

LIBRARY Michigan State 2 University

This is to certify that the dissertation entitled

POLYMER-MODIFIED PLATES FOR ENRICHMENT OF PHOSPHOPEPTIDES PRIOR TO ANALYSIS BY MATRIX-ASSISTED LASER DESORPTION/IONIZATOIN MASS SPECTROMETRY

presented by

Jamie D. Dunn

has been accepted towards fulfillment of the requirements for the

Ph.D.	degree in	Chemistry
	Merli Major Pro	fessor's Signature
	12/1	3/2007
		Date

MSU is an affirmative-action, equal-opportunity employer

PLACE IN RETURN BOX to remove this checkout from your record. **TO AVOID FINES** return on or before date due. **MAY BE RECALLED** with earlier due date if requested.

DATE DUE	DATE DUE	DATE DUE
0 8 2 1 0 9 NUV 1 4 2009		

5/08 K:/Proj/Acc&Pres/CIRC/DateDue indd

POLYMER-MODIFIED PLATES FOR ENRICHMENT OF PHOSPHOPEPTIDES PRIOR TO ANALYSIS BY MATRIX-ASSISTED LASER DESORPTION/IONIZATION MASS SPECTROMETRY

By

Jamie D. Dunn

A DISSERTATION

Submitted to
Michigan State University
in partial fulfillment of the requirement
for the degree of

DOCTOR OF PHILOSOPHY

Department of Chemistry

2007

ABSTRACT

POLYMER-MODIFIED PLATES FOR ENRICHMENT OF PHOSPHOPEPTIDES PRIOR TO ANALYSIS BY MATRIX-ASSISTED LASER DESORPTION/IONIZATION MASS SPECTROMETRY

By

Jamie D. Dunn

Protein phosphorylation is a key cellular regulatory mechanism, so identifying phosphorylation sites on regulatory proteins is vital for understanding diseases such as cancer and finding new pharmaceutical targets. While mass spectrometry (MS) is a useful for identifying phosphorylation sites, low degrees of phosphorylation make detection of these species difficult. To overcome this challenge, immobilized metal affinity chromatography (IMAC), which isolates phosphopeptides based on their affinity for an immobilized metal-ligand complex such as Fe(III)-nitrilotriacetate (Fe(III)-NTA), can be used to enrich phosphopeptides prior to MS analysis. However, the use of IMAC decreases throughput and can result in sample loss because of a large number of processing steps.

This dissertation describes development of a metal affinity-based purification procedure that occurs directly on a gold-coated sample plate that can be inserted into a mass spectrometer for analysis. Fe(III)-NTA complexes were covalently linked to polymers that were grafted to the gold-coated plates. Deposition of protein digests on the polymer-modified plates, followed by rinsing with an acetic acid solution, addition of matrix, and subsequent analysis by matrix-assisted laser desorption/ionization (MALDI) MS yielded mass spectra dominated by peaks corresponding to phosphopeptides.

In initial experiments, we grafted thin polymer films (\sim 30 Å) of poly(acrylic acid) (PAA) onto the MALDI plate, and the PAA was subsequently derivatized with the Fe(III)-NTA complexes. The use of the Fe(III)-NTA-PAA-modified gold plates afforded mass spectra that were dominated with peaks due to singly and multiply phosphorylated peptides from β -casein and other digests since nonphosphorylated peptides were virtually removed during rinsing. In these experiments, the matrix 2',4',6'-trihydroxy-acetophenone mixed with diammonium hydrogen citrate proved to be much better than α -cyano-4-hydroxycinnamic acid for the detection of phosphopeptides.

We also examined the utility of poly(2-hydroxyethyl methacylate) (PHEMA) brushes modified with Fe(III)-NTA complexes for on-plate enrichment. These brushes are 10-fold thicker than the Fe(III)-NTA-PAA films and thus have greater binding capacities. These Fe(III)-PHEMA-NTA brushes exhibited a higher recovery of β-casein phosphorylated peptides compared to Fe(III)-NTA-PAA-modified plates, allowing detection of trace-levels of phosphopeptide impurities. The Fe(III)-NTA-PHEMA brushes have a phosphopeptide binding capacity of 0.6 μg/cm² and exhibited a phosphopeptide recovery of ~73%, whereas thin films of Fe(III)-NTA-PAA afforded a recovery of only ~23% and a monolayer of Fe(III)-NTA had a mere recovery of ~9%. Lastly, we compared the use of the Fe(III)-NTA-PHEMA-modified plates with commercially available IMAC and metal oxide materials. The phosphopeptide recoveries of the commercial enrichment methods were lower than that of the PHEMA brushes with the exception of a TiO₂ microtip, which had a similar recovery of ~68%. However, the TiO₂ microtip exhibited significant impurities in its eluent.

ACKNOWLEDGEMENTS

Merlin, thank you for giving me my second home at MSU. My experience in your group has been very rewarding, and I have learned much since I earned my masters degree. I have found a love for surface chemistry, and am excited to use my skills in a new career. Thank you for being supportive, understanding, and most of all, fun over the past 3 years. I wish you the best and hope you find a new student that is as sassy as I am.

Sam, Amanda, and Jennie, it was a pleasure working with you, and I will see you at future conferences. Lizzy, I will miss you. You are a smart, beautiful lady, and I know you will do well. Gavin, Jetze, and Gary thank you for being on my committee. Thanks for your help and insightful discussions. I would also like to thank the Chemistry Department staff for their help, and the NSF and MSU for funding my research.

The support and understanding that I have received from my family is unbelievable. Thanks for coming to MI for my commencement! My best friend, Steph, and dear friend, Amy Jo, have also been very supportive. Steph, your laugh is unforgettable and I keep it close to my heart. I love you all dearly, and I'm excited to spend more time with you. I couldn't ask for a better family or friends. I would also like to thank my long distance chemistry friends, Sri, Lei, Anne, Doug, and Heather, for keeping in touch and encouraging me to keep going. I miss you all.

D.J., what can I say? You're amazing, and have given me so much love & support over the past 4 years. I'm blessed to have you as my fiancé, and thank God for bringing us together. I would also like to thank D.J.'s family for their support and welcoming me into their home.

TABLE OF CONTENTS

LIST OF FIGURES
Chapter One: Introduction
1.1 Outline
1.2 Protein Phosphorylation
1.3 Phosphoprotein/Phosphopeptide Characterization
1.3.1 Sanger's Reagent and Edman Degradation
1.3.1 Sanger's Reagent and Edman Degradation
1.3.2 Mass Spectrometry
1.3.2.1Ionization Sources.91.3.2.1.1Electrospray Ionization.101.3.2.1.2Matrix-assisted Laser Desorption/Ionization.101.3.2.2Mass Analyzers Compatible with MALDI.121.3.2.2.1Time-of-Flight Mass Spectrometer.121.3.2.2.2Linear Ion Trap Mass Spectrometer.151.3.2.3Identification of Phosphopeptides Using Chemical Methods and Subsequent Analysis by MALDI-MS.201.3.2.4Identification of Phosphopeptides Using Post Source Decay and Tandem Mass Spectrometry.211.3.2.5Challenges in Phosphopeptide Detection by Mass Spectrometry.231.4Enhancement or Enrichment Techniques for the Analysis of Phosphopeptides.241.4.1Matrices and Additives for MALDI-MS.241.4.1.1Use of Ammonium Salts to Enhance Phosphopeptide Detection.241.4.1.2Enhanced Ionization of Phosphopeptides Using 2',4',6'-Trihydroxyacetophenone as a Matrix.251.4.1.3Phosphoric Acid as a Matrix Additive for Analysis of Phosphopeptides.251.4.2Affinity Chromatography.261.4.2.1Background.261.4.2.2Immunoprecipitation of Phosphoproteins Using Phospho-specific
1.3.2.1.1 Electrospray Ionization
1.3.2.1.2 Matrix-assisted Laser Desorption/Ionization
1.3.2.2 Mass Analyzers Compatible with MALDI
1.3.2.2.1 Time-of-Flight Mass Spectrometer
1.3.2.2 Linear Ion Trap Mass Spectrometer
1.3.2.3 Identification of Phosphopeptides Using Chemical Methods and Subsequent Analysis by MALDI-MS
Subsequent Analysis by MALDI-MS
1.3.2.4 Identification of Phosphopeptides Using Post Source Decay and Tandem Mass Spectrometry
Mass Spectrometry
1.3.2.5 Challenges in Phosphopeptide Detection by Mass Spectrometry
1.4. Enhancement or Enrichment Techniques for the Analysis of Phosphopeptides 24 1.4.1 Matrices and Additives for MALDI-MS
1.4.1 Matrices and Additives for MALDI-MS
1.4.1.1 Use of Ammonium Salts to Enhance Phosphopeptide Detection
1.4.1.2 Enhanced Ionization of Phosphopeptides Using 2',4',6'-Trihydroxyacetophenone as a Matrix
2',4',6'-Trihydroxyacetophenone as a Matrix
1.4.1.3Phosphoric Acid as a Matrix Additive for Analysis of Phosphopeptides
1.4.2 Affinity Chromatography261.4.2.1 Background261.4.2.2 Immunoprecipitation of Phosphoproteins Using Phospho-specific
1.4.2.1 Background
1.4.2.2 Immunoprecipitation of Phosphoproteins Using Phospho-specific
Antibodies27
1.4.2.3 Immobilized Avidin Affinity Chromatography for Phosphopeptides28
1.4.2.4 Immobilized Metal Affinity Chromatography for Phosphopeptide
Purification
1.4.3 Metal Oxide Affinity Chromatography
1.4.3.1 Titanium Dioxide-based Enrichment
1.4.3.2 Enrichment Using Zirconium Dioxide
1.4.4 Magnetic Beads
1.4.4.1 Magnetic Nanoparticles Coated with Metal Oxide Materials
1.4.4.2 Fe(III)-Iminodiacetate Immobilized on Magnetic Microspheres
1.4.5 Reversible Covalent Enrichment
1.4.5.1 Chemical Derivatization of Phosphopeptides and Solid-state Purification48

1.4.6 MALDI On-plate Enrichment Techniques
1.4.6.1 Background on Surface-enhanced Affinity Capture Technology54
1.4.6.2 Recent Advancements in MALDI On-plate Enrichment Techniques
for Phosphopeptides59
1.4.6.2.1 Nitrilotriacetic Acid Self-assembled Monolayers Immobilized on Gold
Plates
1.4.6.2.2 Photochemically Immobilized Iminodiacetic Acid on Silicon Supports61
1.4.6.2.3 Polymer-modified Gold MALDI Probes
1.4.6.2.4 Zirconium-phosphonate-modified Porous Silicon Plates
1.4.6.2.5 TiO ₂ -coated Gold Nanoparticles Immobilized on Glass Plates
1.5 Research Overview
1.6 References
1.0 References/1
Chapter Two: Detection of Phosphopeptides Using Fe(III)-Nitrilotriacetate
Complexes Immobilized on a MALDI Plate
2.1 Introduction
2.2 Experimental
2.2.2 Protein Digestion
2.2.3 Fabrication of Fe(III)-NTA Plates
2.2.4 Sample Preparation for Analysis by MALDI-MS
2.2.5 Instrumentation and Data Analysis
2.3 Results and Discussion
2.3.1 Fabrication and Characterization of Fe(III)-NTA-Modified Plates87
2.3.2 Analysis of Phosphoangiotensin by MALDI-MS90
2.3.3 Analysis of Phosphoprotein Digests by MALDI-MS94
2.3.4 Comparison of THAP and α-CHCA as Matrices for Phosphopeptide
Detection on Modified Plates102
2.4 Conclusions
2.5 References
Chapter Three: High-capacity Polymer Brushes Immobilized onto a MALDI
Plate for the Analysis of Phosphopeptides by MS108
3.1 Introduction
3.2 Experimental112
3.2.1 Materials and Solutions
3.2.2 Protein Digestion and Methyl Esterification
3.2.3 Fabrication of Fe(III)-NTA-PHEMA-modified Plates
3.2.4 Quantitation of Phosphopeptide Binding Using Ellipsometry
3.2.5 Protocol for Using the Polymer-modified MALDI Plates
3.2.6 Instrumentation and Data Analysis
3.3 Results and Discussion
3.3.1 Synthesis and Characterization of Fe(III)-NTA-PHEMA-modified Plates119
3.3.2 Identification of Phosphopeptides Using Tandem MS
3.3.3 Quantitation of Phosphopeptide Binding to Fe(III)-NTA-PHEMA-modified
Plates Using Ellipsometry

3.3.4	Analysis of Tryptic Phosphoprotein Digests by MS Using Fe(III)-NTA-	
	PHEMA-modified MALDI Plates.	131
3.3.4		
3.3.4		
3.3.5	· · · · · · · · · · · · · · · · · · ·	
	NTA-PHEMA-modified MALDI Plates.	149
3.4	Conclusions.	
3.5	References	
Char	pter Four: Comparison of Phosphopeptide Enrichment Techniques	157
4.1	Introduction	
4.2	Experimental	
4.2.1		
4.2.2		
4.2.3		
4.2.4	=	
4.2.5		
4.2.6		
4.3	Results and Discussion.	
4.3.1	Calibration	
4.3.2		
4.3.3		
4.3.4		
4.3.4 4.4		
	Conclusions	
4.5	References	201
_	pter Five: Conclusions and Future Research	
5.1	Conclusions and Future Research	
5.2	References	206

LIST OF TABLES

Chapter Three: High-capacity Polymer Brushes Immobilized onto a MALDI Plate

for the Analysis of Phosphopeptides by MIS
Table 3:1: Phosphopeptide-related ions observed in the positive-ion mass spectra of tryptic β-casein digests. The numbers of phosphorylated, aspartic acid (D) and glutamic acid (E) residues in each sequence are also listed. Unless specified, ions correspond to the [M+H] ⁺ ion
Table 3:2: Nonphosphorylated peptides that were frequently observed in the mass spectra of 1 pmol, 500 fmol, 125 fmol, and 62 fmol ovalbumin digest when the spectra were obtained using the Fe(III)-NTA-PHEMA-modified plate. The number of histidine (H),
glutamic acid (E), and aspartic acid (D) residues for each peptide sequence are

given......148

Chapter Four: Comparison of Phosphopeptide Enrichment Techniques

LIST OF FIGURES

Chapter One: Introduction

Figure 1.1: Phosphorylation of serine catalyzed by a protein kinase in the presence ATP
Figure 1.2: Reversible protein phosphorylation and the change in protein conformation due to the addition of the phosphate group. Kinases catalyze phosphorylation whereas phosphatases catalyze dephosphoyrlation
Figure 1.3: Use of Sanger's reagent to cleave a polypeptide at the terminal amide bond for subsequent analysis
Figure 1.4: Use of Edman degradation to cleave a peptide at the terminal amide bond for subsequent sequencing using chromatography or electrophoresis. The process must be repeated to determine each residue
Figure 1.5: Schematic diagram of a basic mass spectrometer8
Figure 1.6: Schematic diagram of MALDI sample preparation and analysis. After deposition of the analyte and matrix solution onto the MALDI plate, the solvent evaporates, co-crystallizing the matrix with the analyte
Figure 1.7: Schematic diagram of a MALDI time-of-flight mass spectrometer with linear- and reflectron-mode capabilities. The ion path is shown for linear-mode TOF MS
Figure 1.8: Mass scan line for the linear ion trap. U_{DC} is zero, hence, a_x is zero. Grey circles are the ions in the stable region, and the relative size of the circle corresponds to the relative size of the m/z value.
Figure 1.9: General schematic of the Thermo 2-D linear ion trap. Ions are trapped in the center section and the front and back sections reduce distortion of the electric field of the center section, thus, the ion trapping efficiency is improved. Ions are radially (a direction) ejected from the center section through the slot (0.25 mm x 30 mm) of the two exit rods
Figure 1.10: Schematic diagram of the Thermo vMALDI LTQ XL instrument19
Figure 1.11: β-Elimination of (a) phosphoserine and (b) phosphothreonine, forming dehydroalanine and dehydroaminobutyric acid, respectively, which are subsequently reacted with ethanedithiol (Michael addition)21
Figure 1.12: Cleavage of a tripeptide backbone shows the x, y, and z ions and the a, b and c ions. The most common sequence ions are the y and b type23

Figure 1.13: Labeling of a phosphopeptide with biotin and capture of this peptide using avidin immobilized on beads
Figure 1.14: Labeling of a phosphopeptide with biotin and capture of this peptide using avidin immobilized on beads
Figure 1.15: Labeling of a phosphopeptide with biotin and capture of this peptide using avidin immobilized on beads
Figure 1.16: Structures of a) IDA and b) NTA
Figure 1.17: Methyl esterification of carboxylic acid groups in the peptide using acety chloride and an excess of methanol: a) reaction shows generation of HCl and b) reaction shows the acid-catalyzed methyl esterification of the carboxylic acid groups
Figure 1.18: General protocol for the enrichment of phosphopeptides using commercial IMAC column packed with Fe(III)-NTA beads. Reverse phase (RP) C18 column is used for sample desalting
Figure 1.19: Structures of 2,5-DHB, salicylic acid, pththalic acid, benzoic acid39
Figure 1.20: Adsorption of salicylic acid and phosphoric acid to the surface of TiO ₂ 40
Figure 1.21: Fabrication of TiO ₂ -coated magnetic nanoparticles. Zirconia- and alumina coated magnetic nanoparticles are prepared in a similar fashion
Figure 1.22: Preparation of magnetic beads modified with Fe(III)-IDA47
Figure 1.23: Six-step solid-phase enrichment using carbodiimide condensation and glass beads derivatized with iodoacetyl groups. Figure shows only 5 steps
Figure 1.24: Reversible solid-phase enrichment of phosphoserine and phosphothreoine-containing peptides using β-elimination and Michael addition followed by enrichment on a dithiopyridino-modified resin
Figure 1.25: Reversible solid-phase enrichment using an α-diazo resin. Cleavage of the phosphopeptide can be accomplished by using either trifluoroacetic acid (TFA) of NH ₄ OH. Note that when NH ₄ OH is used, the methyl ester is hydrolyzed back to the original phosphopeptide
Figure 1.26: Three-step solid phase enrichment using carbodiimide condensation52
Figure 1.27: Reversible solid-phase enrichment of protected phosphopeptides using an oxidation-reduction condensation reaction

Figure 1.28: Capture of an antigen for probe affinity mass spectrometry using an antibody immobilized on a self-assembled monolayer on a MALDI target
Figure 1.29: On-probe affinity enrichment using an antibody anchored to a grafted polymer to capture the antibody of interest
Figure 1.30: Formation of a self-assembled monolayer of octadecanethiol and derivatization using maleimide-terminated NTA. Further NTA complexation with Ga(III or Fe(III) is not shown here
Figure 1.31: Immobilization of a monolayer of an IDA derivative on porous silicon using photochemistry
Figure 1.32: Fabrication of polymer-modified MALDI gold plates for phosphopeptide capture and concentration. A hydrophobic pattern is created first, followed by the immobilization of polymers onto the 200- µm diameter gold wells
Figure 1.33: Immobilization of gold nanoparticles (NPs) coated with titania on glass substrates
Chapter Two: Detection of Phosphopeptides Using Fe(III)-Nitrilotriacetate Complexes Immobilized on a MALDI Plate
Figure 2.1: Immobilization of Fe(III)-NTA complexes onto a gold-coated substrate. Surface modification: a) immobilized PAA, b) activated PAA, c) NTA-derivatized PAA, and d) Fe(III)-NTA complex
Figure 2.2: Reflectance FTIR spectra of PAA films after different steps during functionalization of these films with Fe(III)-NTA: a) immobilized PAA, b) activated PAA, c) NTA-derivatized PAA, and d) immobilized Fe(III)-NTA-PAA88
Figure 2.3: Positive ion MALDI mass spectra of a mixture of 2 pmol of angiotensin and 2 pmol of phosphoangiotensin obtained using a) Fe(III)-NTA-modified gold and b conventional gold plates. After the peptide mixture was applied to the modified plate, a rinse with 25 mM acetic acid was used to remove angiotensin. The matrix was saturated α-CHCA
Figure 2.4: Positive ion MALDI mass spectra of a 10-pmol myoglobin digest spiked with 1 pmol of angiotensin and 1 pmol of phosphoangiotensin. The spectra were obtained using a) a Fe(III)-NTA-modified plate and b) a conventional gold plate. After the peptide mixture was applied to the surface-modified plate, it was rinsed with 50 mM

Figure 2.5: Positive ion MALDI mass spectra of a 7-pmol β -case in digest analyzed using a) conventional gold and b) Fe(III)-NTA-modified gold plates. After the peptide mixture was applied to the modified plate, it was rinsed with acetic acid in 30% acetonitrile prior to addition of THAP/DAHC
Figure 2.6: Positive ion MALDI mass spectra of a 3.8-pmol ovalbumin digest analyzed using a) conventional gold, b) Fe(III)-NTA-PAA-modified (30 Å thickness) gold, and c) Fe(III)-NTA-PAA-modified (90 Å thickness) gold plates. Spectrum d) was obtained using a 6.5-pmol ovalbumin digest and a Fe(III)-PAA-modified gold plate. After the peptide mixtures were applied to the modified plates, they were rinsed with acetic acid in 30% acetonitrile prior to addition of THAP/DAHC. The arrows indicate peaks corresponding to phosphorylated peptides at m/z 2090, 2513, and 290398
Figure 2.7: Positive ion MALDI mass spectra of a 7.3-pmol ovalbumin digest analyzed using the Fe(III)-NTA-modified gold plate with different matrices: (a) α -CHCA/DAHC and (b) THAP/DAHC. After the peptide mixture was applied to the modified plates, they were rinsed with acetic acid in 30% acetonitrile. The arrows indicate peaks corresponding to phosphopeptides at m/z 2090, 2513, and 2903
Chapter Three: High-capacity Polymer Brushes Immobilized onto a MALDI Plate for the Analysis of Phosphopeptides by MS
Figure 3.1: Cartoon of "grafting to" versus "grafting from" methods of film growth109
Figure 3.2: General mechanism for transition-metal-catalyzed ATRP. k_{act} , k_{deact} , k_p , and k_t are the rate constants for activation, deactivation, polymerization, and termination, respectively
Figure 3.3: Fabrication of an Fe(III)-NTA-PHEMA-modified gold MALDI plate121
Figure 3.4: Reflectance FTIR spectra of a) a PHEMA brush immobilized on a gold substrate, and the same brush after b) derivatization with succinic anhydride, c) activation of carboxylic acid groups, d) derivatization with NTA, and e) complexation with ferric ions
Figure 3.5: CID MS/MS spectrum of a monophosphorylated peptide (m/z 2088) isolated from 500 fmol of an ovalbumin digest: a) full mass range and b) enlarged region (600 – 1950). Prior to obtaining the mass spectrum, the phosphopeptide was enriched on a Fe(III)-NTA-PHEMA-modified plate
Figure 3.6: CID MS/MS spectrum of a monophosphorylated peptide (m/z 2511) isolated from 500 fmol of an ovalbumin digest: a) full mass range and b) enlarged region (800 – 2300). Prior to obtaining the mass spectrum, the phosphopeptide was enriched on a Fe(III)-NTA-PHEMA-modified plate

Figure 3.7: CID MS/MS spectrum of a monophosphorylated peptide (m/z 2901) isolated from 3.5 pmol of an ovalbumin digest: a) full mass range and b) enlarged region (800 – 2300). Prior to obtaining the mass spectrum, the phosphopeptide was enriched on a Fe(III)-NTA-PHEMA-modified plate
Figure 3.8: Plot of the amount of pA bound to PHEMA-NTA-Fe(III) films on a gold substrate as a function of pA concentration. The solid line represents the fit to the Langmuir adsorption isotherm, and the inset shows an expanded view of the data at low pA concentrations
Figure 3.9: Positive-ion MALDI mass spectra of 7 pmol of β -casein digest. Spectra were obtained using a) conventional analysis and b) a Fe(III)-NTA-PHEMA-modified plate with incubation and rinsing. In spectrum b, peaks labeled with triangles represent doubly charged phosphopeptides, peaks labeled with stars are due to fragmentation of phosphopeptides, and peaks labeled with circles stem from α -S1-casein and α -S2-casein phosphorylated peptides. Numbers in parentheses are peak intensities. Peak identification was facilitated by MS/MS spectra
Figure 3.10: Positive-ion MALDI mass spectra of 1 pmol of β -casein digest. Spectra were obtained using a) conventional analysis and b) a Fe(III)-NTA-PHEMA-modified plate with incubation and rinsing. In spectrum b, peaks labeled with triangles represent doubly charged phosphopeptides, peaks labeled with stars are due to fragmentation of phosphopeptides, and peaks labeled with circles stem from α -S1-casein and α -S2-casein phosphorylated peptide impurities. Numbers in parentheses are peak intensities137
Figure 3.11: Positive-ion MALDI mass spectra of 500 fmol of β -casein digest. The spectra were obtained using a) conventional analysis and b) a Fe(III)-NTA-PHEMA-modified plate with incubation and rinsing. In spectrum b, peaks labeled with triangles are due to doubly charged phosphopeptides, peaks labeled with stars are due to fragmentation of phosphopeptides, and peaks labeled with circles stem from α -S1-casein and α -S2-casein phosphorylated peptides. The number in parentheses is peak intensity.
Figure 3.12: Positive-ion MALDI mass spectra of 125 fmol of β -casein digest. The spectra were obtained using a) conventional analysis and b) a Fe(III)-NTA-PHEMA-modified plate with incubation and rinsing. In spectrum b, peaks labeled with triangles are due to doubly charged phosphopeptides, peaks labeled with stars are due to fragmentation of phosphopeptides, and peaks labeled with circles stem from α -S1-casein and α -S2-casein phosphorylated peptide impurities. The number in parentheses is peak intensity

Figure 3.13: Positive-ion MALDI mass spectra of 31 fmol of β -casein digest. Spectra were obtained using a) conventional analysis and b) a Fe(III)-NTA-PHEMA-modified plate with incubation and rinsing. In spectrum b, the peak labeled with a triangle represents a doubly charged phosphopeptide, the peak labeled with a star is due to fragmentation of phosphopeptides, and the peak labeled with a circle stem from an α -S1-casein phosphorylated peptide impurity
Figure 3.14: Positive-ion MALDI mass spectra of 15 fmol of β-casein digest. The spectra were obtained using a) conventional analysis and b) a Fe(III)-NTA-PHEMA-modified plate with incubation and rinsing. The number in parentheses is peak intensity
Figure 3.15: Positive-ion MALDI mass spectra of 1 pmol of ovalbumin digest. Spectra were obtained using a) conventional analysis and b) a Fe(III)-NTA-PHEMA-modified plate with incubation and rinsing. Numbers in parentheses are peak intensities144
Figure 3.16: Positive-ion MALDI mass spectra of 500 fmol of ovalbumin digest. Spectra were obtained using a) conventional analysis and b) a Fe(III)-NTA-PHEMA-modified plate with incubation and rinsing. Numbers in parentheses are peak intensities
Figure 3.17: Positive-ion MALDI mass spectra of 125 fmol of ovalbumin digest. Spectra were obtained using a) conventional analysis and b) a Fe(III)-NTA-PHEMA-modified plate with incubation and rinsing. The number in parentheses is peak intensity
Figure 3.18: Positive-ion MALDI mass spectra of 62 fmol of ovalbumin digest. Spectra were obtained using a) conventional analysis and b) a Fe(III)-NTA-PHEMA-modified plate with incubation and rinsing. The number in parentheses is peak intensity149
Figure 3.19: Positive-ion MALDI mass spectra of a) 250 fmol of β-casein digest and b) 250 fmol of methyl esterified β-casein digest. The spectra were obtained using an Fe(III)-NTA-PHEMA-modified plate with 1-h incubation and rinsing with 3:30:67 acetic acid:acetonitrile:water
Figure 3.20: Enlarged region (2125 – 2275) of the positive-ion MALDI mass spectra of 250 fmol of a methyl esterified β-casein digest. The spectrum, which was obtained using enrichment on an Fe(III)-NTA-PHEMA-modified plate, shows peaks due to side products from deamidation with subsequent methyl esterification
Chapter Four: Comparison of Phosphopeptide Enrichment Techniques
Figure 4.1: Synthesis of a Fe(III)-NTA-MUA-modified MALDI plate158
Figure 4.2: Fabrication of the Fe(III)-NTA-PAA-modified MALDI plate160

Figure 4.3: a) Millpore ZipTip _{MC} and b) structure of iminodiacetate (IDA)161
Figure 4.4: Qiagen Mass Spec Focus IMAC Chip for purification and concentration of phosphopeptides. The enlargement shows the hydrophobic zone, the analysis zone, and the affinity capture zone. Figure adapted from the Qiagen manual that accompanies the chips
Figure 4.5: Several views of Qiagen NuTips, which contain embedded metal oxide chromatographic material. The end of the tip is flattened as shown in the side view presumably to maximize the surface area of the tip in contact with the sample164
Figure 4.6: Sequence of the labeled synthetic phosphopeptides a) H ₅ peptide and b) D ₅ peptide with their respective m/z values
Figure 4.7: Calibration curved prepared by plotting the ratio of the peak intensities due to the H ₅ and D ₅ peptides (I _{H5} /I _{D5}) in MALDI mass spectra. 125 fmol of D ₅ peptide was present in all samples, and the amount of H ₅ peptide was varied from 8 to 125 fmol
Figure 4.8: Procedure used to recover H ₅ peptide (no digest) using Fe(III)-NTA-MUA-modified or Fe(III)-NTA-PHEMA-modified plates
Figure 4.9: MALDI mass spectrum of 125 fmol of the H ₅ peptide (no protein digest). The spectra were obtained using a) the Fe(III)-NTA-MUA-modified plate and b) the Fe(III)-NTA-PHEMA-modified plate. After the sample was applied to the plates and rinsed, 125 fmol of D ₅ peptide was added as an internal standard
Figure 4.10: Protocol used for determining the recovery of the H ₅ peptide from a protein digest mixture using Fe(III)-NTA-MUA-modified, Fe(III)-NTA-PAA-modified, or Fe(III)-PHEMA-modified plates
Figure 4.11: Analysis of 1 pmol of a protein digest mixture containing 125 fmol of the H ₅ peptide. 125 fmol of the D ₅ peptide was added as an internal standard. Spectra were obtained using a) conventional MALDI-MS analysis, and b) and c) a Fe(III)-NTA-MUA-modified plate with incubation and rinsing. Spectrum c) is an expanded portion of spectrum b)
Figure 4.12: Analysis of 1 pmol of a protein digest mixture containing 125 fmol of the H ₅ peptide. 125 fmol of the D ₅ peptide was added as an internal standard. Spectra were obtained using a) conventional MALDI-MS analysis, and b) and c) a Fe(III)-NTA-PAA-modified plate with incubation and rinsing. Spectrum c) is an expanded portion of spectrum b)

Figure 4.13: Analysis of 1 pmol of a protein digest mixture containing 125 fmol of the H ₅ peptide. 125 fmol of the D ₅ peptide was added as an internal standard. Spectra were obtained using a) conventional MALDI-MS analysis, and b) and c) a Fe(III)-NTA-PHEMA-modified plate with incubation and rinsing. Spectrum c) is an expanded portion of spectrum b)
Figure 4.14: Analysis of 1 pmol of protein digest mixture containing 125 fmol of the H_5 peptide and 125 fmol of the D_5 peptide (internal standard) using a) conventional MALDI-MS analysis, b) conventional MALDI-MS analysis with precursor ion isolation with m/z 1396.4 and a m/z window of 10 (no fragmentation), and c) the Fe(III)-NTA-PHEMA-modified plate with incubation and rinsing. In spectrum c), the D_5 peptide was added just prior to addition of matrix
Figure 4.15: CID MS/MS spectrum of m/z 1399.6 observed in the MS spectrum of the peptides recovered from the H ₅ peptide/protein digest mixture using an Fe(III)-NTA-PHEMA-modified plate a) m/z region 400 – 1400 and b) enlarged m/z region 500 – 1300. The b and y ions are due to the peptide shown, which originates from BSA187
Figure 4.16: CID MS/MS spectrum of the H_5 peptide (selected precursor ion at m/z 1393.6) a) m/z region 400 – 1400 and b) enlarged m/z region 500 – 1295190
Figure 4.17: CID MS/MS spectrum of the D_5 peptide (selected precursor ion at m/z 1398.6) a) m/z region 400 – 1400 and b) enlarged m/z region 500 – 1295191
Figure 4.18: CID MS/MS analysis of 1 pmol of a protein digest mixture containing 125 fmol of the H ₅ peptide. 125 fmol of the D ₅ peptide was added to the digest solution prior to conventional analysis and to the Fe(III)-NTA-PHEMA-modified plate after enrichment. Spectra were obtained using a) conventional MALDI-MS analysis and b) enrichment using a Fe(III)-NTA-PHEMA-modified plate. In both a and b, the precursor ion isolation was m/z 1396.4 with a m/z window of 10
Figure 4.19: Enlarged m/z region $1240 - 1390$ of the CID MS/MS analysis of 1 pmol of a protein digest mixture containing 125 fmol of the H ₅ peptide. Spectra were obtained using a) conventional MALDI-MS analysis and b) enrichment on a Fe(III)-NTA-PHEMA-modified plate. 125 fmol of the D ₅ peptide was added to the digest solution prior to conventional analysis and to the Fe(III)-NTA-PHEMA-modified plate after enrichment. In both a and b, the selected precursor ion had a m/z 1396.4 with a m/z window of 10
Figure 4.20: Mass spectra of the peptides extracted using a Millipore ZipTip _{MC} and a solution containing a protein digest mixture (1 pmol) and 125 fmol of the H ₅ peptide. a) m/z range 500 - 2500 and b) enlarged m/z region 1390 - 1404. The D ₅ peptide (125 fmol) was added as an internal standard to the extracted peptides

Figure 4.21: Mass spectra of the peptides extracted onto a Qiagen Mass Spec Focus IMAC chip from a solution containing a protein digest mixture (1 pmol) and 125 fmol of the H_5 peptide. a) m/z range $500 - 2500$ and b) enlarged m/z region $1390 - 1404$. The Depeptide was added as an internal standard to the extracted peptides
Figure 4.22: Mass spectra of the peptides extracted using a Glygen TiO_2 NuTip and a solution containing a protein digest mixture (1 pmol) and 125 fmol of the H_5 peptide. a) m/z range $1000 - 2000$ and b) enlarged m/z region $1390 - 1404$. The D_5 peptide (125 fmol) was added as an internal standard to the extracted peptides
Figure 4.23: Mass spectra of the peptides extracted using a Glygen ZrO_2 NuTip and a solution containing a protein digest mixture (1 pmol) and 125 fmol of the H_5 peptide. a) m/z range $1000 - 2000$ and b) enlarged m/z region $1390 - 1404$. The D_5 peptide (125 fmol) was added as an internal standard to the extracted peptides

LIST OF ABBREVIATIONS

ADP	. adenosine diphosphate
amino-terminated NTA	. $N_{\alpha}N_{\alpha}$ -bis(carboxymethyl)-L-lysine hydrate
ATP	. adenosine triphosphate
ATRP	. atom transfer radical polymerization
Biotin-HPDP	N-[6-(biotinamido)hexyl]-3'-(2'-pyridyldithio)propionamide
bpy	. 2,2'-bipyridine
BSA	. bovine serum albumin
α-CHCA	α-cyano-4-hydroxycinnamic acid
CID	collision-induced dissociation
DAHC	diammonium hydrogen citrate
2,5-DHB	2,5-dihydroxybenzoic acid
D/I	desorption/ionization
DIPEA	N,N'-diisopropylethylamine
DMAP	. 4-dimethylaminopyridine
DMF	dimethylformamide
DSP	. dithiobis-succinimidyl propionate
DTT	dithiothreitol
EDC	N,N'-dimethylaminopropyl ethyl carbodiimide
EDT	1,2-ethanedithiol
ESI	. electrospray ionization

FD	field desorption
FT-ICR	Fourier transform ion cyclotron resonance
FTIR	.Fourier transform infrared
GC-MS	gas chromatography/mass spectrometry
GLYMO	.3-glycidoxypropyltrimethoxysilane
HDT	. hexadecanethiol
IAC	.immobilized affinity chromatography
IDA	iminodiacetic acetate
IMAC	immobilized metal affinity chromatography
LC	. liquid chromatography
LD	. laser desorption
LIT	. linear ion trap
MALDI	. matrix assisted laser desorption/ionization
MUA	. mercaptoundecanoic acid
MUD	. 11-mercaptoundecanol
MS	mass spectrometry
MS/MS	.tandem mass spectrometry
m/z	mass-to-charge ratio
NHS	. N-hydroxysuccinimide
NP	. nanoparticle
NTA	. nitrilotriacetate
1P	. monophosphorylated peptide
4P	. tetraphosphorylated peptide

pA	. phoshoangiotensin II
PAA	. poly(acrylic acid)
PAMS	probe affinity mass spectrometry
PDMS	polydimethylsiloxane
PEI	. polyethylenimine
РНЕМА	. poly(2-hydroxyethyl methacrylate)
phos b	. phosphorylase b
PPh ₃	. triphenylphosphine
pS	. phosphoserine
PSD	. post-source decay
pT	phosphothreonine
PTBA	. poly(tert-butyl acrylate)
PTM	posttranslational modification
pY	. phosphotyrosine
PySSPy	2,2'-dithiopyridine
QIT	quadrupole ion trap
q-TOF	quadrupole time-of-flight
RP	. reverse phase
SALDI	surface-assisted laser desorption/ionization
SAM	self-assembled monolayer
SEAC	. surface-enhanced affinity capture
SIMS	secondary-ion mass spectrometry
S/N	. signal-to-noise ratio

tBOC	t-butyl-dicarbonate
TEA	triethylamine
TEOS	tetraethyl orthosilicate
TFA	trifluoroacetic acid
THAP	2',4',6'-trihydroxyacetophenone
TOF	time-of-flight
UV	ultraviolet
XPS	x-ray photoelectron spectroscopy

xxi

Chapter One: Introduction

1.1 Outline

This chapter first discusses (sections 1.2 and 1.3) the importance of phosphoproteins and the main methods that are used to characterize them, Edman degradation and mass spectrometry (MS). Although MS is the primary technique currently used to analyze phosphoproteins, the inherent challenges in phosphoprotein and phosphopeptide detection have led to the development of methods for enriching these species prior to analysis. Thus, section 1.4 provides background on several enrichment techniques, most notably immobilized metal affinity chromatography (IMAC). My research has focused on modifying MALDI sample plates with polymers that can effect on-plate enrichment in a manner similar to IMAC. On-plate enrichment is advantageous in that it allows for minimal sample handling, high throughput, and low sample loss, and section 1.4.6 describes prior work in this area. Finally, section 1.5 provides a brief outline of the research described in the thesis.

1.2 Protein Phosphorylation

Although reversible protein phosphorylation is just one of over 200 different posttranslational modifications (PTMs),¹ it is one of the major mechanisms by which cellular activity is regulated. This PTM, which is regulated by kinases and phosphatases, is essential for numerous cellular functions such as gene expression and membrane transport.²⁻⁹ The importance of reversible protein phosphorylation as a biological regulatory mechanism was acknowledged in 1992 when Edmond H. Fischer and Edwin G. Krebs won the Nobel Prize for demonstrating that the inactive form of glycogen

phosphorylase (phosphorylase b) is converted into the active form (phosphorylase a) by reversible phosphorylation when a divalent metal ion is present.¹⁰

In the phosphorylation process of eukaryotes, hydroxyl groups on the side chains of serine, threonine, or tyrosine residues participate in phosphoryl transfer, but the susceptibility of these amino acids to phosphorylation is sequence dependent. As shown in Figure 1.1, adenosine triphosphate (ATP) serves as a source of phosphate, and in the presence of a kinase, ATP loses its gamma phosphate to form adenosine diphosphate (ADP).¹¹ The addition of one phosphate increases the molecular weight of a protein by 80 Da (when the phosphate is fully protonated) and decreases the protein charge by 2 units at high pH.

Figure 1.1: Phosphorylation of serine catalyzed by a protein kinase in the presence of ATP. Figure adapted from Walsh.¹¹

Phosphorylation is regulated by networks of protein kinases and phosphatases that catalyze phosphorylation and dephosphorylation of serine, threonine and tyrosine

residues. As shown in Figure 1.2, the addition of a phosphate group can cause a protein to undergo a change in conformation, often yielding an active enzyme. The phosphorylation site can serve as a docking station for proteins to interact with other proteins, molecules or ions in the cell. The malfunction of kinases often leads to diseases such as cancer so an understanding of phosphorylation process has important biomedical implications. The activity of kinases can be followed by monitoring the concentration of phosphorylated proteins, but in addition to detecting phosphorylation events, it is important to determine on what residues these events occur. Identification of these residues will allow better understanding of cellular regulation as well as development of new pharmaceutical targets. However, a protein may contain many serine, tyrosine, or threonine residues, so identifying a specific site of phosphorylation is challenging. Nevertheless, these determinations can be carried out using either Edman degradation or mass spectrometry as discussed in sections 1.3.1 and 1.3.2 below.

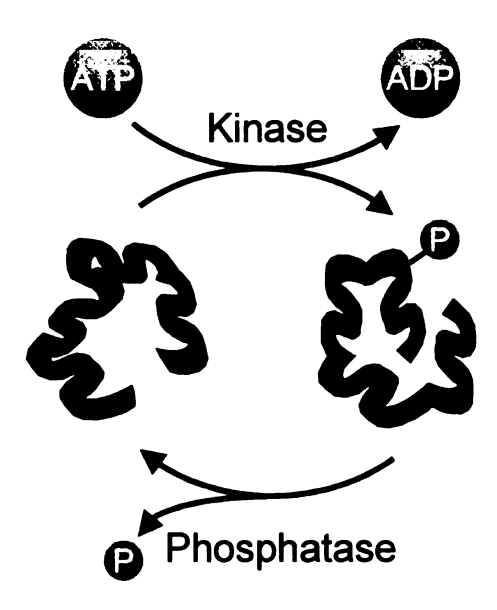


Figure 1.2: Reversible protein phosphorylation and the change in protein conformation due to the addition of the phosphate group. Kinases catalyze phosphorylation whereas phosphatases catalyze dephosphorylation.

1.3 Phosphoprotein/Phosphopeptide Characterization

1.3.1 Sanger's Reagent and Edman Degradation

Frederick Sanger, who won the Nobel Prize in 1958, was the first to use a chemical reagent¹³ to help determine the complete sequence of insulin, a protein containing 51 amino acid residues. As depicted in Figure 1.3, Sanger utilized fluorodinitrobenzene (Sanger's reagent) as an electrophile to form a stable covalent bond to the amino group (the strongest nucleophile in the peptide chain) of the N-terminus of the peptide. Once the peptide is labeled, the amide bond is hydrolyzed and the labeled amino acid can be identified. Unfortunately, use of Sanger's reagent leads to some hydrolysis of other amide bonds in the peptide, hence, this method is not an efficient approach to identifying the sequence of a peptide or protein.

the state of the s

Figure 1.3: Use of Sanger's reagent to cleave a polypeptide at the terminal amide bond for subsequent analysis.

Pehr V. Edman also developed a chemical method to determine the sequence of peptides, but the reagent employed, N-phenyl isothiocyanate, serves as both an electrophile and a nucleophile and can form a stable, 5-atom ring when it binds to the amino acid at the N-terminus of the peptide (Figure 1.4). This avoids the hydrolysis of the other peptide bonds in the chain. After cleavage, the labeled amino acid can be identified using chromatography or electrophoresis.

Figure 1.4: Use of Edman degradation to cleave a peptide at the terminal amide bond for subsequent sequencing using chromatography or electrophoresis. The process must be repeated to determine each residue.

The main disadvantages of these two techniques are that they require many steps, large quantities of pure peptide and several hours to days to sequence the peptide. Edman degradation typically requires 1 pmol of peptide, and although this technique is now automated, it still takes about a day to sequence a peptide/protein containing 50 amino acids (~5 kDa peptide). Additionally, coupling is inhibited by modifications of the terminal amine such as formylation and acetylation, which is another disadvantage of chemical sequencing methods.⁸

For many years, Edman degradation was the primary technique that was used to characterize proteins. Within the last 20 years, however, mass spectrometry has become the workhorse for analyzing proteins due to the development of electrospray ionization (ESI) and matrix-assisted laser desorption/ionization (MALDI).

1.3.2 Mass Spectrometry

Mass spectrometry (MS) is now the method of choice for determining the sequence of proteins because it is much faster than Edman degradation and requires less sample, and much research is currently aimed at utilizing mass spectrometric techniques for the identification of phosphorylation sites. Below I first provide information on MS instrumentation and then discuss challenges that need to be overcome in the identification of phosphorylation sites.

MS was first introduced in 1897 by Sir Joseph J. Thomson, ¹⁴ and since then it has become practical for a wide range of applications. There are several mass spectrometry instruments that can be utilized, and the selection of the instrument greatly depends on the analyte being examined. The two most important parts of any MS instrument are the ionization source and the mass analyzer, and the basic design of an instrument is shown in Figure 1.5. Although the MS experiment requires ions that are in the gas phase, samples can be initially introduced to the instrument in a solid or liquid form. The ionization source converts the sample into gas-phase ions, and the mass analyzer separates these ions based on their mass-to-charge ratio (m/z). Subsequently, the ions are collected and counted by the detector, and a mass spectrum is produced.

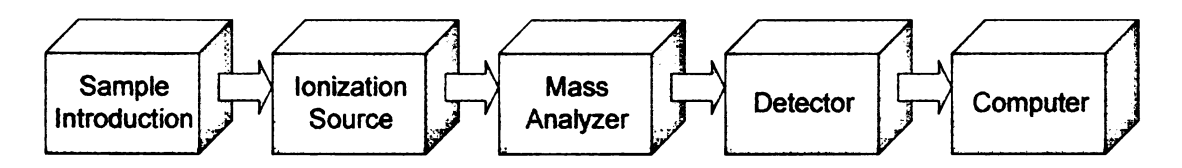


Figure 1.5: Schematic diagram of a basic mass spectrometer.

Initially, mass spectrometry methods including gas chromatography/mass spectrometry (GC-MS), which utilizes electron impact (EI) as the ionization method, were limited to the analysis of volatile (high vapor pressure) compounds because EI ionization requires gas-phase samples. The challenging issue of sample volatility and thermal stability was overcome by the development of desorption/ionization (D/I) techniques, which yield gas phase ions from condensed phase analytes. Mass spectrometric D/I methods encompass field desorption (FD), laser desorption (LD), matrix-assisted laser desorption/ionization (MALDI), secondary-ion mass spectrometry (SIMS), and fast atom bombardment (FAB).

The methods of field desorption and laser desorption have limited utility. FD requires the analyte on the sample probe to be heated with a high electric field (10⁷ – 10⁸ V/cm).¹⁵ The basic idea of LD was to focus a pulsed laser onto a solid target such that a a portion of the sample could be heated to several hundred degrees in a few nanoseconds. At this point, desorption can occur at rates faster than those for chemical degradation (although some fragmentation is observed), resulting in desorption of intact molecules. A portion of the sample is not only desorbed, but it is also ionized. However, the use of LD was limited to compounds with molecular weights of approximately 1000 Daltons (Da) and less.¹⁶ The relatively new method MALDI is a D/I technique related to laser desorption, but it incorporates a matrix to assist in the desorption/ionization of the

analyte. MALDI circumvented the mass limitation of LD, allowing high molecular weight species such as proteins and oligonucleotides to be analyzed using MS. MALDI will be discussed further in section 1.3.2.1.2.

LD (including MALDI) is a pulsed ionization technique that generates bursts of ions on the timescale of nanoseconds, and the time-of-flight (TOF) mass analyzer was the first instrument used with LD.¹⁷ The TOF spectrometer is capable of separating high molecular weight, singly-charged ions.¹⁷ More recently, MALDI has been coupled with other mass analyzers with tandem MS capabilities. Some of these mass spectrometers include the quadrupole-TOF (q-TOF), TOF-TOF, quadrupole ion trap, and Fourier transform ion cyclotron resonance (FT-ICR) mass analyzers. In our experiments, we utilized MALDI coupled with TOF, as well as the linear quadrupole ion trap mass analyzer for the analysis of phosphopeptides. These two mass analyzers will be discussed further in section 1.3.2.2.

1.3.2.1 Ionization Sources

The development of the soft desorption/ionization techniques such as matrix-assisted laser desorption/ionization (MALDI) and electrospray ionization (ESI) around 1985 paved the way for the analysis of biomolecules by mass spectrometry. The importance of soft ionization methods for the analysis of macromolecules was recognized in 2002 when John Fenn and Koichi Tanaka shared the Nobel prize.

THE HOLD COME TO SECURE A SECURE OF THE PROPERTY OF THE PROPER

1.3.2.1.1 Electrospray Ionization

Electrospray ionization (ESI) is not a D/I technique, but it is also capable of ionizing non-volatile compounds and was developed about the same time as MALDI. ESI is an attractive method relative to D/I techniques since ions can be formed and detected as multiply-charged species. Analytes are injected as liquids and pumped continuously through a needle with a flow rate of roughly 1-10 μL/min. Nanoliter flow rates (50-400 nL/min) are also possible. Charged droplets are sprayed from the end of the needle due to an applied potential (3-5 kV), and drying gas causes the droplets to desolvate. As a result of solvent evaporation, Coulombic explosions due to charge repulsion result in the formation of ions with different degrees of charge for the same species. Analytes that have several ionization sites will be highly charged. ESI is also capable of analyzing species that lack sites of ionization, but this usually requires an acidic or basic additive in order for the analyte to be detected.

1.3.2.1.2 Matrix-assisted Laser Desorption/Ionization

The principle of MALDI and the term "matrix-assisted LD" were first published in 1985 by Hillenkamp and Karas.¹⁹ They showed that tryptophan assisted in the molecular ion formation of alanine by LD-MS. For this experiment, the laser threshold irradiance (2 x 10⁷ W/cm² at 266 nm, 10-μm spot area, 10-ns pulse width, and 20 nJ at the sample) was that of tryptophan, which is about 10-fold less than that required for ionization of alanine. After this initial discovery, it was not until 1988 that MALDI was used to analyze proteins with molecular weights exceeding 10 kDa¹⁹ and 100 kDa.²⁰ These studies showed that MALDI is a soft ionization method, and is ideal for thermally

the first of the second of the

labile molecules such as oligonucleotides, proteins, and peptides. Current MALDI-MS methods are capable of detecting low picomole (pmol) to attamole (amol) amounts of analytes.¹

Conventional MALDI sample plates are typically made from stainless steel and in some cases may be coated with gold, depending on the manufacturer. The diameters of the sample wells are ~2-3 mm, and sample preparation for conventional ultraviolet (UV) MALDI is minimal. A 10,000-fold excess of low molecular weight, UV-absorbing, organic matrix is simply co-crystallized with the analyte on the MALDI sample plate.¹ Some UV-MALDI matrices that are commonly used today were discovered between and include 2,5-dihydroxybenzoic acid (2,5-DHB),²¹ α-cvano-4-1990-1992 hydroxycinnamic acid (α-CHCA),²² and 3,5-dimethoxy-4-hydroxycinnamic acid (sinapinic acid).²³ The first two matrices are typically used for peptide analysis whereas the latter is used for protein analysis. After the matrix solution (e.g., 20 mg/mL matrix in 60% acetonitrile, 0.1% trifluoroacetic acid)²⁴ is applied to the sample plate, the solvent rapidly evaporates, incorporating the analyte molecules into the matrix crystals. As portrayed in Figure 1.6, when the pulsed, 337-nm laser is fired at the sample, the analyte molecules (M) are desorbed and ionized intact, forming singly-charged ions with little fragmentation. Typically, each peak observed in the positive-ion MALDI mass spectrum corresponds to a single, intact peptide that is singly protonated, $[M+H]^+$. There may also be other peaks in the mass spectrum resulting from adducts of the same peptide with alkali metal ions. For example, in positive-ion mode, a peptide (M) may be ionized by either a proton [M+H]⁺ or by a sodium ion [M+Na]⁺, yielding two peaks in the mass spectrum. The abundance of sodium adducts can usually be reduced by sample desalting prior to conventional MS analysis.

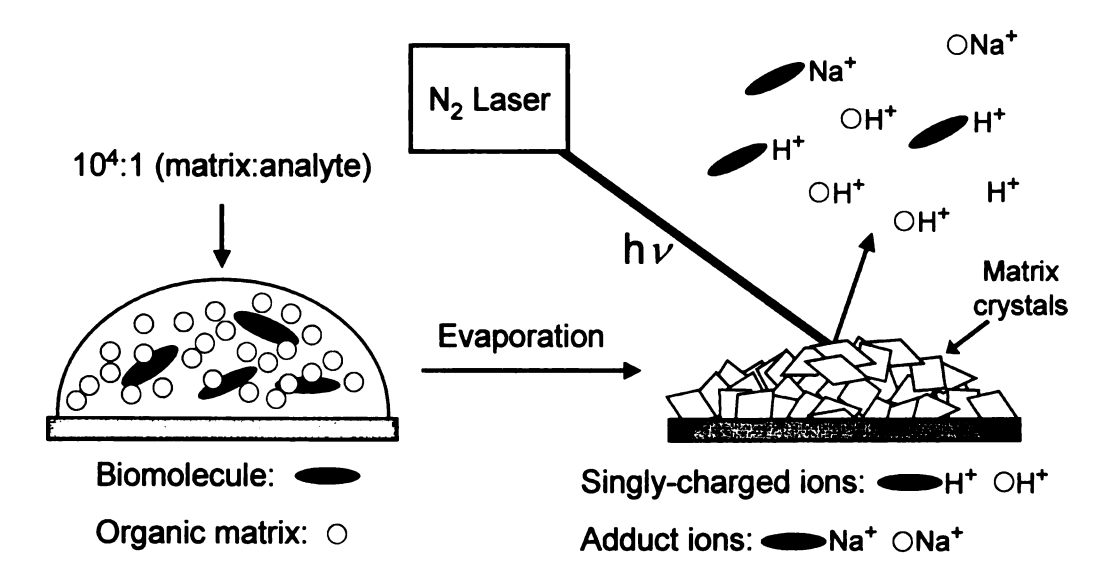


Figure 1.6: Schematic diagram of MALDI sample preparation and analysis. After deposition of the analyte and matrix solution onto the MALDI plate, the solvent evaporates, co-crystallizing the matrix with the analyte.

1.3.2.2 Mass Analyzers Compatible with MALDI

1.3.2.2.1 Time-of-Flight Mass Spectrometer

Since the introduction of time-of-flight (TOF) mass analyzers between 1940 and 1950, substantial developments involving improved resolution due to time-lag focusing using delayed extraction and reflectron modes have been made. A schematic of an axial TOF mass spectrometer is shown in Figure 1.7.

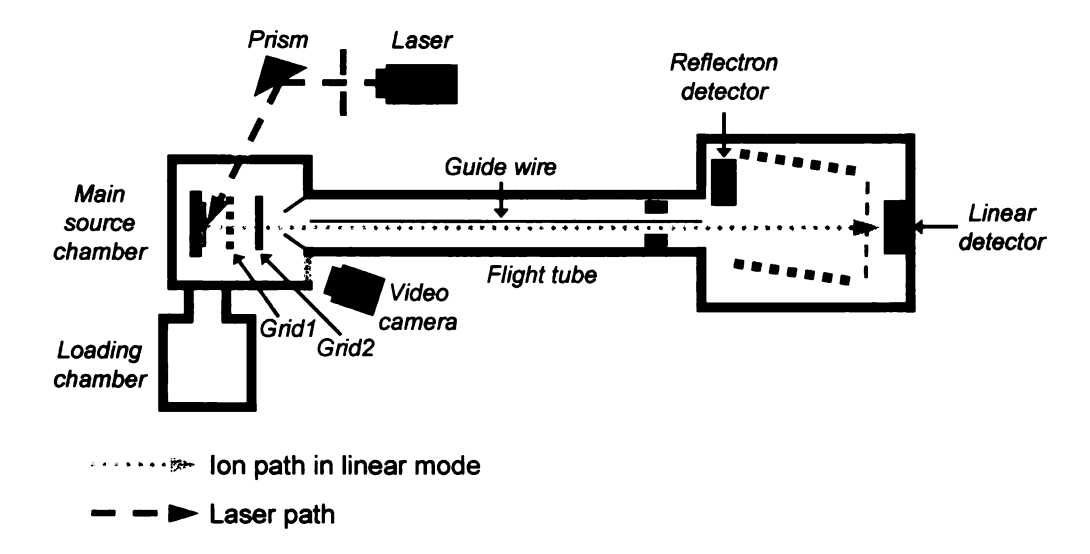


Figure 1.7: Schematic diagram of a MALDI time-of-flight mass spectrometer with linear- and reflectron-mode capabilities. The ion path is shown for linear-mode TOF-MS.

After the sample plate is inserted into the instrument, the pulsed laser with a typical wavelength of 337 nm is fired, and the peptides are desorbed/ionized. A burst of ions forms, and these are held between the sample plate and the variable-voltage grid for a short duration (\sim 100-200 ns) before the ions are accelerated. This delayed extraction parameter limits the spatial distribution of the ions. The guide wire voltage is 0.05% in magnitude of the accelerating voltage and helps to guide or refocus the ions down the flight tube to prevent collisions with the wall. As the ions travel through the field-free flight tube, they are separated based on their m/z values, hence, the heaviest ions travel the slowest and will reach the detector last as indicated by Equations 1.1-1.3.

Equation 1.1:
$$E_k = \frac{1}{2} \text{ mv}^2 = zeV$$

Equation 1.2: $v = d/t$

Equation 1.3: $t = (md/2zeV)^{1/2}$

Equations 1.1 and 1.2 are used to derive Equation 1.3. Equation 1.1 states that the ion's kinetic energey (E_k) is proportional to its mass (m) and the square of its velocity (v), or alternatively the product of ion charge in coulombs (ze; $e = 1.6 \times 10^{-19} \text{ C}$) and the accelerating voltage (V). The ion's velocity is equal to distance traveled (d) divided by the ion's flight time (t), so d/t can be substituted for v to give Equation 1.3. According to Equation 1.3, an ion's flight time is proportional to the mass-to-charge (m/z). This simply means that an ion with the smallest m/z value will have the smallest flight time, so it will reach the detector first and vice versa for the ion with the largest m/z value. The length of the flight tube is typically about 1 to 2 m and is limited by the ion's mean free path (the distance an ion can travel without colliding with another ion) with a vacuum pressure of 1.2 x 10⁻⁷ Torr. One of the main advantages of the MALDI-TOF instrument is that collection of mass spectra is very rapid (Calculation 1.1 shows an estimated flight time of an ion with m/z 4000 in a 2 m flight tube with an accelerating voltage of 20 kV is ~50 us), making this a high-throughput technique. It takes less than a minute to acquire an average spectrum where several spectra are accumulated and averaged to increase signal to noise ratio (S/N). Additionally, the mass range of TOF is in principle unlimited. Karas et al. demonstrated that a protein with a molecular weight of over 300 kDa can be analyzed.25

Calculation 1.1:
$$t = (md/2zeV)^{1/2}$$

$$t = \frac{\left[(4000 \text{ g/mol})(1 \text{ kg/}1000 \text{ g})(1 \text{ mol/}6.02 \text{ x } 10^{23} \text{ molecules})(2 \text{ m})}{2(1)(1.6 \text{ x } 10^{-19} \text{ C})(20,000 \text{ V})} \right]^{1/2}$$

$$t = 50 \text{ } \mu\text{s}$$

We initially utilized the Applied Biosystems Voyager delayed-extraction STR (reflectron capability) mass spectrometer for the analysis of phosphopeptides and

proteolytic digests. Typically, we acquired the mass spectra in positive-ion, linear mode instead of using negative-ion or reflectron modes because the sensitivity and the S/N were best under these conditions. The use of the reflectron mode corrects for the initial kinetic energy distribution, leading to improved resolution and mass accuracy, but the reflectron mode phosphopeptide signals are often low due to metastable ion fragmentation.²⁶ Metastable ion fragmentation occurs in the TOF drift region, so the metastable ions will have the same kinetic energy as their precursor ion. Thus, the metastable and precursor ions will arrive at the linear detector simultaneously, and signal will be preserved in spite of fragmentation. However, if the ions pass through an electric field (i.e. reflectron region), then the metastable and precursor ions will be separated and these ions will be observed in the mass spectrum at their corresponding m/z values. The phosphate groups on serine and threonine residues are especially labile and undergo βelimination, resulting in decreased signal from the intact phosphopeptide ion in reflectron mode. Typically, metastable fragmentation is due to the loss of phosphoric acid (-H₃PO₄, -98 Da) from phosphorylated serine and threonine residues.²⁷ However, similar fragmentation can also occur for phosphotyrosine-containing peptides (loss of 80 Da due to HPO₃), but less frequently since these residues are more stable.²⁷ In spite of lower signals, post-source decay (PSD) MS (section 1.3.2.4) can be used to characterize phosphopeptides based on mass losses of 98 and 80 Da.²⁷

1.3.2.2.2 Linear Ion Trap Mass Spectrometer

The Nobel prize was awarded to Wolfgang Paul in 1989 for the invention of the quadrupole ion trap (QIT), which is also known as the Paul trap. In 1993, the coupling

of MALDI with the quadrupole ion trap (QIT) mass analyzer was accomplished independently by the research groups of Yates and Bier. ^{28,29} Linear ion trap (LIT) mass analyzers are similar to three-dimensional (3-D) QITs, but only take into account the ion-trapping fields of the two-dimensional (x-y plane) quadrupole. ³⁰ Hence linear ion traps are also known as two-dimensional (2-D) traps. The motion of positive ions in oscillating electric fields in the x and y directions can be described by Equations 1.4-1.7, where $\xi = \Omega t/2$, m = mass, e = electric charge, U_{DC} is the magnitude of the DC voltage, V_{RF} is the RF amplitude (ramped from zero to 10 kV), $\Omega = v2\pi$, which is the applied RF frequency (v = 1.2 MHz), and r_0 is the distance from the middle of the trap to the exit ($r_0 = 4.12 \text{ mm}$). ³⁰⁻³² The positive-ion LIT stability diagram, plotted a_x versus q_x , ³² is shown in Figure 1.8. The mass scan line is determined by the a-q stability diagram, ³² and for the LIT, when U_{DC} is equal to zero, a_x is zero according to Equation 1.6. Thus, ions in the linear ion trap are stable when q_x is less than 0.908.

Equation 1.4:
$$\frac{d^{2}x}{d\xi^{2}} + (a_{x} - 2q_{x}\cos 2\xi) = 0$$
Equation 1.5:
$$\frac{d^{2}y}{d\xi^{2}} + (a_{y} - 2q_{y}\cos 2\xi) = 0$$
Equation 1.6:
$$a_{x} = \frac{8eU_{DC}}{mr_{0}^{2}\Omega^{2}}$$
Equation 1.7:
$$q_{x} = \frac{4eV_{RF}}{mr_{0}^{2}\Omega^{2}}$$

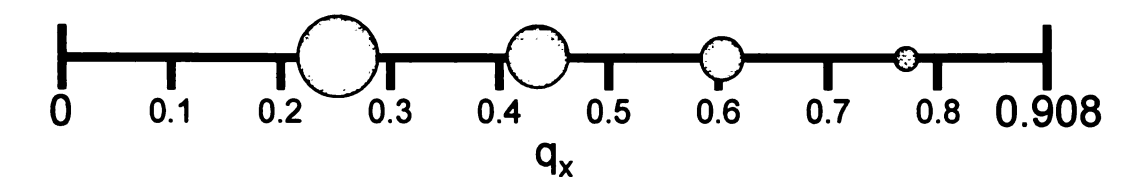


Figure 1.8: Mass scan line for the linear ion trap. U_{DC} is zero, hence, a_x is zero. Grey circles are the ions in the stable region, and the relative size of the circle corresponds to the relative size of the m/z value. See Douglas et al. for a-q stability diagram.³²

In 1969, the first LIT was developed,³³ and Thermo was the first company to file a patent on this new instrumentation in 1994.³⁰ The main advantage of the LIT over a QIT is that the 2-D trap can contain a larger volume of ions and the sensitivity is greater (i.e. lower detection limit) due to a higher trapping efficiency. It was estimated that the sensitivity should be at least 6 times greater than that of the traditional 3-D QIT.³⁴

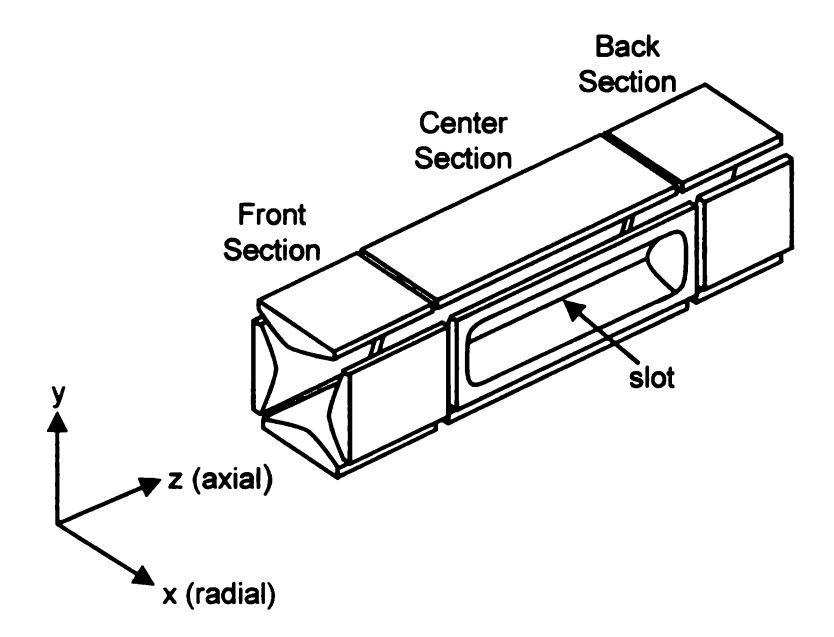


Figure 1.9: General schematic of the Thermo 2-D linear ion trap. Ions are trapped in the center section and the front and back sections reduce distortion of the electric field of the center section, thus, the ion trapping efficiency is improved. Ions are radially (x direction) ejected from the center section through the slot (0.25 mm x 30 mm) of two exit rods. Figure is redrawn from the Thermo LTQ XL instrument manual.

A diagram of the Thermo 2-D linear ion trap is shown in Figure 1.9. The trap is made up of four parallel hyperbolic-shaped rods, which are segmented into three sections to avoid unintended axial ejection due to distortion of the electric field at the front and back lenses.³¹ Positive ions are focused into the 2-D trap in the z direction using DC voltages, and subsequently axially (z direction) trapped in the center section. The ions are also stabilized radially (x, y-direction) by an RF electric field, producing a 2-D quadrupole field. A supplemental AC voltage is applied to the x rods for isolation, activation, and ejection of the ions.³¹ Ions are radially ejected from the trap through the two slots (0.25 x 30 mm) in the exit rods using a resonance voltage. Radial (x direction) ion ejection is efficient, and dual detectors (see Figure 1.10) allow for most of the ions to be detected, leading to increased sensitivity.

Tandem MS can be easily performed using the linear ion trap and consists of isolation, excitation, and ejection. To perform a tandem MS (MS^2) experiment, a precursor ion for a particular m/z value is first isolated in the trap while the other ions are ejected. Next, a resonance excitation AC voltage is applied, giving the precursor ion enough kinetic energy to collide with the helium collision gas, causing it to internally fragment. Finally, the product ions are ejected by ramping the main RF voltage from low to high voltage and simultaneously applying the resonance ejection AC voltage to the exit rods at a constant frequency while increasing amplitude.

The continue that we that he extra the first of the set of the set of the

In our recent experiments, we utilized a Thermo vMALDI LTQ XL instrument, which contains a linear ion trap. A schematic of the vMALDI LTQ instrument is shown in Figure 1.10. The vMALDI (v stands for vacuum) source houses the sample plate, a fiber optic cable directing the N₂ laser, a camera, and a modified quadrupole (Q00). The

vMALDI source is operated at 170 mTorr, which is a much higher pressure than that of the MALDI source on the axial TOF mass spectrometer (PerSeptive Biosystems Voyager STR), but lower than that of an atmospheric pressure MALDI source. The diagram shows the N_2 laser (337 nm) irradiating the sample at an incident angle of ~30°, and the typical laser spot diameter for this instrument is 80-120 µm. 35,36 Following the vMALDI source is the Rf quadrupole (Q0) and octapole (Q1), which guide the ions into the linear ion trap. The Q00 quadrupole increases the translational kinetic energy of the ions, and the Q0 quadrupole imparts a downhill potential gradient to help guide the ions. Similar to quadrupole Q00, the octapole Q1 increases the translation kinetic energy of the ions. Inside the linear ion trap is a bath gas of helium (10⁻³ Torr), which is used as the ion damping gas (i.e. energetically slows the ions down) as well as the collision gas for collision-induced dissociation (CID) experiments. The upper m/z limit for the Thermo vMALDI LTQ XL instrument is 4000 and is determined based on r₀ (4.12 mm), v (1.2 mHz), and a maximum V_{RF} (10 kV) as shown in Calculation 1.2. Thus, digestion of proteins prior to analysis by MALDI-MS is required. In all of our experiments we utilized this "bottom-up" approach to analyze phosphoproteins.

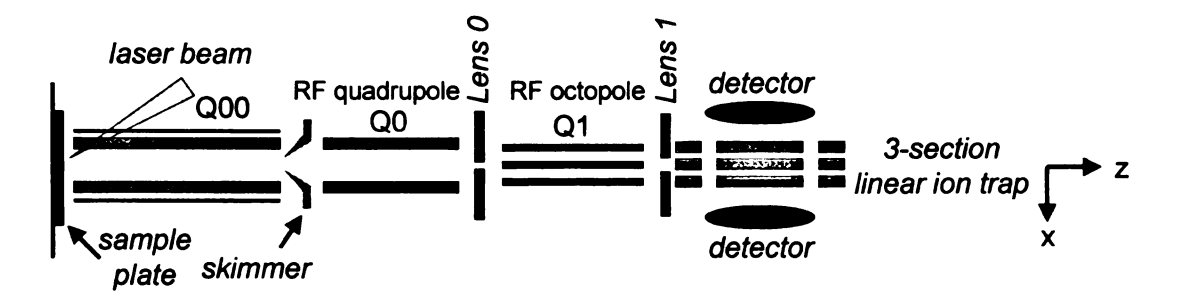


Figure 1.10: Schematic diagram of the Thermo vMALDI LTQ XL instrument. Figure redrawn from Garrett et al.³⁶

Calculation 1.2:
$$m_{max} = \frac{4eV_{RFmax}}{q_x r_0^2 (v2\pi)^2}$$

$$m_{max} = \frac{4(1.6x10^{-19} \text{ C})(10,000 \text{ V})}{0.908(0.00412 \text{ m})^2 [1.2 \text{ x} 10^6 \text{ Hz} (2\pi)]^2} = 7.8 \text{ x} 10^{-24} \text{ kg/molecule}$$

$$m_{max} = 7.8 \text{ x} 10^{-24} \text{ kg/molecule} (6.02 \text{ x} 10^{23} \text{ molecule/mol})(1000g/kg)$$

$$m_{max} = 4,400 \text{ g/mol}$$

1.3.2.3 Identification of Phosphopeptides Using Chemical Methods and Subsequent Analysis by MALDI-MS

Several chemical methods have been employed to remove or replace phosphate groups in order to facilitate identification of phosphorylation by MS. The use of phosphatase to dephosphorylate peptides prior to analysis by MALDI-MS, for example, has previously been used to identify phosphopeptides.³⁷ Comparison of mass spectra before and after treatments allows identification of phosphorylated peptides by specific changes in m/z values (i.e. loss of HPO₃ would result in a new signal 80 m/z units lower than in the untreated sample). Additionally, β-elimination can be used under strongly alkaline conditions to remove the phosphate group of phosphoserine and phosphothreonine-containing peptides,³⁸ and then the peptide is reacted with a nucleophile such as ethanedithiol to yield an S-ethyl cysteine derivative (Michael Addition) (Figure 1.11).³⁸ β-elimination is not applicable to phosphotyrosine-containing peptides. Additionally, O-glycosidic linkages present due to glycosylation, another posttranslational modification, can also undergo β-elimination.²⁴ Another approach has relied on chemical affinity tags to enrich the phosphoprotein/phosphopeptide sample prior to MS analysis, and this method will be discussed further in section 1.4.2.3.

(a)
$$O=P-OH$$

$$O=P-OH$$

$$O=P-OH$$

$$O=P-OH$$

$$O+D$$

Figure 1.11: β-Elimination of (a) phosphoserine and (b) phosphothreonine, forming dehydroalanine and dehydroaminobutyric acid, respectively, which are subsequently reacted with ethanedithiol (Michael addition).

1.3.2.4 Identification of Phosphopeptides Using Post Source Decay and Tandem Mass Spectrometry

Mass spectrometry such as post-source decay (PSD) and tandem mass spectrometry have also been used to characterize phosphopeptides. These approaches typically use a characteristic neutral loss to identify phosphopeptides. Due to metastable fragmentation (ions fragment in the time-of-flight tube, after they have been accelerated, and will reach the detector at the same time as their precursor ion), PSD can be used in reflectron mode TOF to characterize phosphoserine and phosphothreonine peptides by monitoring the neutral loss of H₃PO₄.²⁷ Reflectron mode separates metastable ions from precursor ions by using an applied electric field. If the peptide contains more than one phosphate, then multiple losses of H₃PO₄ will be observed in the mass spectrum. The

PSD fragmentation of phosphotyrosine-containing peptides will show a loss of HPO₃ (-80 Da from the precursor ion) in the positive-ion mass spectrum.²⁷ Collision-induced dissociation (CID) tandem MS can be used in ion traps to monitor similar neutral losses in positive-ion mode as well as product ions at m/z 79 (PO₃⁻) and m/z 89 (H₂PO₄⁻) in negative-ion mode.²⁴ Occasionally, CID MS/MS signals due to [M+H-H₃PO₄]⁺ are low due to competing fragmentation pathways that involve water loss [M+H-H₂O]⁺, but this can be overcome by using wideband activation of the precursor ion. Wideband activation works by applying resonance excitation energy to the selected phosphopeptide precursor ion as well as to any product ions 20 m/z units below the precursor ion, i.e. [M+H-H₂O]⁺, giving rise to a peak due to [M+H-H₂O-H₃PO₄]⁺ with a neutral loss of 116 Da.

Since the presence of phosphate groups on peptides hinders the fragmentation of the peptide backbone using CID, often there are few product ions that give sequence information. Typically, when a protonated nonphosphorylated peptide (precursor ion) is fragmented using low energy CID, the most frequent product ions formed are the $b_{(n\geq 2)}$ and y_n type (b_1 type ions are unstable unless the N-terminal amino acid is lysine, histidine, or methionine) due to the amide bond cleavage along the peptide backbone (Figure 1.12). These types of ions are used to sequence the peptide since each sequential amide bond cleavage corresponds to the loss of an amino acid residue. However, as mentioned above for phosphorylated peptides other fragmentation pathways such as loss of H_3PO_4 may dominate, so MS^3 may be required to obtain sequence ions.

the first temperature for the control of the state of the control of the control

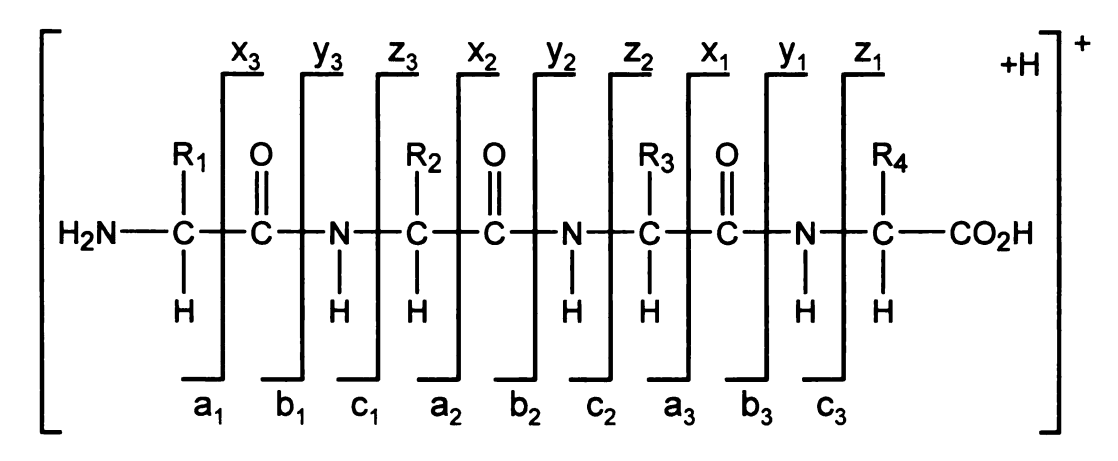


Figure 1.12: Cleavage of a tripeptide backbone shows the x, y, and z ions and the a, b, and c ions. The most common sequence ions are the y and b type.

1.3.2.5 Challenges in Phosphopeptide Detection by Mass Spectrometry

There are several challenges when detecting phosphopeptides by MS. In general, the amount of phosphorylated protein in eukaryotic cells and the degree of phosphorylation are relatively low, which makes detecting phosphopeptides challenging by any technique. Phosphorylated tyrosine residues are the least abundant among the phosphorylated residues (ratio of pS:pT:pY is 1800:200:1), which presents further difficulties in detecting phosphotytrosine sites. Additionally, it has bee reported that phosphopeptides are difficult to detect by MS in the presence of nonphosphorylated species. The MALDI-MS, this suppression effect is because desorption/ionization efficiencies for phosphopeptides are roughly an order of magnitude lower than those for their nonphosphorylated counterparts, and ionization of phosphorylated peptides becomes more difficult as the number of phosphorylation sites increases. However, there is recent literature that suggests phosphorylated peptides are not difficult to detect over nonphosphorylated peptides.

1.4. Enhancement or Enrichment Techniques for the Analysis of Phosphopeptides

As mentioned above mass spectrometric analysis of phosphoproteins is difficult because of their low abundance. Below we describe new matrix formulations that are used to help increase MS signals due to phosphorylated species as well as enrichment techniques aimed at overcoming the low abundance of these species.

1.4.1 Matrices and Additives for MALDI-MS

1.4.1.1 Use of Ammonium Salts to Enhance Phosphopeptide Detection

One method used to increase MS signals of phosphopeptides over nonphosphopeptides was the addition of ammonium salts to the matrix. In 1999, Asara and Allison introduced diammonium hydrogen citrate (DAHC) and ammonium acetate to the MALDI matrix for enhanced detection of phosphorylated peptides using positive-ion mode MALDI-TOF-MS.⁴² Specifically, they examined the utility of DAHC and 2,5-DHB to increase the relative signals of multiply phosphorylated peptides associated with an incomplete β-casein digest. The incorporation of DAHC generated a mass spectrum where the most intense peaks corresponded to two miscleaved, tetraphosphorylated peptides (average m/z 3124 and 3479) while the signals for the nonphosphorylated peptides were significantly reduced when compared to the conventional MALDI-MS analysis of the β-casein digest. The authors' explanation for this effect was that the citrate is effective at "capturing" the sodium ions, precipitating as sodium citrate, which leaves the ammonium ions to form a precipitate with the phosphate of the phosphorylated peptide. Simply put, the use of ammonium salts reduce alkali metal ion adduction, thus, alleviating suppression of phosphopeptide signals.

Control of the Colombia Control of the Control of t

1.4.1.2 Enhanced Ionization of Phosphopeptides Using 2',4',6'-Trihydroxyacetophenone as a Matrix

In 2004, Yang et al. introduced DAHC with 2',4',6'-trihydroxyacetophenone (THAP) as an alternative matrix to 2,5-DHB or α -CHCA for the analysis of phosphopeptides. However, the goal of their research was to enhance phosphopeptide signals in positive-ion mode MALDI-TOF-MS while maintaining signals due to nonphosphorylated peptides, so both species could be analyzed. When THAP with DAHC was used as a matrix instead of α -CHCA with DAHC, the peak intensities of the mono- and tetraphosphorylated peptides (m/z 2062 and 3122) increased by 10-fold while the signals due to nonphosphorylated peptides were approximately the same as when the α -CHCA matrix was used. However, the β -casein digest was purified using Millipore ZipTip C18 pipette tips prior to analysis. It would be interesting to see results from unpurified digest.

1.4.1.3 Phosphoric Acid as a Matrix Additive for Analysis of Phosphopeptides

In 2004, Kjellström and Jensen demonstrated the use of phosphoric acid, after examining five acids (acetic acid, formic acid, trifluoroacetic acid, heptafluorobutyric acid, and phosphoric acid), as a suitable matrix additive to enhance phosphopeptide signals in MALDI-TOF-MS. They utilized 2,5-DHB as a matrix for their studies since it is considered a "cool" matrix (i.e. little, if any, fragmentation of peptides results) and compared the use of phosphoric acid in positive-ion and negative-ion modes. In both ionization modes, when 200 fmol of α -casein was analyzed, the use of phosphoric acid in the matrix solution yielded increased signals from all four observed phosphopeptides.

Interestingly, the signal intensities of the phosphopeptides were stronger relative to nonphosphorylated signals in negative-ion mode, but the absolute intensities of phosphopeptide signals were stronger when using positive-ion mode, which has been observed previously. The authors also analyzed 100 fmol of β -casein digest using positive-ion mode and found that the ionization of the tetraphosphorylated peptide was enhanced in the presence of phosphoric acid. This peptide was not detected when TFA, rather than phosphoric acid, was used in the matrix solution. The authors suggest that the phosphoric acid-enhanced detection of phosphorylated peptides is due to a "salting out" effect, as PO_4^{3-} is known to be the best anion for precipitating proteins.

1.4.2 Affinity Chromatography

1.4.2.1 Background

Shortly after the introduction of liquid chromatography (LC), affinity chromatography was launched by Starkenstein in 1910 when an enzyme was bound to insoluble starch.⁴⁷ However, it was not until 1936 that Landsteiner and van der Scheer covalently bonded an affinity ligand, hapten, to a support material for antibody purification by immobilized affinity chromatography (IAC).⁴⁷ Affinity chromatography differs from conventional LC in that it employs stronger and more specific interactions that provide higher retention and selectivity than is found in typical LC.

Affinity ligands can be classified as either 1) high-specificity ligands, which bind one or a few closely related target species, or 2) group-specific ligands, which bind a larger group of related species.⁴⁷ High-specificity ligands include antibodies or enzyme inhibitors, while group-specific ligands include immunoglobulin-binding proteins,

boronates, synthetic dyes, and metal-ion complexes. Hence, affinity chromatography is comprised of several subsets, including bioaffinity, immunoaffinity, DNA affinity, boronate affinity, dye-ligand affinity, biomimetic affinity, and immobilized metal affinity chromatography. An extensive discussion on these affinity techniques can be found in the "Handbook of Affinity Chromatography."

Immunoprecipitation is related to affinity chromatography and it has been used towards the purification of phosphorylated proteins, so its application will be discussed in section 1.4.2.2 below. Additionally, immobilized avidin affinity chromatography and immobilized metal affinity chromatography will be discussed in sections 1.4.2.3 and 1.4.2.4, respectively, because these IAC methods can be used for the enrichment of phosphoproteins or phosphopeptides.

1.4.2.2 Immunoprecipitation of Phosphoproteins Using Phospho-specific Antibodies

Immunoprecipitation utilizes antibodies to form insoluble complexes with the antigen. ⁴⁷ In the case of phosphorylated proteins, this technique is predominantly limited to phosphorylated tyrosine-containing proteins, and there are several commercial antibodies that bind these proteins. It should be noted that these antibodies are not effective in precipitating phosphopeptides, and a study by Marcus et al. showed that the yield of immunoprecipiated tyrosine-phosphopeptides was a mere 2%. ⁴⁸ In 2002, Grønborg and coworkers demonstrated that anti-phosphoserine and antiphosphothreonine antibodies could be used to enrich proteins with phosphoserine and phosphothreonine residues, respectively. ⁴⁹ However, the specificity of these antibodies is limiting.

1.4.2.3 Immobilized Avidin Affinity Chromatography for Phosphopeptides

In 2001, Oda et al. demonstrated the use of avidin affinity chromatography for the purification of phosphoserine and phosphothreonine proteins or peptides prior to MS.⁵⁰ The chemical modification of the phosphorylated proteins/peptides is depicted in Figure 1.13. Oxidation of cysteine residues is followed by \(\beta\)-elimination of the phosphorylated serine or threonine residues, which is carried out under strongly alkaline conditions. This yields α,β-unsaturated dehydroalanine or dehydroaminobutyric acid residues, and these readily react with 1,2-ethanedithiol, a nucleophile, leaving a free sulfhydryl group to react with a maleimide-terminated biotinylated affinity tag. The proteins are digested using trypsin, and the tagged peptides are then captured on a column containing beads with immobilized avidin. The interaction between avidin and biotin is one of the strongest noncovalent interactions known, with an association constant of 1.6 x 10¹³ M⁻ Moreover, the binding is reversible and once the column has been rinsed, the immobilized biomolecules can be eluted with free biotin (5 mM). The eluted biotinlabeled protein is subsequently digested with trypsin and the tryptic fragments containing the biotin label are purified using another avidin column. Oda et al. applied this method towards the analysis of phosphopeptides from β -casein and ovalbumin digests (0.05 – 1 mg).⁵⁰ The B-casein phosphoprotein was isolated from a mixture of 6 proteins using biotin labeling and avidin affinity chromatography, and the β-casein recovery was about 90%. After digestion and further avidin purification, one β-casein monophosphorylated peptide dominated the mass spectrum. This IAC technique was also applied towards the recovery of ovalbumin phosphopeptides from a whole-cell yeast extract containing 2

wt% ovalbumin. Three phosphorylated peptides were recovered, while signals due to nonphosphorylated peptides were minimal.

Figure 1.13: Labeling of a phosphopeptide with biotin and capture of this peptide using avidin immobilized on beads. Figure adapted from Oda et al.⁵⁰

Adamczyk et al. utilized a similar procedure that employed a biotin derivative (N-[6-(biotinamido)hexyl]-3'-(2'-pyridyldithio)propionamide, Biotin-HPDP), which contains a free thiol group.⁵¹ The protocol (Figure 1.14) that was used is as follows: 1) β-elimination of the phosphorylated serine and threonine residues of the protein, 2) reaction with 1,2-ethanedithiol (EDT), 3) formation of a disulfide bond between Biotin-HPDP and the thiol-derivatized protein, 4) tryptic digestion of the protein, 5) immobilization of the biotin-labeled peptides to an avidin column, 6) removal of non-biotinylated peptides, and 7) cleavage of the disulfide bond using a reducing agent (i.e. DTT) to release the bound peptides. At this point Biotin-HPDP is still bound to the

avidin column and the freed peptides contain only the EDT label. Using this technique, 8 phosphopeptides from a digest mixture of α -casein (20 μ g), β -casein (10 μ g), and ovalbumin (20 μ g) were detected. Moreover, the EDT label could be used to identify the location of the phosphorylation site using CID MS/MS.

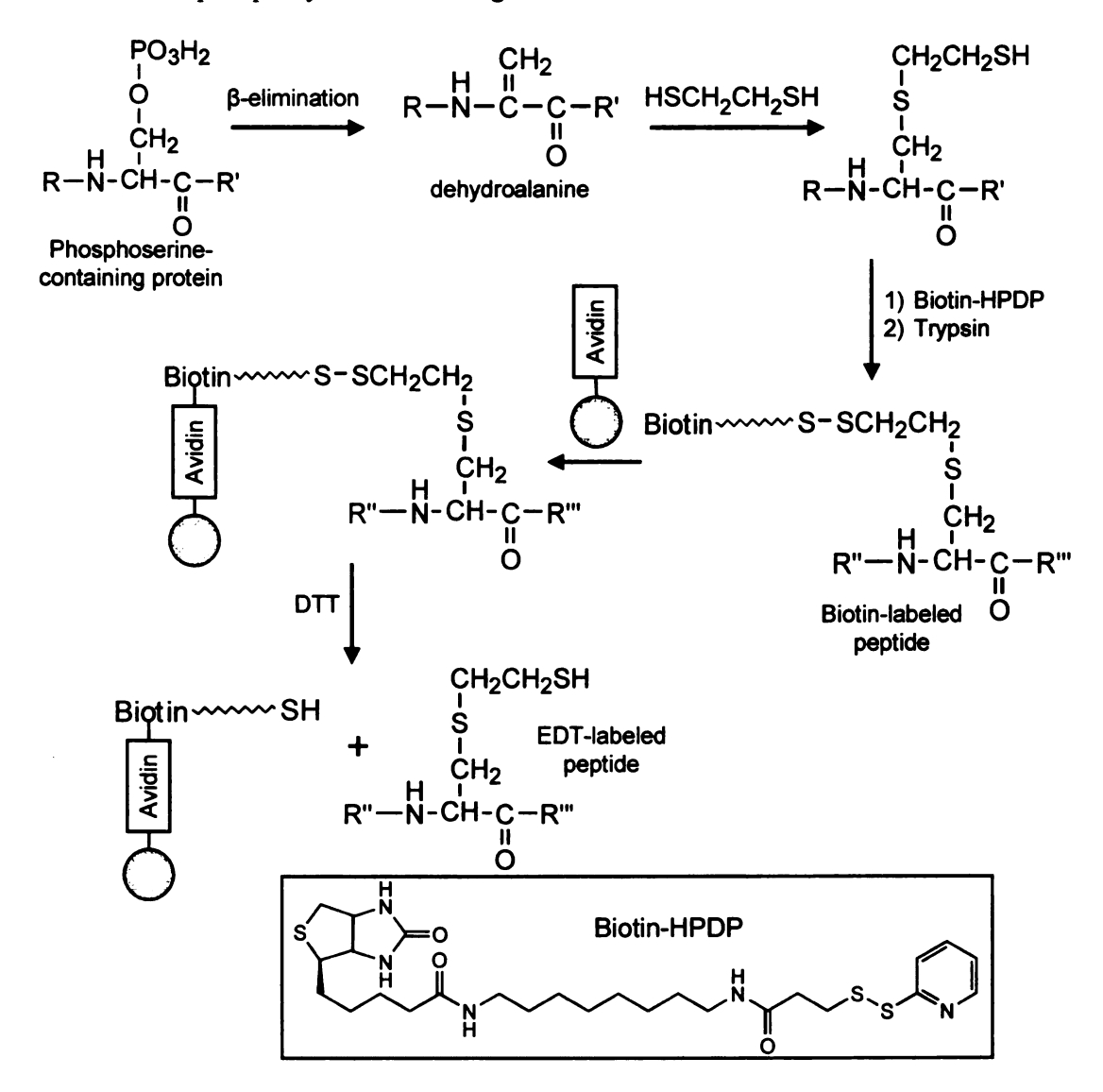


Figure 1.14: Labeling of a phosphopeptide with biotin and capture of this peptide using avidin immobilized on beads. Figure adapted from Adamczyk et al.⁵¹

In 2002, Goshe et al. utilized deuterated EDT and iodoacetyl-terminated biotin to incorporate phosphoprotein isotope affinity tags into β -casein (Figure 1.15).⁵² The

tagged phosphoproteins were digested and the labeled peptides were captured on an avidin column. After rinsing the column to remove unbound peptides, the captured peptides were subsequently eluted using TFA (30% acetonitrile/0.4% TFA) and further analyzed using liquid chromatography MS. This technique detected a single monophosphopeptide from β -casein and 2 phosphopeptides from α -casein impurities. Additonally, the isotope tag allowed identification of the phosphorylation site using CID MS/MS. The incorporation of the isotope tags demonstrated that quantitation of phosphoproteins by comparing tagging with isotopic and nonisotopic labels would be possible if a high resolution mass spectrometer (TOF or FTICR) was implemented.

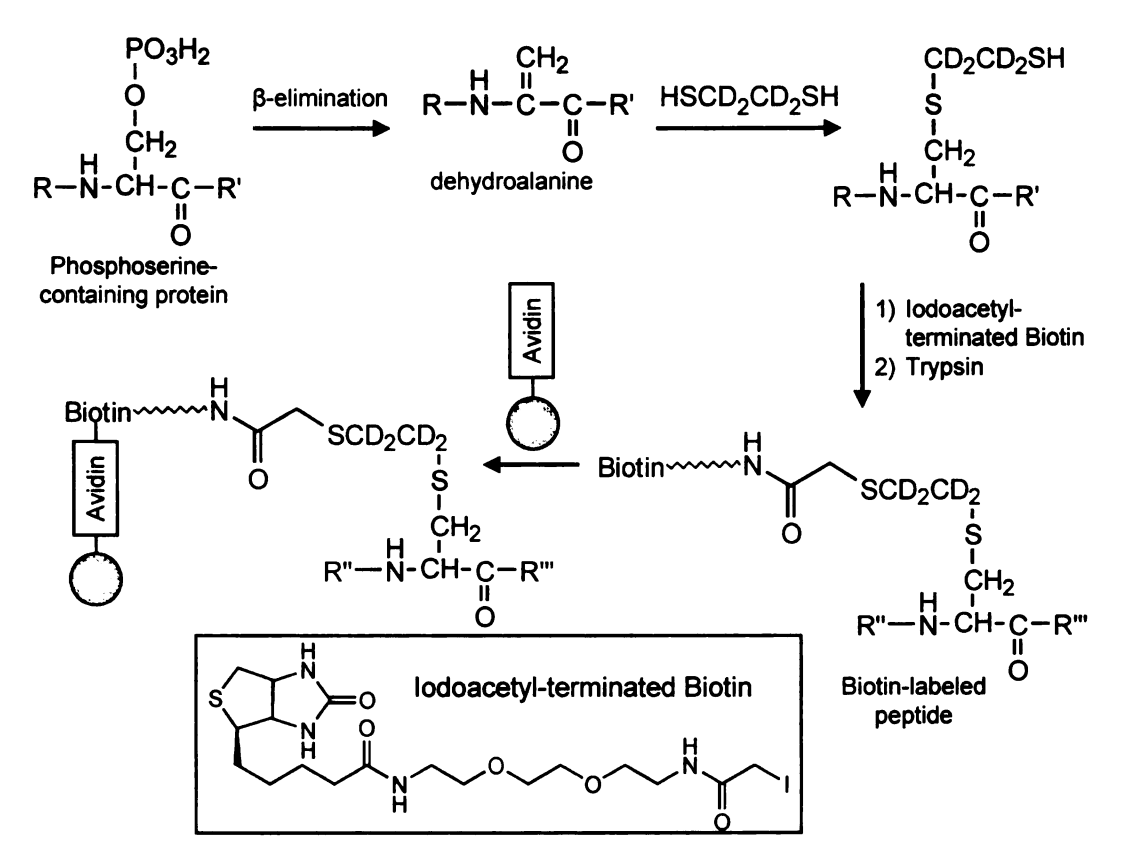


Figure 1.15: Labeling of a phosphopeptide with biotin and capture of this peptide using avidin immobilized on beads. Figure adapted from Goshe et al.⁵²

1.4.2.4 Immobilized Metal Affinity Chromatography for Phosphopeptide Purification

Immobilized metal affinity chromatography (IMAC) is a type of IAC that relies on the interactions between metal-ligand complexes and specific functional groups such as phosphates. Although less specific than other affinity methods, the lower specificity of IMAC makes it applicable to a wide range of separations. Introduced in 1975 by Porath, ⁵³ IMAC is currently the most common method used to enrich phosphopeptides prior to analysis by MS.

The most common ligands employed in IMAC are iminodiacetate (IDA) and nitrilotriacetate (NTA), which are shown in Figure 1.16. NTA was introduced in 1987 by Hochuli, ⁵⁴ and Fe(III)-NTA complexes are among the most popular metal ion complexes for enriching phosphopeptides. However, other metal ions have been investigated for their affinity towards phosphorylated peptides, including hard metal ions such as Ga(III) and Zr(IV). ⁵⁵, ⁵⁶ IDA is a tridentate ligand whereas NTA is a tetradentate ligand, hence, the latter should bind more strongly to the metal ion to better prevent leaching. For this reason, we chose to immobilize Fe(III)-NTA complexes on our polymer substrates. Typical metal affinity resins are fairly inexpensive (\$60 for 5 mL of iminodiacetic acid-sepharose resin from Aldrich).

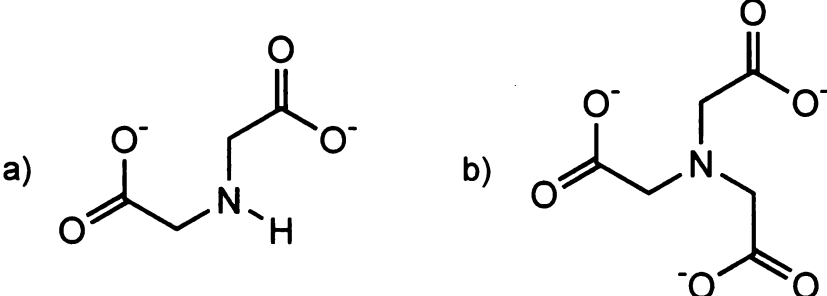


Figure 1.16: Structures of a) IDA and b) NTA.

There are several challenges that are associated with using IMAC. Since the metal ions are not covalently bound to the substrate, there is a possibility for these ions to be leached out of the column during the enrichment steps, leading to loss of phosphopeptides or contamination of peptides with metal ions. However, thorough washing of the substrate before use and judicial choice of binding ligands can minimize these problems.

A second challenge is nonspecific binding of peptides containing the acidic residues, glutamic and aspartic acid. To overcome this problem, the carboxyl groups of amino acid residues can be methyl esterified as demonstrated by Ficarro et al.⁵⁷ Peptides are typically esterified by reaction with acetyl chloride in an excess of methanol (methanolic HCl), as shown in Figure 1.17. More recently (2006), thionyl chloride (SOCl₂) has been used instead of acetyl chloride for the methyl esterification of phosphopeptides. 58.59 This reagent showed a higher efficiency for the conversion of carboxylic acid groups to methyl esters than did methanolic HCl. Increasing the ionic strength of the buffer or rinse solution can also help minimize electrostatic interactions between acidic residues and metal-ion complexes. Seeley et al. showed a reduction in non-specific binding to Ga(III)-IMAC resin by using the endoproteinase Glu-C instead of trypsin during digestion.⁶⁰ Glu-C cleaves the protein at the C-terminus of glutamic and aspartic acid residues; hence, only one acidic residue will be present in the peptide chains, thus alleviating nonspecific binding to due to interactions between IMAC resins and multiple acidic residues.

(a)
$$CH_3-OH$$
 + H_3C CI H_3C OCH_3 + HCI OCH_3 + HCI OCH_3 + H_2O OCH_3 OCH_3 + OCH_3 OCH_3 + OCH_3 + OCH_3 OCH_3 + OCH_3

Figure 1.17: Methyl esterification of carboxylic acid groups in the peptide using acetyl chloride and an excess of methanol: a) reaction shows generation of HCl and b) reaction shows the acid-catalyzed methyl esterification of the carboxylic acid groups.

Another challenge that has been reported in the use of IMAC is that the technique is more specific for multiply phosphorylated peptides than monophosphorylated peptides since multiply phosphorylated peptides are more acidic and bind stronger to the IMAC resin than singly phosphorylated peptides. 57.61.62 However, this probably also depends on IMAC variables such as the affinity ligand, the binding capacity of the support material, and the binding, rinsing, and elution conditions. 63 Recently, Ndassa et al. reported that the use of a high capacity IMAC material in conjuction with an optimized binding and rinsing buffer (33:33:33 acetonitrile/methanol/water with 0.1% acetic acid) led to enhanced phosphopeptide recovery and uniform LC-MS detection of multiply and singly phosphorylated peptides.⁵⁸ (Peptides were methyl esterified.) Reducing the concentration of acetic acid from 1 to 0.1% yielded an increase in the number of phosphorylated peptides detected, and the recovery of phosphorylated peptides from a cell lysate doubled when using 33:33:33 acetonitrile/methanol/water with 0.1% acetic acid instead of 25:75 acetonitrile/water, 1% acetic acid, and 100 mM NaCl as the loading and washing solutions. In other experiments, the use of 100 mM NaCl had the greatest effect on the recoveries of monophosphorylated peptides, which were reduced by half when the NaCl was used. This study also showed that using an IMAC support with a higher capacity allowed for a uniform recovery of singly and multiply phosphorylated peptides. If the IMAC column does not have a large enough capacity for all of the phosphorylated peptides in the mixture, then the multiply phosphorylated peptides will bind preferentially over the monophosphorylated peptides.

Perhaps the most difficult challenge in IMAC is that it can lead to sample loss due to multiple rinsing and elution steps. Typically, commercial IMAC techniques used to enrich phosphopeptides require several steps prior to the MALDI-MS analysis as shown in Figure 1.18. First, the protein digest is purified using reverse-phase chromatography to desalt the sample and remove other reagents that may interfere with phosphopeptide binding to the metal-affinity resin. The purified peptide mixture is then loaded onto the IMAC column, and the nonphosphorylated peptides are rinsed away. Generally, a phosphate buffer is then employed to elute or displace the phosphopeptides from the affinity resin, but this buffer is not compatible with MALDI, so it needs to be removed, again using reverse-phase chromatography. Finally, the enriched phosphopeptide solution is mixed with a matrix on a conventional sample plate, dried, and subsequently analyzed by MALDI-MS.

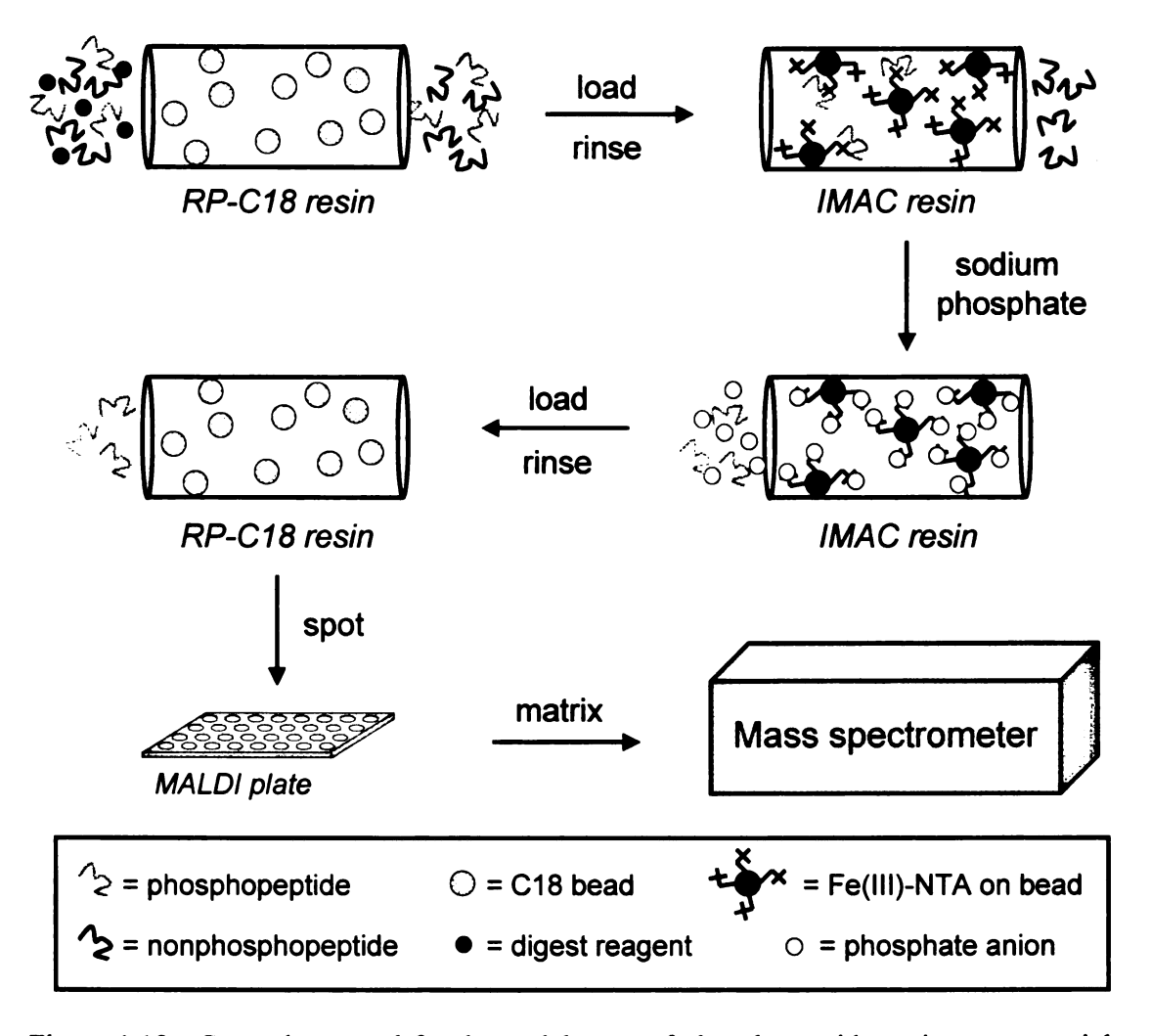


Figure 1.18: General protocol for the enrichment of phosphopeptides using commercial IMAC column packed with Fe(III)-NTA beads. Reverse phase (RP) C18 column is used for sample desalting.

1.4.3 Metal Oxide Affinity Chromatography

1.4.3.1 Titanium Dioxide-based Enrichment

Between 2004 and 2005, the use of TiO₂ resins for the enrichment of phosphorylated peptides was demonstrated by Sano, Pinkse, and Larsen.⁶⁴⁻⁶⁷ At a low pH, this metal oxide has a positively charged surface that selectively adsorbs phosphopeptides and exhibits outstanding enrichment behavior.

Pinkse et al. utilized 2D-nanoLC-ESI-MS/MS and TiO₂ precolumns to analyze a synthetic phosphopeptide as well as proteolytic digests of cGMP-dependent protein kinase. 65 The protocol called for using a phosphopeptide loading solution in 0.1 M acetic acid, a rinsing solution of 0.1 M acetic acid in 80% acetonitrile, and an ammonium bicarbonate eluent (pH 9.0). When an equimolar mixture of of 125 fmol of RKIpSASEF, a synthetic phosphorylated peptide derived from cGMP-dependent protein kinase (PKG), and 125 fmol of its nonphosphorylated counterpart were analyzed using the TiO₂ precolumn, the percent recovery of the RKIpSASEF was above 90%. Additionally, 11 phosphorylated peptides were recovered from the analysis of a PKG tryptic digest. However, nonphosphorylated peptides were also retained on the titanium dioxide precolumn. The authors thought that the acidic nature of these nonphosphorylated peptides caused them to have an affinity for TiO₂ so they compared the affinity of the [Glu¹]-fibrinopeptide of В methylated and non-methylated forms (EGVNDNEEGFFSAR) for titania. Their studies showed that about 98% of the nonmethylated peptide was retained on the TiO₂ precolumn under the phosphopeptide loading and washing procedure, and then eluted under basic conditions. In contrast, the methylated form appeared to have very little affinity for TiO₂.

In other developments with TiO₂, Larsen and coworkers⁶⁴ incorporated 0.1% TFA and 2,5-DHB in the phosphopeptide loading buffer and rinsing solution instead of 0.1 M acetic acid (used by Pinkse et al.⁶⁵). The pH values of 0.1% TFA and 0.1 M acetic acid solutions are 1.9 and 2.7, respectively, hence, the TFA solution was used to promote protonation of acidic residues and prevent adsorption of nonphosphorylated peptides to TiO₂. Moreover, an NH₄OH eluent at pH 10.5 allowed higher recovery of

phosphopeptides (4 additional phosphopeptides were observed from an α-casein digest when using NH₄OH rather than a pH 9.0 ammonium bicarbonate eluent). Remarkably, when they used 2,5-DHB in the binding and rinsing solution and NH₄OH, pH 10.5 as the eluent, they detected 20 phosphorylated peptides in the MALDI-MS spectrum of 500 fmol α-casein digest, while virtually no signals due to nonphosphorylated peptides were observed.⁶⁴ Larsen and coworkers also optimized conditions when they analyzed a more complex digest mixture containing equimolar amounts (500 fmol) of 3 nonphosphorylated proteins (bovine serum albumin, β-lactoglobulin, and carbonic anhydrase) and 3 phosphoproteins (β -casein, α -casein, and ovalbumin). Using enrichment with TiO₂ along with the loading solutions and eluents mentioned above, they were able to recover 18 phosphorylated peptides while the majority of peaks due to nonpshosphorylated peptides were virtually eliminated. After the TiO₂ column, these studies typically used a Poros Oligo R3 microcolumn for sample desalting and concentration. Occasionally, phosphopeptides were not retained on the Oligo material and required further purification using a graphite microcolumn. Larsen and coworkers also examined enrichment with Fe(III)-NTA-IMAC beads (PHOS-selectTM, Sigma) using the mixture of digested proteins described above.⁶⁴ They showed that the performance of their TiO₂ material was better than the IMAC resin with respect to the number of phosphorylated peptides detected and the reduction in nonphosphopeptide signals.⁶⁴ In these experiments, the amount of nonphosphorylated protein digests were 10-fold and 50fold greater than that of the phosphoprotein digests. Larsen et al. also compared the use of MALDI and ESI for phosphopeptide analysis.⁶⁴ They noted that LC-ESI-MS/MS

favored monophosphorylated peptide detection, and multiphosphorylated peptides frequently were not detected⁶⁴ in accord with studies by Gruhler.⁶⁸

In addition to examining 2,5-DHB in loading solution, Larsen and coworkers also studied the competing effects of other acids (some structures are shown in Figure 1.19) on the binding of nonphosphorylated peptides on TiO₂.⁶⁴

Figure 1.19: Structures of 2,5-DHB, salicylic acid, pththalic acid, benzoic acid.

They observed the following order of ability to inhibit nonphosphopeptide binding: 2,5-DHB \sim salicylic acid \sim phthalic acid > benzoic acid \sim cyclohexane carboxylic acid > phosphoric acid > TFA > acetic acid. As noted by the authors, IR spectroscopy showed that substituted aromatic carboxylic acids interact more strongly with TiO₂ than do aliphatic carboxylic acids containing one –COOH group.⁶⁹ Phosphoric acid ($K_A = 4 \times 10^4 \text{ M}^{-1}$) and substituted aromatic carboxylic acids ($K_A = 10^4 - 10^5 \text{ M}^{-1}$) have similar binding affinities for TiO₂, but the coordination geometry of salicylate and phosphate to TiO₂ are different as shown in Figure 1.20. Salicylic acid creates a chelating bidentate structure with the TiO₂ surface, whereas a bridging bidentate complex forms when phosphate (from phosphoric acid) binds to the surface. Due to the differences in coordination, Larsen suggested that 2,5-DHB predominantly competes for binding sites with nonphosphorylated peptides and not phosphorylated peptides.

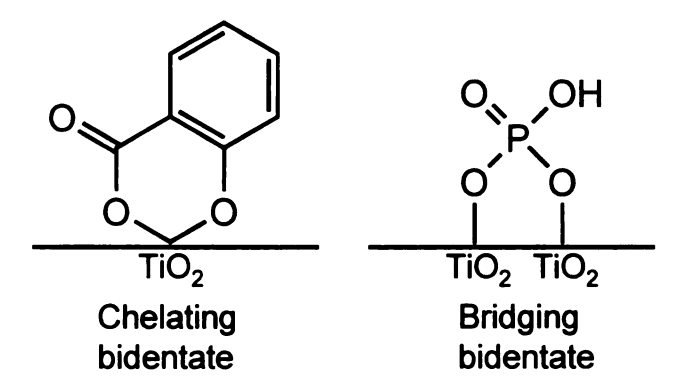


Figure 1.20: Adsorption of salicylic acid and phosphoric acid to the surface of TiO₂. Figure adapted from Larsen et al.⁶⁴

In 2006, Olsen et al. utilized a similar protocol to that of Larsen et al. for phosphopeptide enrichment using TiO₂ and 2,5-DHB in the loading solutions.⁶³ Prior to the enrichment, phosphoprotein digests were fractionated using strong cation exchange chromatography. Enriched samples were analyzed using liquid chromatography mass spectrometry. This methodology resulted in the detection of over 10,000 phosphopeptides, and the identification of 6,600 phosphorylation sites on 2,244 proteins.⁶³

1.4.3.2 Enrichment Using Zirconium Dioxide

Like titanium dioxide, zirconium dioxide is positively charged at low pH and capable of binding phosphopeptides. Additionally, ZrO₂ has been shown to have a higher binding affinity towards phosphate than carboxylate anions. ^{70,71} Moreover, ZrO₂ has been used previously as a chromatographic material due to its physical and thermal stability, and thus it is a promising material for phosphopeptide enrichment.

In 2006, Kweon et al. utilized zirconium dioxide microtips (Glygen) for the enrichment of phosphorylated peptides and compared the specificity and recovery

achieved to that obtained with titanium dioxide microtips (Glygen) when using the same protocol (same binding, rinsing and elution solutions).⁷² The optimal procedure for the enrichment of 100-pmol tryptic α-casein and β-casein digests using 50-μg ZrO₂ microtips with subsequent analysis by negative-ion mode ESI-FT-ICR MS was determined to include a 3.3% formic acid (pH 2.0) binding solution, a water rinse, and a 0.5% piperidine (pH 11.5) elution solution. Under these conditions, 10α -casein phosphorylated peptides and only one nonphosphorylated peptide were detected using the ZrO₂ tips, while 8 phosphopeptides and one nonphosphorylated peptide were detected using the TiO₂ tips. Similarly, when a \(\beta\)-casein digest was analyzed using ZrO₂ tips, 5 phosphopeptides and 2 nonphosphopeptides were detected, while use of TiO₂ yielded only captured 4 phosphopeptides and at least one nonphosphopeptide. Overall, TiO₂ microtips were more selective for multiply phosphorylated peptides in α -casein and β casein digests, whereas the ZrO₂ tips enriched primarily monophosphorylated peptides. The authors presume that the selectivity of ZrO₂ for monophosphorylated peptides could be due to either the higher acidity of zirconia or the higher coordination number compared to titania. However, the surface properties of these metal oxide materials are not well understood.

Additionally, tryptic and Glu-C digests were compared using ZrO₂ and TiO₂ tips.⁷² The use of Glu-C was previously demonstrated to reduce nonspecific binding of nonphosphorylated peptides to a Ga(III)-IMAC column as mentioned above (section 1.4.2.4).⁶⁰ If complete Glu-C cleavage occurs, then only one acidic residue (E or D) will be present in the peptide chains. However, Kweon et al. found that Glu-C digestion did

he de Millering Miller of the State of the

not provide a significant advantage over tryptic digestion in the enrichment of casein phosphopeptides by either ZrO₂ or TiO₂ tips.

1.4.4 Magnetic Beads

The use of magnetic beads for phosphopeptide enrichment is attractive since the beads can be easily collected using an external magnetic field. Moreover, the development of nano-sized magnetic beads makes the technique even more attractive since the high surface area to volume ratio provides a high binding capacity. The use of magnetic beads modified with metal oxide or IMAC materials are discussed below.

1.4.4.1 Magnetic Nanoparticles Coated with Metal Oxide Materials

The use of magnetic nanoparticles coated with metal oxides (e.g., titania, zirconia, and alumina) for the analysis of phosphopeptides began in 2005.⁷³⁻⁷⁵ Figure 1.21 shows the fabrication of metal oxide-coated magnetic nanoparticles. Briefly, magnetic (Fe₃O₄) nanoparticles were coated with a thin layer of SiO₂ either using tetraethyl orthosilicate (TEOS) or sodium silicate, and the metal oxide, TiO₂, ZrO₂, or Al₂O₃, was then formed on the silica using titanium butoxide, zirconium butoxide, or aluminum isopropoxide, respectively. This procedure resulted in the formation of ~50-, ~170-, and ~20-nm diameter titania-, zirconia-, and alumina-coated Fe₃O₄ particles, respectively.



Figure 1.21: Fabrication of TiO₂-coated magnetic nanoparticles. Zirconia- and aluminacoated magnetic nanoparticles are prepared in a similar fashion.

The protocol for using the metal oxide-coated magnetic nanoparticles to enrich phosphopeptides is fairly simple. For example, 25 μ g of magnetic beads is mixed with ~50 μ L of protein digest in 0.15% TFA in a microcentrifuge tube, incubated for 30 seconds, rinsed with 50% acetonitrile containing 0.15% TFA and the solution is decanted while using a magnet to secure the nanoparticles to the wall of the tube. The beads are either applied to the MALDI plate without the addition of matrix (Fe₃O₄/TiO₂ surface-assisted laser desoption/ionization (SALDI)) or they are mixed with 2,5-DHB containing phosphoric acid and then applied to the MALDI plate for direct MALDI-TOF-MS analysis. The Fe₃O₄/TiO₂ SALDI method is attractive since no elution step or matrix is necessary.

The estimated binding capacity of alumina-coated magnetic nanoparticles is 60 µg of phosphopeptide per milligram of nanoparticle. Using this capacity, 25 µg of magnetic beads should be capable of isolating 1.5 µg of phosphopeptide, which for a phosphopeptide with a molecular weight of 2500 Da corresponds to 600 pmol. This high capacity could lead to nonspecific binding. The binding capacities for the other metal oxide-coated magnetic nanoparticles were not specified.

Chen et al. examined the utility of titania-coated magnetic nanoparticles as phosphopeptide affinity devices and as an effective SALDI matrix (a citrate buffer containing DAHC was added to help desorption/ionization of the analyte).⁷⁵ Based on the absorption spectroscopy of β-casein phosphopeptides that had been eluted from Fe₃O₄/TiO₂ nanoparticles, these materials are capable of relatively high phosphopeptide recoveries of 51%. The analysis of 500 fmol of a β-casein casein digest using SALDI with Fe₃O₄/TiO₂ nanoparticles for phosphopeptide capture resulted in a mass spectrum that showed predominantly peaks due to three phosphorylated peptides (m/z 2062, 2556, and 3122). However, compared to a conventional MALDI mass spectrum, the Fe₃O₄/TiO₂ SALDI technique showed a 3-fold enhancement in the absolute intensity of the peak at m/z 2062, but the other phosphopeptide peaks seemed to be about the same intensity in the two spectra. The detection limit for the Fe₃O₄/TiO₂ SALDI technique is 50 fmol for the m/z 2062 peak, but it was higher (500 fmol) for the other two phosphorylated peptides (m/z 2556 and 3122). The Fe₃O₄/TiO₂ nanoparticles seem to have some affinity towards acidic nonphosphorylated peptides since several nonphosphopeptides were present in the mass spectrum of casein phosphopeptides enriched from a cytochrome c digest, which was in 20-fold excess. Perhaps, the use of 2,5-DHB in the binding and rinsing protocol would help alleviate this nonspecific binding, as demonstrated by Larsen.⁶⁴ Notably, in addition to using Fe₃O₄/TiO₂ nanoparticles for SALDI, Chen et al. showed that the incorporation of a matrix such as 2,5-DHB containing phosphoric acid prior to MS analysis gave a ~12-fold increase the signal-to-noise (S/N) in mass spectra and afforded a more linear baseline. The irregularshaped baseline in SALDI could be due to an increase in laser power, which, would probably be needed when no matrix was used.

In 2006, Lo et al. implemented zirconia-coated magnetic nanoparticles in a 30-sec phosphopeptide enrichment technique.⁷³ Based on the detection of a single phosphopeptide (m/z 2062) from a β -casein digest, this 30-sec enrichment protocol has a detection limit of ~45 fmol. Again, two other phosphopeptides (m/z 2556 and 3122) were only detected at higher amounts (450 fmol). At longer incubation times of 1 h, the signals from phosphopeptides in a β -casein digest are ~4-fold stronger.

As might be expected, at higher concentrations (280 pmol of α-casein digest), multiply phosphorylated peptides are preferentially detected over singly phosphorylated peptides when using metal oxide magnetic nanoparticles.⁷³ When the amount of digest was reduced by a factor of 800, only monophosphorylated peptides were observed in the mass spectrum. This again suggests that at high concentrations of phosphoprotein digest, the multiply phosphorylated peptides are preferentially bound over monophosphorylated species. When the binding capacity is much greater than the amount of phosphopeptide, however, the monophosphorylated species also bind and show a stronger signal, probably due to higher ionization efficiency.

Most recently, the Chen group utilized alumina-coated magnetic nanoparticles for enriching phosphopeptides. They incubated protein digests with the magnetic nanoparticles for 30 sec and estimated that it takes 5 min to use their enrichment method and perform subsequent MS characterization. Using the alumina-coated beads, the authors analyzed as little as 25 fmol of α -casein digest. Eight phosphopeptides from the 25-fmol α -casein digest were detected, but signals due to half these peptides are barely

detectable (i.e. the S/N appears to be below 3). Unlike the titania-coated magnetic beads, the alumina-coated beads do not appear to have affinity towards acidic nonphosphorylated peptides as demonstrated by the analysis of a digest mixture of two phosphoproteins (2.5 pmol of α- and β-casein) and two nonphosphorylated proteins (125 pmol of cytochrome c and BSA). Even though the amounts of nonphosphoproteins in the digests were 50-fold greater than those of the phosphorylated proteins, virtually no signals due to nonphosphorylated peptides from cytochrome c and BSA were observed. This is a significant improvement over the titania-coated magnetic beads, but it would be interesting to see the performance of the Fe₃O₄/Al₂O₃ nanoparticles when lower levels of phosphopeptides are analyzed in the presence of nonphosphorylated protein digests.

1.4.4.2 Fe(III)-Iminodiacetate Immobilized on Magnetic Microspheres

In 2006, Xu et al. fabricated magnetic microspheres that were derivatized with Fe(III)-iminodiacetate (IDA) and used these particles for enriching phosphopeptides prior to analysis in positive-ion mode MALDI-TOF/TOF MS.⁷⁶ In short, the 0.2-0.3-μm magnetic particles were prepared by a solvothermal reaction, coated with 70 nm of silica using tetraethyl orthosilicate (TEOS), modified with 3-glycidoxypropyltrimethoxysilane, GLYMO), reacted with IDA and charged with Fe(III) as shown in Figure 1.22. The utility of the beads was demonstrated by the analysis of β-casein digests. The β-casein digest was incubated with the Fe(III)-NTA-modified magnetic beads for 90 min, washed with 20% acetonitrile, and then the magnet-isolated beads were dispersed in 10 μL of 50% acetonitrile. No phosphopeptide elution step was necessary since the bead slurry (0.4 μL) was applied directly to the MALDI sample plate followed by addition of 2,5-

DHB containing phosphoric acid, which should desorb the phosphopeptides from the beads.

Figure 1.22: Preparation of magnetic beads modified with Fe(III)-IDA. Figure adapted from Xu et al.⁷⁷

The mixing of 40 pmol of digest with the Fe(III)-IDA-modified magnetic microspheres (10 μ L, 1 mg/mL) resulted in a mass spectrum that was dominated by signals due to mono- and tetraphosphorylated peptides (m/z 2061 and 3122) of β -casein. Although, there were a few peaks in the conventional MALDI mass spectrum due to nonphosphorylated peptides, the signal intensities for these peaks were reduced when the phosphopeptides were enriched. When the amount of digest was reduced by 10-fold, the magnetic beads were still able to enrich the phosphorylated peptides although the absolute signals had decreased.

1.4.5 Reversible Covalent Enrichment

1.4.5.1 Chemical Derivatization of Phosphopeptides and Solid-state Purification

In 2001, Zhou et al. developed a six-step, solid-phase enrichment technique that can be applied to phosphotyrosine peptides in addition to phosphoserine and phosphothreonine-containing peptides.⁷⁸ The method is portrayed in Figure 1.23. Prior to tryptic digestion, any cysteine residues of the protein mixture are reduced and alkylated. After digestion, the amino groups of the peptides are first protected using tbutyl-dicarbonate (Boc), followed by carbodiimide (N,N'-dimethylaminopropyl ethyl carbodiimide, EDC) mediated reaction of ethanolamine with the carboxlyate and phosphate groups, yielding amide and phosphoramidate bonds, respectively. phosphate group is regenerated by acid hydrolysis (10% TFA), and cystamine is attached to the phosphate group via carbodiimide-catalyzed condensation. Finally, the attached cystamine is reduced using dithiothreitol (DTT) and the free sulfhydryl group is then reacted with iodoacetyl groups immobilized on glass beads. After rinsing the beads to remove nonphosphorylated peptides, the phosphopeptides are cleaved from the surface, and the tBoc protecting groups are removed using 100% TFA. Using this enrichment strategy for the analysis of the phoshotyrosine peptide TTHpYGSLPQK, recovery was ~20%.

the state of the s

Figure 1.23: Six-step solid-phase enrichment using carbodiimide condensation and glass beads derivatized with iodoacetyl groups. Figure shows only 5 steps. Figure adapted from Zhou et al.⁷⁸

β-elimination chemistry provides a considerably simpler method for enriching phosphopeptides. In this chemistry, strong bases such as NaOH or Ba(OH)₂ can be used to cleave the phosphoester bonds of phosphoserine and phosphothreonine, forming the respective dehydroalanine or dehydroaminobutyric acid analogs, which can then react with different nucleophiles, such as thiol, amine, or alcohol groups. As shown in Figure 1.24, Thaler et al. used these reactions to cleave the phosphate ester of α-casein phosphopeptides from a tryptic digest (cysteines were oxidized to cysteic acid prior to digestion).⁷⁹ The peptides were subsequently reacted with propanedithiol, followed by and covalently binding of the peptides to a solid support derivatized with reactive dithiopyridine groups. After the resin was rinsed thoroughly, the bound peptides were simply cleaved using DTT and the free thiol groups were alkylated. The sample was then desalted and analyzed using MALDI-TOF-MS. However, when combined with MALDI-MS, this method revealed only 2 tryptic phosphopeptides from a 20-μg (~820 pmol) α-

casein digest. (α -Casein contains α -S1 and α -S2 protein forms, and complete tryptic digestion of these proteins yield 4 and 5 phosphopeptides, respectively.)

Figure 1.24: Reversible solid-phase enrichment of phosphoserine and phosphothreoine-containing peptides using β -elimination and Michael addition followed by enrichment on a dithiopyridino-modified resin. Figure adapted from Thaler et al. ⁷⁹

In 2003, Lansdell and Tepe demonstrated the use of an α-diazo functionalized resin to reversibly and covalently bind the phosphate group of phosphopeptides. Since β-elimination or another technique is not required to chemically derivatize the phosphopeptide prior to solid-phase enrichment, this technique can be applied to phosphorylated serine, threonine, and tyrosine peptides. The immobilization procedure is shown in Figure 1.25. In order to prevent carboxylate groups of the peptides from covalently binding to the resin, these groups were first protected by methyl esterification using acetyl chloride in an excess of methanol. The authors used their strategy to enrich 500 fmol of phosphorylated anigoteinsin II (DRVpYIHPF) from a mixture of three nonphosphorylated peptides. After the peptide mixture was incubated with the α-diazo resin, the nonphosphopeptides were rinsed away, and the immobilized phosphopeptide

were cleaved with either TFA or NH₄OH. The resulting phosphopeptides were analyzed using MALDI-TOF MS, and the mass spectrum showed only the peak representing phosphorylated angiotensin (m/z 1127).

Figure 1.25: Reversible solid-phase enrichment using an α -diazo resin. Cleavage of the phosphopeptide can be accomplished by using either trifluoroacetic acid (TFA) or NH₄OH. Note that when NH₄OH is used, the methyl ester is hydrolyzed back to the original phosphopeptide. Figure adapted from Lansdell et al.⁸⁰

In 2005, Tao et al. created a 4-step enrichment process (Figure 1.26) for the immobilization of methyl esterified phosphopeptides onto an amino-terminated dendrimer using EDC coupling.⁸¹ This one-pot chemistry avoids the need for the amino groups on the N-terminus and lysine or arginine residues to be protected.⁷⁸ Once the

Marie St. No. of Street, Street, Street, St.

phosphoprotein digest had incubated with the dendrimer (concentration of amine group is 1 M), it was rinsed and the phosphopeptides were liberated using 10% TFA due to cleavage of the phosphoramidate bonds. This technique was employed in analyzing digests of 10 pmol β-casein, and the phosphopeptide recovery was greater than 35%.

$$\begin{array}{c} \text{amino-terminated} \\ \text{dendrimer} \\ \text{H}_2\text{N} \\ \text{C} \\ \text$$

Figure 1.26: Three-step solid phase enrichment using carbodiimide condensation. Figure adapted from Tao et al.⁸¹

More recently, Warthaka et al. utilized a three-step solid-phase enrichment technique, consisting of the protection/oxidation-reduction condensation of phosphopeptides with glycine-derivatized Wang resin⁸² as shown in Figure 1.27. In the first step, carboxylic acid-containing residues are protected using methyl esterification. Next, the methylated phosphopeptides are covalently coupled to the glycine Wang resin in the presence of triphenylphosphine (PPh₃), 2,2'-dithiopyridine (PySSPy), and N,N'-diisopropylethylamine (DIPEA). The phosphopeptide is bound to the glycine-derivatized resin via a phosphoramidate bond, which is cleavable by TFA. Subsequently, the resin is washed and the phosphopeptides are eluted with 95% TFA and analyzed using MALDI-

TOF MS. By using this enrichment strategy, the recovery of a monophosphopeptide from 30 nmol of β -casein digest was ~37%, which is comparable to that of the carbodiimide solid-phase enrichment technique used by Tao et al.⁸¹

Figure 1.27: Reversible solid-phase enrichment of protected phosphopeptides using an oxidation-reduction condensation reaction. Figure adapted from Warthaka et al. 82

1.4.6 MALDI On-plate Enrichment Techniques

On-plate enrichment is at the heart of this dissertation, and thus the following section discusses on-plate enrichment of both phosphopeptides and other species. The first section presents the development of on-plate enrichment by affinity capture, and subsequent sections discuss more recent developments in affinity capture of phosphopeptides.

1.4.6.1 Background on Surface-enhanced Affinity Capture Technology

In 1993, Hutchens and Yip established the use of surface-enhanced affinity capture (SEAC) using agarose beads derivatized with single-stranded DNA as the affinity probe to capture lactoferrin, an 80-kDa glycoprotein found in the infant urine. Urine from premature infants was mixed with the modified agarose beads, and the beads were rinsed to remove unwanted species, mixed with a sinapinic acid matrix solution, and spotted on the sample plate for subsequent analysis using MALDI-TOF-MS. Notably, lactoferrin could be analyzed without prior pretreatment of the urine. However, beads applied to the MALDI target caused complications in the TOF-MS analysis as shown by Papac and coworkers.⁸³ Surface heterogeneities caused variations in the ion's flight time, leading to peak broadening, and higher laser energies were required when analyzing samples from beads. Papac et al. used sepharose charged with Cu(II) or Fe(III) as an affinity support. They analyzed cytochrome c, apotransferrin, and lactoferrin using the Cu(II)-IMAC resin and an equimolar mixture of phosphokemptide (LRRApSLG) and nonphosphorylated kemptide using an Fe(III)-IMAC support. After applying the proteins or peptides to the IMAC beads and rinsing, an aliquot of the bead slurry was added to the MALDI sample plate, followed by addition of matrix and analysis by MALDI-TOF-MS. For comparison, they also eluted the captured biomolecules from the IAC and IMAC beads and analyzed the eluent by conventional MALDI-TOF-MS. Interestingly, a stronger signal (2-fold greater) was observed for the proteins/peptides when they were analyzed directly from the IMAC beads relative to when the analyte was eluted from the beads and subsequently analyzed by MALDI-TOF-MS.

In 1995, Brockman and Orlando were the first to derivatize the MALDI target itself in order to capture specific biomolecules.⁸⁴ They termed their technique probe affinity MS (PAMS). In their initial work, antibodies were immobilized to the gold MALDI plate via derivatization of a self-assembled monolayer (SAM). As shown in Figure 1.28, the gold substrate was immersed in a solution of 10 mM dithiobissuccinimidyl propionate (DSP) to form a SAM. The antibody was then coupled to the DSP SAM via amide bond formation. Lastly, the affinity probe was incubated in a complex solution containing the protein of interest. After 20 minutes, the probe was rinsed to remove unbound proteins or impurities, matrix was spotted onto the probe, and the sample was analyzed using MALDI-TOF-MS. Brockman and Orlando demonstrated that biotinylated proteins can be selectively captured on the MALDI probe while nonbiotinyl proteins including mygoglobin, cyctochrome c, and ribonuclease B are not retained by the affinity probe.⁸⁴ Their study not only showed selective capture and detection of the proteins of interest, but also demonstrated that PAMS does not cause peak broadening. Moreover, the alkali metal ion adducts typically seen in conventional MALDI analysis were not observed in the PAMS experiment since salts were removed when the probe was rinsed prior to the addition of the matrix. Remarkably, compared to conventional MALDI-MS the resolution was 2-fold greater when the affinity probe was used.

Company of the Compan

Figure 1.28: Capture of an antigen for probe affinity mass spectrometry using an antibody immobilized on a self-assembled monolayer on a MALDI target. Figure adapted from Brockman and Orlando.⁸⁴

In a subsequent study, Brockman and Orlando grafted a polymer onto the MALDI probe in order to increase the binding capacity for the protein of interest. 85 As shown in Figure 1.29, the gold probes were first immersed in 10 mM 3-mercapto-1-propanol (MP) to form the SAM, and the hydroxyl group of the MP SAM was activated with epichlorohydrin in the presence of triethylamine (TEA), yielding a glycidyl ether. Dextran (500 kDa) was then covalently coupled to the epichlorohydrin-activated hydroxyl groups under basic conditions, and sodium periodate (NaIO₄) was added to oxidize the adjacent hydroxide groups on the dextran to aldehyde moieties. Antibodies to YINF (or alternatively any species containing a primary amine group) were then coupled to the oxidized dextran via an amide bond in the presence of a catalyst, NaCNBH₃. The antibody-dextran-modified probes were immersed into a mixture of an interferon protein, YINF (16 kDa), and cytochrome c (12 kDa). After a 20-30-min immersion in the sample, the probe was rinsed to remove cytochrome c and other impurities, and sinapinic acid was applied for direct MALDI-MS analysis of γINF. The γINF-antibody-dextranmodified probes showed minimal non-specific binding whereas the γINF-antibody-SAM films modified using the DSP chemistry afforded binding of non-specific proteins. Brockman noted that DSP is readily reactive with water (half-life of the *N*-hydroxysuccinimide group of DSP in water is about 20 min), and could have formed carboxylic acid groups during the immobilization of the antibody onto the surface. Through electrostatic interactions, proteins containing primary amine groups can be captured onto surfaces containing carboxylic acid groups. They also demonstrated that the antibody-polymer-modified probes are capable of binding 500 times more protein than the antibody-SAM-modified plates that they initially fabricated. Although, Brockman and Orlando did not use these polymer-modified probes to analyze phosphopeptides, the potential application is apparent.

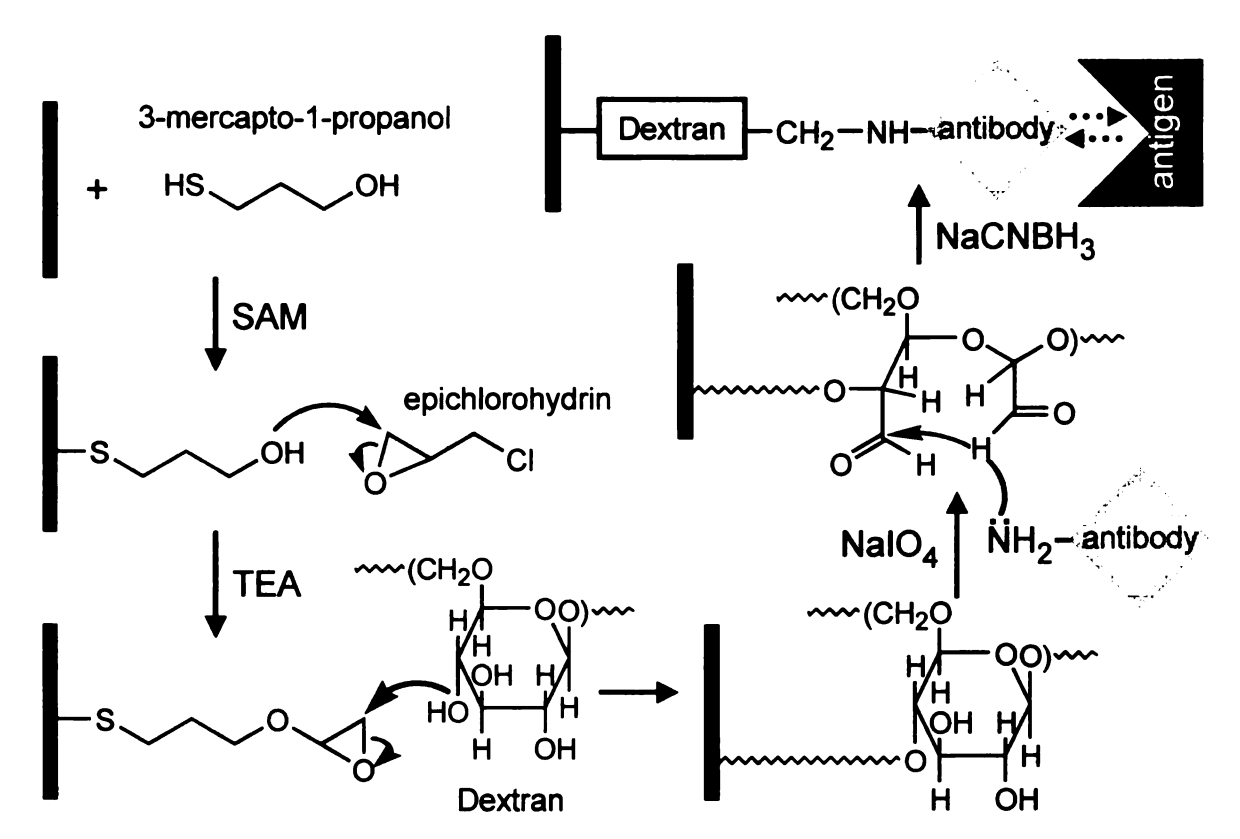


Figure 1.29: On-probe affinity enrichment using an antibody anchored to a grafted polymer to capture the antibody of interest. Figure adapted from Brockman and Orlando.⁸⁵

Ciphergen Biosystems (Palo Alto, CA) commercially developed a ProteinChip System, consisting of a ProteinChip Reader (i.e. linear TOF MALDI mass spectrometer), ProteinChip Software, and related accessories that are used in conjunction with ProteinChip Arrays. The ProteinChip System and ProteinChip Arrays utilizing affinity MALDI probes were first available to the market in 1997⁸⁶ and have been typically applied toward biomarker assays and protein analysis of biological fluids. 86 However, in 2004, analysis of phosphorylated peptides was demonstrated and kinase activity was monitored using IMAC-Gallium ProteinChip Arrays (IMAC chips were charged using a solution of 50 mM gallium nitrate).⁸⁷ A mixture of three mono-phosphorylated peptides with of sequences KRPpSQRHGSKY, TRDIYETDYpYRK, and KRELVEPLpTPSGEAPNQALLR and their nonphosphorylated counterparts were analyzed simultaneously. The nonphosphorylated peptides (1-3 pmol) were in a 10-fold excess compared to the phosphorylated analogs, but all three phosphorylated peptides showed greater signals in the mass spectrum greater than their nonphosphorylated forms. Thulasiraman et al. also showed that peptide substrates phosphorylated by 3 specific kinases could be detected simultaneously using the IMAC ProteinChip Array.⁸⁷

In November 2006, Bio-Rad Laboratories acquired Ciphergen's proteomics instrument business, and currently, the ProteinChip technology is offered through Bio-Rad. Unfortunately, the use of these chips requires the Ciphergen TOF mass spectrometer, as the ProteinChip Arrays are not compatible with other commercial mass spectrometers.

1.4.6.2 Recent Advancements in MALDI On-plate Enrichment Techniques for Phosphopeptides

1.4.6.2.1 Nitrilotriacetic Acid Self-assembled Monolayers Immobilized on Gold Plates

The immobilization of self-assembled monolayers (SAMs) derivatized with NTA analogs has been established since 1996.⁸⁸⁻¹⁰⁷ These NTA SAMs have been used for the study of histidine-nickel, protein-protein, protein-antibody, protein-DNA, or protein-ligand interactions and for biotechnology applications including microarrays, biosensors, catalysis, and biocompatible coatings.

$$-s \longleftrightarrow_{4}^{SH} \xrightarrow{\text{maleimide-terminated NTA}} -s \longleftrightarrow_{4}^{SH} \xrightarrow{\text{opt SAM}}$$

Figure 1.30: Formation of a self-assembled monolayer of octadecanethiol and derivatization using maleimide-terminated NTA. Further NTA complexation with Ga(III) or Fe(III) is not shown here. Figure adapted from Shen et al. 108

However, it was not until 2005 that Shen and coworkers used NTA SAMs immobilized on gold MALDI plates to capture phosphorylated peptides for direct MALDI-TOF-MS analysis. In short, a SAM of 1,8-octanedithiol was formed overnight on a gold substrate, maleimide-terminated NTA (N-[5-(3'-maleimidopropylamido)-1-carboxypentyl]-iminodiacetic acid) was coupled to the SAM, and the immobilized NTA ligand was charged with Ga(III) using 200 mM gallium nitrate (Figure 1.30). Using these

Ga(III)-NTA-SAM-modified plates, Shen et al. investigated on-probe enrichment of a mixture containing two synthetic phosphopeptides, DLDVPIPGRFDRRVpSVAAE and KIGDFGMTRDIYETDpYpYRKGGK, four nonphosphorylated peptides, and angiotensin I, ACTH 1-17, ACTH 18-39, and ACTH 7-39 (ACTH is an abbreviation for adrenocorticotropic hormone). In the conventional MS analysis of the mixture, the four nonphosphorylated peptides showed signals compared the stronger to monophosphorylated peptide, and the diphosphorylated peptide was not detected. In contrast, when the same mixture was analyzed using the Ga(III)-NTA-SAM-modified probe, both phosphopeptides were detected while the peaks due to the nonphosphorylated peptides were eliminated or reduced. (The matrix employed in their analyses was α-CHCA.) However, even though the MS signal due to the nonphosphorylated peptide ACTH 18-39 was significantly reduced, it was still more intense than the peaks due to the phosphorylated peptides.

Shen and coworkers also analyzed a tryptic digest of β-casein using the Ga(III)-NTA-SAM-modified plates. The conventional MS analysis generated signals for a few nonphosphorylated peptides in addition to a relatively low intensity peak for the monophosphorylated peptide. However, the signal for the monophosphorylated peptide increased by about 3-fold when the SAM-modified probe was used rather the conventional MALDI-MS analysis. No signal for the tetraphosphorylated peptide was observed in either the conventional analysis or when the modified plate was used, however. Nonspecific adsorption of nonphosphorylated peptides was also apparent in the mass spectrum when the digest was applied to the Ga(III)-NTA-SAM-modified probe.

The authors state that they saw better reproducibility in the mass spectra when Ga(III) was used rather than Fe(III) as the metal ion.

1.4.6.2.2 Photochemically Immobilized Iminodiacetic Acid on Silicon Supports

Recently, Xu et al. derivatized a porous silicon surface with IDA-1,2-epoxy-9-decene via a photochemical reaction.⁷⁶ In brief, excess IDA was reacted with 1,2-epoxy-9-decene, forming a photochemically reactive IDA derivative. The electrochemically-etched porous silicon substrate was immersed in a solution of the IDA derivative and exposed to light from a 1000-W Hg lamp. After 2 h, IDA-1,2-epoxy-9-decene was assumed to be immobilized onto the silicon surface as shown in Figure 1.31. The IDA-derivatized silicon surface was then immersed in a 100 mM FeCl₃ solution.

Figure 1.31: Immobilization of a monolayer of an IDA derivative on porous silicon using photochemistry. Figure adapted from Xu et al.⁷⁶

The Fe(III)-IDA-derivatized porous silicon plates were employed to analyze tryptic digests of β -casein using 2,5-DHB containing 1% phosphoric acid as a matrix solution. The conventional mass spectrum of the digest revealed the presence of three phosphorylated peptides with m/z 2062, 2556, and 3122 along with several peaks due to nonphosphorylated peptides. When a 1 pmol digest was applied to the Fe(III)-IDA-modified silicon probe, only peaks due to the phosphorylated peptides were present. However, there was significant background noise in the mass spectrum, and the signal intensity due to the phosphopeptides decreased compared to the conventional mass

spectrum. When the amount of digest was decreased from 1 pmol to 300 fmol, all three phosphopeptides were still detected when the modified silicon plate was used while nonspecific adsorption from other peptides was minimal. At the lower amount of digest, the peak intensities of the phosphopeptides appeared to be higher than those observed in the conventional MALDI mass spectrum of the same amount of digest. The authors identified the phosphorylated peptide, giving rise m/z2556. to IEKFQpSEEQQQTEDELQDK. However, this m/z value does not correlate with the phosphorylated peptide that they suggested. The correct value for this peptide would be m/z 2432. The peak at m/z 2556 is most likely due to FQpSEEQQQTEDELQDKIHPF as reported elsewhere. 109,110 Although TPCK-treated trypsin was used in these studies, it appears that some cleavage due to chymotrypsin resulted in the peak at m/z 2556. (TPCK-treated trypsin inhibits chymotrypsin activity without affecting the activity of trypsin, and chymotrypsin is responsible for cleaving proteins at the carboxyl side of tyrosine (Y), tryptophan (W), and phenylalanine (F)).

1.4.6.2.3 Polymer-modified Gold MALDI Probes

Our research group has previously used polymer-modified, patterned MALDI plates as phosphopeptide affinity probes. These patterned affinity probes served to both purify and concentrate the analyte. Xu et al. prepared these substrates as shown in Figure 1.32.

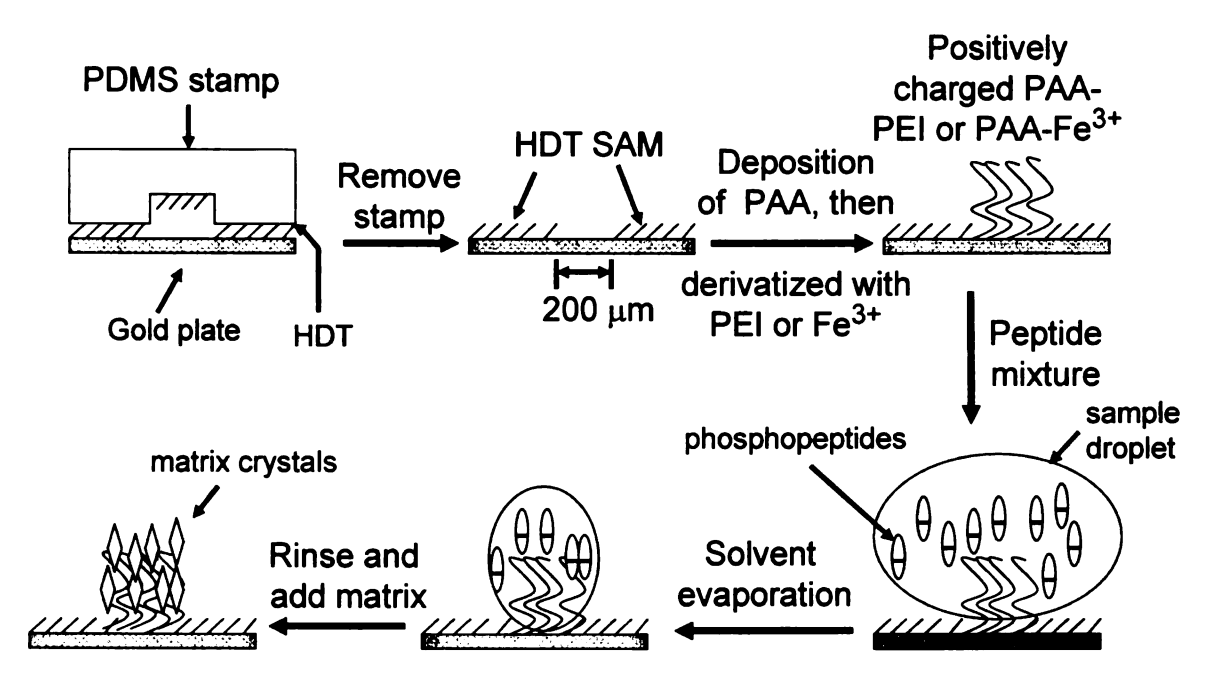


Figure 1.32: Fabrication of polymer-modified MALDI gold plates for phosphopeptide capture and concentration. A hydrophobic pattern is created first, followed by the immobilization of polymers onto the 200-µm diameter gold wells.

The gold substrates were first patterned with 200-µm diameter spots by using a poly(dimethylsiloxane) (PDMS) stamp, according to methods developed by Whitesides. The patterned-PDMS stamp was painted with hexadecanethiol (HDT) and gently pressed onto the surface of a gold substrate, and the HDT-patterned substrate was then immersed into a solution of mercaptoundecanoic acid (MUA) to form a SAM in the areas that were not exposed to HDT. The carboxylic acid groups of MUA were activated using ethyl chloroformate and subsequently reacted with amino-terminated poly(*tert*-butyl acrylate) (PTBA) or polyethylenimine (PEI). If PTBA was immobilized on the surface, then the *t*-butyl ester groups were hydrolyzed by immersing the substrate in a solution of methanesulfonic acid, forming poly(acrylic acid) (PAA). The PAA-modified gold substrate was finally immersed in solution of 100 mM Fe(NO₃)₃. Both the Fe(III)-PAA-modified gold plates and the PEI-modified gold substrates were used as positively-

charged affinity probes for the capture and analysis of phosphopeptides by MALDI-TOF-MS. The matrix used in the phosphospeptide analyses was α -CHCA.

The patterned polymer-modified probes where used to examine phosphorylated protein digests of ovalbumin and β-casein. When the Fe(III)-PAA-modified plate was used to enrich the phosphopeptides from 1 pmol of ovalbumin digest, signals due to the phosphopeptides were enhanced compared to those observed in the conventional MS analysis, but the mass spectrum of the enriched sample was still dominated with peaks due to nonphsophorylated peptides. The surface may not be completely saturated with Fe(III), leaving negatively-charged sites due to carboxylate groups to bind positivelycharged peptides via electrostatic interactions. Perhaps more stringent rinsing, including acetic acid and/or acetonitrile, could have alleviated adsorption due to nonspecific peptides. The use of the PEI-modified plate also showed improved signal for two of the phosphorylated peptides (m/z 2090 and 2903) from the ovalbumin digest compared to the conventional MS analysis. However, one of the phosphorylated peptides was not detected (m/z 2513). Additionally, the mass spectrum showed fewer peaks due to nonphosphopeptides compared to the conventional mass spectrum. In order to confirm the presence of phosphorylated peptides, the samples were incubated with phosphatase on the polymer-modified plates and then analyzed by MALDI-MS. After treatment, two peaks were observed in the mass spectra at m/z values that were 80 Da less than m/z 2090 and 2513, which indicated the phosphopeptides were correctly assigned.

Xu et al. also demonstrated that PEI-modified plates could be used to capture the phosphorylated peptides from 100 fmol of β -casein digest. The signals due to the monophosphorylated and tetraphosphorylated peptides dominated the mass spectrum

when the PEI-modified plate was used. However, in addition to the phosphoryl groups present in the peptides, there are several acidic amino acid residues (D and E) that could be attracted to the positively-charged PEI surface.

1.4.6.2.4 Zirconium-phosphonate-modified Porous Silicon Plates

Immobilization of zirconium-phosphonate onto substrates has been demonstrated and has potential applications in catalysis, sensing, electronics, protein immobilization, and separations. ¹¹³⁻¹²⁵ It is known that Zr(IV) binds strongly to immobilized phosphonate monolayers due to metal ion-ligand crosslinking (Zr(IV) ions coordinate to more than one phosphonate molecule). Thus, these Zr(IV)-phosphonate monolayers are highly stable.

In 2006, Zhou et al. prepared zirconium-phosphonate monolayers immobilized on porous silicon as phosphopeptide affinity probes for MALDI-TOF-MS.¹¹⁰ To form the phosphonate-silicon surface, a modified etched silicon susbstrate was placed in a solution of phosphorous oxychloride (POCl₃) and 2,4,6-trimethylpyridine (collidine), and the surface was charged with Zr(IV) by immersing the phosphonate-modified silicon substrate into 20 mM ZrOCl₂ (zirconyl chloride). All of the analyses were performed using linear TOF-MS and utilizing 2,5-DHB containing 1% H₃PO₄ as a matrix. The Zr(IV)-phosphonate-modified plates were used to analyze digests of β-casein containing 2 pmol, 20 fmol, and 2 fmol of protein, using 2,5-DHB as a matrix (contained 1% phosphoric acid). As mentioned before the tryptic digestion of β-casein typically results in the formation of two phosphorylated peptides, monophosphorylated and tetraphosphorylated species. Enrichment of phosphopeptides from the β-casein digest using the Zr(IV)-phosphonate silicon substrate yielded signals for both phosphopeptides

at the 2-pmol and 20-fmol levels. Moreover, another phosphorylated peptide (FQpSEEQQQTEDELQDKIHPF), gave rise to a peak at m/z 2556. As discussed previously, the presence of this peptide is due to chymotrypsin cleavage. When 2 fmol of β -casein was analyzed using the porous silicon plates only phosphopeptide peaks at m/z 2061 and 2556 were observed in the mass spectrum, while no signal for the tetraphosphorylated peptide was seen. Virtually, no nonphosphorylated peptides were detected in all three experiments.

Additionally, β-casein was combined with a tryptic digest of bovine serum albumin (BSA), a nonphosphorylated protein, and analyzed at β-casein to BSA ratios of 1:1, 1:10, and 1:100 (the amount of β-casein in the digest was maintained at 1 pmol). Impressively, the use of the derivatized porous silicon plates nearly eliminated all signals corresponding to peptides from the BSA digest. However, when the amount of BSA was 100-fold greater than β-casein, the signals for the monophosphorylated peptides (*m/z* 2061 and 2556) dramatically decreased. For comparison, they also applied the mixture to Fe(III)-IMAC beads (Poros MC beads, PerSeptive Biosystems) that contain an IDA ligand. The Fe(III)-IDA beads suffered from nonspecific adsorption at high amounts of the BSA digest (10-pmol and 100-pmol amounts), which is a frequent limitation of IMAC. However, it would have been interesting if the authors had used Zr(IV)-IMAC beads, in addition to the Fe(III)-IMAC beads, to make a comparison with their modified substrates.

Zhou et al. were able to isolate 15 phosphorylated peptides from a 2-pmol α -casein digest using the Zr(IV)-phosphonate-modified silicon plate. (A number of these peptides arise from missed cleavages.) Even though 14 of the phosphorylated

peptides were observed in the conventional MALDI mass spectrum, the modified silicon plate simplified the mass spectrum by practically eliminating all signals due to nonphosphorylated peptides. The Zr(IV)-phosphonate-modified porous silicon probes were highly selective for phosphopeptides from the β - and α -casein digests. However, many of the phosphopeptides from these digests are highly acidic and it would be interesting to see how these modified silicon substrate performed when analyzing other phosphorylated protein digests.

1.4.6.2.5 TiO₂-coated Gold Nanoparticles Immobilized on Glass Plates

As described in section 1.4.3.1, TiO₂ has been previously used for the analysis of phosphopeptides. Lin and coworkers immobilized TiO2-coated gold nanoparticles on a glass plate for analysis of phosphopeptides by MALDI-TOF-MS.¹²⁶

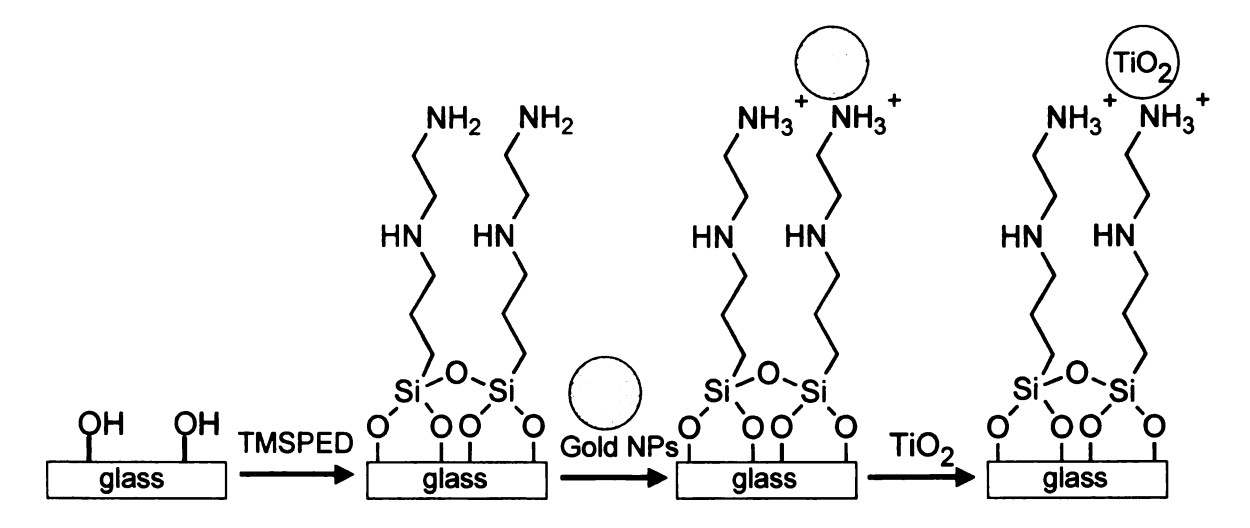


Figure 1.33: Immobilization of gold nanoparticles (NPs) coated with titania on glass substrates. Figure adapted from Lin et al. 126

The scheme in Figure 1.33 shows the fabrication of the TiO₂-gold-nanoparticle (TiO₂-gold-NP) glass plate. Using the Frens method, ¹²⁷ the gold nanoparticles were prepared

with an average bead diameter of 26 nm. To prepare the glass slide for the attachment of the gold nanoparticles. thin film of **TMSPED** (N-[3-(trimethoxysilyl)propyllethylenediamine) was bound to the oxidized glass surface. Gold nanoparticles were then immobilized onto the TMSPED-treated surface, and a solution of titanium isopropoxide was spin coated onto the substrate, followed by annealing. The coverage of the 26-nm diameter gold nanoparticles on the glass slide was estimated to be ~618 nanoparticles/um² (34% coverage). Tryptic digests were applied to the modified glass plates in 500-µL aliquots, and once the sample had incubated for 1 hr, the surface was rinsed to remove unwanted species, and 2,5-DHB containing H₃PO₄ was added. Subsequent MS analysis was carried out using a TOF mass spectrometer.

The TiO₂-gold-NP-modified glass plates were applied to the analysis of β -case in digests containing relatively high amounts of protein (50 pmol and 500 pmol). Three phosphorylated peptides (m/z 3122, 2556, and 2062) were captured and detected using the TiO₂-gold-NP plate, but nonspecific adsorption was observed when the 500-pmol sample (500 μ L of 1- μ M β -case in digest) was analyzed with the modified glass plate. The authors made no comparisons to the conventional analysis of the digests.

Using the modified glass plate, they also analyzed two more complex samples: 1) an equimolar mixture (50 pmol of each) of cytochrome c and β -casein and 2) milk, which contains α -S1-, α -S2-, and β -casein. Interestingly, there were almost no peaks due to peptides from cytochrome c, a nonphosphorylated protein, in the mass spectrum when the equimolar digest mixture was analyzed using the TiO₂-gold-NP-modified glass plate. Milk contains several proteins, including the caseins. The milk digest was applied to the modified plate and 4 phosphopeptides (m/z 3122, 3008, 2556, and 1952), one being due

to chymotrypsin cleavage and one being due to miscleavage of α -S1-casein, were detected. This number of phosphopeptides detected is quite low since α -S1- and α -S2-casein are highly phosphorylated (there are over 20 phosphorylation sites between the two proteins). If all three casein proteins are digested completely (i.e. no miscleavage), then 11 phosphorylated peptides should result. Hence, only 18% of non-miscleaved, phosphorylated peptides were detected in the milk digest using the titania bead-modified target. Conventional MALDI-MS analyses of the digests would be useful for comparison.

1.5 Research Overview

The research described in this dissertation focuses on the design, fabrication, and implementation of polymer-modified MALDI sample plates derivatized with metal affinity complexes for enrichment and analysis of phosphopeptides by mass spectrometry. This direct sampling technique has the potential to reduce sample preparation time and loss of the analyte compared to conventional IMAC-based approaches, and the use of polymer brushes should provide a much higher enrichment capacity than the on-probe enrichment techniques described above. In Chapter Two, immobilization of Fe(III)-nitrilotriacetate-poly(acrylic acid) onto gold plates was demonstrated, and the use of these plates were shown to be highly selective for enrichment of phosphopeptides over nonphosphopetides. Although the binding capacity of these polymer-modified plates was greater than that of monolayer-derivatized plates, higher binding capacity was still needed. To increase the capacity, thicker poly(2-hydroxyethyl methacrylate) brushes grown on gold substrates using atom-transfer radical

polymerization were used. Chapter Three demonstrated the remarkable capacity of derivatized brushes for analyzing phosphoprotein digests, and Chapter Four showed that the percent recovery of phosphopeptides by these systems is around 70%. Lastly, the high-capacity polymer modified plates were compared with commercial IMAC and metal oxide affinity techniques, and these results are in Chapter Four. To compare the techniques, the use of labeled synthetic phosphopeptides for quantitation by MALDI-MS was implemented. The polymer-brush-modified plates show superior performance to all of the commercial techniques we investigated. Chapter Five briefly summarizes the conclusion of this work and points to future research directions.

1.6 References

- (1) Hillenkamp, F.; Peter-Katalinic, J. MALDI MS: A Practical Guide to Instrumentation, Methods and Applications; Wiley-VCH Verlag GmbH & Co.: KGaA, 2007
- (2) Krebs, E. G. Philosophical Transactions of the Royal Society of London Series B-Biological Sciences 1983, 302, 3-11.
- (3) Adams, J. A. Chemical Reviews **2001**, 101, 2271-2290.
- (4) Hunter, T. Cell **2000**, 100, 113-127.
- (5) Johnson, L. N.; Lewis, R. J. Chemical Reviews 2001, 101, 2209-2242.
- (6) Krebs, E. G.; Beavo, J. A. Annual Review of Biochemistry 1979, 48, 923-959.
- (7) Pawson, T.; Nash, P. Genes & Development 2000, 14, 1027-1047.
- (8) Simpson, R. J. Proteins and Proteomics: A Laboratory Manual; Cold Spring Harbor Laboratory Press: Cold Spring Harbor, 2003 Ch. 8.
- (9) Whitmarsh, A. J.; Davis, R. J. Cellular and Molecular Life Sciences 2000, 57, 1172-1183.
- (10) Fischer, E. H.; Krebs, E. G. *Journal of Biological Chemistry* **1955**, *216*, 121-132.
- (11) Walsh, C. T. *Posttranslation Modification of Proteins*; Roberts and Company: Englewood, **2006** 35-36.
- (12) Marks, F. Protein Phosphorylation.; Wiley-VCH Verlag GmbH: KGaA, 1996 269-281.
- (13) Stryer, L. *Biochemistry*; 4th ed.; W.H. Freeman and Company: New York, **1995**
- (14) Siuzdak, G. The Expanding Role of Mass Spectrometry; 2nd ed.; MCC Press: San Diego, 2006
- (15) Watson, J. T. *Introduction to Mass Spectrometry*; Lippencott-Raven Publishing: Philadelphia, **1997**
- (16) Denoyer, E.; Vangrieken, R.; Adams, F.; Natusch, D. F. S. Analytical Chemistry 1982, 54, A26-&.
- (17) Cotter, R. J. Time-of-Flight Mass Spectrometry: Intrumentation and Applications in Biological Research; American Chemical Society: Washington, DC, 1997

- (18) De Hoffmann, E.; Charette, J.; Stroobant, V. Mass Spectrometry Principles and Applications; John Wiley & Sons: Chichester, 1996
- (19) Karas, M.; Bachmann, D.; Hillenkamp, F. Analytical Chemistry 1985, 57, 2935-2939.
- (20) Tanaka, K.; Waki, H.; Ido, Y.; Akita, I. S.; Yoshida, Y.; Yoshida, T. Rapid Communications in Mass Spectrometry 1988, 2, 151-153.
- (21) Strupat, K.; Karas, M.; Hillenkamp, F. International Journal of Mass Spectrometry and Ion Processes 1991, 111, 89-102.
- (22) Beavis, R. C.; Chaudhary, T.; Chait, B. T. *Organic Mass Spectrometry* **1992**, *27*, 156-158.
- (23) Beavis, R. C.; Chait, B. T. Proceedings of the National Academy of Sciences of the United States of America 1990, 87, 6873-6877.
- (24) Simpson, R. J. Purifying Proteins for Proteomics: A Laboratory Manual; Cold Spring Harbor Laboratory Press: Cold Spring Harbor, 2004 Ch. 21.
- (25) Karas, M.; Ingendoh, A.; Bahr, U.; Hillenkamp, F. Biomedical and Environmental Mass Spectrometry 1989, 18, 841.
- (26) Kjellstrom, S.; Jensen, O. N. *Analytical Chemistry* **2004**, *76*, 5109-5117.
- (27) Annan, R. S.; Carr, S. A. Analytical Chemistry 1996, 68, 3413-3421.
- (28) Jonscher, K.; Currie, G.; McCormack, A. L.; Yates, J. R. Rapid Communications in Mass Spectrometry 1993, 7, 20-26.
- (29) Schwartz, J. C.; Bier, M. E. Rapid Communications in Mass Spectrometry 1993, 7, 27-32.
- (30) Todd, R. E. M. a. J. F. J. *Quadrupole Ion Trap Mass Spectrometry*; 2nd ed.; John Wiley & Sons: Hoboken, **2005**; Vol. 165
- (31) Schwartz, J. C.; Senko, M. W.; Syka, J. E. P. Journal of the American Society for Mass Spectrometry 2002, 13, 659-669.
- (32) Douglas, D. J.; Frank, A. J.; Mao, D. M. Mass Spectrometry Reviews 2005, 24, 1-29.
- (33) Church, D. A. Journal of Applied Physics 1969, 40, 3127-&.

- (34) Quarmby, S. T.; Yost, R. A. International Journal of Mass Spectrometry 1999, 191, 81-102.
- (35) Garrett, T. J.; Prieto-Conaway, M. C.; Kovtoun, V.; Bui, H.; Izgarian, N.; Stafford, G.; Yost, R. A. *International Journal of Mass Spectrometry* **2007**, *260*, 166-176.
- (36) Garrett, T. J.; Yost, R. A. Analytical Chemistry **2006**, 78, 2465-2469.
- (37) Liao, P. C.; Leykam, J.; Andrews, P. C.; Gage, D. A.; Allison, J. Analytical Biochemistry 1994, 219, 9-20.
- (38) Meyer, H. E.; Hoffmannposorske, E.; Heilmeyer, L. M. G. Methods in Enzymology 1991, 201, 169-185.
- (39) Hubbard, M. J.; Cohen, P. Trends in Biochemical Sciences 1993, 18, 172-177.
- (40) Craig, A. G.; Hoeger, C. A.; Miller, C. L.; Goedken, T.; Rivier, J. E.; Fischer, W. H. Biological Mass Spectrometry 1994, 23, 519-528.
- (41) Steen, H.; Jebanathirajah, J. A.; Rush, J.; Morrice, N.; Kirschner, M. W. Molecular & Cellular Proteomics 2006, 5, 172-181.
- (42) Asara, J. M.; Allison, J. Journal of the American Society for Mass Spectrometry 1999, 10, 35-44.
- (43) Yang, X. F.; Wu, H. P.; Kobayashi, T.; Solaro, R. J.; van Breemen, R. B. Analytical Chemistry 2004, 76, 1532-1536.
- (44) Janek, K.; Wenschuh, H.; Bienert, M.; Krause, E. Rapid Communications in Mass Spectrometry 2001, 15, 1593-1599.
- (45) Ma, Y. L.; Lu, Y.; Zeng, H. Q.; Ron, D.; Mo, W. J.; Neubert, T. A. Rapid Communications in Mass Spectrometry 2001, 15, 1693-1700.
- (46) Wolfender, J. L.; Chu, F. X.; Ball, H.; Wolfender, F.; Fainzilber, M.; Baldwin, M. A.; Burlingame, A. L. *Journal of Mass Spectrometry* **1999**, *34*, 447-454.
- (47) Hage, D. S. *Handbook of Affinity Chromatography*; 2nd ed.; Taylor & Francis: Boca Raton, **2006**
- (48) Marcus, K.; Immler, D.; Sternberger, J.; Meyer, H. E. *Electrophoresis* **2000**, *21*, 2622-2636.

- (49) Gronborg, M.; Kristiansen, T. Z.; Stensballe, A.; Andersen, J. S.; Ohara, O.; Mann, M.; Jensen, O. N.; Pandey, A. *Molecular & Cellular Proteomics* **2002**, *1*, 517-527.
- (50) Oda, Y.; Nagasu, T.; Chait, B. T. *Nature Biotechnology* **2001**, *19*, 379-382.
- (51) Adamczyk, M.; Gebler, J. C.; Wu, J. Rapid Communications in Mass Spectrometry 2001, 15, 1481-1488.
- (52) Goshe, M. B.; Veenstra, T. D.; Panisko, E. A.; Conrads, T. P.; Angell, N. H.; Smith, R. D. Analytical Chemistry 2002, 74, 607-616.
- (53) Porath, J.; Carlsson, J.; Olsson, I.; Belfrage, G. *Nature* **1975**, *258*, 598-599.
- (54) Hochuli, E.; Dobeli, H.; Schacher, A. Journal of Chromatography 1987, 411, 177-184.
- (55) Posewitz, M. C.; Tempst, P. Analytical Chemistry 1999, 71, 2883-2892.
- (56) Feng, S.; Ye, M. L.; Zhou, H. J.; Jiang, X. G.; Jiang, X. N.; Zou, H. F.; Gong, B. L. *Molecular & Cellular Proteomics* **2007**, *6*, 1656-1665.
- (57) Ficarro, S. B.; McCleland, M. L.; Stukenberg, P. T.; Burke, D. J.; Ross, M. M.; Shabanowitz, J.; Hunt, D. F.; White, F. M. *Nature Biotechnology* **2002**, *20*, 301-305.
- (58) Ndassa, Y. M.; Orsi, C.; Marto, J. A.; Chen, S.; Ross, M. M. *Journal of Proteome Research* **2006**, *5*, 2789-2799.
- (59) Moser, K.; White, F. M. Journal of Proteome Research 2006, 5, 98-104.
- (60) Seeley, E. H.; Riggs, L. D.; Regnier, F. E. Journal of Chromatography B-Analytical Technologies in the Biomedical and Life Sciences 2005, 817, 81-88.
- (61) Nousiainen, M.; Sillje, H. H. W.; Sauer, G.; Nigg, E. A.; Korner, R. Proceedings of the National Academy of Sciences of the United States of America 2006, 103, 5391-5396.
- (62) Nuhse, T. S.; Stensballe, A.; Jensen, O. N.; Peck, S. C. Molecular & Cellular Proteomics 2003, 2, 1234-1243.
- (63) Olsen, J. V.; Blagoev, B.; Gnad, F.; Macek, B.; Kumar, C.; Mortensen, P.; Mann, M. Cell **2006**, 127, 635-648.
- (64) Larsen, M. R.; Thingholm, T. E.; Jensen, O. N.; Roepstorff, P.; Jorgensen, T. J. D. *Molecular & Cellular Proteomics* **2005**, *4*, 873-886.

- (65) Pinkse, M. W. H.; Uitto, P. M.; Hilhorst, M. J.; Ooms, B.; Heck, A. J. R. *Analytical Chemistry* **2004**, *76*, 3935-3943.
- (66) Sano, A.; Nakamura, H. Analytical Sciences 2004, 20, 861-864.
- (67) Sano, A.; Nakamura, H. Analytical Sciences 2004, 20, 565-566.
- (68) Gruhler, A.; Olsen, J. V.; Mohammed, S.; Mortensen, P.; Faergeman, N. J.; Mann, M.; Jensen, O. N. Molecular & Cellular Proteomics 2005, 4, 310-327.
- (69) Dobson, K. D.; McQuillan, A. J. Spectrochimica Acta Part a-Molecular and Biomolecular Spectroscopy 2000, 56, 557-565.
- (70) Blackwell, J. A.; Carr, P. W. Journal of Chromatography 1991, 549, 43-57.
- (71) Blackwell, J. A.; Carr, P. W. *Journal of Chromatography* **1991**, *549*, 59-75.
- (72) Kweon, H. K.; Hakansson, K. Analytical Chemistry 2006, 78, 1743-1749.
- (73) Lo, C. Y.; Chen, W. Y.; Chen, C. T.; Chen, Y. C. *Journal of Proteome Research* **2007**, *6*, 887-893.
- (74) Chen, C. T.; Chen, W. Y.; Tsai, P. J.; Chien, K. Y.; Yu, J. S.; Chen, Y. C. *Journal of Proteome Research* **2007**, *6*, 316-325.
- (75) Chen, C. T.; Chen, Y. C. Analytical Chemistry **2005**, 77, 5912-5919.
- (76) Xu, S. Y.; Zhou, H. J.; Pan, C. S.; Fu, Y.; Zhang, Y.; Li, X.; Ye, M. L.; Zou, H. F. Rapid Communications in Mass Spectrometry 2006, 20, 1769-1775.
- (77) Xu, X. Q.; Deng, C. H.; Gao, M. X.; Yu, W. J.; Yang, P. Y.; Zhang, X. M. *Advanced Materials* **2006**, *18*, 3289-+.
- (78) Zhou, H. L.; Watts, J. D.; Aebersold, R. *Nature Biotechnology* **2001**, *19*, 375-378.
- (79) Thaler, F.; Valsasina, B.; Baldi, R.; Jin, X.; Stewart, A.; Isacchi, A.; Kalisz, H. M.; Rusconi, L. Analytical and Bioanalytical Chemistry 2003, 376, 366-373.
- (80) Lansdell, T. A.; Tepe, J. J. Tetrahedron Letters 2004, 45, 91-93.
- (81) Tao, W. A.; Wollscheid, B.; O'Brien, R.; Eng, J. K.; Li, X. J.; Bodenmiller, B.; Watts, J. D.; Hood, L.; Aebersold, R. *Nature Methods* **2005**, *2*, 591-598.
- (82) Warthaka, M.; Karwowska-Desaulniers, P.; Pflum, M. K. H. ACS Chemical Biology 2006, 1, 697-701.

- (83) Papac, D. I.; Hoyes, J.; Tomer, K. B. Analytical Chemistry 1994, 66, 2609-2613.
- (84) Brockman, A. H.; Orlando, R. Analytical Chemistry 1995, 67, 4581-4585.
- (85) Brockman, A. H.; Orlando, R. Rapid Communications in Mass Spectrometry 1996, 10, 1688-1692.
- (86) Tang, N.; Tornatore, P.; Weinberger, S. R. Mass Spectrometry Reviews 2004, 23, 34-44.
- (87) Thulasiraman, V.; Wang, Z.; Katrekar, A.; Lomas, L.; Yip, T. T. Simultaneous Monitoring of Mulitple Kinase Activities by SELDI-TOF Mass Spectrometry; Humana Press: Totowa, 2004; Vol. 264 205-215.
- (88) Valiokas, R.; Klenkar, G.; Tinazli, A.; Tampe, R.; Liedberg, B.; Piehler, J. Chembiochem 2006, 7, 1325-1329.
- (89) Ataka, K.; Heberle, J. *Biopolymers* **2006**, 82, 415-419.
- (90) Klenkar, G.; Valiokas, R.; Lundstrom, I.; Tinazli, A.; Tampe, R.; Piehler, J.; Liedberg, B. *Analytical Chemistry* **2006**, 78, 3643-3650.
- (91) Ataka, K.; Richter, B.; Heberle, J. Journal of Physical Chemistry B 2006, 110, 9339-9347.
- (92) Tinazli, A.; Tang, J. L.; Valiokas, R.; Picuric, S.; Lata, S.; Piehler, J.; Liedberg, B.; Tampe, R. Chemistry-a European Journal 2005, 11, 5249-5259.
- (93) Johnson, D. L.; Martin, L. L. Journal of the American Chemical Society 2005, 127, 2018-2019.
- (94) Rigler, P.; Ulrich, W. P.; Vogel, H. Langmuir 2004, 20, 7901-7903.
- (95) Maly, J.; Masci, A.; Masojidek, J.; Sugiura, M.; Pilloton, R. Analytical Letters **2004**, *37*, 1645-1656.
- (96) Gamsjaeger, R.; Wimmer, B.; Kahr, H.; Tinazli, A.; Picuric, S.; Lata, S.; Tampe, R.; Maulet, Y.; Gruber, H. J.; Hinterdorfer, P.; Romanin, C. *Langmuir* **2004**, *20*, 5885-5890.
- (97) Lee, J. K.; Kim, Y. G.; Chi, Y. S.; Yun, W. S.; Choi, I. S. *Journal of Physical Chemistry B* **2004**, *108*, 7665-7673.
- (98) Maly, J.; Di Meo, C.; De Francesco, M.; Masci, A.; Masojidek, J.; Sugiura, M.; Volpe, A.; Pilloton, R. *Bioelectrochemistry* **2004**, *63*, 271-275.

- (99) Trammell, S. A.; Wang, L. Y.; Zullo, J. M.; Shashidhar, R.; Lebedev, N. Biosensors & Bioelectronics 2004, 19, 1649-1655.
- (100) Wegner, G. J.; Lee, N. J.; Marriott, G.; Corn, R. M. Analytical Chemistry **2003**, 75, 4740-4746.
- (101) Makower, A.; Halamek, J.; Skladal, P.; Kernchen, F.; Scheller, F. W. Biosensors & Bioelectronics 2003, 18, 1329-1337.
- (102) Rigler, P.; Ulrich, W. P.; Hoffmann, P.; Mayer, M.; Vogel, H. *Chemphyschem* **2003**, *4*, 268-275.
- (103) Luk, Y. Y.; Tingey, M. L.; Hall, D. J.; Israel, B. A.; Murphy, C. J.; Bertics, P. J.; Abbott, N. L. *Langmuir* **2003**, *19*, 1671-1680.
- (104) Kada, G.; Riener, C. K.; Hinterdorfer, P.; Kienberger, F.; Stoh, C. M.; Gruber, H. J. Single Molecules 2002, 3, 119-125.
- (105) Scheibler, L.; Dumy, P.; Stamou, D.; Duschl, C.; Vogel, H.; Mutter, M. *Polymer Bulletin* **1998**, *40*, 151-157.
- (106) Stora, T.; Hovius, R.; Dienes, Z.; Pachoud, M.; Vogel, H. *Langmuir* **1997**, *13*, 5211-5214.
- (107) Sigal, G. B.; Bamdad, C.; Barberis, A.; Strominger, J.; Whitesides, G. M. *Analytical Chemistry* **1996**, *68*, 490-497.
- (108) Shen, J. W.; Ahmed, T.; Vogt, A.; Wang, J. Y.; Severin, J.; Smith, R.; Dorwin, S.; Johnson, R.; Harlan, J.; Holzman, T. Analytical Biochemistry 2005, 345, 258-269.
- (109) Stensballe, A.; Jensen, O. N. Rapid Communications in Mass Spectrometry 2004, 18, 1721-1730.
- (110) Zhou, H. J.; Xu, S. Y.; Ye, M. L.; Feng, S.; Pan, C.; Jiang, X. G.; Li, X.; Han, G. H.; Fu, Y.; Zou, H. *Journal of Proteome Research* **2006**, *5*, 2431-2437.
- (111) Xu, Y. D.; Bruening, M. L.; Watson, J. T. Analytical Chemistry **2004**, 76, 3106-3111.
- (112) Xia, Y. N.; Whitesides, G. M. Angewandte Chemie-International Edition 1998, 37, 551-575.
- (113) Mazur, M.; Krysinski, P.; Blanchard, G. J. Langmuir 2005, 21, 8802-8808.

- (114) Nonglaton, G.; Benitez, I. O.; Guisle, I.; Pipelier, M.; Leger, J.; Dubreuil, D.; Tellier, C.; Talham, D. R.; Bujoli, B. *Journal of the American Chemical Society* **2004**, *126*, 1497-1502.
- (115) Benitez, I. O.; Bujoli, B.; Camus, L. J.; Lee, C. M.; Odobel, F.; Talham, D. R. Journal of the American Chemical Society 2002, 124, 4363-4370.
- (116) Clearfield, A.; Poojary, D. M.; Zhang, B. L.; Zhao, B. Y.; Derecskei-Kovacs, A. Chemistry of Materials 2000, 12, 2745-2752.
- (117) Kumar, C. V.; Chaudhari, A. Journal of the American Chemical Society 2000, 122, 830-837.
- (118) Kohli, P.; Blanchard, G. J. Langmuir 2000, 16, 695-701.
- (119) Nixon, C. N.; Le Claire, K.; Odobel, F.; Bujoli, B.; Talham, D. R. Chemistry of *Materials* **1999**, 11, 965-976.
- (120) Byrd, H.; Whipps, S.; Pike, J. K.; Ma, J. F.; Nagler, S. E.; Talham, D. R. Journal of the American Chemical Society 1994, 116, 295-301.
- (121) Frey, B. L.; Hanken, D. G.; Corn, R. M. Langmuir 1993, 9, 1815-1820.
- (122) Byrd, H.; Pike, J. K.; Talham, D. R. Chemistry of Materials 1993, 5, 709-715.
- (123) Hong, H. G.; Sackett, D. D.; Mallouk, T. E. Chemistry of Materials 1991, 3, 521-527.
- (124) Putvinski, T. M.; Schilling, M. L.; Katz, H. E.; Chidsey, C. E. D.; Mujsce, A. M.; Emerson, A. B. *Langmuir* **1990**, *6*, 1567-1571.
- (125) Lee, H.; Kepley, L. J.; Hong, H. G.; Akhter, S.; Mallouk, T. E. *Journal of Physical Chemistry* **1988**, 92, 2597-2601.
- (126) Lin, H. Y.; Chen, C. T.; Chen, Y. C. Analytical Chemistry 2006, 78, 6873-6878.
- (127) Frens, G. Nature-Physical Science 1973, 241, 20-22.

Chapter Two: Detection of Phosphopeptides Using Fe(III)-Nitrilotriacetate Complexes Immobilized on a MALDI Plate

2.1 Introduction

Protein phosphorylation, a post-translational modification regulated by kinases and phosphatases, is essential for numerous cellular functions such as gene expression and membrane transport, 1-8 so identification of phosphorylation sites is vital to understanding many biochemical processes. While mass spectrometry is a useful technique for identifying such sites, low ionization efficiencies of phosphorylated fragments or a low degree of phosphorylation in a given sample can make detection of phosphorylated species difficult. To overcome this challenge, immobilized metal affinity chromatography (IMAC) can be used to enrich phosphopeptides prior to analysis. IMAC isolates phosphopeptides based on their affinity for a metal-ligand complex that is immobilized on a chromatographic support, and typical complexes for capturing phosphopeptides contain six-coordinate metal ions, such as Fe(III), bound to tetradentate ligands like nitrilotriacetate (NTA). Such complexes have two metal-coordination sites available to bind to a phosphoryl group present on serine, threonine, or tyrosine residues. 12.13

Despite the success of IMAC, the use of this technique complicates analyses and decreases throughput because the sample mixture must be loaded onto a column, rinsed to remove unbound species, and then eluted to collect the fragments of interest. The eluted sample then can be examined by electrospray ionization mass spectrometry or mixed with matrix on a conventional sample plate and analyzed by matrix-assisted laser desorption/ionization mass spectrometry (MALDI-MS). This report describes our efforts

to perform a similar, but simpler, procedure directly on a modified gold MALDI sample plate. We immobilize Fe(III)-NTA complexes on the surface of a MALDI plate, add unpurified sample to the plate for a 5-10 min incubation period, and then rinse the plate to remove unbound peptide fragments along with salts and other contaminants. Subsequent addition of matrix allows analysis by MALDI-MS.

Two previous studies employed a similar approach where IMAC beads were applied to the MALDI probe. 9,15 However, in those methods, phosphopeptides were adsorbed on beads that were subsequently applied to the MALDI probe, so off-probe steps were required. Although MALDI probes modified with arrays of surface spots capable of IMAC are commercially available through Ciphergen, 16 to our knowledge they have not been extensively used for detection of phosphopeptides.

We covalently bind an NTA derivative to the gold MALDI probe surface via derivatization of immobilized poly(acrylic acid) (PAA) as shown in Figure 2.1. This results in a homogeneously derivatized substrate along with a high density of NTA complexes. We recently employed similar PAA-modified MALDI-MS probes (without NTA) to improve the detection of phosphorylated peptides from proteolytic digests. In that case, PAA immobilized on a gold MALDI probe was derivatized with polyethyleneimine or complexed directly with Fe(III) and used as a cationic substrate for the adsorption of phosphopeptides from ovalbumin and β -casein tryptic digests. The experiments described here demonstrate, however, that NTA-modified surfaces exhibit substantially greater signals for a wide range of phosphopeptides than do the Fe(III)-PAA films, as well as greater selectivity over nonphosphorylated peptides. Fe(III)-NTA-modified surfaces are very effective in isolating all phosphopeptides in ovalbumin, β -

casein, and phosphopeptide-doped myoglobin digests. Additionally, we show that 2',4',6'-trihydroxyacetophenone (THAP), a matrix recently used for the analysis of phosphopeptides in conventional MALDI-MS,¹⁹ is a significantly better matrix for these experiments than α -cyano-4-hydroxycinnamic acid (α -CHCA).

2.2 Experimental

2.2.1 Materials and Solutions

Horse skeletal muscle myoglobin, bovine β-casein, and chicken egg ovalbumin were purchased from Sigma and digested using sequencing grade modified trypsin obtained from Promega. Human angiotensin II and phosphorylated angiotensin II, DRVpYIHPF, were acquired from Calbiochem. Chemicals employed in the preparation of surface-modified gold plates were $N_{\alpha}N_{\alpha}$ -bis(carboxymethyl)-L-lysine hydrate (Fluka), FeCl₃ (Spectrum), ethyl chloroformate (Aldrich), 4-methylmorpholine (Aldrich), methanesulfonic acid (Mallinckrodt), and amino-terminated poly(tert-butyl acrylate) (PTBA), which was synthesized as previously reported.²⁰ THAP (Fluka) matrix solutions were prepared by mixing a 10-mg/mL THAP solution in methanol:water (1:1) with an aqueous solution containing 10 mg/mL of diammonium hydrogen citrate (DAHC, J. T. Baker) in a 9:1 ratio. A 10-mg/mL solution of α-CHCA in acetonitrile:0.2% trifluoroacetic acid (1:1) also was combined with the aqueous DAHC solution in a ratio of 9:1 to compare the effects of THAP and α -CHCA on the detection of phosphopeptides. Saturated α-CHCA in acetonitrile:0.2% aqueous trifluoroacetic acid (1:1) was sometimes employed in the detection of phosphoangiotensin.

2.2.2 Protein Digestion

Solutions (10 μ g/ μ L) of horse heart myoglobin, bovine β -casein, and chicken ovalbumin were prepared in 6 M urea containing 50 mM Tris-HCl, and 20- μ L aliquots of these protein solutions were heated in a water bath at 70 °C for 1 hour. For the ovalbumin solution, 5 μ L of 10 mM 1,4-dithio-DL-threitol (DDT) was added prior to heating to cleave the disulfide bond. After cooling, 180 μ L of 50 mM ammonium bicarbonate was added to each protein solution, and a 10- μ L aliquot of 100 mM iodoacetamide was added to the ovalbumin solution, which was placed in the dark for 30 min. Subsequently, 10 μ L of 0.5 μ g/ μ L modified trypsin was added, and the solutions were incubated for ~20 hours at 37 °C. The digestions were quenched with addition of sufficient glacial acetic acid (~12 μ L) to achieve a 5% solution. The final concentrations of myoglobin, β -casein, and ovalbumin in the digests were ~1 μ g/ μ L. No purification of these digest solutions was carried out prior to applying them to unmodified or Fe(III)-NTA-modified gold plates.

2.2.3 Fabrication of Fe(III)-NTA Plates

Gold-coated Si wafers (1.3 x 2.8 cm) were modified with PAA using a previously described method. Briefly, UV/ozone-cleaned wafers were immersed in 1 mM mercaptoundecanoic acid in ethanol for 1 hour to form a monolayer of carboxylic acid groups on the gold surface. These functional groups were activated to form mixed anhydrides by a 10-min immersion in 10 mL of anhydrous *N,N*-dimethylformamide (DMF) to which 100 µL of 4-methylmorpholine and 100 µL of ethyl chloroformate were added. After rinsing and drying, the wafers were immediately placed in a solution of

amino-terminated PTBA (0.4 mg in 12 mL DMF) for 1 hour, and hydrolysis of immobilized PTBA to PAA was carried out using 1% methanesulfonic acid in CH_2Cl_2 for 10 minutes. In some cases, a second layer of PAA was attached to the previously grafted polymer using the same procedure. To attach an amino-terminated NTA derivative $(N_{co}N_{co}-bis(carboxymethyl)-L-lysine hydrate)$ to PAA, a rinsed and dried film was activated using 4-methylmorpholine and ethyl chloroformate as described above for activation of the monolayer. After rinsing with ethyl acetate and drying with N₂, the activated wafer was immersed for 1 hour in aqueous 0.1 M $N_{co}N_{co}-bis(carboxymethyl)-L-lysine hydrate that was adjusted to pH 10 with NaOH; rinsed with water; and dried with N₂. Lastly, the NTA-modified substrate was placed in an aqueous 100 mM FeCl₃ solution for 30 minutes, rinsed with ethanol, and dried using N₂. The attachment of Fe(III)-NTA to PAA is depicted in Figure 2.1.$

2.2.4 Sample Preparation for Analysis by MALDI-MS

Solutions containing phosphoangiotensin/angiotensin or 1-ug/µL protein digests were applied to the Fe(III)-NTA-modified wafers by spreading 20 or 40 µL of solution over the entire 3.6 cm²-surface and drying with a gentle stream of nitrogen gas for 5-10 minutes, at which time all of the solvent had evaporated. The plate was rinsed with 4-6 acid mL of appropriate solution (25 mMaqueous acetic for angiotensin/phosphoangiotensin mixtures, 50 mM acetic acid containing 30% acetonitrile angiotensin-spiked myoglobin digests, and 3:30:67 glacial acid:acetonitrile:water for proteolytic digests) to remove unbound species, and flowing N₂ was used to remove any remaining rinsing solution and to dry the wafer completely. Matrix solution was spotted in 0.2- to 0.5- μ L aliquots on these substrates and allowed to crystallize before using superglue to secure the gold-modified wafers on a commercial MALDI plate (Applied Biosystems) that had been altered with a 32 x 29 x 0.5-mm cavity to accommodate the modified wafers in the mass spectrometer. In conventional MALDI experiments, 1 μ L of protein digest was added directly to the sample well of a 64-well, gold plate (Applied Biosystems), and addition of 1 μ L of matrix immediately followed. The volume of sample applied to the metal-affinity plates was larger than in conventional MALDI because there are no sample wells on the surface of the modified wafers. To compare the sensitivity of the modified plates with that of conventional wells, we normalized the amount of sample added to that covering the same area as a conventional sample well (2 mm diameter, 0.031 cm²). For example, when 40 μ L of a solution containing 60 pmol/ μ L of both angiotensin and phosphoangiotensin was spotted on the Fe(III)-NTA-modified wafer (1.3 x 2.8 cm), we estimated that 20 pmol of each peptide was actually applied to an area of 0.031 cm².

2.2.5 Instrumentation and Data Analysis

Analyses by MALDI-MS were carried out using a PerSeptive Biosystems Voyager STR MALDI TOF mass spectrometer. The instrument utilized a pulsed nitrogen laser (337-nm, 3-nanosecond pulses at 3 Hz) and was operated in the linear mode. The user-selected parameters included an accelerating voltage of 20 kV for the detection of positive ions, an intermediate source grid voltage that is 94% of the accelerating voltage, a guide wire voltage that is opposite bias and 0.05% in magnitude of the accelerating voltage, and an extraction delay time of 100 ns. MALDI mass spectra

resulting from 150 or more laser pulses were collected and averaged for each acquisition. and signals were assigned to specific peptides using Protein Prospector (http://prospector.ucsf.edu). Calibration was performed using intense peaks corresponding to identified peptides. The MALDI mass spectra shown here are representative of the data. Each experiment was repeated three times or more using different modified plates. Occasionally, a spot of matrix on the modified plates crystallized in dense sheets and vielded little to no signal only in the analyses of ovalbumin digests. However, this occurred in less than 25% of cases. The thicknesses of polymer films on modified plates were determined using a rotating analyzer spectroscopic ellipsometer (J. A. Woollam, M-44), assuming a film refractive index of 1.5. Reflectance FTIR spectra of the modified plates were collected using a Nicolet Magna 560 spectrophotometer with a Pike grazing angle (80°) accessory. photoelectron spectroscopy measurements were carried out using a Physical Electronics PHI-5400 ESCA workstation with a polychromatic Mg x-ray operating at 300 W and 15 kV with a take-off angle of 45°.

a) S
$$\stackrel{\text{H}}{\longrightarrow}$$
 R $\stackrel{\text{NH}_2}{\longrightarrow}$ A-methylmorpholine ethyl chloroformate b) S $\stackrel{\text{H}}{\longrightarrow}$ R $\stackrel{\text{NH}_2}{\longrightarrow}$ N_a-bis(carboxymethyl)-L-lysine (pH 10) C $\stackrel{\text{H}}{\longrightarrow}$ R = (CH₂)₂NHCO(CH₂)₂C(CN)(CH₃)

Figure 2.1: Immobilization of Fe(III)-NTA complexes onto a gold-coated substrate. Surface modification: a) immobilized PAA, b) activated PAA, c) NTA-derivatized PAA, and d) Fe(III)-NTA complex.

2.3 Results and Discussion

2.3.1 Fabrication and Characterization of Fe(III)-NTA-Modified Plates

Each step during the fabrication of the modified plates (Figure 2.1) was monitored using reflectance FTIR spectroscopy. The FTIR spectra in Figure 2.2 confirm the attachment of NTA to PAA and the formation of the Fe(III) complexes on a gold plate. In Figure 2.2a, the most intense peak in the spectrum (1730 cm⁻¹) is due to the acid carbonyl group of PAA immobilized on the gold substrate. Activation of PAA results in the formation of mixed anhydrides as depicted in Figure 2.1b and gives rise to carbonyl absorbances at 1810 and 1770 cm⁻¹ in the IR spectrum (Figure 2.2b). Anhydrides readily react with primary amine groups, such as that in $N_{\alpha}N_{\alpha}$ -bis(carboxymethyl)-L-lysine (amino-terminated NTA) to form amides as shown in Figure 2.1c, but prior studies suggest that only ~50% of the anhydride groups actually react to form amides, as represented by the stoichiometry of y to z in Figure 2.1c.²⁰ The yield in derivatization with amino-terminated NTA might be even lower because derivatization with this compound had to be performed in aqueous solutions at pH 10 due to its low solubility in organic solvents. At this pH, a significant fraction of the mixed anhydrides may hydrolyze back to carboxylate groups. In the IR spectrum of NTA-derivatized films, the broad peak around 1660 cm⁻¹ (Figure 2.2c) is due primarily to the carboxylate groups of NTA.²¹ Unfortunately, the broad carboxylate peak of NTA overlaps with the acid carbonyl peak of PAA, precluding direct estimation of the yield of the derivatization reaction from the decrease in the intensity of the PAA acid carbonyl stretch. However, the carboxylate absorbance of water-rinsed NTA-PAA films is about 1.5-fold greater than that for deprotonated PAA films before derivatization, and this would suggest a derivatization yield of about 50%. (A water rinse leaves NTA in the deprotonated state, but protonates PAA.)

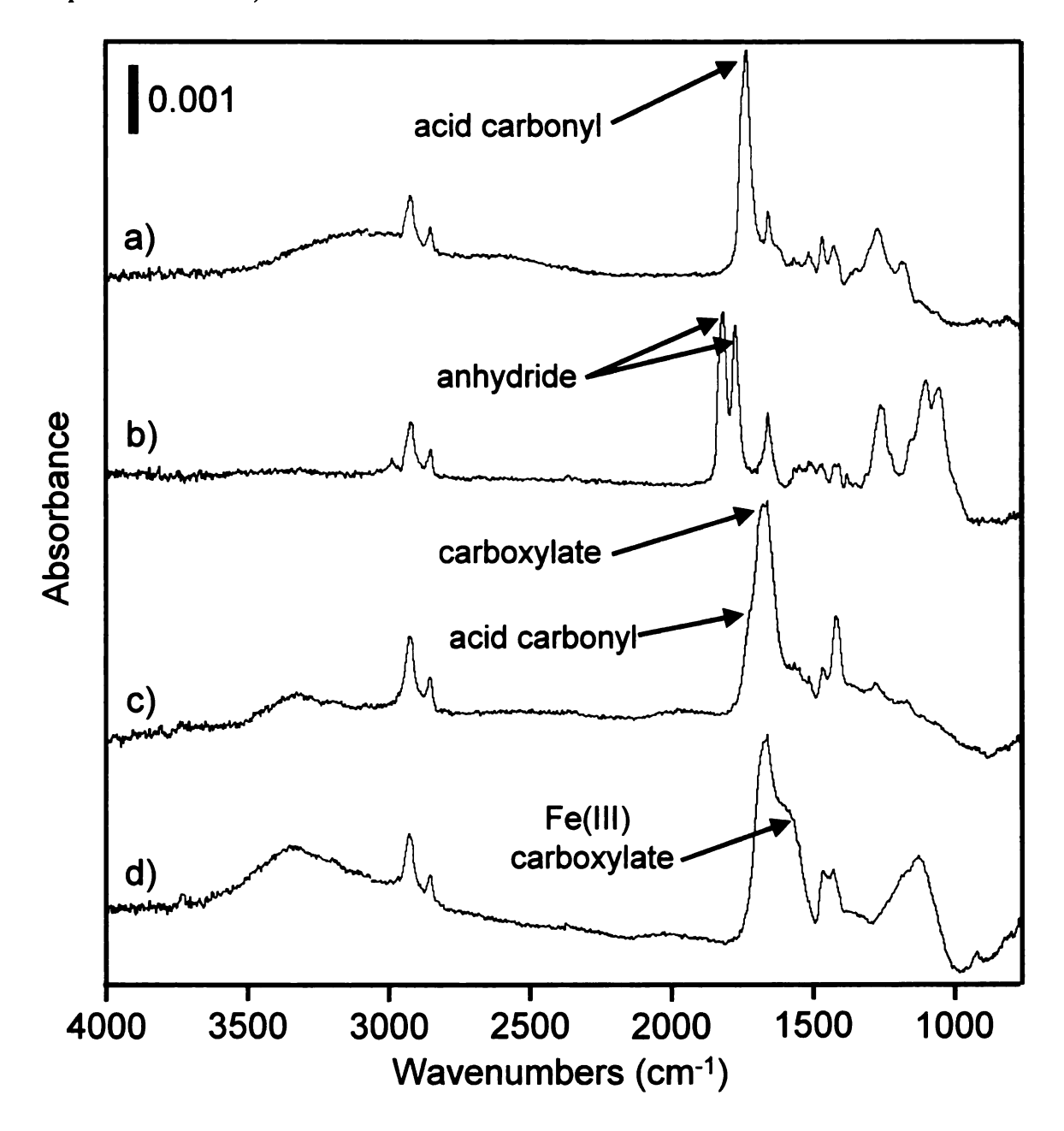


Figure 2.2: Reflectance FTIR spectra of PAA films after different steps during functionalization of these films with Fe(III)-NTA: a) immobilized PAA, b) activated PAA, c) NTA-derivatized PAA, and d) immobilized Fe(III)-NTA-PAA.

When the NTA-modified plate was exposed to a ferric chloride solution, a shoulder appeared at ~1585 cm⁻¹ (Figure 2.2d), suggesting the formation of the Fe(III)-NTA

complex. Absorbances from Fe(III)-PAA complexes also could contribute to this peak, but NTA is a much stronger Fe(III) binder than PAA. Deconvolution of the carboxylate/acid carbonyl absorbances from 1480 to 1800 cm⁻¹ into two peaks with maxima at 1668 and 1580 cm⁻¹ suggests that about 50% of the carboxylate/carboxylic acid groups in these films form complexes with Fe(III). (This rough estimation neglects possible amide absorbances and assumes that acid carbonyl peaks and carboxylates have similar extinction coefficients.) X-ray photoelectron spectroscopy of 2-layer PAA films showed a Fe to O ratio of 1:11, implying that about 60% of the total carboxylate/carboxylic acid groups in these films (from both NTA and PAA) bind Fe(III) (assuming a stoichiometry of three carboxylate groups to one Fe(III), no water in the film, and a 50% yield in derivatization of PAA with NTA). Thus, the FTIR and XPS data provide similar values for the fraction of carboxylate/carboxylic acid groups binding to Fe(III).

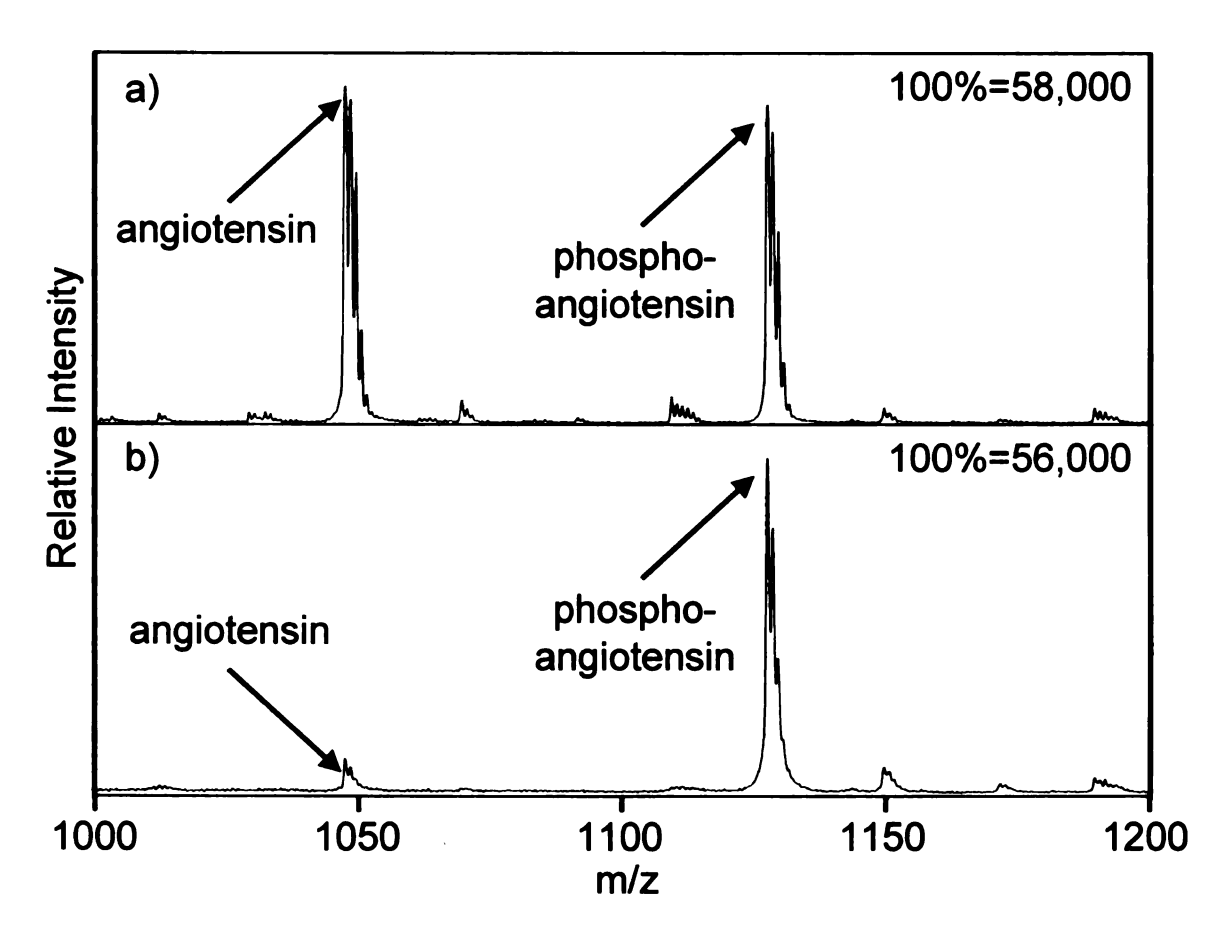


Figure 2.3: Positive ion MALDI mass spectra of a mixture of 2 pmol of angiotensin and 2 pmol of phosphoangiotensin obtained using a) Fe(III)-NTA-modified gold and b) conventional gold plates. After the peptide mixture was applied to the modified plate, a rinse with 25 mM acetic acid was used to remove angiotensin. The matrix was saturated α -CHCA.

2.3.2 Analysis of Phosphoangiotensin by MALDI-MS

Our initial MALDI-MS experiments examined whether Fe(III)-NTA-derivatized probes could selectively capture phosphoangiotensin from simple, equimolar phosphoangiotensin/angiotensin mixtures. The equimolar solutions were applied directly to the modified probes, rinsed with acetic acid solutions, and dried. The addition of matrix to these films created spot diameters of about 2 mm, and the MALDI mass spectrum (Figure 2.3a) of a mixture containing 2 pmol of each peptide (per spot diameter

of 2 mm) shows peak intensities for phosphoangiotensin (m/z 1126) that are approximately 10-fold greater than those for angiotensin (m/z 1046). In contrast, the conventional MALDI (unmodified gold probe, no rinse) mass spectrum in Figure 2.3b shows approximately equal signals for the two peptides. Even when a solution containing 20 fmol of each peptide (per spot diameter of 2 mm) was analyzed, the peak associated with phosphorylated angiotensin was still 10-fold greater than the nonphosphorylated counterpart on surface-modified sample probes, while conventional MALDI-MS yielded comparable signals for both species.

To test whether this selectivity can be maintained during analysis of a more complex mixture, a tryptic myoglobin digest containing urea, Tris-HCl, and ammonium bicarbonate was spiked with an equimolar mixture of angiotensin and phosphoangiotensin. Without prior sample purification, the mixture was applied to the surface-modified Fe(III)-NTA plate. The stability of Fe(III)-NTA films at acidic pH and in organic solvents allows for tailoring of the rinsing protocol to remove hydrophilic as well as hydrophobic nonphosphorylated peptides. To decrease the number of peptides remaining on the surface from the myoglobin digest, 30% acetonitrile was used in the acetic acid rinsing solution. Figure 2.4 shows a conventional MALDI mass spectrum of this peptide mixture along with a spectrum obtained using a Fe(III)-NTA-modified plate. The most intense peak in the mass spectrum obtained using the modified plate (Figure 2.4a) is due to phosphoangiotensin, whose signal was at least 6.5-fold greater than that for angiotensin and 3.5-fold greater than any signal due to peptides from the myoglobin digest. In contrast, the conventional MALDI mass spectrum (Figure 2.4b) shows similar signals for angiotensin and phosphoangiotensin as well as even more intense peaks for some of the peptides of the digested myoglobin. Even when the sample contained 100-fold more myoglobin than phosphoangiotensin (20 pmol myoglobin, 200 fmol phosphoangiotensin, spectrum not shown), the signal for phosphoangiotensin was twice that of the most intense peak due to a myoglobin fragment, while the corresponding phosphoangiotensin signal in conventional MALDI was difficult to detect.²² At a 1000:1 ratio of myoglobin to phosphoangiotensin (20 pmol myoglobin, 20 fmol phosphoangiotensin, spectrum not shown), the signal for phosphoangiotensin was about the same intensity as those for myoglobin fragments when using the modified plates, and conventional MALDI showed no phosphoangiotensin signal.²³ These data suggest that low amounts of phosphorylation in a given protein can be readily detected. However, in extremely large excesses of background protein compared to phosphorylated species, such as might be found in whole-cell extracts, the modified MALDI plates may not be capable of revealing low-level phosphorylated species.

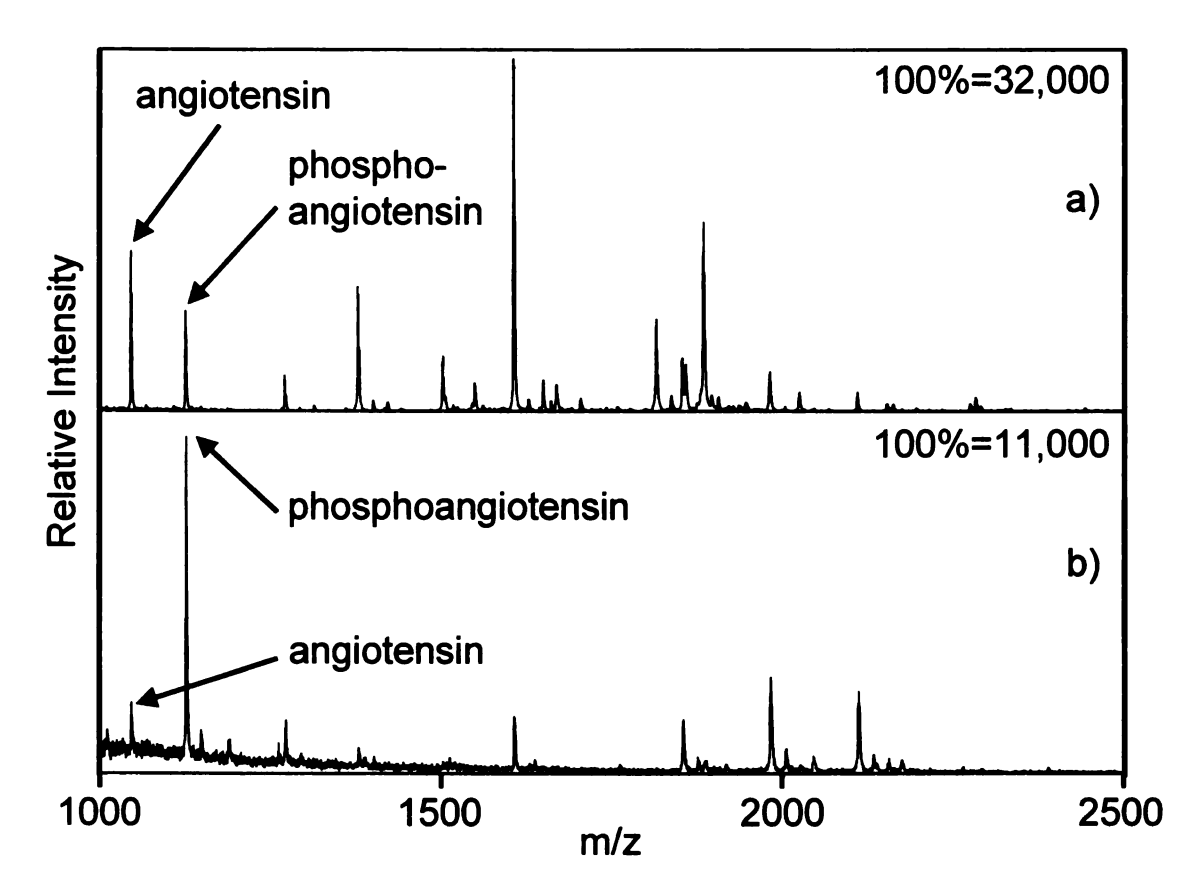


Figure 2.4: Positive ion MALDI mass spectra of a 10-pmol myoglobin digest spiked with 1 pmol of angiotensin and 1 pmol of phosphoangiotensin. The spectra were obtained using a) a Fe(III)-NTA-modified plate and b) a conventional gold plate. After the peptide mixture was applied to the surface-modified plate, it was rinsed with 50 mM acetic acid in 30% acetonitrile prior to the addition of saturated α -CHCA

As seen in Figure 2.4a, five nonphosphorylated peptides from the myoglobin digest were retained on the NTA-modified surface after rinsing with the acid solution. All of these peptides contain one or more histidine residues and at least one acidic residue, so one is tempted to infer that these amino acids are important in binding to the Fe(III)-NTA complexes. However, 6 out of the 8 fragments seen in conventional MALDI (mass range of m/z 1000 to 5000) contain at least one histidine and one acidic residue, and two of these 6 peptides did not appear in the spectrum obtained using the modified plate. Thus, it is not possible to draw a conclusion as to whether peptides

containing histidine and acidic residues are more difficult to remove from the modified plate.

2.3.3 Analysis of Phosphoprotein Digests by MALDI-MS

We also studied the utility of the modified probes in analyzing digests of two phosphorylated proteins, β-casein and ovalbumin. β-casein is a pentaphosphorylated protein frequently used to test methods for detection of phosphorylated peptides. Tryptic digestion of this protein yields three phosphorylated fragments, one monophosphorylated peptide (FQpSEEQQQTEDELQDK, [M+H]⁺ at m/z 2063), and two tetraphosphorylated peptides (ELEELNVPGEIVEpSLpSpSpSEESITR, [M+H]⁺ at m/z 2967, and RELEELNVPGEIVEpSLpSpSpSEESITR, [M+H]⁺ at m/z 3124). As shown in Figure 2.5, use of the Fe(III)-NTA-modified probe allowed detection of all three phosphopeptides, while use of conventional MALDI afforded a signal only for the monophosphopeptide. The most intense peaks in the mass spectrum obtained with the modified probe were due to the tetraphosphorylated peptides, and these peaks were at least 6.5-fold and 4-fold greater than any signals assigned to nonphosphorylated peptides. (Peaks neighboring the signals of the tetraphosphopeptides correspond to adduct ions, primarily [M+Na]⁺ and [M+K]⁺, of these two phosphorylated species. Additionally. there is a peak 43 m/z units higher than the peaks for each of the two $[M+H]^{+}$ corresponding to the tetraphosphorylated peptides, which may be due to carbamylation of the peptides. Heating of protein digests containing urea can lead to this modification.²³ Frequently, there is also a peak 55 ± 1 m/z units higher than the peak for each of the singly-protonated peaks assigned to the tetraphosphorylated peptides, which is possibly

due to an iron adduct). Even the signal intensity for the monophosphopeptide on the metal-affinity plate was as a minimum 2-fold greater than any signals associated with the nonphosphorylated β-casein fragments. However, the absolute signal for this peptide dropped by a factor of 2.5 relative to that in the conventional MALDI mass spectrum in Figure 2.5a. Because the peptide-binding capacity of the metal affinity plate is limited, signals due to peptides that ionize well in conventional MALDI will generally be greater in conventional MALDI-MS than when applying the modified plate and a rinsing protocol. The advantages of the Fe(III)-NTA-modified plates lie in analyzing phosphorylated peptides that are difficult to detect in conventional MALDI-MS and in decreasing the number of signals due to nonphosphorylated species, thereby simplifying spectral interpretation.

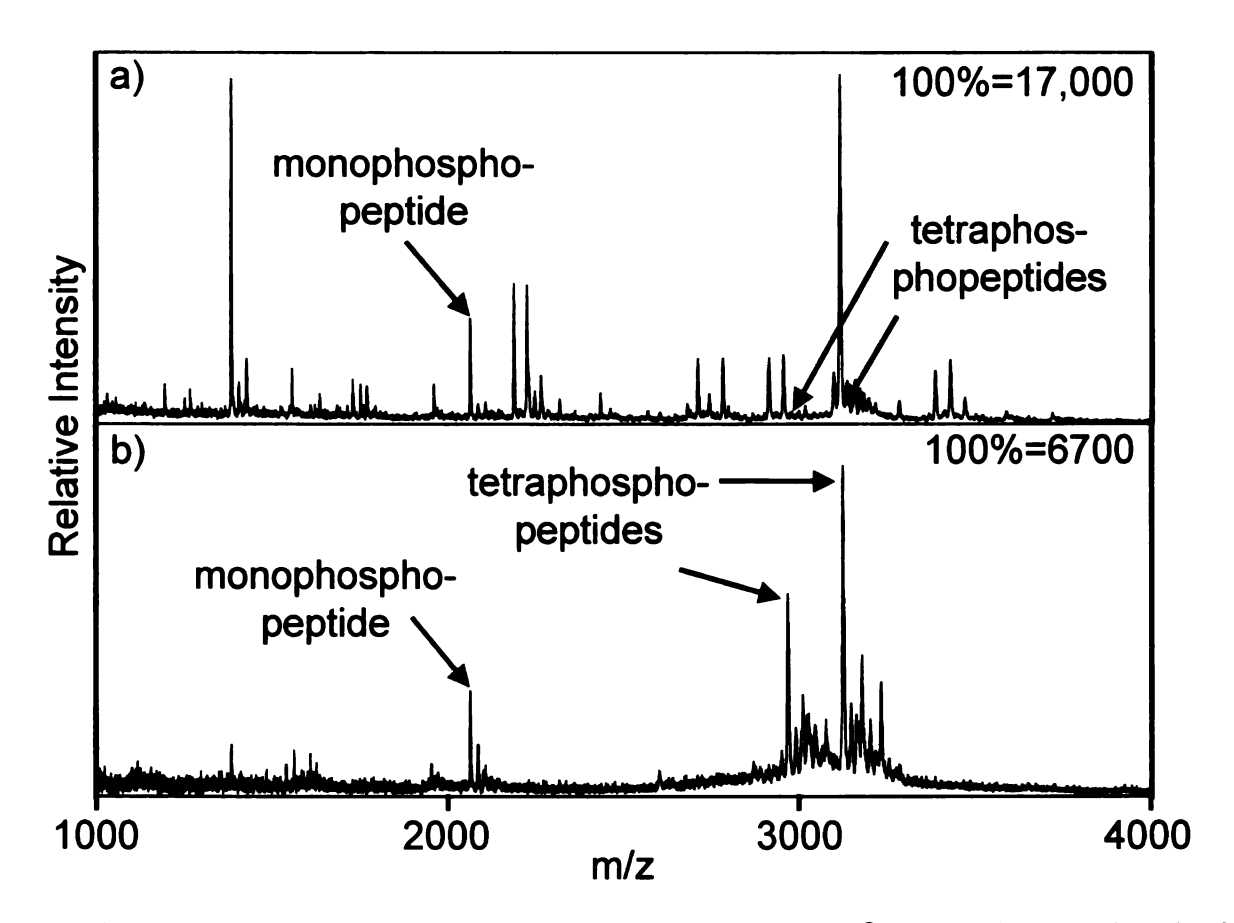


Figure 2.5: Positive ion MALDI mass spectra of a 7-pmol β -casein digest analyzed using a) conventional gold and b) Fe(III)-NTA-modified gold plates. After the peptide mixture was applied to the modified plate, it was rinsed with acetic acid in 30% acetonitrile prior to addition of THAP/DAHC.

Ovalbumin is an example of a diphosphorylated protein that contains a disulfide bond. Reduction of the disulfide bond is essential for formation of one monophosphorylated peptide (L63-R85) as well as four nonphosphorylated species. Thus, DTT and iodoacetamide were added to ovalbumin digests for the respective cleavage of the disulfide bond and the carbamidomethylation of the resulting cysteine residues. Compared to the β-casein digest, the ovalbumin sample should be more challenging to analyze for phosphopeptides because it contains both an increased number of tryptic fragments and two additional reagents, DTT and iodoacetamide, that could interfere with the binding of phosphorylated peptides to surface-modified plates. Analysis of the ovalbumin digest by conventional MALDI-MS resulted in detection of three monophosphorylated peptides at m/z 2090 (EVVGpSAEAGVDAASVSEEFR), 2513 2903 (LPGFGDpSIEAQCGTSVNVHSSLR), and (FDKLPGFGDpSIEAQCGTSVNVHSSLR) as indicated in Figure 2.6a. Although the conventional mass spectrum shows signals due to all of the expected phosphorylated peptides in the mixture, use of the Fe(III)-NTA-modified plate greatly simplifies identification of the monophosphorylated peptides by virtually eliminating all signals due to nonphosphorylated species (Figure 2.6b). The strongest signal at m/z 2090 was up to 13-fold greater than that of any nonphosphorylated fragment when the Fe(III)-NTA plate was used. Even the weakest phosphopeptide signal at m/z 2903 was usually 1.5-times greater than any signals attributed to nonphosphorylated peptides adsorbed to the modified plate. These experiments show that the binding of the phosphorylated peptides to the Fe(III)-NTA-modified surface was not prohibited by the presence of DTT and iodoacetamide, nor did these reagents damage the surface-modified plate.

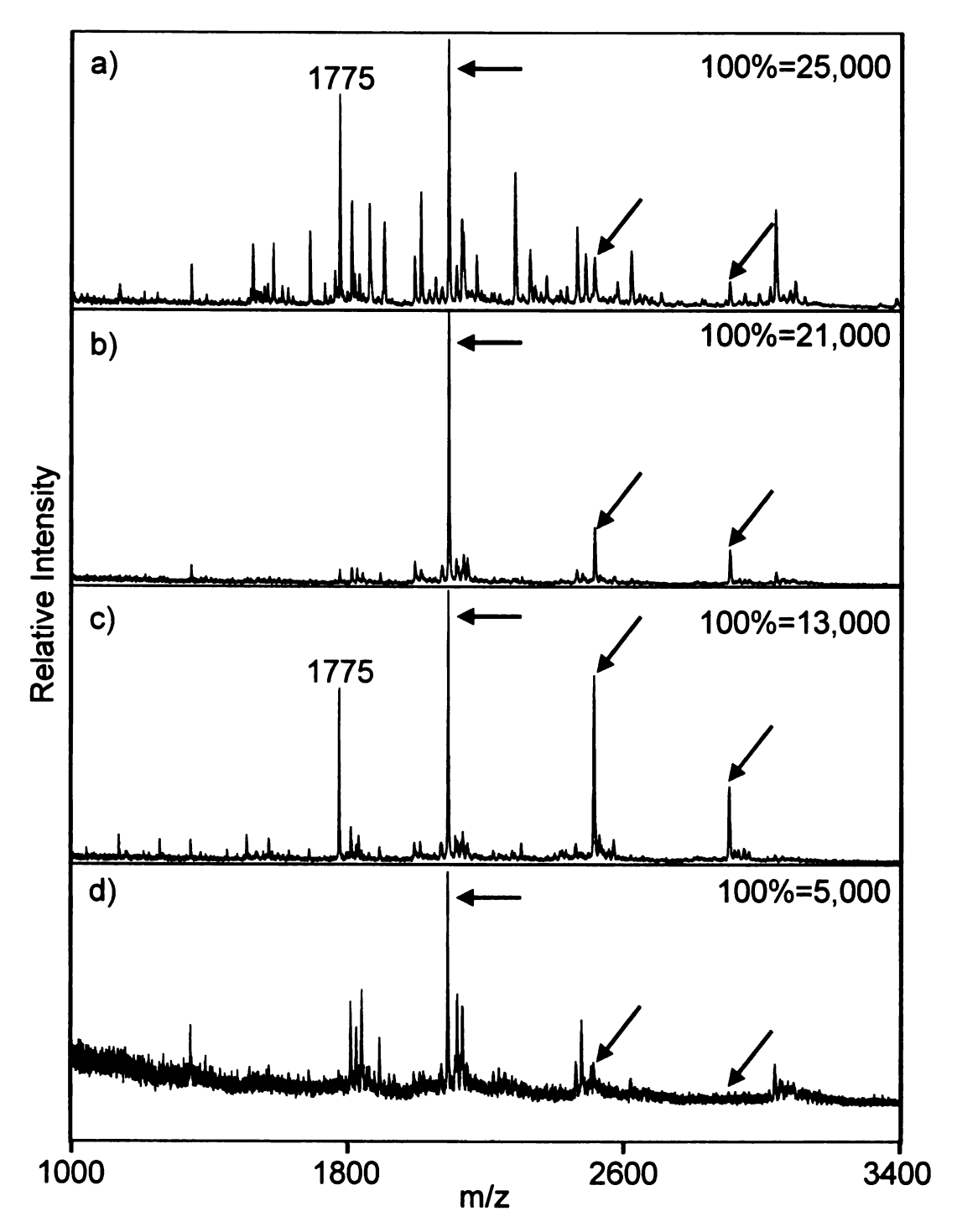


Figure 2.6: Positive ion MALDI mass spectra of a 3.8-pmol ovalbumin digest analyzed using a) conventional gold, b) Fe(III)-NTA-PAA-modified (30 Å thickness) gold, and c) Fe(III)-NTA-PAA-modified (90 Å thickness) gold plates. Spectrum d) was obtained using a 6.5-pmol ovalbumin digest and a Fe(III)-PAA-modified gold plate. After the peptide mixtures were applied to the modified plates, they were rinsed with acetic acid in 30% acetonitrile prior to addition of THAP/DAHC. The arrows indicate peaks corresponding to phosphorylated peptides at m/z 2090, 2513, and 2903.

The thickness of the NTA-derivatized films on the gold substrate can be increased by grafting additional PAA layers prior to attachment of the amino-terminated NTA derivative. 24.25 Increasing the thickness of the Fe(III)-NTA-polymer film should augment the number of binding sites available for capture of phosphopeptides and, perhaps, yield greater signal intensities for these species during analysis by MALDI-MS. To form a second grafted layer of PAA, amino-terminated PTBA is attached to previously immobilized, activated PAA, and then hydrolyzed using methanesulfonic acid as described in the experimental section. Two layers of Fe(III)-NTA-derivatized PAA had a thickness of 80-100 Å, whereas a single layer of PAA modified with the affinity complex had a thickness of about 30 Å. Additional layers of PAA can be attached as desired. We investigated the use of multilayer Fe(III)-NTA-PAA-modified films with thicknesses from 80 Å up to 500 Å for the detection of phosphopeptides in an ovalbumin digest by MALDI-MS. Plates modified with a Fe(III)-NTA-PAA film that was 90 Å thick showed a modest increase in signal for the ovalbumin phosphopeptides at m/z 2513 and 2903 along with a slightly smaller signal at m/z 2090 (Figure 2.6c) compared to the previously used plates modified with a 30-Å thick film (Figure 2.6b). Films with thicknesses greater than 90 Å did not show a significant improvement in capturing phosphopeptides, and results were similar to those shown in Figure 2.6c. One drawback to the performance of thicker films was that they gave a relatively strong signal for a nonphosphorylated peptide at m/z 1775 (Figure 2.6c). Most likely the amino acid sequence of this peptide is ISQAVHAAHAEINEAGR, which contains two histidine and two glutamic acid residues, which as discussed above, could have some affinity for Fe(III)-NTA complexes. 13,26,27 Increasing the thickness of the film may have created an excess of Fe(III)-NTA sites that allowed this particular nonphosphorylated peptide to bind. If desired, glutamic acid, aspartic acid, histidine, and cysteine residues could be derivatized to minimize their adsorption, 11.28.29 but this would detract from the advantages of rapid analysis using surface-modified plates.

Overall, increasing the thickness of Fe(III)-NTA-PAA films does not substantially improve the performance of the modified plates. To better understand this phenomenon, we utilized reflectance FTIR spectroscopy to examine the degree of phosphoangiotensin binding to Fe(III)-NTA-PAA films with different numbers of PAA layers. Exposure of a plate modified with a single layer of Fe(III)-NTA-PAA film to a 1.2 mM solution of phosphoangiotensin in 5% acetic acid resulted in a surface coverage of about 800 fmol/mm². This coverage was determined by calibrating the amide absorbance due to adsorbed phosphoangiotensin using a plot of ellipsometric thickness versus the absorbance due to spin-coated bovine serum albumin. (The amide absorbance per thickness should be essentially independent of the protein, and we assumed a film density of 1 g/cm³.) Most importantly, on going from 1 to 3 layers of Fe(III)-NTA-PAA, the amide peak intensity at 1670-1680 cm⁻¹ increased by only ~25%. These data suggest that binding occurs primarily at the film surface to yield monolayer coverages when using high concentrations of phosphoangiotensin. Exposure of the modified plate to matrix solution followed by rinsing with water and ethanol, resulted in the disappearance of the amide absorbance, suggesting that the matrix removes essentially all of the phosphoangiotensin from the film. Unfortunately, the relatively low sensitivity of infrared studies does not allow an examination of binding at lower phosphoangiotensin concentrations that would be more relevant to analysis. Still, these data suggest that

thicker Fe(III)-NTA-PAA films will not provide substantially increased levels of phosphoangiotensin binding.

As mentioned in the introduction, we previously employed Fe(III) complexes of PAA (no NTA present) to capture phosphorylated peptides. Figure 2.6d shows, however, that these films are inferior to Fe(III)-NTA-PAA films for capturing phosphopeptides. Not only were the signals more than 2-fold greater for the phosphorylated peptides when the Fe(III)-NTA-PAA plate, rather than the Fe(III)-PAA plate, was used, but all three of the peptides were detected. With the Fe(III)-PAA-modified probe, one of the phosphorylated peptides (m/z 2903) was not detected and another one (m/z 2513) was difficult to distinguish from the surrounding background and the more intense peaks due to nonphosphorylated peptides (Figure 2.6d).³⁰ Furthermore, when a β-casein digest was analyzed using both Fe(III)-PAA- and Fe(III)-NTA-PAA-modified plates, the monophosphorylated peptide was seldom detected with Fe(III)-PAA probes, and the signals for the tetraphosphorylated peptides were also not as intense as when using Fe(III)-NTA-PAA films. The superior performance of the Fe(III)-NTA-PAA films may result from stronger interactions between Fe(III) and NTA than between Fe(III) and PAA, which could result in less leaching of Fe(III) from the NTA film. A comparable trend was observed when Fe(III)-iminodiacetic acid and Fe(III)-NTA resins were compared for isolating phosphopeptides using IMAC. 15,31 The NTA resin was more specific for phosphopeptide adsorption than iminodiacetic acid (IDA) because of the higher affinity between NTA and Fe(III). 15,32 The logarithms of the stability constants for Fe(III)-NTA and Fe(III)-IDA complexes are roughly 15.9 and 10.7, respectively, whereas the corresponding value for a Fe(III)-carboxylate complex similar to PAA, Fe(III)-(acetate)₃, is only 8.3.³²

2.3.4 Comparison of THAP and α -CHCA as Matrices for Phosphopeptide Detection on Modified Plates

Recent work showed that the use of THAP in acetonitrile/water mixed with DAHC yielded enhanced detection of phosphopeptides from β-casein and cardiac troponin I protein digests relative to analysis with an α -CHCA matrix.¹⁹ Thus, we compared THAP and α-CHCA matrices for detection of phosphorylated peptides from modified plates. However, the THAP matrix that we employed was prepared in 1:1 methanol/water to allow better crystallization of THAP/DAHC on the modified plates. Figure 2.7 shows mass spectra of an ovalbumin digest obtained using a surface-modified plate and α -CHCA or THAP matrices. When using an unsaturated solution of α -CHCA mixed with DAHC, two of the peaks due to the phosphorylated peptides from the ovalbumin digest were difficult to detect, and they were nearly an order of magnitude less intense than when using the THAP/DAHC matrix. Even the intensity of the strongest signal due to a monophosphorylated peptide was 2-fold greater when using THAP than when using α -CHCA as a matrix. Additionally, a saturated α -CHCA matrix solution worked well for the detection of phosphoangiotensin on modified plates, but when the same matrix was applied to the analysis of the phosphorylated protein digests, little, if any, signal for the phosphopeptides could be detected using surface-modified plates.

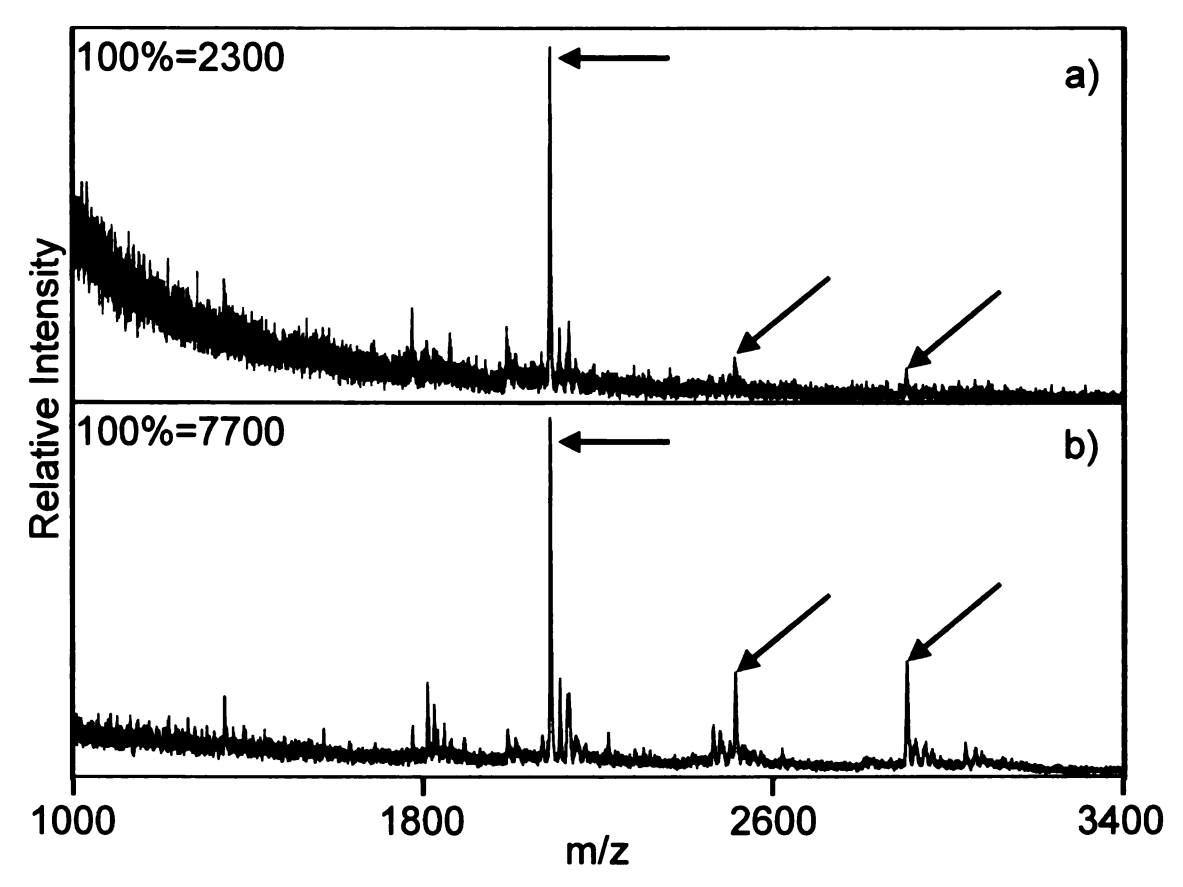


Figure 2.7: Positive ion MALDI mass spectra of a 7.3-pmol ovalbumin digest analyzed using the Fe(III)-NTA-modified gold plate with different matrices: (a) α -CHCA/DAHC and (b) THAP/DAHC. After the peptide mixture was applied to the modified plates, they were rinsed with acetic acid in 30% acetonitrile. The arrows indicate peaks corresponding to phosphopeptides at m/z 2090, 2513, and 2903.

2.4 Conclusions

The Fe(III)-NTA-modified plates allow enrichment of phosphopeptides from protein digests without prior sample purification. A simple, acidic rinsing-step removes most nonphosphorylated peptides and digestion reagents from the plate, while phosphopeptides remain bound to the immobilized Fe(III)-NTA complexes. Notably, all three phosphopeptides, including mono- and tetraphosphorylated species, derived from β -casein were detected using the NTA-modified plate, while the two tetraphosphorylated peptides were not observed in the MALDI mass spectrum when a conventional plate was

employed. Utilization of the modified plate also decreases or eliminates signals due to nonphosphorylated peptides during analysis by MALDI-MS. Finally, the use of a THAP matrix mixed with DAHC enhances the detection of the phosphorylated peptides relative to that observed when using the α -CHCA matrix. The combination of the THAP matrix and the modified Fe(III)-NTA plate provides a simple, rapid method for the detection of phosphopeptides during analysis of proteolytic digests by MALDI-MS.

2.5 References

- (1) Adams, J. A. Chemical Reviews **2001**, 101, 2271-2290.
- (2) Hunter, T. Cell 2000, 100, 113-127.
- (3) Johnson, L. N.; Lewis, R. J. Chemical Reviews **2001**, 101, 2209-2242.
- (4) Krebs, E. G. Philosophical Transactions of the Royal Society of London Series B-Biological Sciences 1983, 302, 3-11.
- (5) Krebs, E. G.; Beavo, J. A. Annual Review of Biochemistry 1979, 48, 923-959.
- (6) Pawson, T.; Nash, P. Genes & Development 2000, 14, 1027-1047.
- (7) Simpson, R. J. *Proteins and Proteomics: A Laboratory Manual*; Cold Spring Harbor Laboratory Press: Cold Spring Harbor, **2003**.
- (8) Whitmarsh, A. J.; Davis, R. J. Cellular and Molecular Life Sciences 2000, 57, 1172-1183.
- (9) Raska, C. S.; Parker, C. E.; Dominski, Z.; Marzluff, W. F.; Glish, G. L.; Pope, R. M.; Borchers, C. H. *Analytical Chemistry* **2002**, *74*, 3429-3433.
- (10) Stensballe, A.; Andersen, S.; Jensen, O. N. *Proteomics* **2001**, *1*, 207-222.
- (11) Zeller, M.; Konig, S. Analytical and Bioanalytical Chemistry 2004, 378, 898-909.
- (12) Hochuli, E.; Dobeli, H.; Schacher, A. Journal of Chromatography 1987, 411, 177-184.
- (13) Holmes, L. D.; Schiller, M. R. Journal of Liquid Chromatography & Related Technologies 1997, 20, 123-142.
- (14) Ueda, E. K. M.; Gout, P. W.; Morganti, L. Journal of Chromatography A 2003, 988, 1-23.
- (15) Zhou, W.; Merrick, B. A.; Khaledi, M. G.; Tomer, K. B. *Journal of the American Society for Mass Spectrometry* **2000**, *11*, 273-282.
- (16) Merchant, M.; Weinberger, S. R. *Electrophoresis* **2000**, *21*, 1164-1177.
- (17) Xu, Y. D.; Bruening, M. L.; Watson, J. T. Analytical Chemistry 2004, 76, 3106-3111.

- (18) Xu, Y. D.; Watson, J. T.; Bruening, M. L. Analytical Chemistry 2003, 75, 185-190.
- (19) Yang, X. F.; Wu, H. P.; Kobayashi, T.; Solaro, R. J.; van Breemen, R. B. Analytical Chemistry 2004, 76, 1532-1536.
- (20) Bruening, M. L.; Zhou, Y. F.; Aguilar, G.; Agee, R.; Bergbreiter, D. E.; Crooks, R. M. *Langmuir* **1997**, *13*, 770-778.
- (21) The FTIR spectrum in Figure 2.2c was taken after rinsing the film with water, and under these conditions PAA films show a predominant peak at 1730 cm⁻¹ and negligible absorbance due to carboxylates.
- (22) This analysis employed THAP as a matrix.
- (23) McCarthy, J.; Hopwood, F.; Oxley, D.; Laver, M.; Castagna, A.; Righetti, P. G.; Williams, K.; Herbert, B. *Journal of Proteome Research* **2003**, *2*, 239-242.
- (24) Zhou, Y. F.; Bruening, M. L.; Bergbreiter, D. E.; Crooks, R. M.; Wells, M. Journal of the American Chemical Society 1996, 118, 3773-3774.
- (25) Zhou, Y. F.; Bruening, M. L.; Liu, Y. L.; Crooks, R. M.; Bergbreiter, D. E. Langmuir 1996, 12, 5519-5521.
- (26) Andersson, L. International Journal of Biochromatography 1996, 2, 25-36.
- (27) Andersson, L.; Porath, J. Analytical Biochemistry 1986, 154, 250-254.
- (28) Ficarro, S.; Chertihin, O.; Westbrook, V. A.; White, F.; Jayes, F.; Kalab, P.; Marto, J. A.; Shabanowitz, J.; Herr, J. C.; Hunt, D. F.; Visconti, P. E. Journal of Biological Chemistry 2003, 278, 11579-11589.
- (29) Ficarro, S. B.; McCleland, M. L.; Stukenberg, P. T.; Burke, D. J.; Ross, M. M.; Shabanowitz, J.; Hunt, D. F.; White, F. M. *Nature Biotechnology* **2002**, *20*, 301-305.
- (30) Better detection of the phosphopeptides occurred with Fe(III)-PAA films when these coatings were used as 0.2-mm diameter spots on hydrophobic plates with a different matrix.¹⁸ However, those results showed more intense signals due to nonphosphorylated species compared to signals of phosphopeptides and were still inferior to those detected when using Fe(III)-NTA-PAA-modified plates.
- (31) Neville, D. C. A.; Rozanas, C. R.; Price, E. M.; Gruis, D. B.; Verkman, A. S.; Townsend, R. R. *Protein Science* **1997**, *6*, 2436-2445.

(32) Martell, A. E.; Smith, R. M. *Critical Stability Constants*; Plenum Press: New York; Vol. 2 **1974**, 118 & 142, and Vol. 3 **1977**, 5.

Chapter Three: High-capacity Polymer Brushes Immobilized onto a MALDI Plate for the Analysis of Phosphopeptides by MS

3.1 Introduction

Chapter Two described modification of MALDI plates using poly(acrylic acid) films that were grafted to a gold surface and then modified with Fe(III)-NTA complexes. The "grafting to" approach typically yields rather thin films with low chain densities because after grafting a few chains to the surface, it is difficult for additional chains to access reactive sites. This chapter describes modification of MALDI plates using a "grafting from" technique, where polymerization occurs from initiators that are anchored to a substrate. The "grafting from" technique results in thicker films than "grafting to" methods because small monomers are readily capable of diffusing to growing polymer chains (Figure 3.1) These thicker films should have outstanding capacity for selective enrichment of phosphopeptides, due to their large number of binding sites. In addition to briefly presenting the "grafting from" procedure that we employed, which has been demonstrated by our group and others, this chapter examines the utility of "grafted from" polymer films in enriching phosphopeptides for MALDI-MS analysis. The films allow selective detection of tryptic phosphopeptides with low femtomole detection limits and minimal sample preparation.

m = monomer

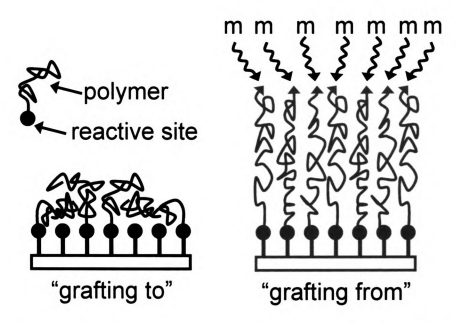


Figure 3.1: Cartoon of "grafting to" versus "grafting from" methods of film growth.

Although many types of polymerization can be used to grow polymers from surfaces, we utilized surface-initiated atom transfer radical polymerization (ATRP) to rapidly grow thick polymers onto gold substrates (i.e. MALDI plates). Further derivatization of these polymer-modified plates with NTA complexes of Fe(III) yields substrates capable of binding phosphopeptides from proteolytic digests. ATRP was developed by Matyjaszewski and Sawamoto in 1995, ^{1,2} and is attractive for polymerization from surfaces for several reasons, most notably for its controlled growth of polymers and use of simple, commercially-available transition-metal catalysts (copper complexes) and initiators (alkyl halides).³ The controlled growth leads to polymers with a narrow molecular weight distribution,⁴ which is ideal for growing uniform polymer brushes on surfaces. The basis of this controlled growth is a low concentration of active

chain ends, due to the fact that the rate of activation of dormant halogen-terminated chain ends by oxidation of Cu(I) is much slower than the reverse reaction (Figure 3.2). Because termination is second order with respect to radical concentration, a low radical concentration favors polymerization over termination, and gives a relatively constant polymerization rate. Additional information on transition metal catalyzed ATRP can be found in an extensive review (covers literature published 1995-2000) by Matyjaszewski.⁴

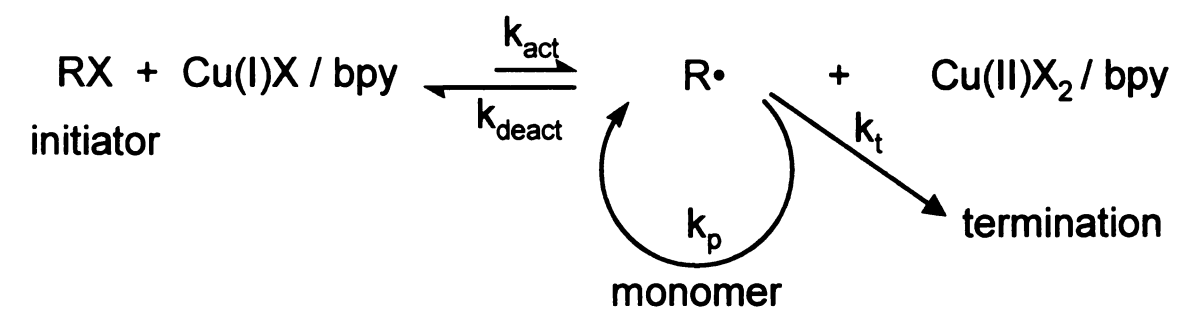


Figure 3.2: General mechanism for transition-metal-catalyzed ATRP (scheme adapted from Matyjaszewski, Chemical Reviews 2001, 101, 2921-2990). k_{act} , k_{deact} , k_p , and k_t are the rate constants for activation, deactivation, polymerization, and termination, respectively.

In the late 1990's, a number of groups demonstrated surface-initiated ATRP using polymerization temperatures of 90 °C and higher.⁵ However, such temperatures are incompatible with some substrate-initiator systems such as thiols on gold.⁶⁻⁹ To overcome this problem, Kim et al. showed that surface-initiated ATRP could be implemented at room temperature when using highly active Cu(I) complexes that were first used by Matyjaszewski in solution polymerization. Solvent also plays a critical role in the rate of ATRP, and water can greatly accelerate polymer growth.¹⁰ Using water as a solvent, Wang et al. used ATRP to grow poly(2-hydroxyethyl methacrylate) (PHEMA) films with thicknesses of several hundred nanometer in just a few hours at room temperature. Others have also demonstrated water-accelerated ATRP.^{11,12}

Using these rapid polymerization methods, our group grew PHEMA films on flat surfaces and in membranes and showed that immobilized PHEMA derivatized with Cu(II)-NTA and Ni(II)-NTA complexes is capable of binding the equivalent of many monolayers of protein. 13-15 Most recently, Jain et al. purified His-tagged proteins using Ni(II)-NTA-PHEMA-modified alumina membranes. 15 The research presented here focuses on using PHEMA films modified with a different complex, Fe(III)-NTA, to capture phosphopeptides from proteolytic digests for direct analysis by MALDI-MS. The use of Fe(III)-NTA-PHEMA-modified MALDI plates for enriching phosphopeptides is very simple and similar to the procedure described in Chapter Two: phosphoprotein digest is applied to the Fe(III)-NTA-PHEMA-modified plate, 2) the plate is rinsed thoroughly with an acetic acid/acetonitrile solution to remove nonphosphorylated peptides as well as any salts or other reagents from the digest, and 3) 2,5-dihydroxybenzoic acid (2,5-DHB) matrix solution containing phosphoric acid is applied to the plate and dried for subsequent analysis using MALDI-MS. 2,5-DHB both elutes the phosphopeptides and serves as a matrix, and was chosen in part because Hart et al. previously showed that 2,5-DHB is effective in eluting phosphopeptides from beads derivatized with Fe(III)-NTA. 16 This chapter demonstrates that this simple procedure yields remarkable specificity and low detection limits in the analysis of phosphopeptides found in tryptic digests of phosphorylated proteins.

3.2 Experimental

3.2.1 Materials and Solutions

Bovine β-casein and chicken egg ovalbumin were purchased from Sigma and digested using sequencing grade modified trypsin obtained from Promega. Other reagents employed in the digestion include Tris-HCl (Invitrogen), urea (J.T. Baker), 1,4dithio-DL-threitol (BioChemika), iodoacetamide (Sigma), and ammonium bicarbonate (Columbus Chemical Industries). Anhydrous methanol (Mallinckrodt) and acetyl chloride (Aldrich) were used for the methyl esterification of the protein digests. Human phosphorylated angiotensin II, DRVpYIHPF, was acquired from Calbiochem. Goldcoated Silicon wafers (Silicon Quest International) were prepared by sputter coating the Si with 20 nm of Cr and subsequently 200 nm of gold. The coating was performed by Lance Goddard Associates, Foster City, CA. The reagents employed in the preparation of surface-modified gold plates were 11-mercaptoundecanol (Aldrich), triethylamine (Jade Scientific), 2-bromoisobutyryl bromide (Aldrich), 2-hydroxyethyl methacrylate (Aldrich), cuprous chloride (Aldrich), cupric bromide (Aldrich), 2,2'-bipyridine (Aldrich), succinic anhydride (J.T. Baker), 4-dimethylaminopryridine (Sigma), N-(3-Ndimethylaminopropyl)-N'-ethylcarbodiimide hydrochloride (Sigma), hydroxysuccinimide (Aldrich), $N_{\alpha}N_{\alpha}$ -bis(carboxymethyl)-L-lysine hydrate (Fluka), ferric chloride hexahydrate (Sigma), and glacial acetic acid (Spectrum). Dimethylformamide (DMF, Spectrum) was dried using 3-Å molecular sieves (Spectrum), and deionized water was obtained using a Millipore purification system (Milli-Q, 18 MΩcm). HPLC grade acetonitrile (EMD), HPLC grade methanol (Sigma), isopropyl alcohol (EMD), and ammonium hydroxide (Columbus Chemical Industries) were used to clean the conventional stainless steel MALDI plate according to Thermo's "deep cleaning" procedure. In this cleaning, the plate was rinsed with isopropanol and methanol, sonicated for 10 min in a solution containing 451 mL of acetonitrile, 451 mL of water, and 108 mL of NH₄OH, and finally rinsed with methanol and water and dried. To create a hydrophobic surface on the plate, HPLC grade hexane (J.T. Baker) was rubbed over the plate using a cotton swab, which was then rinsed with hexane and dried and stored in a nitrogen glove bag when not in use. The matrix used in all MS experiments was 2,5-DHB (Aldrich) in 1:1 HPLC grade acetonitrile (EMD):1% aqueous phosphoric acid (Aldrich). For conventional MALDI analyses, 1 µL of 10 mg/mL 2,5-DHB solution was applied to the sample wells and mixed on-plate with the protein digest, while for analyses carried out with the polymer-modified plates, 0.25 µL of 40 mg/mL 2,5-DHB solution was added to the sample wells on top of 1 uL of 1% o-phosphoric acid. The solution employed to rinse the polymer-modified plates prior to matrix addition was 3:30:67 acetic acid:acetonitrile:water.

3.2.2 Protein Digestion and Methyl Esterification

In protein digestion, twenty 100 μ g samples of each phosphoprotein (bovine β -casein and chicken ovalbumin) were dissolved separately in 20 μ L of 6 M urea containing 50 mM Tris-HCl, (5 μ g/ μ L). These protein solutions were heated in a water bath at 70 °C for 1 hour. To treat all digests equally, even though β -casein does not contain disulfide linkages, 5 μ L of 10 mM 1,4-dithio-DL-threitol (DDT) was added to the protein solutions prior to heating to cleave any disulfide bonds. After cooling, 160 μ L of 50 mM ammonium bicarbonate was added to each protein solution, and a 10- μ L aliquot

of 100 mM iodoacetamide was added to the solutions, which were placed in the dark for 1 h. Subsequently, 10 μL of 0.5 μg/μL modified trypsin was added to each protein, and the solutions were incubated for ~ 16 hours at 37 °C. The digestions were quenched with addition of sufficient glacial acetic acid ($\sim 11 \mu L$) to achieve a 5% solution. Half of the digests were dispensed into Eppendorff tubes in aliquots of ~20 μL, yielding 100 10-μg samples of each protein, and these were stored in a -70 °C freezer until use. The other half of the samples were dried using a Speedvac, and then methyl esterified using methanolic HCl. Methanolic HCl was prepared by slowly adding 2.4 mL of acetyl chloride dropwise into 15 mL of anhydrous methanol. The dried 50-µg samples were dissolved in 200 µL of methanolic HCl and incubated for 2 h at room temperature. The methyl esterified digests were separated into 100 samples, then dried using a Speedvac, and stored in a -70 °C freezer until use. Digests were diluted in 5% acetic acid (or dissolved in 5% acetic acid in the case of methyl esterified digests) prior to applying them to the Fe(III)-NTA-PHEMA-modified or conventional MALDI plates. Typically, DTT is removed prior to application to the IMAC material since it is a strong reducing agent that can interfere with the affinity resin (i.e. it can reduce the metal ion), ^{17,18} but we did not remove it from the digest or perform any other purification prior to application to the polymer-modified plates.

3.2.3 Fabrication of Fe(III)-NTA-PHEMA-modified Plates

Gold-coated Si wafers (1.3 x 2.8 cm) were UV/ozone-cleaned and immersed in 1 mM 11-mercaptoundecanol (MUD) in ethanol overnight (1 h was also used) to form a monolayer of MUD onto the gold surface. The wafers were rinsed with ethanol and

water and dried completely with a stream of nitrogen gas. Typically, 8 wafers were simultaneously prepared at a given time and then placed in a crystallizing dish inside a N₂-filled glove bag. In the glove bag, triethylamine (0.33 mL in 20 mL DMF) was added to the crystallizing dish, followed by addition of 2-bromoisobutyryl bromide (0.25 mL/20 mL DMF) dropwise, over 10 min. The wafers were then rinsed with DMF, ethyl acetate, ethanol, and water and dried with a stream of nitrogen (the presence of an ester carbonyl peak at ~1730 cm⁻¹ in the reflectance FTIR spectrum was used to verify the attachment of the initiator to the MUD SAM). In a Schlenk flask, 30 mL of 2-hydroxyethyl methacrylate (HEMA) and 30 mL of deionized water were degassed using freeze-pumpthaw-pump cycling. After three cycles, 165 mg CuCl, 108 mg CuBr₂, and 640 mg of bpy were added to the flask and an additional three freeze-pump-thaw-pump cycles were performed. The flask was transferred to a N₂ glove bag, and the solution was equally added to four 20-mL scintillation vials containing two wafers each. The desired thickness of PHEMA was determined by the length of time the wafers were immersed in HEMA solution. Typically, wafers immersed in the HEMA solution for 2 h resulted in PHEMA film thickness of 25-30 nm. The PHEMA brushes were removed from the vials, rinsed with DMF, water, and ethanol, and characterized using reflectance FTIR spectroscopy. These films were then immersed in 10 mL of DMF containing 0.1 g succinic anhydride and 0.2 g of 4-dimethylaminopryridine (DMAP) and heated at 55 °C for 3 h in order to convert the hydroxyl groups of PHEMA to carboxylic acid groups. These films were sonicated in DMF for 10 min, followed by rinsing with water and ethanol and drying with N_2 . The carboxylic acid groups were activated using N-(3dimethylaminopropyl)-N'-ethylcarbodiimide hydrochloride (EDC, 96 mg) and N-

hydroxysuccinimide (NHS, 58 mg) in 10 mL of water for 30 min, followed by an ethanol and water rinse and drying with N₂. To immobilize NTA onto the films, the wafers were immersed in an aqueous solution of 0.1 M $N_{\alpha}N_{\alpha}$ -bis(carboxymethyl)-L-lysine hydrate, an amino-terminated NTA derivative, with a pH of 10 (NaOH was used to adjust the pH) for 1 h. The films were rinsed thoroughly with water and dried using N₂. The NTA-Fe(III) complex was formed by immersing the films into an aqueous solution of 100 mM FeCl₃ for 30 min and then rinsing with ethanol and drying using N_2 . The films were additionally immersed in a solution of 250 mM acetic acid/30% acetonitrile for 15 min and rinsed with ethanol to remove any loosely bound ferric ions. The immobilization of Fe(III)-NTA-PHEMA onto gold wafers is depicted in Figure 3.3. All the steps during the fabrication process were monitored using reflectance FTIR spectroscopy. Initially, the wafer was cut to the dimensions of the sample holder (1.3 x 2.8 cm) of the FTIR instrument. In order for the wafer to fit into the modified stainless steel MALDI sample plate (this plate is machined to hold standard microscope slides with dimensions of 2.5 cm x 7.5 cm x 0.1 cm), the wafers were cut to fit the width (2.5 cm) of the plate. Sample wells were made by lightly scratching 2-mm diameter circles onto the wafer using a tungsten carbide-tipped pen and a mask with an array of circles. Six wells on one wafer were created in this fashion, and these wells were capable of holding a maximum of 2-3 μL of aqueous solution. The wafers were secured to the modified stainless steel MALDI sample plate using double-sided tape. 19

3.2.4 Quantitation of Phosphopeptide Binding Using Ellipsometry. Three gold wafers modified with Fe(III)-NTA-PHEMA films with thicknesses of 61, 55, and 66 nm were immersed in phosphoangiotensin II (pA) solutions in a 33 mm-diameter Petri dish for 1 h. The solutions contained 0.002, 0.003, 0.004, 0.005, 0.01, 0.05, 0.1, or 0.2 mg pA/mL in 5% acetic acid. After incubation in one of the pA solutions, the wafers were rinsed thoroughly with 15 mL of 3:30:67 acetic acid:acetonitrile:water, followed by 6 mL of 250 mM acetic acid in 30% acetonitrile and drying with a stream of nitrogen. Thicknesses were then determined in triplicate using ellipsometry. The wafers were rinsed with ethanol and dried with nitrogen, and thicknesses were measured once again. The amount of bound pA was assumed to be directly proportional to the increase in ellipsometric thickness after exposure to the pA solution. In all cases, the amount bound to the surface was less than 10% of the amount of peptide initially in solution. Between different pA solutions, the films were immersed in ethylenediaminetetraacetic acid (EDTA, Aldrich) solution (50 mM, pH 7.3) for 30 min to remove Fe(III) and pA, rinsed with water and immersed in 250 mM acetic acid in 30% acetonitrile for 15 minutes, followed by rinsing with ethanol and drying with nitrogen. The film was regenerated by exposure to 100 mM FeCl₃, followed by rinsing with ethanol, drying with nitrogen, a 15-minute immersion in 250 mM acetic acid in 30% acetonitrile, and drying with nitrogen. Thicknesses were measured using the ellipsometer. The films were rinsed with ethanol and thicknesses were measured again. Thickness differences were calculated both after the 250 mM acetic acid in 30% acetonitrile rinse and after the ethanol rinse and averaged. Results after the two rinses were similar. A nonphosphorylated angiotensin II solution of 0.2 mg/mL in 5% acetic acid was used as a control, and was applied to three Fe(III)-NTA-PHEMA brushes as described for pA.

3.2.5 Protocol for Using the Polymer-modified MALDI Plates

For the analysis of protein digests, 1 μ L of the solution was spotted into the 2-mm diameter well of the Fe(III)-NTA-PHEMA-modified plate. For all the analyses presented in this chapter, the samples were incubated on the polymer-modified plate for 1 h, rinsed with 15-20 mL of 3:30:67 glacial acetic acid:acetonitrile:water solution, and dried with a stream of N_2 to remove any remaining rinse solution. (During incubation, 0.5- μ L aliquots of 5% acetic acid were periodically added to the droplet to compensate for evaporation.) After incubation, a 1- μ L droplet of 1% phosphoric acid was added to each well immediately followed by 0.25 μ L of 40-mg/mL 2,5-DHB solution (1:1 acetonitrile:1% phosphoric acid). Upon crystallization of the matrix, the wafer was secured to the modified stainless steel MALDI sample plate as described previously for subsequent MS analysis.

3.2.6 Instrumentation and Data Analysis

MALDI mass spectra shown here are representative of many similar spectra, as each experiment was repeated three times or more using different modified plates. All mass spectra shown in this chapter were obtained using a MALDI linear ion trap mass spectrometer (Thermo vMALDI LTQ XL), and peptide sequencing was made possible using low energy collision-induced dissociation (CID). Protein Prospector (http://prospector.ucsf.edu) was used to make preliminary assignments to signals in the

mass spectra, and assignments were confirmed using CID tandem mass spectrometry. The Protein Prospector website was also used to help confirm assignments of product ions observed in the tandem mass spectra. Typically, MS/MS, wideband MS/MS, and MS³ were implemented for the characterization and sequencing of phosphopeptides. The thicknesses of polymer films on modified plates were determined using a rotating analyzer spectroscopic ellipsometer (J. A. Woollam, M-44), assuming a film refractive index of 1.5. Reflectance FTIR spectra of the modified plates were collected using a Nicolet Magna 560 spectrophotometer with a Pike grazing angle (80°) accessory.

3.3 Results and Discussion

3.3.1 Synthesis and Characterization of Fe(III)-NTA-PHEMA-modified Plates

Figure 3.3 shows the procedure for preparing the Fe(III)-NTA-PHEMA-modified MALDI plates. The fabrication steps are: adsorption of a monolayer of mercaptoundecanol on gold (1), formation of an immobilized initiator (2), growth of PHEMA brushes (3), conversion of PHEMA to a film containing carboxylic acid groups (4), creation of an active ester (5), reaction with aminobutyl NTA to give an immobilized NTA derivative (6), and formation of the Fe(III)-NTA complex (7). The film formation process is complicated by the fact that ATRP is generally not compatible with carboxylic acid-containing monomers since the carboxylic acid groups will complex with metal ions, changing their catalytic properties. In 2006, Bao et al. used surface-initiated ATRP to grow 150-nm thick poly(tert-butyl acrylate) (PTBA) onto gold surfaces in only 5 min. This was followed by 10-min hydrolysis using methanesulfonic acid that yielded 60-nm thick poly(acrylic acid) (PAA) films.²⁰ This 15-min method for growing and

functionalizing polymer films with carboxylic acid groups could be an improvement over our method, which takes ~6 h. It would be even nicer to use a method where a carboxylic acid-containing monomer could be polymerized directly, but the exploration of these ideas is beyond the scope of this dissertation.

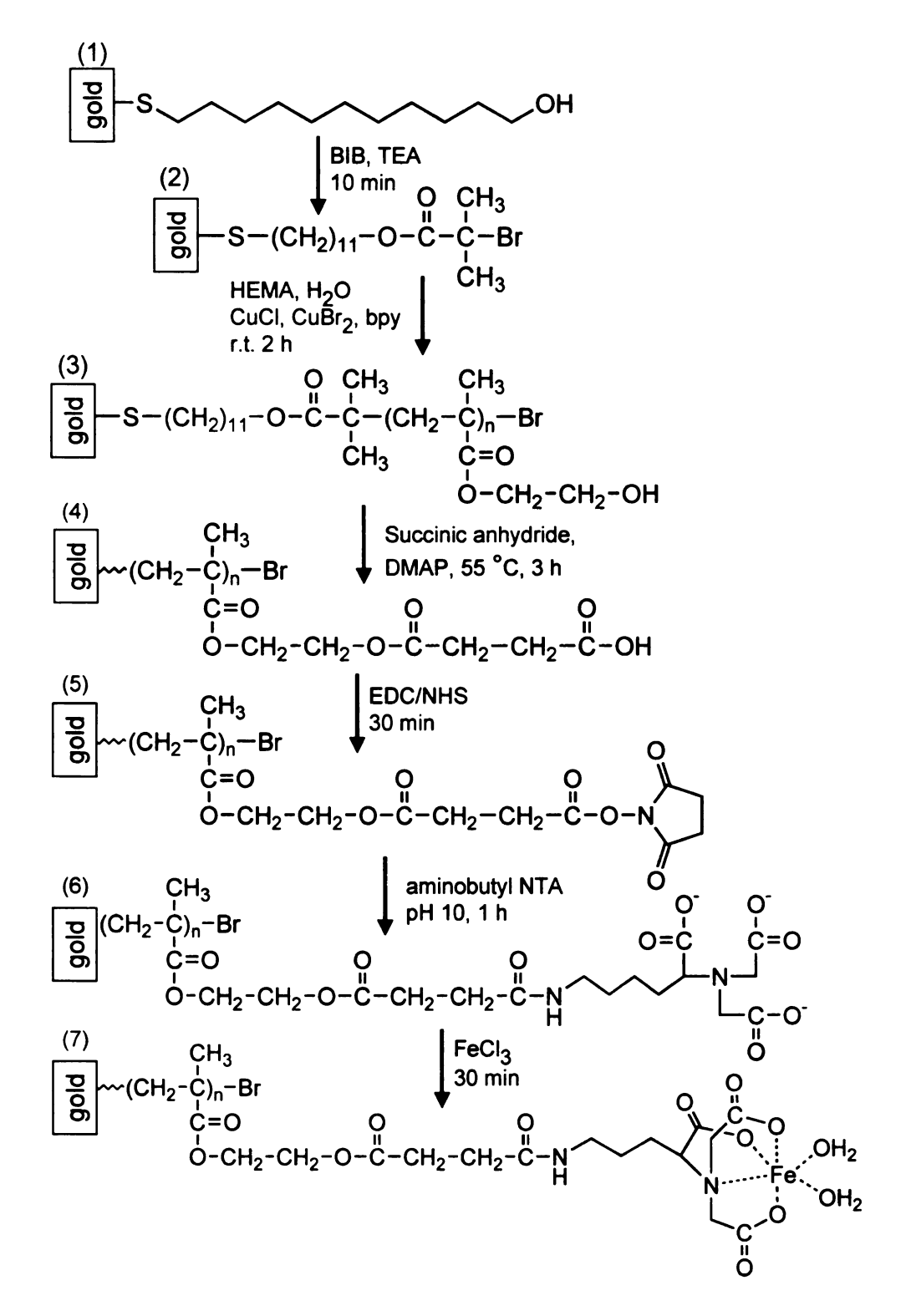


Figure 3.3: Fabrication of an Fe(III)-NTA-PHEMA-modified gold substrate. Abbreviation are defined as follows: Triethylamine (TEA), 2-bromoisobutyryl bromide (BIB), 2-hydroxyethyl methacrylate (HEMA), 2,2'-bipyridine (bpy), 4-dimethylaminopyridine (DMAP), N-(3-dimethylaminopropyl)-N'-ethylcarbodiimide hydrochloride (EDC), N-hydroxysuccinimide (NHS), $N_{\omega}N_{\alpha}$ -bis(carboxymethyl)-L-lysine hydrate (aminobutyl NTA).

Reflectance FTIR characterization of the growth of PHEMA films and their derivatization with Cu(II)-NTA has been reported elsewhere by our group. ¹³ The FTIR results here are similar, although the spectrum of the PHEMA-Fe(III)-NTA complex is somewhat different from the spectrum of the Cu(II)-NTA-PHEMA. Figure 3.4 shows the reflectance FTIR spectra of films at each step of the polymer derivatization process.

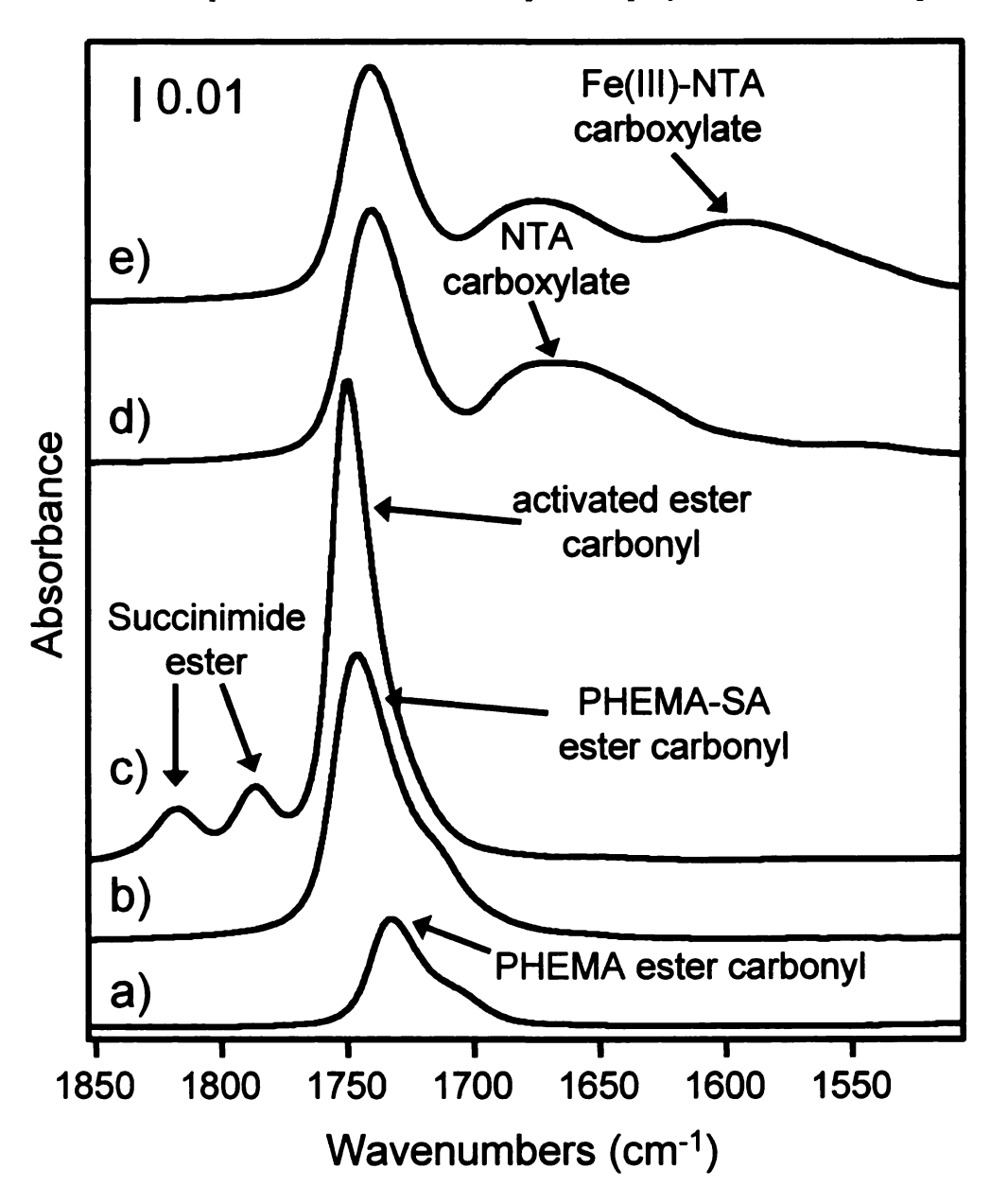


Figure 3.4: Reflectance FTIR spectra of a) a PHEMA brush immobilized on a gold substrate, and the same brush after b) derivatization with succinic anhydride, c) activation of carboxylic acid groups, d) derivatization with NTA, and e) complexation with ferric ions.

In brief, the ester carbonyl absorbance at 1740 cm⁻¹ (Figure 3.4.a) and the hydroxyl stretch at 3650-3100 cm⁻¹ (not shown) confirmed the growth of the PHEMA brush. After derivatization with succinic anhydride, the absorbance of the ester carbonyl approximately doubled due to the additional ester functionality on every repeating unit of the polymer (Figure 3.4b), and the disappearance of the hydroxyl stretch (not shown) also indicated almost complete derivatization. The activation of the carboxylic acid groups by coupling NHS to the polymer is confirmed by the pronounced succinimde ester peaks at 1817 and 1786 cm⁻¹ and the asymmetric stretch of succinimide at ~1750 cm⁻¹ that overlaps with the carbonyl stretch (Figure 3.6c). After the carboxylic acid groups are reacted with amino-terminated NTA, a broad peak at 1664 cm⁻¹ is observed (Figure 3.4.d), which is probably due to the amide bond as well as carboxylate groups of NTA. Lastly, the complexation of Fe(III) to NTA results in the appearance of a peak at 1590 cm⁻¹, which is indicative of Fe(III)-NTA complexes (ferric carboxylate).²¹ The thickness of the film after each step was also monitored using ellipsometry. Typically, after a 25nm thick PHEMA film on a gold wafer was derivatized with Fe(III)-NTA complexes, the film thickness increased to ~50 nm.

3.3.2 Identification of Phosphopeptides Using Tandem MS

Prior to discussing enrichment techniques, it is important to demonstrate how phosphopeptides were identified using tandem MS. Without MS^n techniques it is possible to mistakenly attribute an m/z value to a phosphorylated species. All analyses performed in this section were carried out using a vMALDI linear ion trap mass

spectrometer (Thermo vMALDI LTQ XL), and peptide sequencing was made possible through MSⁿ using low energy collision-induced dissociation (CID).

Typically, when a protonated peptide (precursor ion) is fragmented using low energy CID, the most frequent product ions formed are the $b_{(n\geq 2)}$ and y_n type (b_1 type ions are typically unstable unless the N-terminal amino acid is lysine, histidine, or methionine) due to the amide bond cleavage along the peptide backbone. These types of ions are used to sequence the peptide since each sequential amide bond cleavage corresponds to the loss of an amino acid residue. However, depending on the side groups of the amino acid other fragmentation pathways can dominate, yielding little sequence information. Sometimes this is the case for phosphorylated peptides. Figures 3.5, 3.6, and 3.7 show mass spectra of three phosphorylated peptides from an ovalbumin digest in order to demonstrate the fragmentation of phosphopeptides using low-energy CID.

In some cases, the loss of water from the precursor ion, $[M+H-H_2O]^+$, is dominant and the loss of phosphoric acid from the precursor ion, $[M+H-H_3PO_4]^+$, is barely observed as shown in Figure 3.5. Although $[M+H-H_2O]^+$ is the dominant fragment in the mass range from 600 - 1950 in Figure 3.5b, there are several peaks due to y_n ions, which can be used to verify the sequence of the peptide. These mass spectral data stem from the monophosphopeptide EVVGpSAEAGVDAASVSEEFR ($[M+H]^+$ m/z 2088). Wideband activation MS/MS of m/z 2088 yielded stronger signals due to y_n ions because of additional fragmentation of the $[M+H-H_2O]^+$ ion.

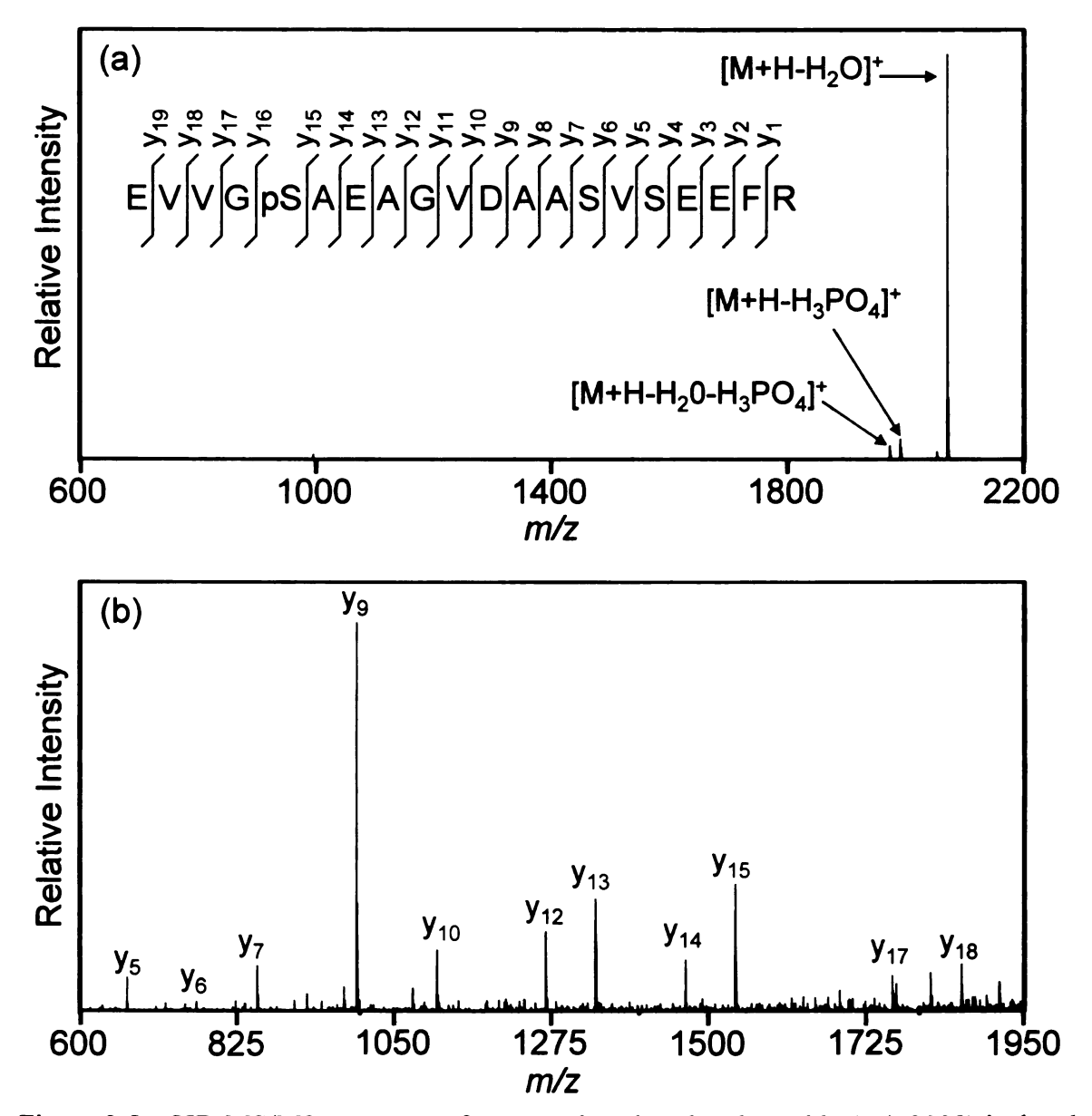


Figure 3.5: CID MS/MS spectrum of a monophosphorylated peptide (m/z 2088) isolated from 500 fmol of an ovalbumin digest: a) full mass range and b) enlarged region (600 – 1950). Prior to obtaining the mass spectrum, the phosphopeptide was enriched on a Fe(III)-NTA-PHEMA-modified plate.

A second phosphopeptide from an ovalbumin digest (LPGFGDpSIEAQCGTSVNVHSSLR, $[M+H]^+$ m/z 2511) showed nearly equal losses of phosphoric acid and water as shown in Figure 3.6, and there were only a few peaks in the mass spectrum that could be used to verify the sequence. To get additional sequence

information, wideband activation MS should be used, which would yield [M+H-H₃PO₄-H₂O]⁺. In principle, this ion could be further fragmented (MS³) to yield sequence ions, but no additional sequence ions were observed in the MS³ spectrum due to low intensities.

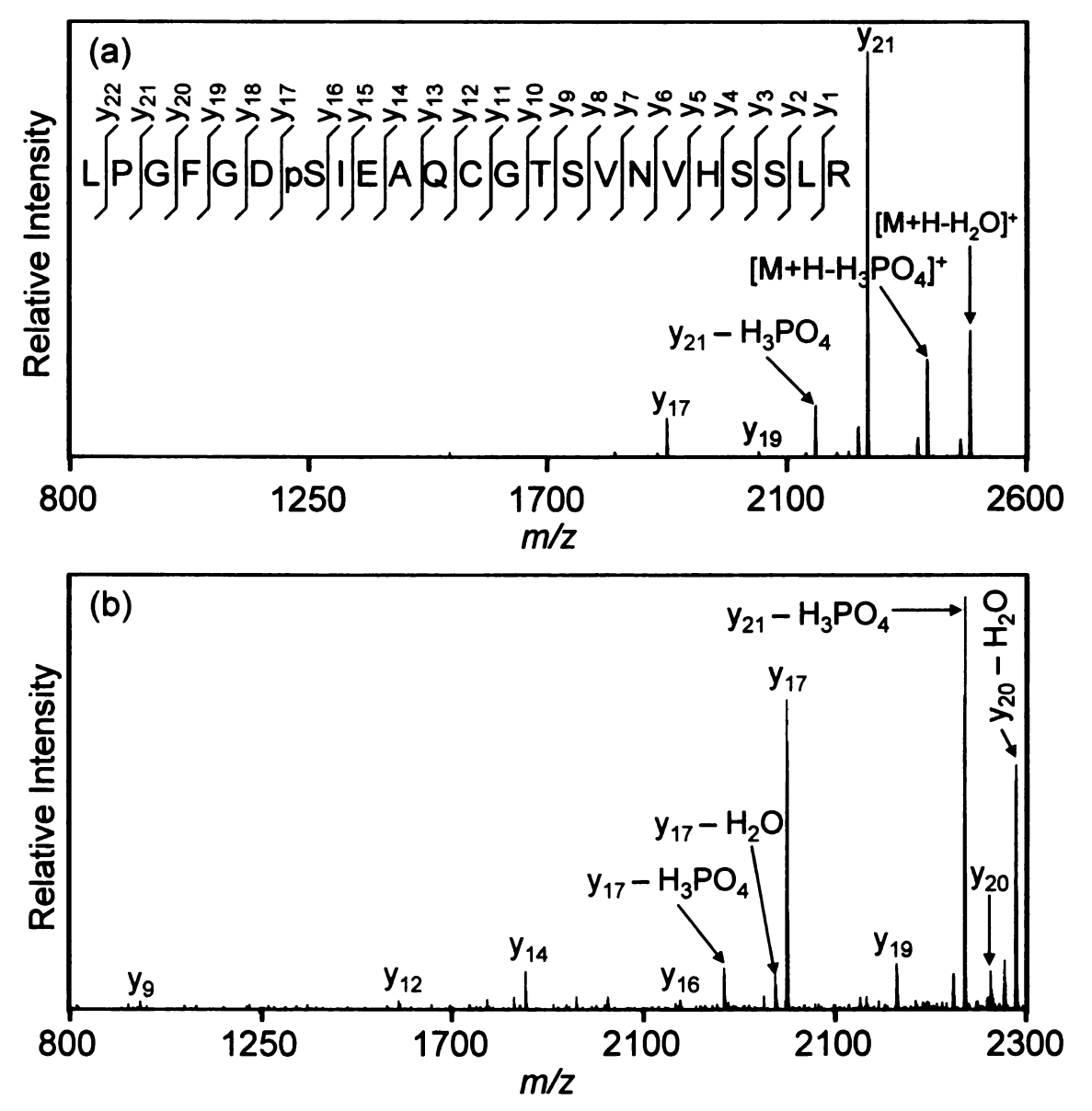


Figure 3.6: CID MS/MS spectrum of a monophosphorylated peptide (m/z 2511) isolated from 500 fmol of an ovalbumin digest: a) full mass range and b) enlarged region (800 – 2300). Prior to obtaining the mass spectrum, the phosphopeptide was enriched on a Fe(III)-NTA-PHEMA-modified plate.

Lastly, when CID MS/MS was performed on the phosphopeptide FDKLPGFGDpSIEAQCGTSVNVHSSLR ($[M+H]^+$ m/z 2901), the predominant loss that was observed was due to -H₃PO₄ (m/z 2803) as shown in Figure 3.7. This strong signal due to [M+H-H₃PO₄]⁺ can be used to easily determine that the peptide is phosphorylated, however, there is little sequence information present in the mass spectrum. As mentioned previously, one could further fragment $[M+H-H_3PO_4]^+$ (MS³) to get more sequence ions. However, usually there was insufficient signal to achieve useful MS³ data for this phosphorylated peptide. One interesting aspect of Figures 3.6b and 3.7b is that they show $y_n-H_3PO_4$ ions. Additionally, the y_{17} ion is due to pSIEAQCGTSVNVHSSLR 1925) and $y_{17}-H_3PO_4$ due (m/z)is to dAIEAQCGTSVNVHSSLR (m/z 1827, dA stands for dehydroalanine) in both cases. Additionally, no peak due to the y_{16} ion was observed in either mass spectrum. Perhaps, this could help to identify the location of the phosphorylation site in some cases.

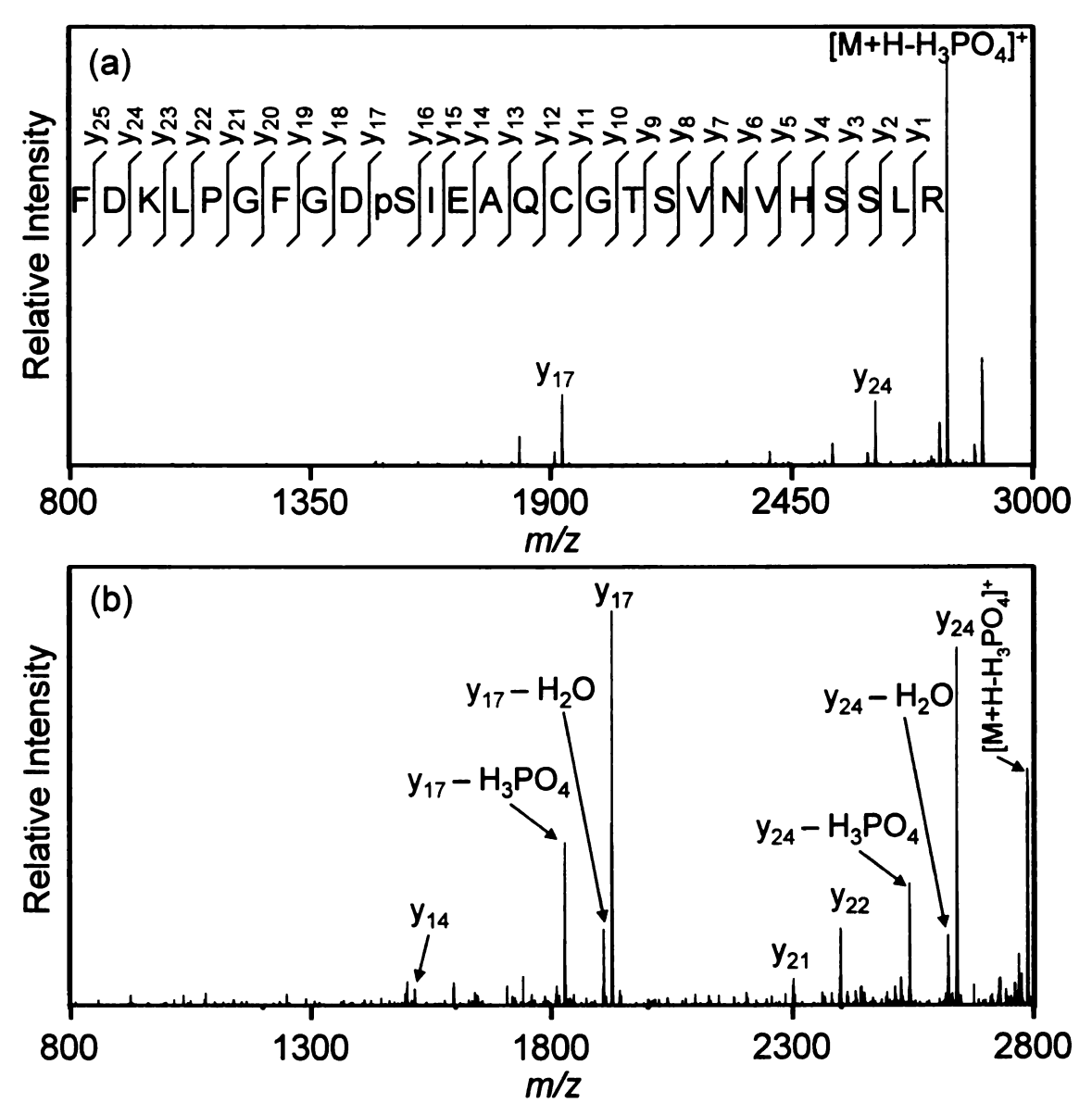


Figure 3.7: CID MS/MS spectrum of a monophosphorylated peptide (m/z 2901) isolated from 3.5 pmol of an ovalbumin digest: a) full mass range and b) enlarged region (800 – 2300). Prior to obtaining the mass spectrum, the phosphopeptide was enriched on a Fe(III)-NTA-PHEMA-modified plate.

3.3.3 Quantitation of Phosphopeptide Binding to Fe(III)-NTA-PHEMA-modified Plates Using Ellipsometry. To determine the phosphopeptide binding capacity of Fe(III)-NTA-PHEMA brushes on gold-coated substrates, ellipsometry was used to measure the thicknesses of three Fe(III)-NTA-PHEMA films on Au before and after immersion in phosphoangiotensin (pA) solutions for 1 h. The increase in ellipsometric thickness (after rinsing) was assumed to be entirely due to bound pA, and Figure 2 shows the resulting pA adsorption isotherm for films with an average thickness of ~60 nm. (A pA density of 1 mg/mL was employed to convert thickness increases to surface coverage, and the large error bars stem in part from the fact that even at saturation, the increase in film thickness is only 4 nm on a 60 nm film.) The maximum amount of pA bound is about 0.6 μg/cm², or 18 pmol in the area of a 2-mm diameter sample spot. Nonphosphorylated angiotensin II was also applied to the polymer-modified plate to see whether its histidine and glutamic acid residues would cause nonspecific binding, and no binding of this peptide was detected even at a solution concentration of 0.2 mg/mL.

Figure 2 shows the fit of the binding data to the Langmuir adsorption isotherm, which is described by Equation 1, where x ($\mu g/cm^2$) is the experimental amount of pA bound to the polymer film, x_m ($\mu g/cm^2$) is the maximum amount of pA that could be bound to the polymer film, c (mg/mL) is the concentration of pA in solution, and K (mL/mg) is the Langmuir constant for the formation of the pA-Fe(III)-NTA complex.

Equation 3.1
$$x = \frac{x_m c}{K^{-1} + c}$$

The fit yields a value of $0.6 \,\mu\text{g/cm}^2$ (1.1 nmol/cm²) for x_m and a K of 250 mL/mg (2.8 x 10^8 mL/mol), but unfortunately, the uncertainty in the data and the fit are not sufficient to predict the amount of pA that would be bound to the film at the low concentrations used in mass spectrometry. However, the phosphopeptide recoveries of 70% described below for solutions initially containing 125 fmol of the H₅ peptide in 2 μ L of solution also give a K of about 250 mL/mg, assuming the binding capacity in a 2-mm diameter spot is 0.6 μ g/cm².

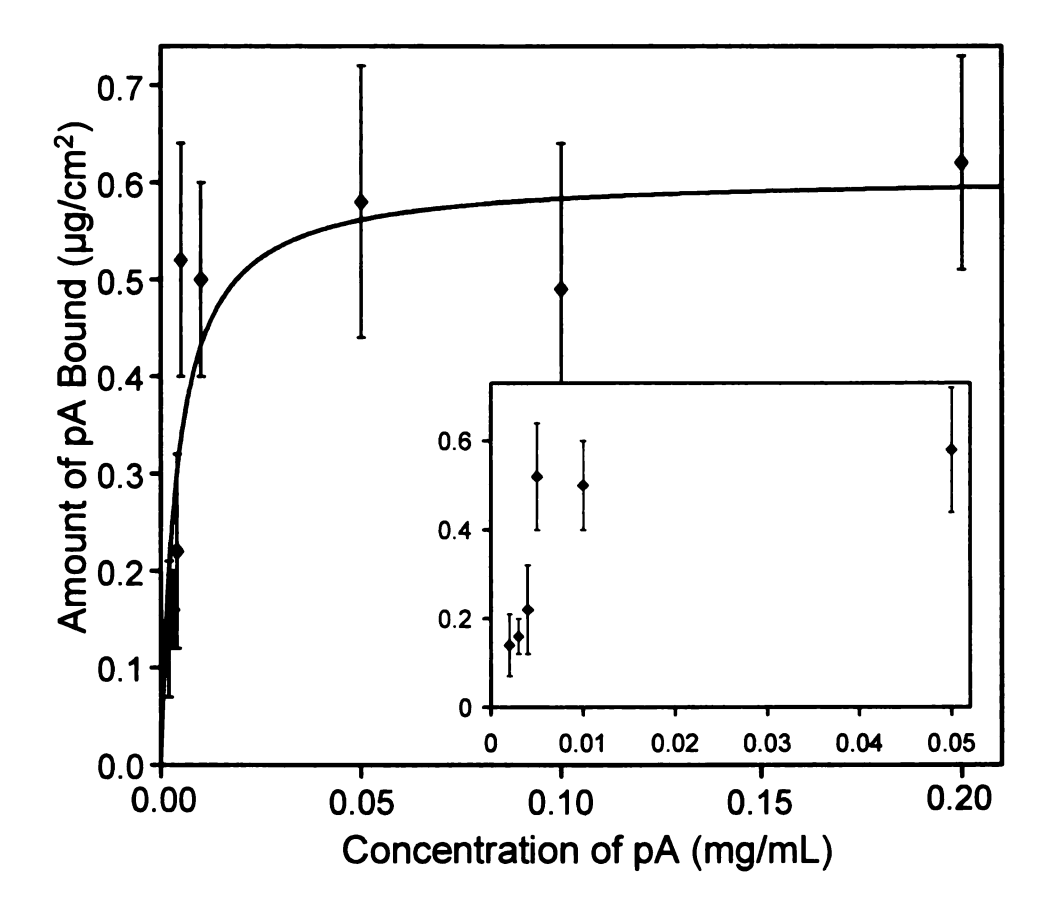


Figure 3.8: Plot of the amount of pA bound to PHEMA-NTA-Fe(III) films on gold substrates as a function of pA concentration. The solid line represents the fit to the Langmuir adsorption isotherm, and the inset shows an expanded view of the data at low pA concentrations.

3.3.4 Analysis of Tryptic Phosphoprotein Digests by MS Using Fe(III)-NTA-PHEMA-modified MALDI Plates

3.3.4.1 Analysis of β-Casein Digests

To compare our enrichment technique to others (see the review of other techniques in Chapter One), we first applied tryptic β-casein digest to our Fe(III)-NTA-PHEMA-modified gold MALDI plates. Tryptic digests of β-casein are perhaps the most common samples used to validate phosphopeptide enrichment techniques. One microliter of the phosphoprotein digest containing 7 pmol, 1 pmol, 500 fmol, 125 fmol, 31 fmol, or 15 fmol was applied to a sample well (2-mm diameter) and incubated for 1 h. To prevent the sample from drying, 0.5-uL increments of 5% acetic acid were applied over the 1-h period. The sample plates were thoroughly washed with 15-20 mL of 3:30:67 acetic acid:acetonitrile:water solution to remove nonphosphorylated peptides and the other digest reagents, and the polymer-modified plates were completely blown dry with nitrogen. A 1-µL aliquot of 1% phosphoric acid was immediately spotted onto each sample well and 0.25 µL of matrix solution was added. All analyses using the Fe(III)-NTA-PHEMA-modified plates were compared with conventional analysis by MALDI-MS, which consisted of spotting the same amount of phosphoprotein digest (1 μ L of 7 pmol, 1 pmol, 500 fmol, 125 fmol, 31 fmol, or 15 fmol) in the 2-mm diameter well of the conventional MALDI plate, followed by addition of 1 µL of 10 mg/mL 2,5-DHB (1:1 acetontrile/1% H₃PO₄).

As mentioned in Chapter Two, β -casein is a pentaphosphorylated protein, and tryptic digestion typically results in the formation of three phosphorylated peptides (FQpSEEQQQTEDELQDK, m/z 2062, $1P_{2062}$; ELEELNVPGEIVEpSLpSpSpSEESITR,

m/z 2966, $4P_{2966}$; and RELEELNVPGEIVEpSLpSpSpSEESITR, m/z 3122, $4P_{3122}$). Mono- and tetraphosphorylated peptides are represented by 1P and 4P, respectively. We also occasionally observed another B-casein phosphorylated peptide (NVPGEIVEpSLpSpSpSEESITR, m/z 2353, 4P₂₃₅₂) due to chymotryptic cleavage.²² Additionally, we frequently found several phosphopeptides from α -S1- and α -S2-caseins, which are present as impurities. (β-Casein is sold as a 90% pure mixture through Sigma-Aldrich.) Table 3.1 lists the peaks due to β -casein, α -S1-casein, and α -S2-casein phosphopeptides that were observed in the positive-ion MALDI mass spectra. The table also lists peaks that were due to doubly-charged phosphopeptide ions, [M+2H]2+, and phosphopeptide ions that underwent fragmentation, resulting in the loss of one or two phosphate groups, [M+H-H₃PO₄]⁺ or [M+H-2H₃PO₄]⁺. No peptide sequences could be assigned to the peaks at m/z 2599, 2603, 2616, and 3042 as shown in Table 3.1. However, these peaks have tentatively been assigned as due to phosphopeptides since the loss of H₃PO₄ was observed in the MS/MS spectra.

Table 3.1: Phosphopeptide-related ions observed in the positive-ion mass spectra of tryptic β -casein digests. The numbers of phosphate groups and aspartic acid (D) and glutamic acid (E) residues in each sequence are also listed. Unless specified, ions correspond to the $[M+H]^+$ ion. Subscripts: a) Doubly protonated peptide, $[M+2H]^{2+}$, b) chymotryptic cleavage reported by Larsen et al., 22 c) reported by Larsen et al., 22 and d) could be due to in source fragmentation, $[M+H-H_3PO_4]^+$ or $[M+H-2H_3PO_4]^+$.

Protein	Phosphopeptide Sequence	Sequence Number	# Phosphate groups	# D	# E	m/z	m/z (methyl esterified peptide)
β-casein	FQpSEEQQQTEDELQDK	33-48	1	2	4	1032	1081
	ELEELNVPGEIVEpSLpSpSpSEESITR	2-25	4	0	7	1484 ^a	1234
	RELEELNVPGEIVEpSLpSpSpSEESITR	1-25	4	0	7	1562 ^a	1618
	FQpSEEQQQTEDELQDK	33-48	1	2	4	2062	2160
	NVPGEIVEpSLpSpSpSEESITR	7-25	4	0	7	2353 ^b	2465
	ELEELNVPGEIVEpSLpSpSpSEESITR	2-25	4	0	7	2966	3078
	RELEELNVPGEIVEpSLpSpSpSEESITR	1-25	4	0	7	3122	3234
α-S1-casein	HIQKEDVPpSER	80-90	1	1	2	1418	1474
	VPQLEIVPNpSAEER	106-119	1	0	3	1661	1717
	YKVPQLEIVPNpSAEER	104-119	1	0	3	1952	2008
	DIGpSEpSTEDQAMEDIK	43-58	2	3	3	1928	2026
	QMEAEpSIpSpSpSEEIVPNpSVEQK	59-79	5	0	5	2721	2805
α-S2-casein	EQLpSTpSEENSK	126-136	2	0	3	1411	1467
	TVDMEpSTEVFTK	138-149	1	1	2	1467	1523
	EQLpSTpSEENSKK	126-137	2	0	3	1540	1596
	NMAINPpSKENLCSTFCK	25-41	1	0	1	2094	2122
	NTMEHVpSpSpSEEpSIISQETYK	2-21	4	0	4	2619	2689
	KNTMEHVpSpSpSEEpSIISQETYK	1-21	4	0	4	2747	2817
	NANEEEYSIGpSpSpSeEpSAEVATEEVK	46-70	4	0	8	3008	3134
	NANEEEYSIGpSpSpSEEpSAEVATEEVK	46-70	5	0	8	3088 ^c	3214
β-casein	FQpSEEQQQTEDELQDK	33-48	- H ₃ PO ₄	2	4	1963 ^d	2061
	ELEELNVPGEIVEpSLpSpSpSEESITR	2-25	- 2 H ₃ PO ₄	0	7	2770 ^d	2882
	ELEELNVPGEIVEpSLpSpSpSEESITR	2-25	- H ₃ PO ₄	0	7	2868 ^d	2980
	RELEELNVPGEIVEpSLpSpSpSEESITR	1-25	-2 H ₃ PO ₄	0	7	2926 ^d	3038
	RELEELNVPGEIVEpSLpSpSpSEESITR	1-25	- H ₃ PO ₄	0	7	3024 ^d	3136
unidentified	na	na	≥1	na	na	2599	na
	na	na	≥1	na	na	2603	na
	na	na	≥1	na	na	2616	na
	na	na	≥1	na	na	3042	na

In the positive-ion, conventional MALDI mass spectrum of 7 pmol of β-casein digest (Figure 3.9a), only phosphopeptide signals due to the monophosphorylated peptide 1P₂₀₆₂ and one of the tetraphosphorylated peptides 4P₂₉₆₆ were observed. However, when the same digest was analyzed using the Fe(III)-NTA-PHEMA-modified plate as shown in Figure 3.9b, we were able to detect all four of the β -casein phosphorylated peptides as well as 14 other α -S1-casein and α -S2-casein phosphorylated peptides. After enrichment, there was an impressive 30-fold increase in the intensities of the phosphorylated peptides relative to that observed in the conventional MS analysis. We observed doubly-charged peaks (indicated by triangles) at m/z 1032, 1484, and 1561 due to the $1P_{2062}$, $4P_{2966}$, and $4P_{3122}$ peptides, respectively. It also appeared that $1P_{2062},\,4P_{2966}$ and $4P_{3122}$ underwent some fragmentation (peaks labeled with stars in the mass spectrum) either during the desorption/ionization process or while in the ion trap, probably because the phosphate group on the serine residue is quite labile. Both of the tetraphosphorylated peptides showed the loss of two phosphate groups whereas the monophosphorylated peptide lost one phosphate group.

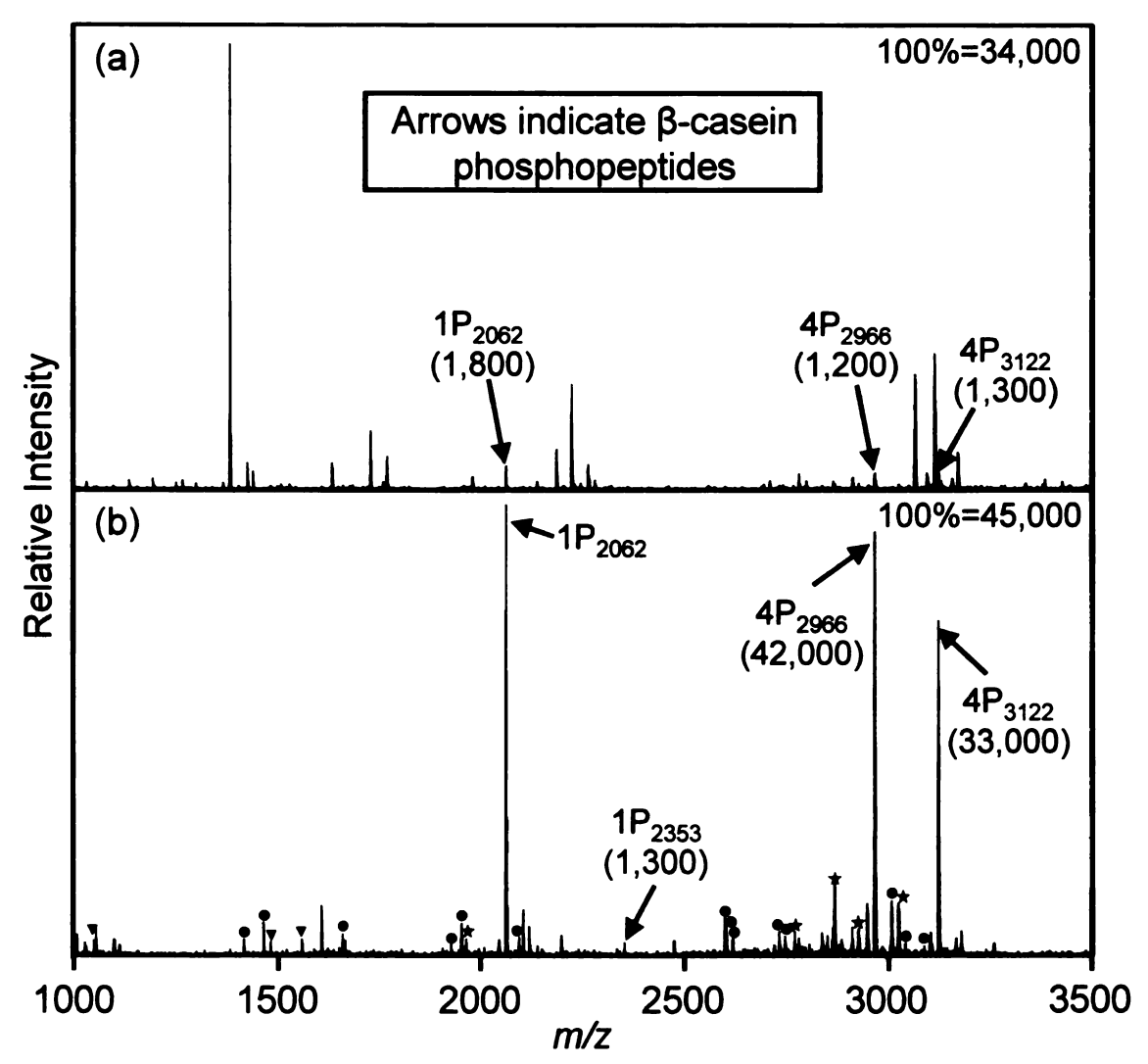


Figure 3.9: Positive-ion MALDI mass spectra of 7 pmol of β -casein digest. Spectra were obtained using a) conventional analysis and b) a Fe(III)-NTA-PHEMA-modified plate with incubation and rinsing. In spectrum b, peaks labeled with triangles represent doubly charged phosphopeptides, peaks labeled with stars are due to fragmentation of phosphopeptides, and peaks labeled with circles stem from α -S1-casein and α -S2-casein phosphorylated peptides. Numbers in parentheses are peak intensities. Peak identification was facilitated by MS/MS spectra.

When the amount of β -casein digest applied was decreased to 1 pmol, the polymer-modified plates showed only a 2-fold increase in the signal due to $1P_{2062}$ relative to the corresponding peptide signal in conventional MS analysis (Figure 3.10). However, neither tetraphosphorylated peptide was observed in the conventional analysis, but the polymer-modified plate was able to readily detect these peptides. No signal due to $1P_{2352}$

was observed when 1 pmol of digest was analyzed on the modified plate, but this result was expected since this peak was only weakly detected when 7 pmol of digest was analyzed, due to minimal chymotryptic cleavage. Additionally, we observed 11 phosphopeptides from α-S1- and α-S2-casein digests and saw doubly protonated phosphopeptides and phosphopeptide fragmentation in the mass spectrum. When 7 pmol of β-casein was analyzed using the Fe(III)-NTA-PHEMA-modified plate the peaks due to the tetraphophorylated peptides were almost the same intensity (or more intense) as the peak due to 1P₂₀₆₂ as in Figure 3.9b. However, when 1 pmol of digest was analyzed using the polymer-modified plate, the signals due to the tetraphosphorylated peptides were less than half the intensity of the peak due to 1P₂₀₆₂. This may suggest that at high amounts of digest, the tetraphosphorylated peptides displace the monophosphorylated peptides, while at low loadings this occurs to a lesser extent. (With 7 pmol of digest, the amount of phosphopeptides approaches the 18 pmol capacity mentioned above.) Because the monophosphopeptide is more readily ionized, under similar loading it would exhibit a higher signal, as shown in the conventional MALDI-MS spectrum.

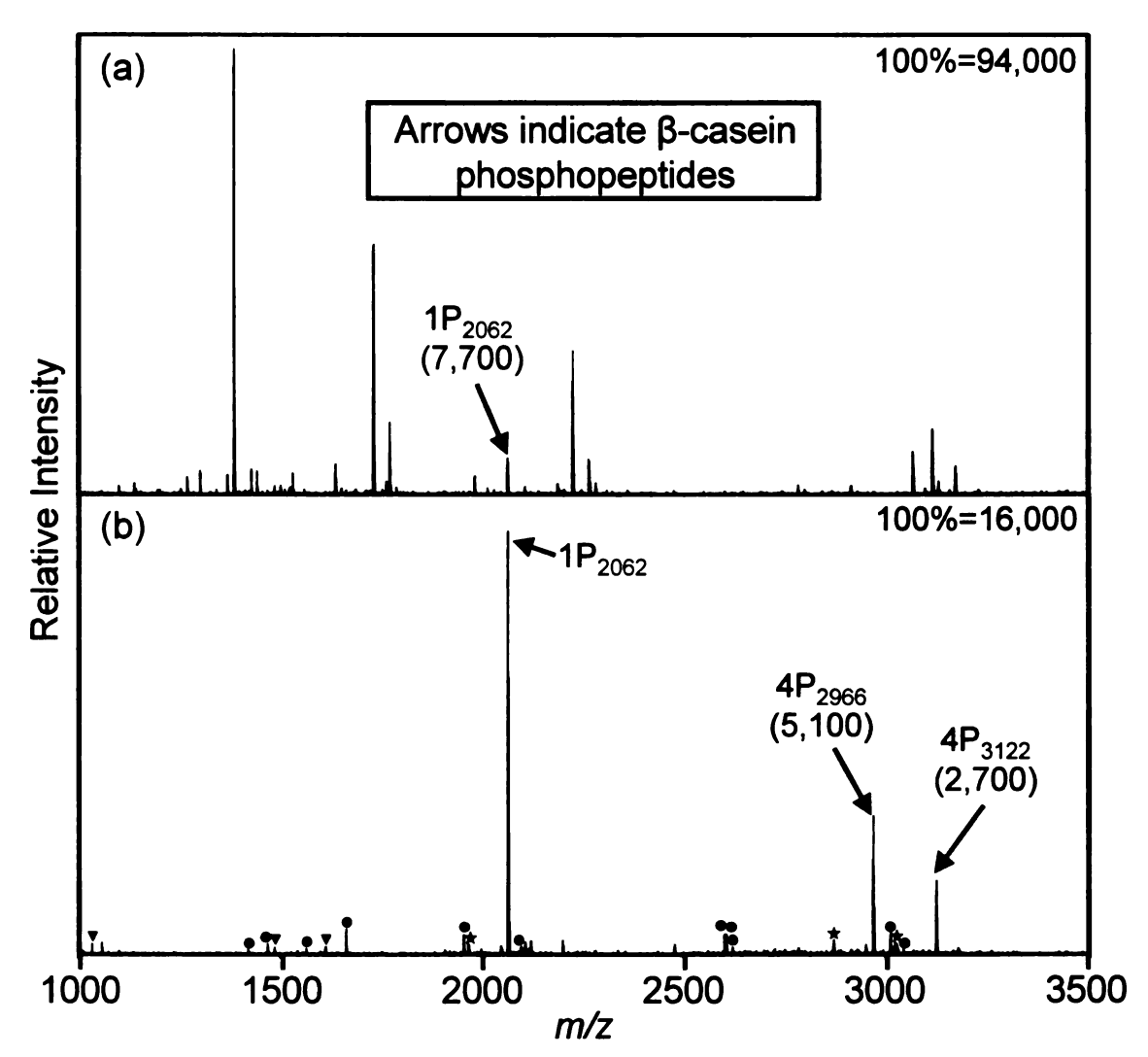


Figure 3.10: Positive-ion MALDI mass spectra of 1 pmol of β -casein digest. Spectra were obtained using a) conventional analysis and b) a Fe(III)-NTA-PHEMA-modified plate with incubation and rinsing. In spectrum b, peaks labeled with triangles represent doubly charged phosphopeptides, peaks labeled with stars are due to fragmentation of phosphopeptides, and peaks labeled with circles stem from α -S1-casein and α -S2-casein phosphorylated peptide impurities. Numbers in parentheses are peak intensities.

When the amount of β -casein digest was decreased to 500 fmol, the polymer-modified plate showed a $1P_{2062}$ signal that was 7-fold greater than the corresponding signal observed in conventional MS analysis (Figure 3.11). However, the number of α -S1- and α -S2-casein phosphorylated peptides decreased (only 7 phosphopeptides were detected), and the two β -casein tetraphosphorylated peptides, $4P_{2966}$ and $4P_{3122}$, were not

detected. An interesting observation is that an α -S2-casein tetraphosphorylated peptide at m/z 3008 due to NANEEEYSIGpSpSpSEEpSAEVATEEVK was detected when 7 pmol, 1 pmol, and 500 fmol (even 125 fmol) of digest were analyzed using the polymer-modified plate. This tetraphosphorylated peptide contains only one more acidic residue than $4P_{2966}$ (ELEELNVPGEIVEpSLpSpSpSEESITR), so we would not expected enrichment to be significantly better for this species. At present, we do not understand the high sensitivity for the m/z 3008 tetraphosphorylated peptide.

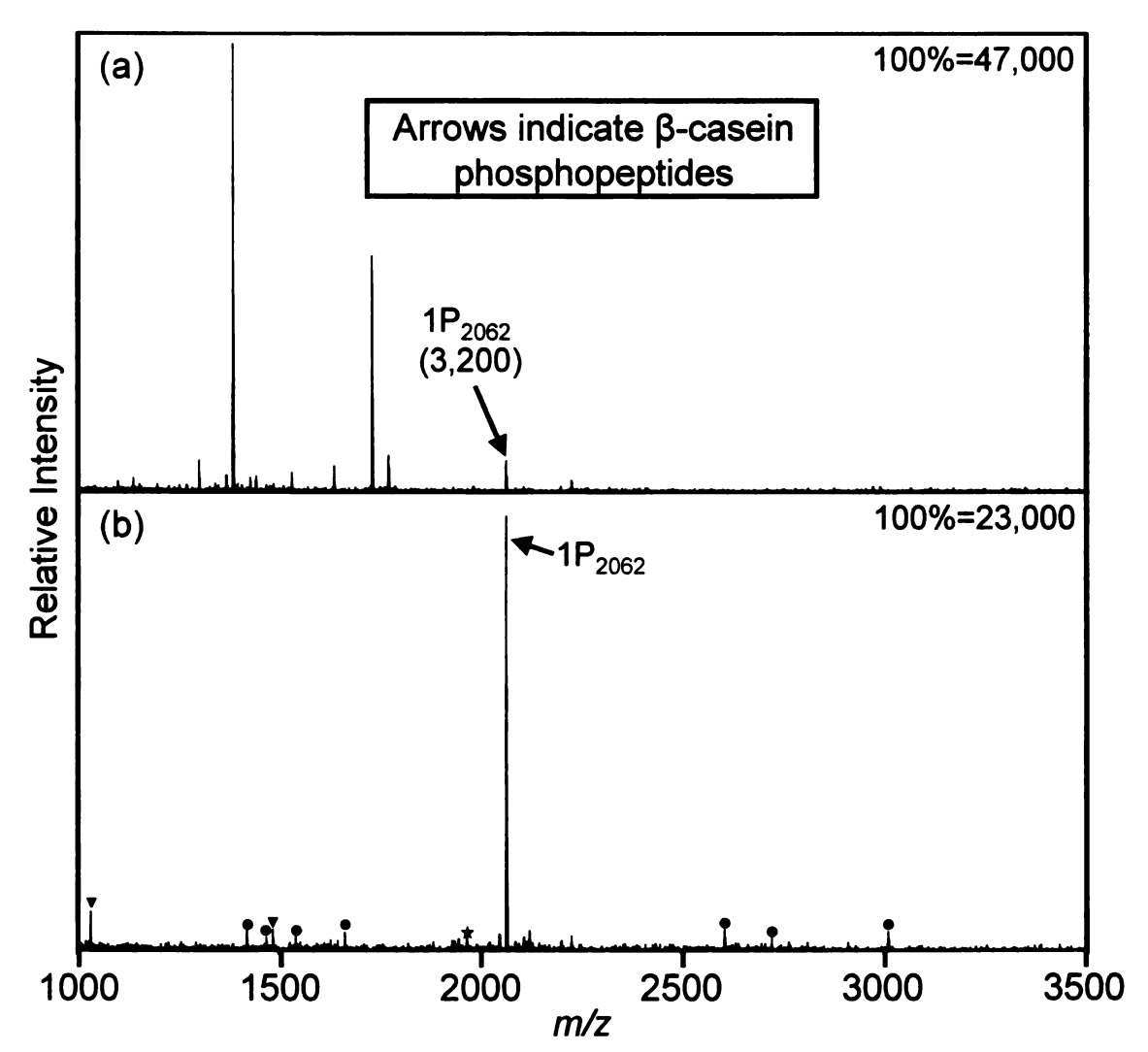


Figure 3.11: Positive-ion MALDI mass spectra of 500 fmol of β -casein digest. The spectra were obtained using a) conventional analysis and b) a Fe(III)-NTA-PHEMA-modified plate with incubation and rinsing. In spectrum b, peaks labeled with triangles are due to doubly charged phosphopeptides, peaks labeled with stars are due to fragmentation of phosphopeptides, and peaks labeled with circles stem from α -S1-casein and α -S2-casein phosphorylated peptides. The number in parentheses is peak intensity.

The results for the analysis of 125 fmol of β -casein digest were similar to those for analysis of the 500 fmol of digest as shown in Figure 3.12. Relative to conventional MALDI-MS, the signal due to $1P_{2062}$ was improved by a factor of 10 when the Fe(III)-NTA-PHEMA-modified plate was used. Six phosphopeptides from the α -casein

contaminants were observed, one of which was due to the tetraphosphorylated peptide at m/z 3008.

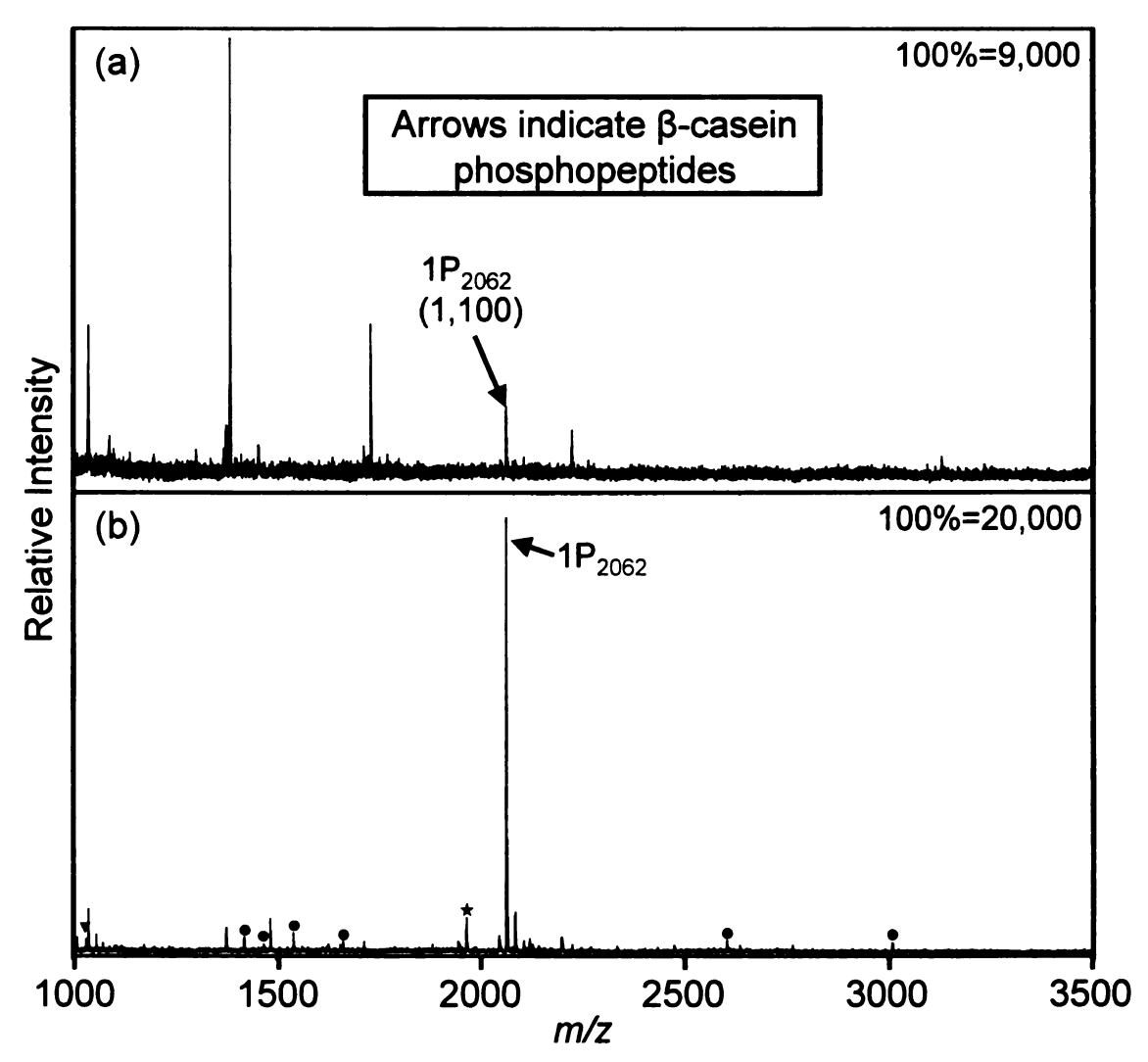


Figure 3.12: Positive-ion MALDI mass spectra of 125 fmol of β -casein digest. The spectra were obtained using a) conventional analysis and b) a Fe(III)-NTA-PHEMA-modified plate with incubation and rinsing. In spectrum b, peaks labeled with triangles are due to doubly charged phosphopeptides, peaks labeled with stars are due to fragmentation of phosphopeptides, and peaks labeled with circles stem from α -S1-casein and α -S2-casein phosphorylated peptide impurities. The number in parentheses is peak intensity.

Figure 3.13 shows the mass spectra when 31 fmol of β -casein was analyzed using the conventional MALDI-MS and the polymer-modified plate. The conventional mass spectrum shows a very weak signal due to $1P_{2062}$ and the signal-to-noise is only 3. When

the digest was applied to the polymer-modified plate, the signal due to $1P_{2062}$ increased by a factor of 2.5 and the signal-to-noise was over 8 times greater. Only one α -casein phosphorylated peptide was observed. Additionally, when 15 fmol of β -casein was analyzed using the conventional analysis the S/N was about 2.4, whereas the S/N observed using the polymer-modified plate was 6.2. The analysis of 15 fmol of β -casein digest is shown in Figure 3.14. From these results the detection limit of conventional analysis by MALDI-MS for β -casein (based on $1P_{2062}$) appears to be around 30 fmol whereas the detection limit when using the enrichment method is below 15 fmol.

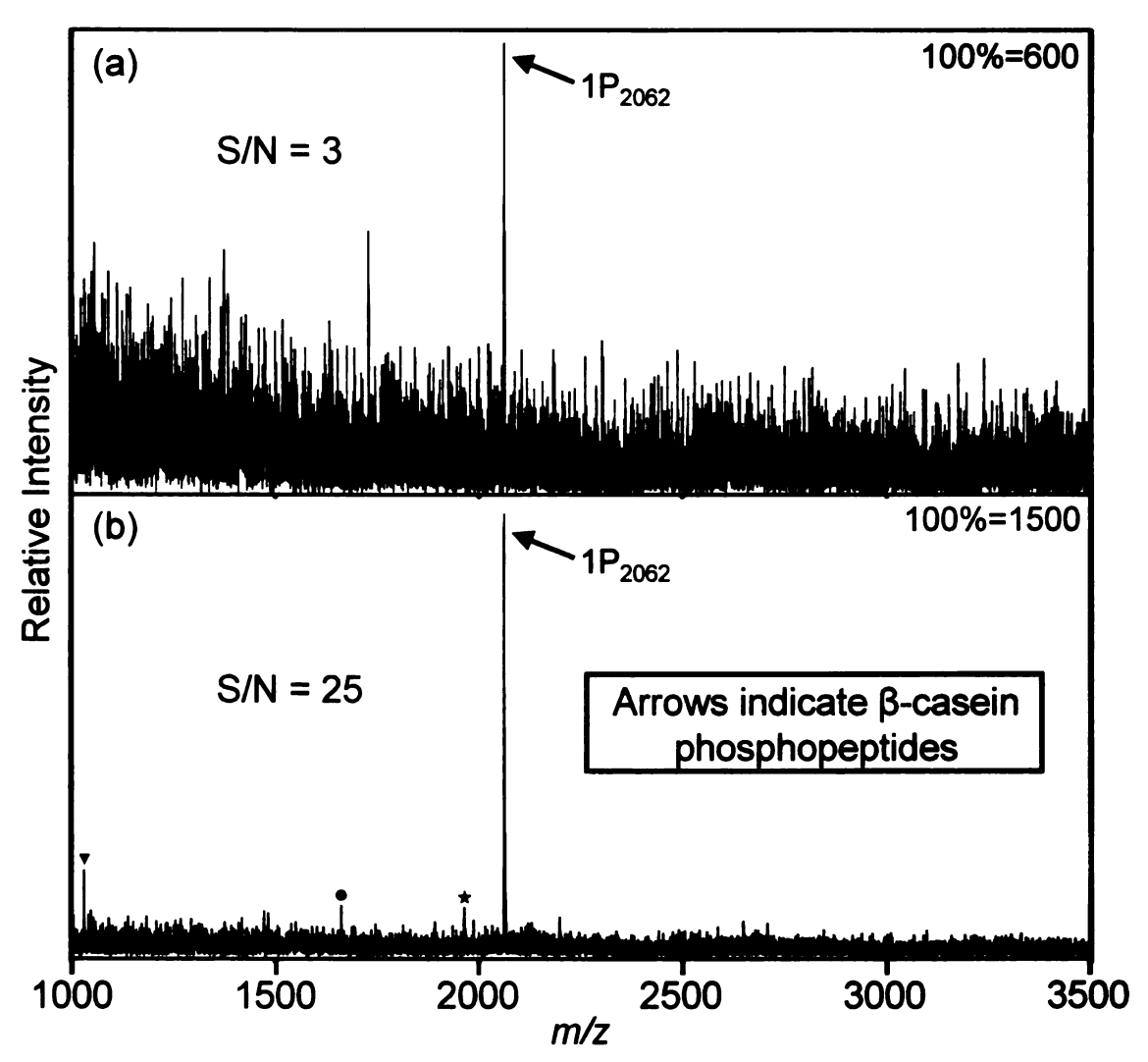


Figure 3.13: Positive-ion MALDI mass spectra of 31 fmol of β -casein digest. Spectra were obtained using a) conventional analysis and b) a Fe(III)-NTA-PHEMA-modified plate with incubation and rinsing. In spectrum b, the peak labeled with a triangle represents a doubly charged phosphopeptide, the peak labeled with a star is due to fragmentation of phosphopeptides, and the peak labeled with a circle stem from an α -S1-casein phosphorylated peptide impurity.

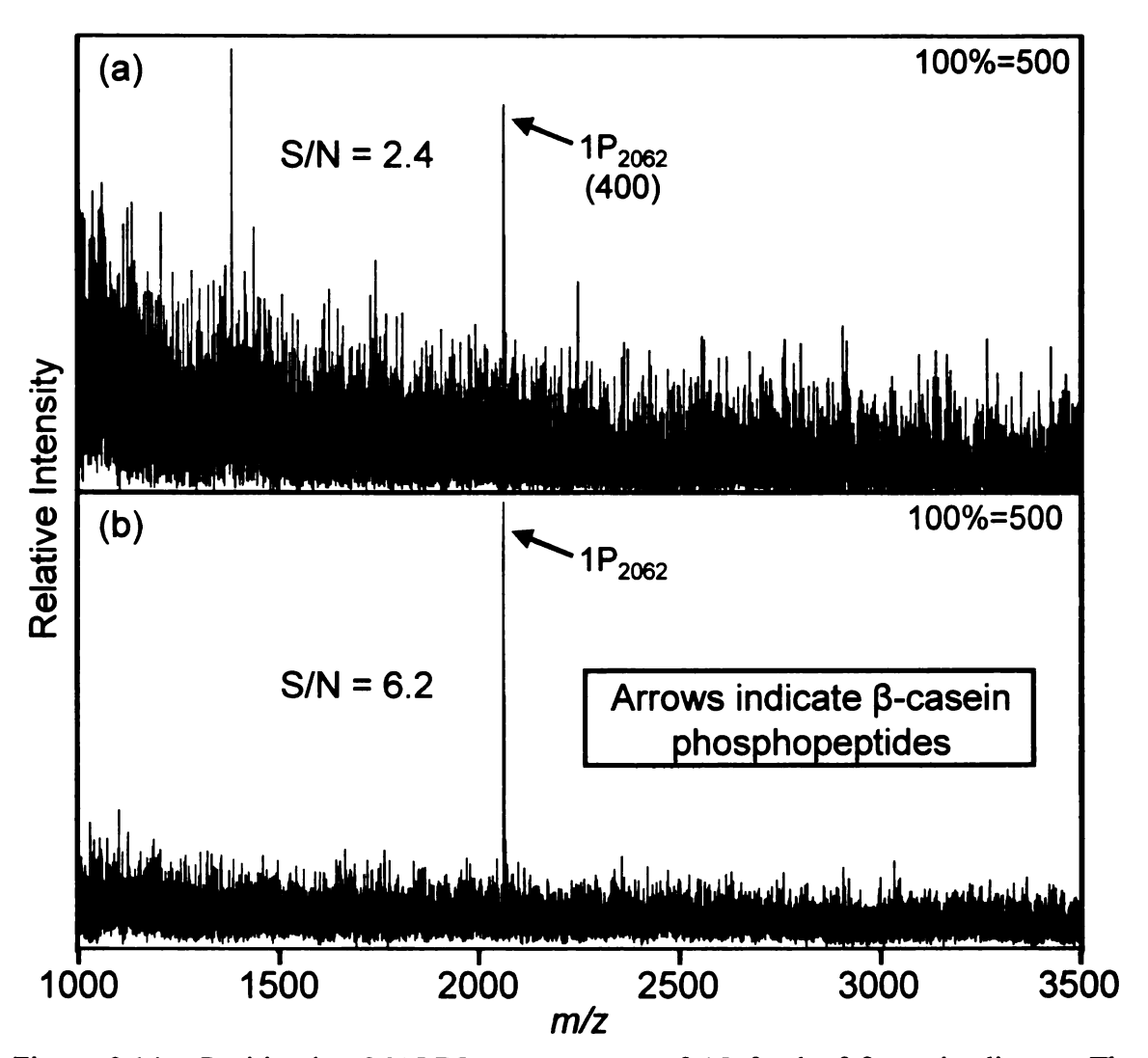


Figure 3.14: Positive-ion MALDI mass spectra of 15 fmol of β -casein digest. The spectra were obtained using a) conventional analysis and b) a Fe(III)-NTA-PHEMA-modified plate with incubation and rinsing. The number in parentheses is peak intensity.

3.3.4.2 Analysis of Ovalbumin Digests

We also analyzed various amounts (1 pmol, 500 fmol, 125 fmol, and 62 fmol) of tryptic digests of ovalbumin, which is a diphosphorylated protein. Tryptic digest of ovalbumin result in the formation of three monophosphorylated (EVVGpSAEAGVDAASVSEEFR, 2088, 1P₂₀₈₈; m/zLPGFGDpSIEAQCGTSVNVHSSLR, 2511, $1P_{2511}$; m/zand FDKLPGFGDpSIEAQCGTSVNVHSSLR, m/z 2901, 1P₂₉₀₁).

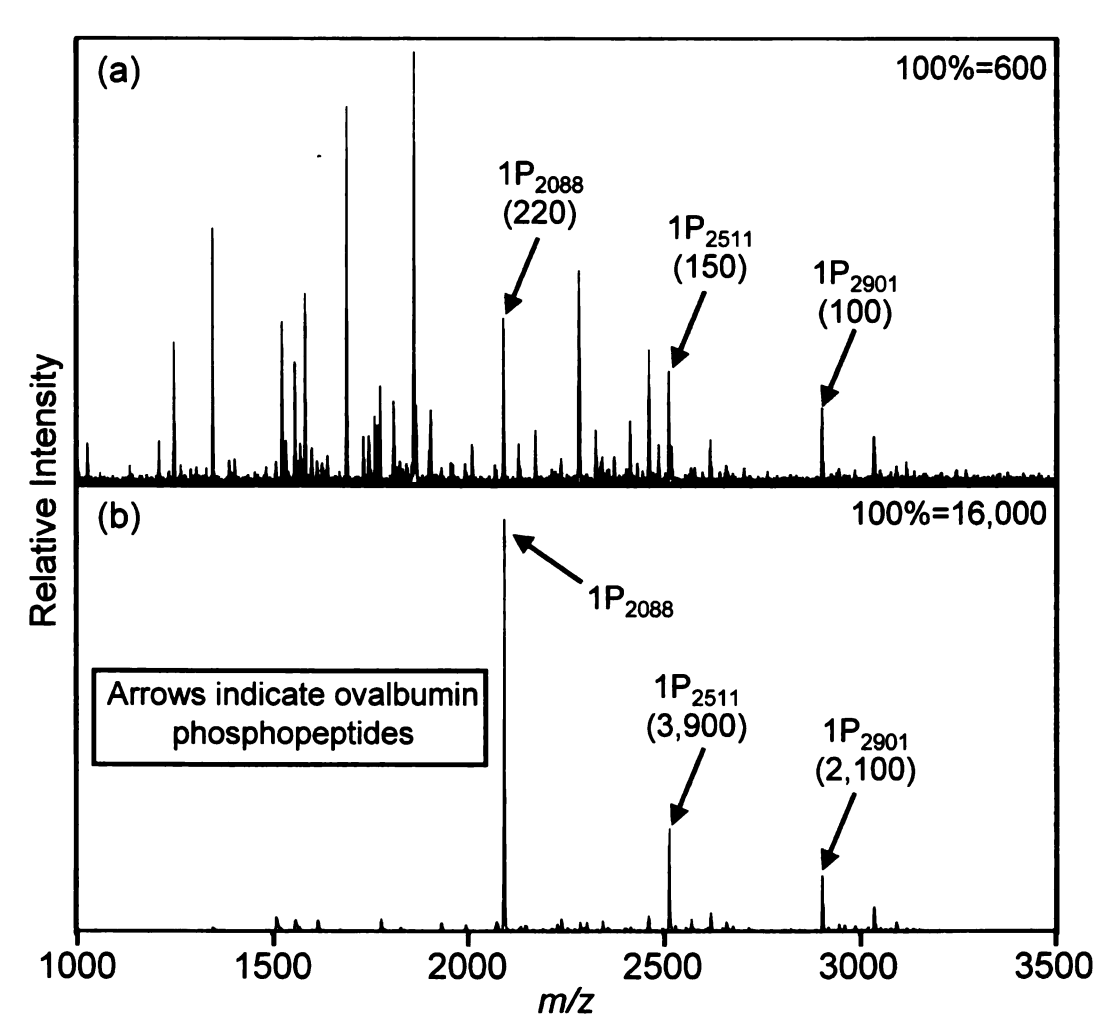


Figure 3.15: Positive-ion MALDI mass spectra of 1 pmol of ovalbumin digest. Spectra were obtained using a) conventional analysis and b) a Fe(III)-NTA-PHEMA-modified plate with incubation and rinsing. Numbers in parentheses are peak intensities.

Shown in Figure 3.15 is the analysis of 1 pmol of ovalbumin digest using conventional MALDI-MS as well as by using the Fe(III)-NTA-PHEMA-modified plate. Even though all three phosphorylated peptides were detected in the conventional analysis, the use of the polymer-modified plate greatly simplifies the mass spectrum. The phosphopeptide peaks dominate the mass spectrum taken on the modified plate because most of the nonphosphorylated peptides were removed during the rinsing step. Moreover, the signals of the phosphorylated peptides increased by a factor of ~40 when

the modified plate was used. The peptide signals in the conventional mass spectrum are most likely low due to the presence of salts in the digest. The use of the Fe(III)-NTA-PHEMA-modified plates allows for capture of phosphopeptides as well as desalting of the sample in a simple rinsing step.

Figure 3.16 shows the analysis of 500 fmol of ovalbumin digest. In this case, the phosphopeptide signals in the conventional MALDI mass spectrum are very weak compared to the nonphosphorylated peptides. In fact, one of the phosphopeptides, $1P_{2901}$, was not detected in the conventional analysis. However, when the same sample was applied to the polymer-modified plates, all three phosphopeptides were readily detected.

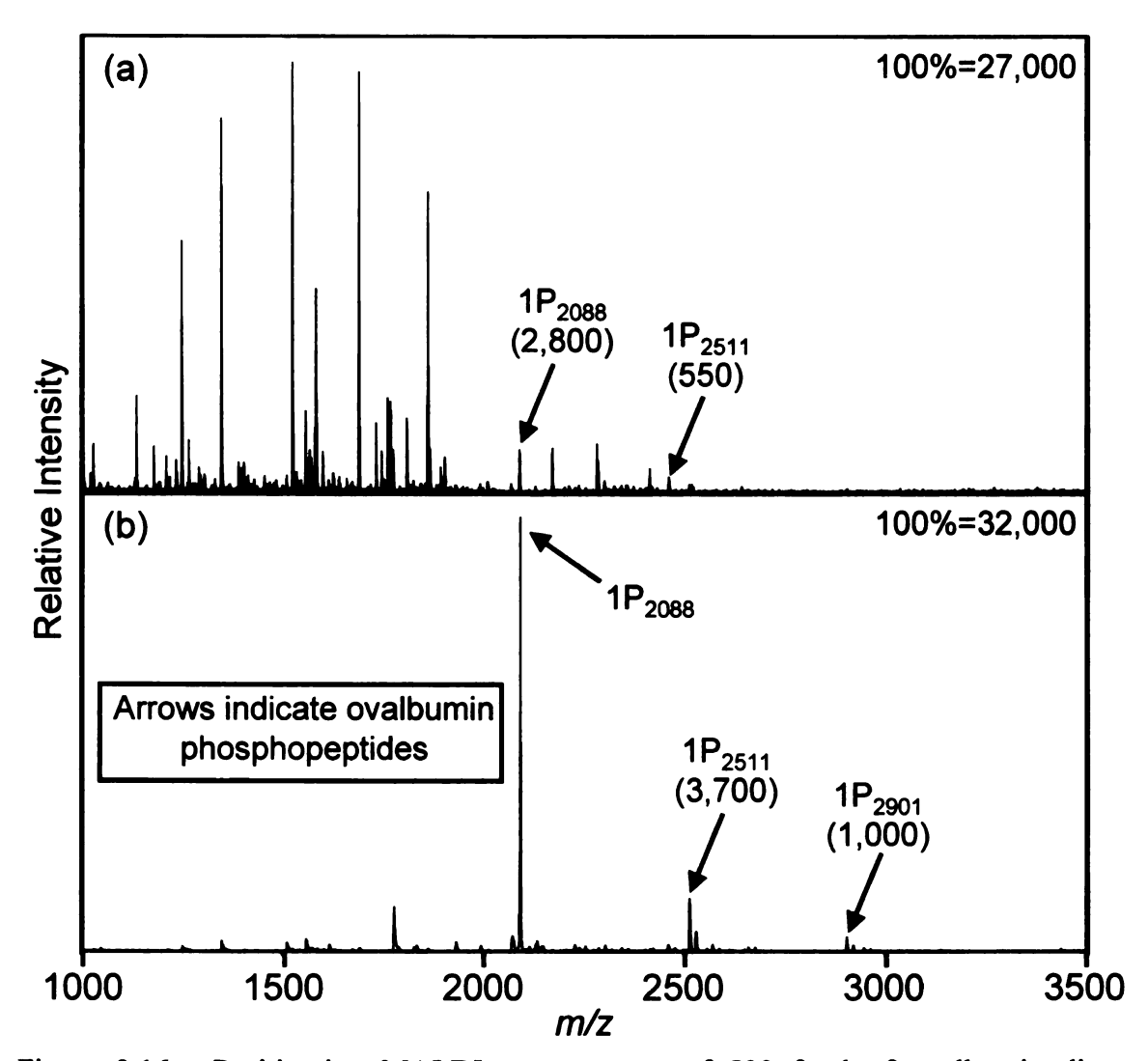


Figure 3.16: Positive-ion MALDI mass spectra of 500 fmol of ovalbumin digest. Spectra were obtained using a) conventional analysis and b) a Fe(III)-NTA-PHEMA-modified plate with incubation and rinsing. Numbers in parentheses are peak intensities.

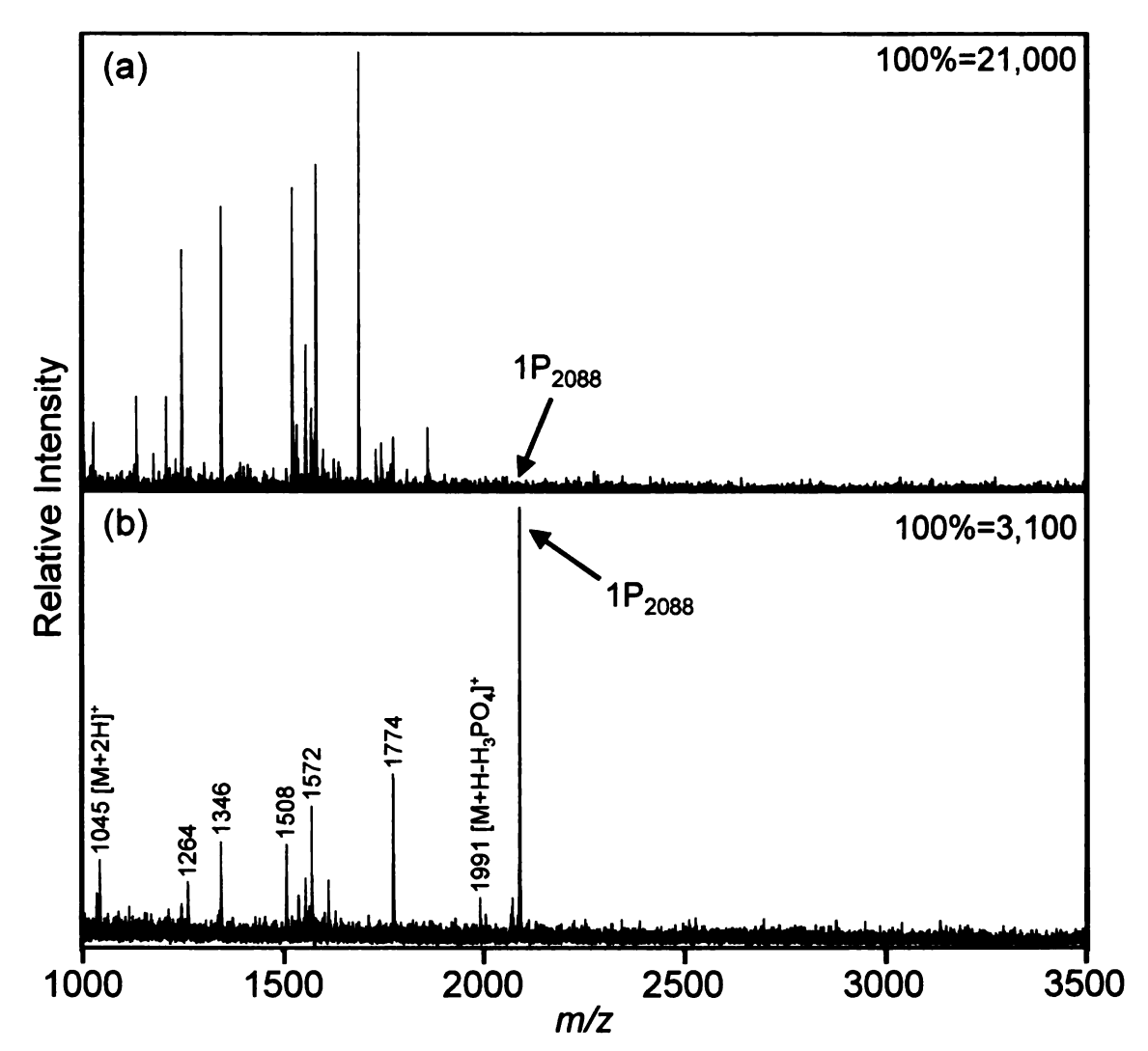


Figure 3.17: Positive-ion MALDI mass spectra of 125 fmol of ovalbumin digest. Spectra were obtained using a) conventional analysis and b) a Fe(III)-NTA-PHEMA-modified plate with incubation and rinsing. The number in parentheses is peak intensity.

The analysis of 125 fmol of ovalbumin digest is shown in Figure 3.17. No phosphopeptides were detected in the conventional MALDI mass spectrum. However, when the digest was applied to the modified plate, one phosphopeptides, $1P_{2088}$, was observed. Unfortunately, there were no signals due to the other two phosphopeptides at m/z 2511 and 2901. Relative to the phosphopeptide peak at m/z 2088, signals due to nonphosphorylated peptides at m/z 1774, 1508, 1346, and 1264 are stronger (1572 was not identified) than at higher digest concentrations. These peaks were characterized

using MS/MS and their assignments can be found in Table 3.2. Ovalbumin contains seven histidine residues and if this protein is digested completely, then the formation of 5 peptides containing at least one histidine residue and 20 peptides without histidine residues results. One of the histidine containing peptides is phosphorylated, 1P₂₀₈₈, and this peptide gives the largest signal of the phosphorylated species. All four of the nonphosphorylated peptides listed in Table 3.2, which contain at least one histidine residue were frequently detected when ovalbumin digests were analyzed using the Fe(III)-NTA-PHEMA-modified plate. Thus, the presence of the histidine residues in the peptides could be contributing to their binding to the polymer-modified plates. Similar results were found when the amount of ovalbumin digest was further decreased to 62 fmol as shown in Figure 3.18. The conventional analysis barely detected one of the phosphorylated peptides (m/z 2088) whereas the use of the polymer-modified plate showed a stronger signal for this phosphopeptide than for the nonphosphorylated peptides. Again, the mass spectrum showed peaks at m/z 1774, 1556, 1508, 1346, and 1248.

Table 3.2: Nonphosphorylated peptides that were frequently observed in the mass spectra of 1 pmol, 500 fmol, 125 fmol, and 62 fmol ovalbumin digest when the spectra were obtained using the Fe(III)-NTA-PHEMA-modified plate. The number of histidine (H), glutamic acid (E), and aspartic acid (D) residues for each peptide sequence are given.

Protein	Peptide Sequence	Sequence Number	# H	# D	# E	m/z
ovalbumin	ADHPFLFCIK	360-369	1	1	0	1248
	HIATNAVLFFGR	370-381	1	0	0	1346
	AFKDEDTQAMPFR	187-199	0	2	1	1556
	ISQAVHAAHAEINEAGR	323-339	2	0	2	1774
	VHHANENIFYCPIAIMSALAMVYLGAK	20-46	2	0	1	3034

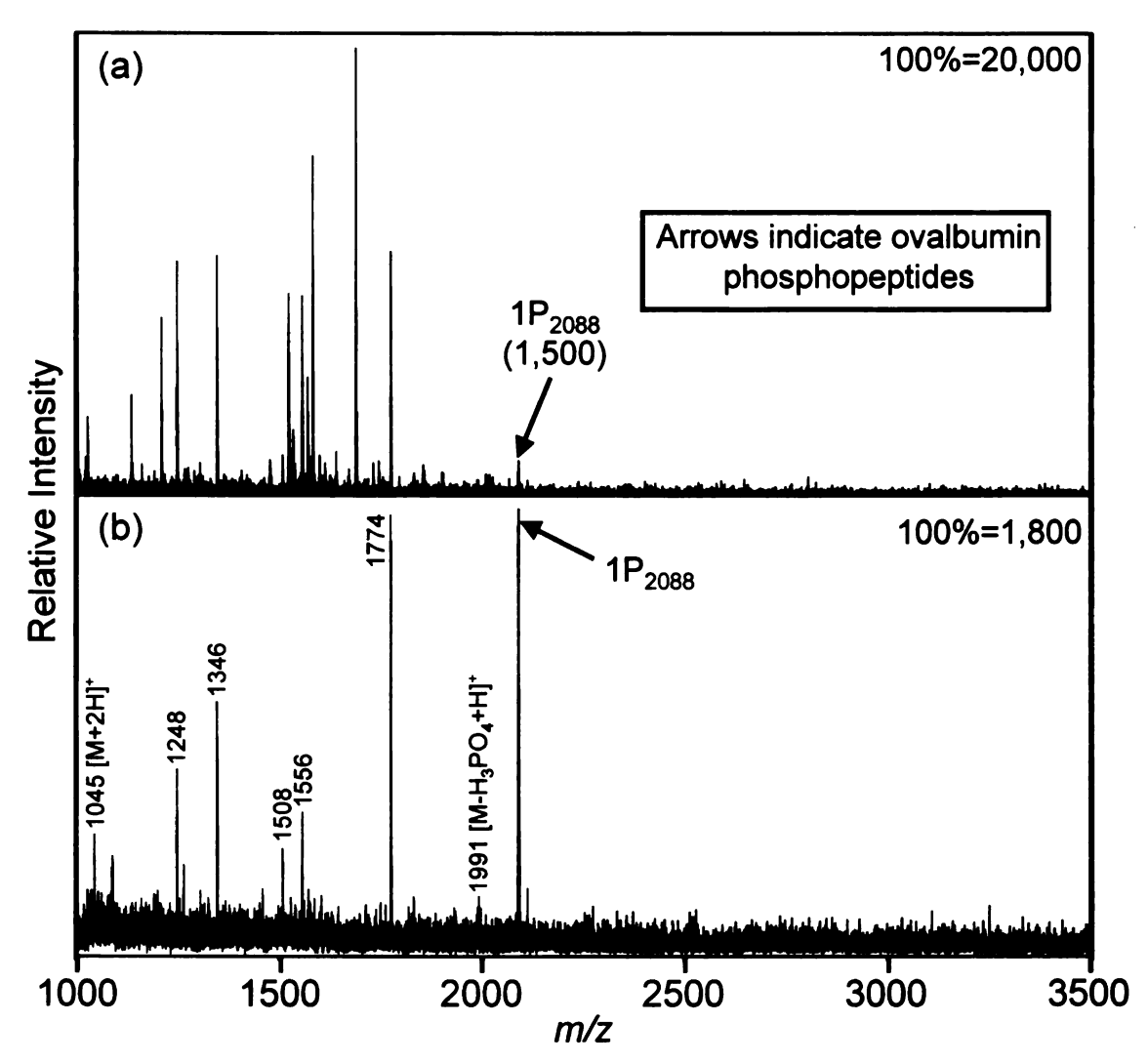


Figure 3.18: Positive-ion MALDI mass spectra of 62 fmol of ovalbumin digest. Spectra were obtained using a) conventional analysis and b) a Fe(III)-NTA-PHEMA-modified plate with incubation and rinsing. The number in parentheses is peak intensity.

3.3.5 Analysis of Methyl Esterified β-Casein Digest by MS Using Fe(III)-NTA-PHEMA-modified MALDI Plates

Although tryptic digests of β -casein are regularly used as a standard phosphoprotein digest to validate enrichment techniques, the tryptic phosphopeptides of β -casein are highly acidic, which could increase the binding affinity of these peptides towards the enrichment medium. Additionally, three of the phosphoserine residues in the tetraphosphorylated peptides are immediately adjacent to one another, and the other

phosphoserine residue is separated from them by a single lysine residue. Thus, the location of the phosphorylation sites in the tetraphosphorylated peptides of β -casein may allow these peptides to bind more strongly to the affinity material than other multiply phosphorylated peptides containing non-neighboring phosphorylation sites. The sequences of the β -casein phosphopeptides can be seen in Table 3.1. To study the effect of the acidic residues on the binding of the phosphopeptides to our Fe(III)-NTA-PHEMA-modified plates, we modified the β -casein digest by converting the carboxylic acid groups of glutamic acid and aspartic acid residues as well as the C-terminus to methyl esters.

The mass spectra in Figure 3.19 show the analysis of 250 fmol of non-methyl esterified and methyl esterified β -casein digests using the Fe(III)-NTA-PHEMA-modified plate. Analyses of the two digests are similar. The predominant peaks in the two mass spectra are due to the monophosphorylated peptides, $1P_{2062}$ and $1P_{2160}$. $1P_{2062}$ contains 7 carboxylic acid groups, so when this peptide is methyl esterified, the resulting peptide will have an m/z value of 2160 (2062 + 7 x 14 = 2160). In addition to the $1P_{2062}$ peak, Figure 3.19a shows other phosphopeptide peaks from α -caseins at m/z 1661, 1952, and 3008. These are the most commonly observed peaks when 250 fmol of β -casein is analyzed using the Fe(III)-NTA-PHEMA-modified plates. The corresponding peptide sequences are listed in Table 3.1. However, these peptides were not detected when the methyl esterified digest was analyzed. Instead, phosphopeptide peaks at m/z 1474 and 1523 are present, again due to α -casein impurities. These peaks correspond to non-methyl esterified phosphopeptides with m/z 1418 (1418 + 4 x 14 = 1474) and 1467 (1467 + 4 x 14 = 1532). From these results it is difficult to conclude if using methyl esterified

casein digest improved our enrichment method. In addition to extraction efficiencies, differences in ionization efficiencies could also cause differences between peptide signals before and after esterification.

In reference to the two peaks at m/z 2175 and 2190 in the spectrum of the esterified digest (Figure 3.20), these are due to side products associated with methyl esterification. Deamidation of glutamine (Q) and asparagine (N) residues to glutamic acid (E) and aspartic acid (D) residues, respectively, can occur as a side reaction.²³ Then the newly formed carboxylic acid groups can be subsequently methyl esterified, resulting in a mass shift of 15 Da. There are five glutamine residues contained in $1P_{2062}$, so multiple additions of 15 Da can be observed and in the mass spectrum in Figure 3.20, two additions of 15 occurred. Also, the peak that is at m/z 2146 is most likely due to incomplete methyl esterification of $1P_{2062}$.

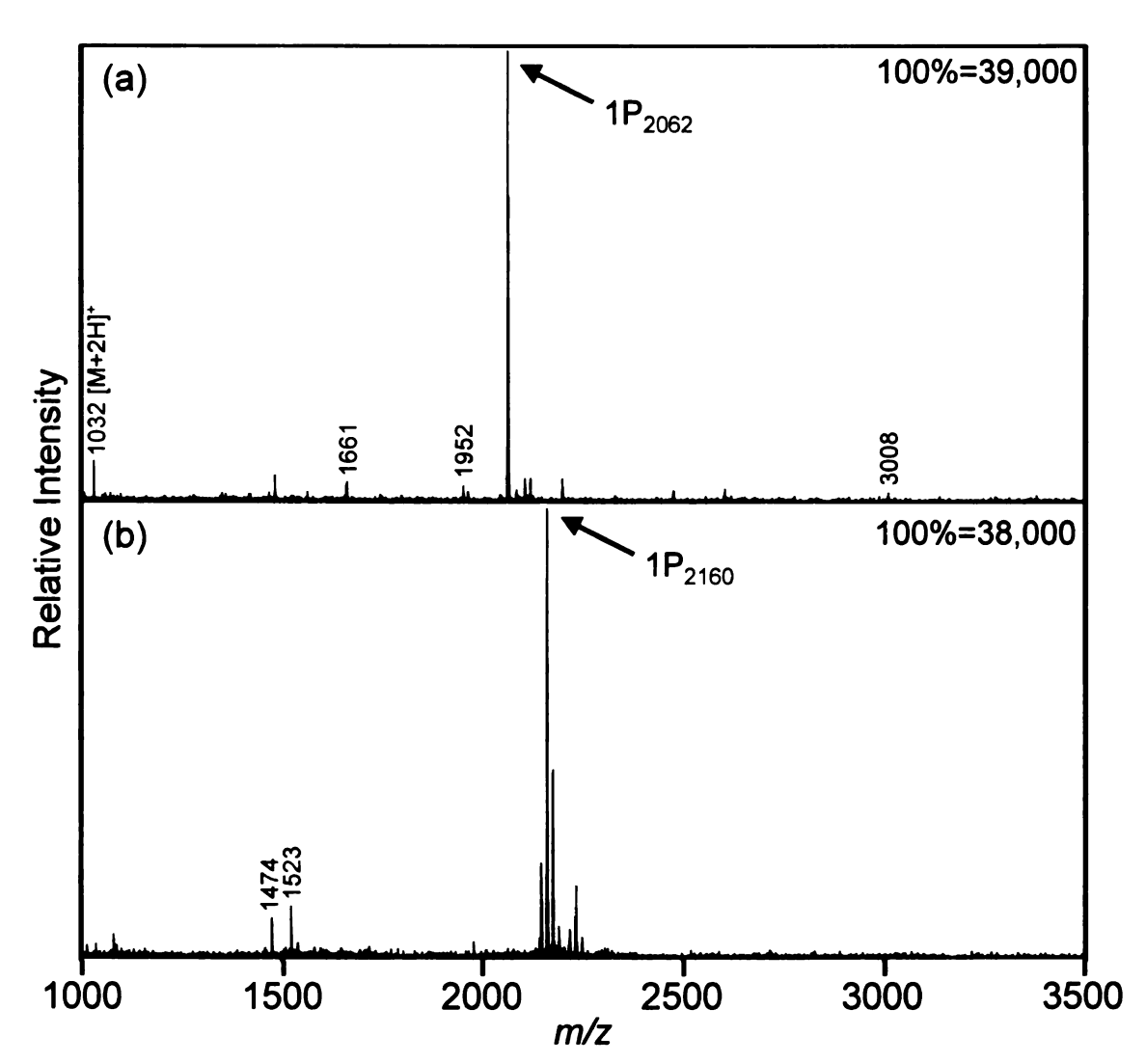


Figure 3.19: Positive-ion MALDI mass spectra of a) 250 fmol of β -casein digest and b) 250 fmol of methyl esterified β -casein digest. The spectra were obtained using an Fe(III)-NTA-PHEMA-modified plate with 1-h incubation and rinsing with 3:30:67 acetic acid:acetonitrile:water.

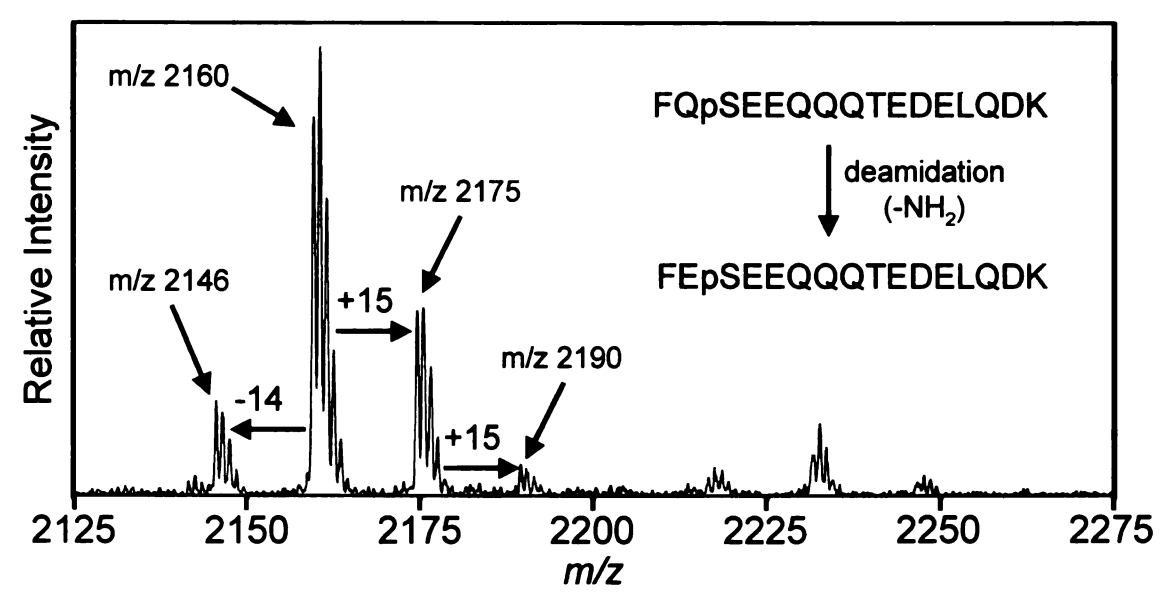


Figure 3.20: Enlarged region (2125 – 2275) of the positive-ion MALDI mass spectra of 250 fmol of a methyl esterified β -casein digest. The spectrum, which was obtained using enrichment on an Fe(III)-NTA-PHEMA-modified plate, shows peaks due to side products from deamidation with subsequent methyl esterification.

3.4 Conclusions

The results presented here demonstrate that the binding capacity of the Fe(III)-NTA-PHEMA-modified gold MALDI plates are 0.6 μg/cm². For a 2-mm diameter sample well this capacity corresponds to ~18 pmol of phosphopeptide. This high capacity should allow for binding of a wide range of phosphopeptides in a given sample and suggests that phosphopeptide recovery should be high. The recovery of low amounts of labeled phosphopeptide will be presented in the following chapter. For a β-casein digest, the limit of detection is less than 15 fmol for the monophosphorylated peptide. Mass spectra of ovalbumin digests clearly show that the use of the Fe(III)-NTA-PHEMA-modified plate greatly simplifies the MS analysis of phosphopeptides. Further studies need to be carried out to better understand the analysis of methyl esterified

phosphoprotein digests. Studies performed here are inconclusive as to whether acidic residues are important in the capture of phosphopeptides.

3.5 References

- (1) Kamigaito, M.; Sawamoto, M.; Higashimura, T. *Macromolecules* **1995**, *28*, 5671-5675.
- (2) Wang, J. S.; Matyjaszewski, K. Journal of the American Chemical Society 1995, 117, 5614-5615.
- (3) Matyjaszewski, K.; Spanswick, J. *Materials Today* **2005**, *8*, 26-33.
- (4) Matyjaszewski, K.; Xia, J. H. Chemical Reviews 2001, 101, 2921-2990.
- (5) Ejaz, M.; Yamamoto, S.; Ohno, K.; Tsujii, Y.; Fukuda, T. *Macromolecules* **1998**, 31, 5934-5936.
- (6) Bain, C. D.; Troughton, E. B.; Tao, Y. T.; Evall, J.; Whitesides, G. M.; Nuzzo, R. G. Journal of the American Chemical Society 1989, 111, 321-335.
- (7) Camillone, N.; Chidsey, C. E. D.; Liu, G. Y.; Scoles, G. *Journal of Chemical Physics* **1993**, *98*, 3503-3511.
- (8) Schlenoff, J. B.; Li, M.; Ly, H. Journal of the American Chemical Society 1995, 117, 12528-12536.
- (9) Shah, R. R.; Merreceyes, D.; Husemann, M.; Rees, I.; Abbott, N. L.; Hawker, C. J.; Hedrick, J. L. *Macromolecules* **2000**, *33*, 597-605.
- (10) Wang, X. S.; Jackson, R. A.; Armes, S. P. *Macromolecules* **2000**, *33*, 255-257.
- (11) Jones, D. M.; Brown, A. A.; Huck, W. T. S. Langmuir 2002, 18, 1265-1269.
- (12) Jones, D. M.; Huck, W. T. S. Advanced Materials 2001, 13, 1256-1259.
- (13) Sun, L.; Dai, J. H.; Baker, G. L.; Bruening, M. L. Chemistry of Materials 2006, 18, 4033-4039.
- (14) Dai, J. H.; Bao, Z. Y.; Sun, L.; Hong, S. U.; Baker, G. L.; Bruening, M. L. *Langmuir* **2006**, *22*, 4274-4281.
- (15) Jain, P.; Sun, L.; Dai, J.; Baker, G. L.; Bruening, M. L. Biomacromolecules 2007, submitted.
- (16) Hart, S. R.; Waterfield, M. D.; Burlingame, A. L.; Cramer, R. Journal of the American Society for Mass Spectrometry 2002, 13, 1042-1051.
- (17) AbDSerotec, http://www.ab-direct.com/about/faq-562.html (August 8, 2007).

- (18) Prochem, http://www.protein-chem.com/faqs-imac.html (August 8, 2007).
- (19) Garrett, T. J.; Prieto-Conaway, M. C.; Kovtoun, V.; Bui, H.; Izgarian, N.; Stafford, G.; Yost, R. A. *International Journal of Mass Spectrometry* **2007**, *260*, 166-176.
- (20) Bao, Z. Y.; Bruening, M. L.; Baker, G. L. Journal of the American Chemical Society 2006, 128, 9056-9060.
- (21) Dunn, J. D.; Watson, J. T.; Bruening, M. L. *Analytical Chemistry* **2006**, *78*, 1574-1580.
- (22) Larsen, M. R.; Thingholm, T. E.; Jensen, O. N.; Roepstorff, P.; Jorgensen, T. J. D. *Molecular & Cellular Proteomics* **2005**, *4*, 873-886.
- (23) Xu, C. F.; Lu, Y.; Ma, J. H.; Mohammadi, M.; Neubert, T. A. Molecular & Cellular Proteomics 2005, 4, 809-818.

Chapter Four: Comparison of Phosphopeptide Enrichment Techniques

4.1 Introduction

This chapter compares the phosphopeptide enrichment by our Fe(III)-NTA-PHEMA-modified plates with enrichment by two other types of modified gold plates that we prepared as well as commercially available IMAC and metal oxide materials. The choice of commercially available IMAC and metal oxide materials for this study was based on their applicably towards small volumes (1-2 µL) and fmol-levels of phosphopeptide. To make the comparison, MALDI-MS was used to quantitate the amount of synthetic phosphopeptide recovered from a given sample. MALDI-MS is not commonly used for quantitative analysis because solid samples (analyte/matrix) are typically heterogeneous, and the ionization efficiencies of peptides can vary widely. However, quantitation of peptides using MALDI-MS can be carried out with an appropriate internal standard such as a stable isotope-labeled peptide.¹ experiments presented here, two synthetic phosphopeptides were used, one being an isotopically labeled internal standard and the other being the recovered (or enriched) phosphopeptide. The linear dynamic range was first determined for the synthetic phosphopeptides to demonstrate over what range the internal standard could be employed. Subsequent experiments showed the unique enrichment properties of Fe(III)-NTA-PHEMA-modified plates

To examine whether relatively thick (thickness) brushes have advantages over monolayer and thin polymer films, we first compared the performance of Fe(III)-NTA-PHEMA-modified gold plates with plates modified with a ~10-Å thick monolayer of Fe(III)-NTA and with a thin ~30-Å thick polymer film derivatized with Fe(III)-NTA

(section 4.3.2). In these experiments, the phosphopeptide-binding moiety is kept constant, but the film architecture is varied. Figure 4.1 shows the procedure employed for fabrication of the plate modified with a monolayer of Fe(III)-NTA.

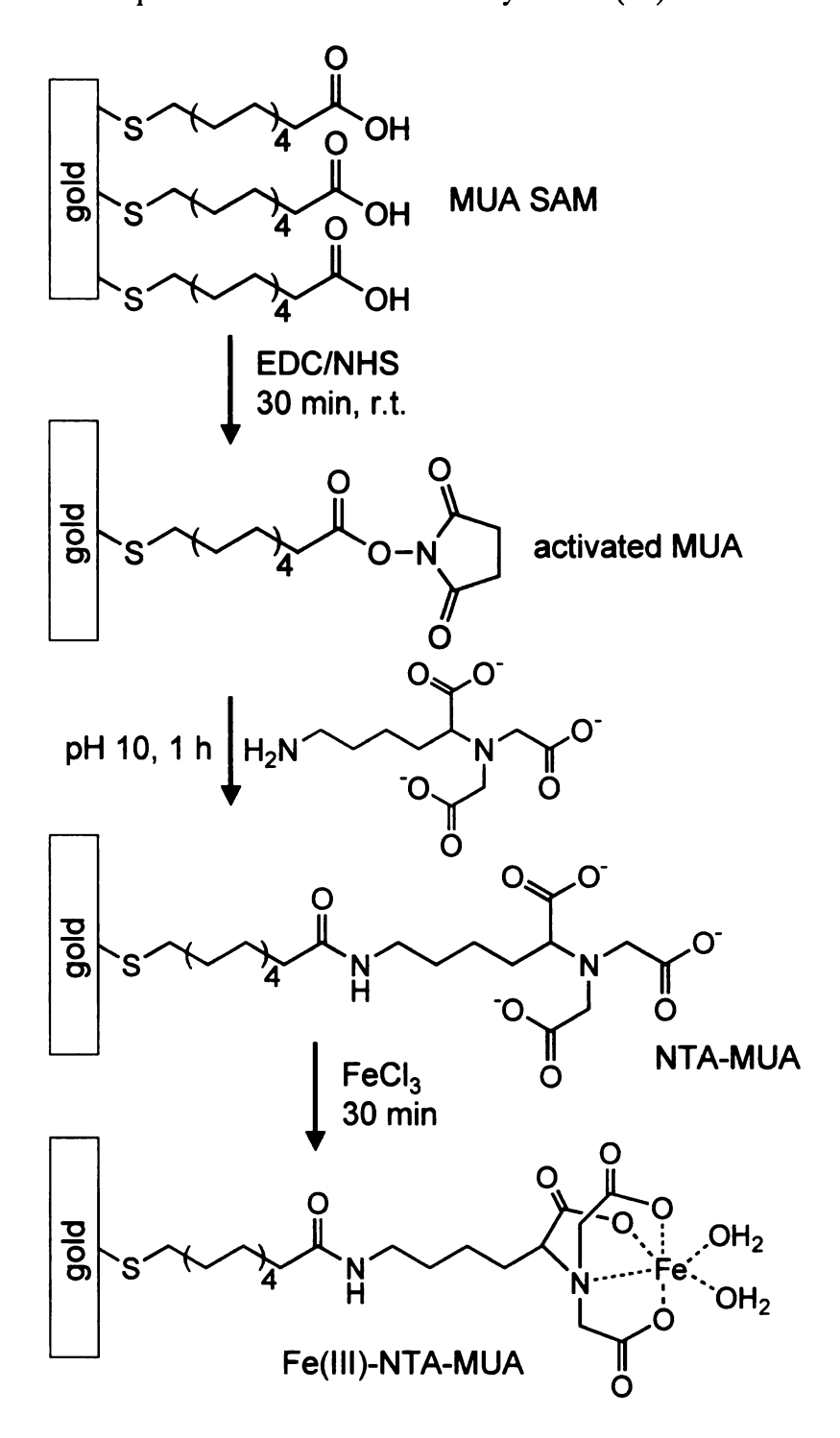


Figure 4.1: Synthesis of a Fe(III)-NTA-MUA-modified MALDI plate.

In brief, the monolayer of Fe(III)-NTA was immobilized onto a gold plate by first forming a self-assembled monolayer (SAM) of mercaptoundecanoic acid (MUA) on the surface. Next, the amino-terminated nitrilotriacetate derivative (NTA) was coupled to the MUA SAM after activation of carboxylic acid groups using EDC/NHS. Lastly, the monolayer was charged with Fe(III) by immersing the substrate into an aqueous ferric chloride solution. In this text, these monolayer-modified gold plates will be referred to as Fe(III)-NTA-MUA.

We also compared our high-capacity Fe(III)-NTA-PHEMA-modified plates with plates coated with a relatively thin (~30 Å), grafted poly(acrylic acid) (PAA) film that was functionalized with Fe(III)-NTA (Fe(III)-NTA-PAA-modified plates). These plates are essentially the same as those described in Chapter Two, but, we slightly modified the procedure by using EDC/NHS instead of ethyl chloroformate/4-methylmorpholine to activate the carboxylic acid groups of PAA as shown in Figure 4.2. Briefly, a MUA SAM is immobilized onto the gold surface and activated using EDC/NHS. Aminoterminated poly(tert-butyl acrylate) (PTBA) is then coupled to the activated monolayer and hydrolyzed with methanesulfonic acid, resulting in the formation of immobilized PAA. Once again, the carboxylic acid groups of PAA are activated with EDC/NHS and allowed to react with the amino-terminated NTA derivative under basic conditions. Lastly, the immobilized Fe(III)-NTA complex is formed using an aqueous ferric chloride solution. The fabrication of these plates was monitored using reflectance FTIR spectroscopy and ellipsometry.

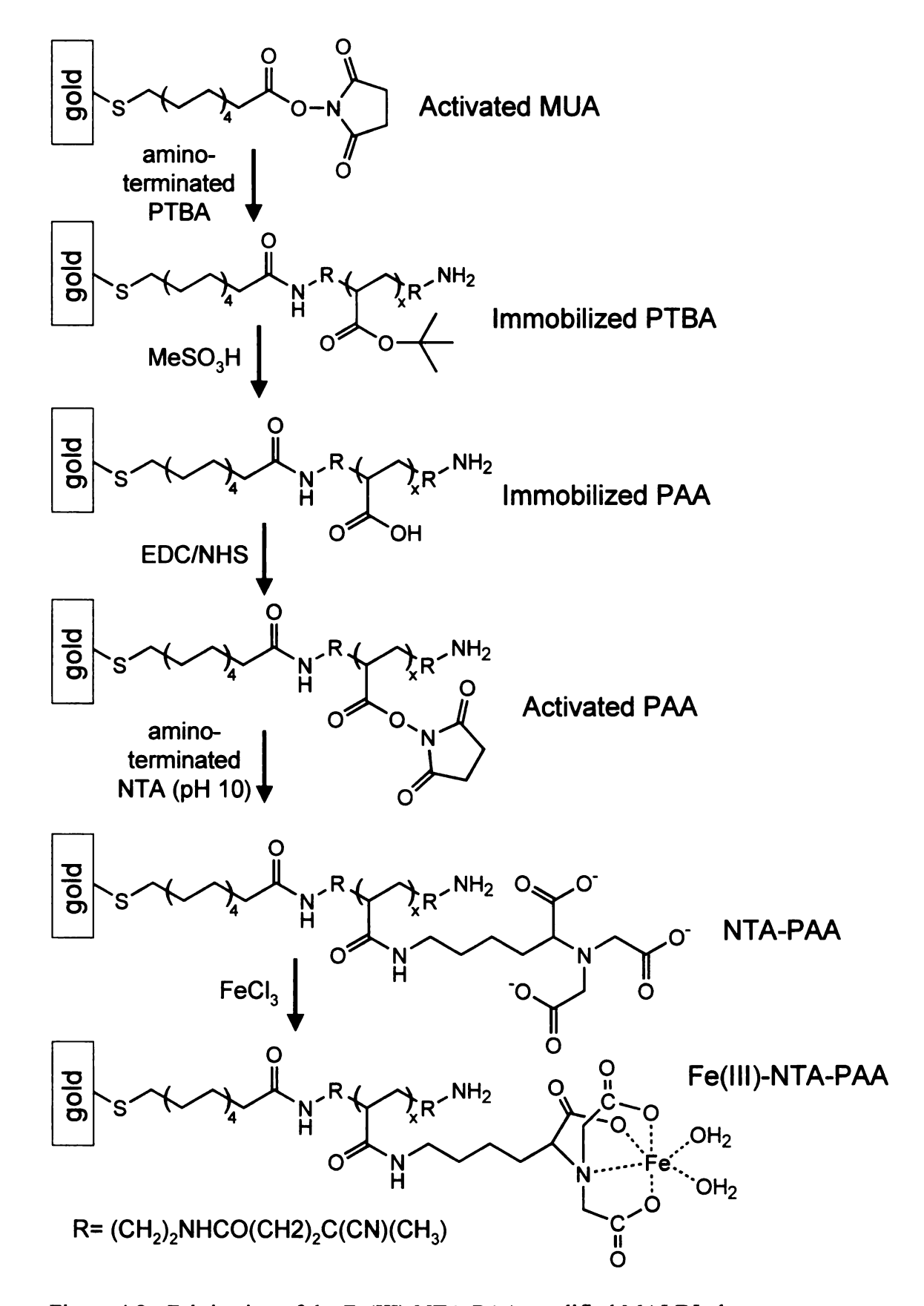


Figure 4.2: Fabrication of the Fe(III)-NTA-PAA-modified MALDI plate.

Section 4.3.3 of this chapter compares the Fe(III)-NTA-PHEMA-modified plates with commercial IMAC materials that also allow rapid and convenient enrichment. The commercial IMAC systems that we examined were Millipore ZipTip_{MC} pipette tips loaded with IMAC resin and Qiagen IMAC Mass Spec Focus Chips. The ZipTip_{MC} (MC stands for metal chelate) system is a 10- μ L pipet tip that is filled with 0.6 μ L of resin containing immobilized iminodiacetate (IDA) ligand (Figure 4.3).

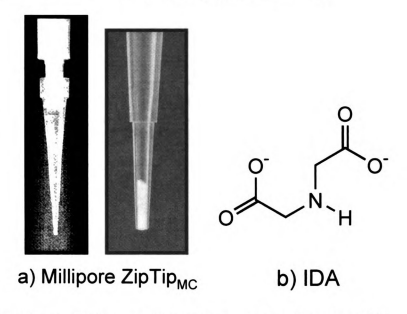


Figure 4.3: a) Millpore ZipTip_{MC} and b) structure of iminodiacetate (IDA).

The company claims that the binding capacity of these tips is 400 ng of peptide, however, a saturating amount of analyte is required to achieve this capacity. These disposable tips can be purchased through Fischer Scientific (8 tips for \$33), and their use seems practical and convenient for phosphopeptide capture and preconcentration since the enriched phosphopeptides can be directly eluted onto the MALDI sample plate for subsequent MS analysis.

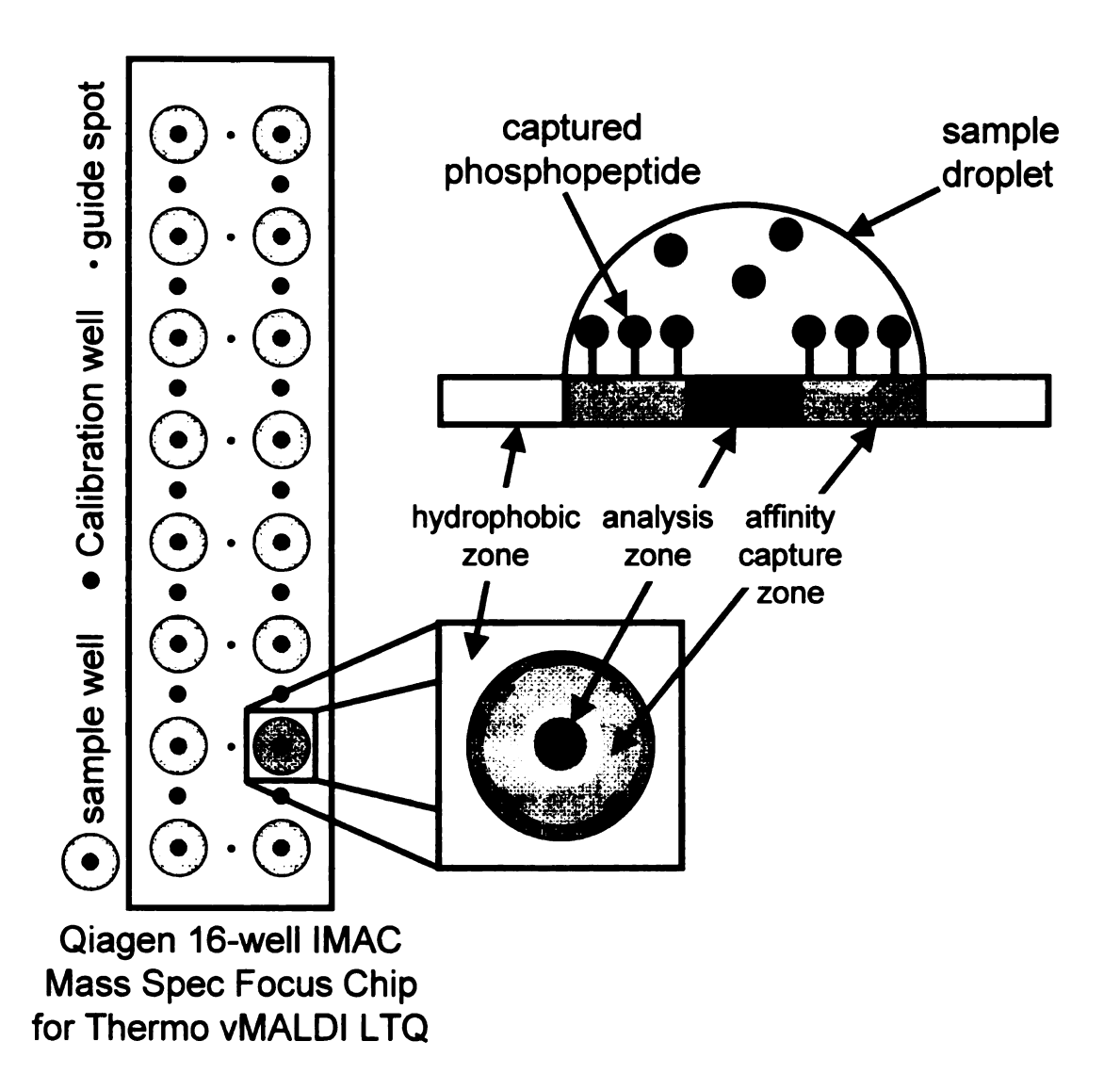


Figure 4.4: Qiagen Mass Spec Focus IMAC Chip for purification and concentration of phosphopeptides. The enlargement shows the hydrophobic zone, the analysis zone, and the affinity capture zone. Figure adapted from the Qiagen manual that accompanies the chips.

The use of IMAC MALDI plates available from Qiagen should, in principle, be equally as convenient as using plates modified with Fe(III)-NTA-PHEMA. Qiagen offers these plates for several MALDI mass spectrometers including Thermo, Applied Biosystems, Waters/Micromass, and Shimadzu/Kratos instruments. The use of these chips with the Thermo vMALDI LTQ mass spectrometer as described here requires a special plate (part number 97155-60125) that can hold the Qiagen IMAC chips. Each

IMAC chip for the vMALDI instrument is equipped with 16 sample wells, and a package of 6 chips can be purchased for \$843 through Qiagen. Figure 4.4 shows a diagram of the 16-well Qiagen IMAC Mass Spec Focus Chips, which contain 16 sample wells along with calibration wells. (The wells are invisible on the chip, so guide spots are present to help direct the spotting of the sample.) The wells are comprised of three regions or zones (Figure 4.4) that allow both purification and isolation of peptides. The white area in the figure is a hydrophobic zone and is used to enclose up to 35 µL of sample within the well. The grey zone contains the affinity ligands that capture the phosphopeptides when charged with Fe(III). When the bound phosphopeptides are eluted from the affinity zone, they are concentrated or focused into the 0.6-mm diameter analysis zone using the matrix solution. The analysis zone is more hydrophilic (more wettable) than the affinity zone, which allows the analyte/matrix to be focused in this region. The manufacturers do not give details on the phosphopeptide binding capacity of these plates or what affinity ligand was used. However, they claim that as little as 10 fmol of β -casein digest can be analyzed. We speculate that the affinity zone consists of a monolayer of NTA. In 2006, Qiagen presented a poster at the American Society for Mass Spectrometry on the use of chips modified with a NTA SAM for phosphopeptide purification and concentration.²

Lastly, due to the increase in popularity of metal oxide materials for phosphopeptide enrichment over the last two years, we wanted to compare our technique with commercially available metal oxide-based enrichment methods that are capable of dealing with low sample volumes and low amounts of analyte. In section 4.3.4, we make a comparison between the use of our high-capacity polymer-modified plates and commercial TiO₂ and ZrO₂ materials. We purchased TiO₂ and ZrO₂-loaded pipet tips

from Glygen. The company offers two types of 10-μL and 100-μL pipet tips, TopTips and NuTips containing these metal oxide materials. The 10-μL TopTips are packed with 4 mg of metal oxide chromatographic material and have a binding capacity of 400 μg, whereas 30 μg of metal oxide material is embedded into the walls of the 10-μL NuTips that have a binding capacity of 1-2 μg. We choose to use the 10-μL Glygen NuTips containing TiO₂ and ZrO₂ since these would require less volume and less analyte.

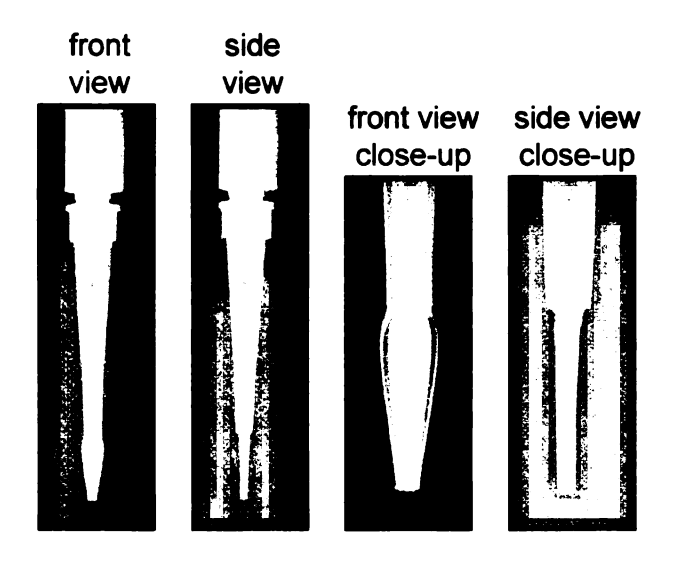


Figure 4.5: Several views of Qiagen NuTips, which contain embedded metal oxide chromatographic material. The end of the tip is flattened as shown in the side view, presumably to maximize the surface area of the tip in contact with the sample.

4.2 Experimental

4.2.1 Materials and Solutions

Bovine serum albumin (BSA, MW ~66 kDa), rabbit phosphorylase b (phos b, MW ~62 kDa), and pig esterase (MW ~97 kDa) were purchased from Sigma and digested using sequencing grade modified trypsin obtained from Promega. Other reagents employed in the digestion included Tris-HCl (Invitrogen), urea (J.T. Baker), 1,4-dithio-DL-threitol (BioChemika), iodoacetamide (Sigma), and ammonium bicarbonate (Columbus Chemical Industries).

The reagents employed in the preparation of surface-modified gold plates were 11-mercaptoundecanol (Aldrich), triethylamine (Jade Scientific), 2-bromoisobutyryl bromide (Aldrich), 2-hydroxyethyl methacrylate (Aldrich), cuprous chloride (Aldrich), cupric bromide (Aldrich), 2,2'-bipyridine (bpy, Aldrich), succinic anhydride (J.T. Baker), 4-dimethylaminopyridine (Sigma), N-(3-dimethylaminopropyl)-N'-ethylcarbodiimide hydrochloride (Sigma), N-hydroxysuccinimide (Aldrich), $N_{\alpha}N_{\alpha}$ -bis(carboxymethyl)-Llysine hydrate (Fluka), ferric chloride hexahydrate (Sigma), and glacial acetic acid (Spectrum). Dimethylformamide (DMF, Spectrum) was dried using 3-Å molecular sieves (Spectrum), and deionized water was obtained from a Millipore ion-exchange system (Milli-Q, 18 MΩcm) or a Barnstead nanopure diamond purification system (Dubuque, Iowa). HPLC grade acetonitrile (EMD), HPLC grade methanol (Sigma), isopropyl alcohol (EMD), and ammonium hydroxide (Columbus Chemical Industries) were used to clean the conventional stainless steel MALDI plate according to Thermo's "deep cleaning" procedure (see Chapter Three for details). The matrix used in all MS experiments was DHB in 1:1 HPLC grade acetonitrile (EMD):1% aqueous phosphoric acid (Aldrich). For conventional MALDI analyses, 1 µL of 10 mg/mL 2,5-DHB solution was applied to the sample wells and mixed on-plate with 1 µL of the protein digest, while for analyses carried out with the polymer-modified plates, 0.25 µL of 40 mg/mL 2,5-DHB solution was added to the sample wells on top of 1 µL of 1% phosphoric acid. The solution employed to rinse the polymer-modified plates prior to matrix addition was 3:33:67 glacial acetic acid:acetonitrile:water.

For peptide synthesis, sequenal grade trifluoroacetic acid (TFA) was obtained from Pierce (Rockford, IL), and N-α-Fmoc-protected amino acids and Wang resins

derivatized with Fmoc-protected amino acids (100-200 mesh) were purchased from EMD Biosciences (San Diego, CA). D₁₀-propionic anhydride was obtained from CDN Isotopes (Pointe-Claire, Quebec, Canada), while propionic anhydride was purchased from Sigma Aldrich (St. Louis, MO). Reagent grade dimethylformamide (DMF) from Spectrum Chemicals (Gardena, CA) was dried with 4-Å molecular sieves.

4.2.2 Digestion of a Mixture of Three Nonphosphorylated Proteins

In protein digestion, 100 µg of each nonphosphorylated protein, bovine serum albumin, rabbit phosphorylase b and pig esterase, were combined and dissolved in 20 μL of 6 M urea containing 50 mM Tris-HCl, (5 μg/μL). This solution was heated in a water bath at 70 °C for 1 hour after addition of 5 µL of 10 mM 1,4-dithio-DL-threitol (DDT) to cleave any disulfide bonds. After cooling, 160 µL of 50 mM ammonium bicarbonate was added to the protein solution, followed by a 30-µL aliquot of 100 mM iodoacetamide, and the mixture was placed in the dark for 1 h. Subsequently, 30 μ L of 0.5 μ g/ μ L modified trypsin was added to the solution, which was then incubated for ~16 hours at 37 °C. The digestions were quenched with addition of sufficient glacial acetic acid (~12 µL) to achieve a 5% solution, dried using a Speedvac, and stored in -20 °C freezer until use. The protein digest mixture was dissolved in 5% acetic acid prior to its application to the Fe(III)-NTA-MUA-, Fe(III)-NTA-PAA-, and Fe(III)-PHEMA-modified MALDI plates. The digest solution applied to the modified plates contained 1.7 µg of each protein: BSA, phos b, and esterase (5 µg total). See section 4.2.5 for the binding solutions used to dissolve the protein digest mixture for the commercial IMAC and metal oxide materials.

4.2.3 Labeled Phosphopeptide Synthesis

CH₃CH₂CO-LFTGHPEpSLEK (H₅ peptide) and CD₃CD₂CO-LFTGHPEpSLEK (D₅ peptide) were prepared using manual stepwise Fmoc-based solid-phase peptide synthesis on Fmoc-Lys(boc)-Wang resins (0.05 mmol). Fmoc amino acids (0.25 mmol) were preactivated thorough with O-(benzotriazol-1-yl)-N,N,N',N',by mixing tetramethyluronium tetrafluoroborate (TBTU) (0.25 mmol), 1-hydroxybenzotriazole hydrate (HOBt) (0.25 mmol), and N,N-diisopropylethylamine (DIPEA) (0.38 mmol) in DMF and then coupled with the peptidyl resin for 15 min. Fmoc-Ser(PO(OBzl)OH-OH was used for phosphoamino acid incorporation and was coupled in a similar fashion as described above except a 3-fold excess of DIPEA was used. Fmoc deprotection was performed with a solution of 30% piperidine in DMF for 25 min while shaking. Nterminal acetylation was performed following the final Fmoc deprotection step by the addition of DIPEA (0.25 mmol) and either d_{10} -propionic anhydride (0.17 mmol) or propionic anhydride (0.17 mmol) in DMF to the resin, while shaking for 15 min. Sidechain protecting groups and the resin were cleaved from the peptide with 2.5% triisopropylsilane and 2.5% water in trifluoroacetic acid for 2 hours. Product peptides were precipitated in diethyl ether, redissolved in 25% aqueous acetic acid, lyophilized, then purified by Reversed Phase-High Performance Liquid Chromatography (RP-HPLC) using an Aquapore RP-300 column (4.6 mm; Perkin Elmer, Wellesley, MA) and a linear gradient elution at a flow rate of 1 mL/min from 0-100% B, where solvent A was 0.1% TFA in water, and solvent B was 0.089% TFA/60% acetonitrile in water. concentrations of aqueous stock solutions of the H₅ and D₅ peptides were determined by amino acid analysis completed by the Genomics Technology Support Facility at Michigan State University. Aliquots (100 pmol) of the stock solutions were concentrated and stored at -20 °C until further use.

4.2.4 Fabrication of Modified MALDI Plates

Gold-coated Si wafers (1.3 x 2.8 cm) were UV/ozone-cleaned and then immersed in 1 mM 11-mercaptoundecanol (MUD) in ethanol overnight (1 h was also used) to form a monolayer of MUD on the gold surface. The wafers were then rinsed with ethanol and water and dried completely with a stream of nitrogen gas. Typically, 8 wafers were simultaneously prepared at a given time. The 8 wafers were placed in a crystallizing dish and inserted into a glove bag under N₂. In the glove bag, triethylamine (0.33 mL in 20 mL DMF) was added to the crystallizing dish, followed by dropwise addition of 2bromoisobutyryl bromide (0.25 mL/20 mL DMF) over 10 min. The wafers were rinsed with DMF, ethyl acetate, ethanol, and water and dried with a stream of nitrogen. The presence of an ester carbonyl peak at ~1730 cm⁻¹ in the reflectance FTIR spectrum was used to verify the attachment of the initiator to the MUD SAM. In a Schlenk flask, 30 mL of 2-hydroxyethyl methacrylate (HEMA) and 30 mL of MilliQ water were degassed using freeze-pump-thaw-pump cycling. After three cycles, 165 mg CuCl, 108 mg CuBr₂, and 640 mg of bpy were added to the flask and an additional three freeze-pump-thawpump cycles were performed. The flask was transferred to an N₂ glove bag, and the solution was equally added to four 20-mL scintillation vials containing two wafers each. The desired thickness of PHEMA was determined by the length of time the wafers were immersed in HEMA solution. Typically, wafers immersed in the HEMA solution for 2 h resulted in PHEMA film thicknesses of 25-30 nm. The PHEMA brushes were removed

from the vials, rinsed with DMF, water, and ethanol, and characterized using reflectance FTIR spectroscopy. These films were then immersed in 10 mL of DMF containing 0.1 g succinic anhydride and 0.2 g of 4-dimethylaminopyridine (DMAP) and heated at 55 °C for 3 h in order to convert the hydroxyl groups of PHEMA to carboxylic acid groups. These films were sonicated in DMF for 10 min, rinsed with water and ethanol and dried with N_2 . The carboxylic acid groups were activated using N-(3-dimethylaminopropyl)-N'-ethylcarbodiimide hydrochloride (EDC, 96 mg) and N-hydroxysuccinimide (NHS, 58 mg) in 10 mL of water for 30 min, followed by ethanol and water rinses and drying with N₂. To immobilized NTA onto the films, the wafers were immersed in an aqueous solution of 0.1 M $N_{\infty}N_{\alpha}$ -bis(carboxymethyl)-L-lysine hydrate, an amino-terminated NTA derivative, at a pH of 10 (pH adjusted using NaOH) for 1 h. The films were rinsed thoroughly with water and dried using N₂. The Fe(III)-NTA complex was formed by immersing the films into an aqueous solution of 100 mM FeCl₃ for 30 min and then rinsing with ethanol and drying using N₂. The films were additionally immersed in a solution of 250 mM acetic acid in 30% acetonitrile for 15 min and rinsed with ethanol to remove any loosely bound ferric ions. The immobilization of Fe(III)-NTA-PHEMA onto gold wafers is depicted in Figure 3.2. All the steps during the fabrication process were monitored using reflectance FTIR spectroscopy. Initially, the wafer was cut to the dimensions of the sample holder (1.3 x 2.8 cm) of the FTIR instrument. However, in order for the wafer to fit into the modified stainless steel MALDI sample plate (this plate is modified to accommodate standard microscope slides with dimensions of 2.5 cm x 7.5 cm x 0.1 cm), the wafers were cut to fit the width (2.5 cm) of the plate and sample wells were made by lightly scratching a 2-mm diameter circle onto the wafer using a tungsten carbide-tipped pen and a mask with circular patterns with 2-mm diameters. Six wells on one wafer were created in this fashion, and each well served to contain the 1- μ L protein digest solution that was spotted onto the wafer. The wells were capable of holding a maximum of 2-3 μ L of aqueous solution, and the wafers were secured to the modified stainless steel MALDI sample plate using double-sided tape.³

4.2.5 Protocols for Determining Phosphopeptide Recovery

Stock solutions containing 100 pmol of either H₅ or D₅ peptides were prepared in 200 μL of deionized water, and all working solutions (125, 62, 31, 16, 8 fmol/μL) were made from the stock solutions using serial dilutions with deionized water. For on-plate enrichment techniques (Fe(III)-NTA-MUA, Fe(III)-NTA-PAA, and Fe(III)-NTA-PHEMA), recovery of the H₅ peptide in the absence of nonphosphorylated protein digest was determined using the following protocol. First, 1 µL of 5% acetic acid was applied to the 2-mm wells on the plates prior to adding 1 μL of aqueous 125-fmol/μL H₅ peptide. The samples were incubated for 1 h (or 10 min in a few cases), and 0.5 µL aliquots of 5% acetic acid were reapplied during the incubation as needed to prevent the sample from The plates were then rinsed with 15-20 mL of 3:30:67 acetic drying. acid:acetonitrile:water solution and completely dried with nitrogen. A 1-µL aliquot of 125 fmol/μL D₅ peptide was applied to the 2-mm well on the plate as an internal standard, followed by 1 µL of 1% phosphoric acid and 0.25 µL of 40 mg/mL 2,5-DHB in 1:1 acetonitrile:1% phosphoric acid. Analysis using MALDI-MS was then performed to compare signals due to the H₅ and D₅ peptides. Recovery of the H₅ peptide in the presence of a digest of BSA, phos b, and esterase was determined using a similar protocol with the exception that 1 μ L of the digest mixture, which contained 1 pmol of protein, was first spotted into the wells, instead of the 5% acetic acid, prior to adding 1 μ L of 125 fmol/ μ L H₅ peptide.

In the case of ZipTipMC pipette tips, the phosphopeptide enrichment protocol provided by the manufacturer was followed. The tips were prerinsed with 0.1% acetic acid in 50% acetonitrile (3 x 10 µL), then charged with 200 mM FeCl₃ in 10 mM HCl (10 x 10 μ L) and subsequently rinsed with deionized water (3 x 10 μ L) followed by 1% acetic acid in 10% acetonitrile (3 x 10 µL). For the analysis involving the recovery of the H₅ peptide from the digest mixture, 1 μL of 1 pmol/μL protein digest mixture together with 1 μL of 125 fmol/μL H₅ peptide was dried completely using a Speedvac. This mixture was reconstituted in 2 µL of 0.1% acetic acid in 10% acetonitrile. The solution was loaded onto the tip and aspirated 10 times. The tip was then rinsed with 0.1% acetic acid in 10% acetonitrile (6 x 10 μ L) and deionized water (3 x 10 μ L). Using 2 μ L of 3 N NH₄OH, the solution was aspirated 6 times to elute the peptides and then this solution was dried and redissolved in 1:1 water:acetonitrile and subsequently spotted onto the stainless steel MALDI plate. A 1 µL aliquot of 125 fmol/µL D₅ peptide (internal standard) and 1 µL of 10 mg/mL 2,5-DHB in 1:1 acetonitrile:1% phosphoric acid were added to the 2 mm well on the conventional plate and allowed to dry prior to MALDI-MS analysis.

For Qiagen MALDI plates, the protocol provided by Qiagen was used for recovery of the H₅ peptide, and this procedure called for the following solutions: wash solution I, 100 mM acetic acid; wash solution II, 100 mM acetic acid, 800 mM urea, 0.1% octyl β-D-glucopyranoside; eluent, 9:1 acetonitrile:0.1% phosphoric acid; and iron

charging solution, 100 mM FeCl₃ hexahydrate in 1 mM acetic acid. Dried samples of the H₅ peptide with or without the digest mixture were dissolved in 5 μL of wash solution II prior to addition to the plate. The matrix solution that was employed was 10 mg/mL 2,5-DHB (20 mg of 2,5-DHB dissolved in 200 µL of 3:13:84 (v:v:v) 0.1% TFA:ethanol:acetonitrile). First, 10 µL of iron charging solution was added to the sample wells and removed with a pipet after 15 min. Each well was rinsed with 10 μL of wash solution I by aspirating the solution up and down 5 times and letting the solution stand for 2 min. The solution was removed and this step was repeated with fresh solution. Each well was also rinsed twice with 10 µL of wash solution II in the same fashion as above. The H_5 peptide-containing sample (5 μ L) was added to the well, incubated for 20 min and then removed with a pipette. The wells were rinsed twice with solution II (10 µL) aspirated 5 times) and twice with solution I (10 µL aspirated 5 times) and allowed to air dry prior to spotting 1 μL of 125 fmol/μL D₅ peptide and 2 μL of the elution solution on the plate, which was in a homemade humidity chamber (a water-soaked sponge was secured against the walls of a glass TLC chamber above a bed of water.) After the sample had focused to the analysis zone, the chip was removed and dried under room conditions. Two microliters of the 2,5-DHB solution was applied to each well and allowed to focus to the analysis zone. Occasionally, spots needed to be refocused using 1 μL of 90:10 acetonitrile:0.1% TFA since the matrix crystallized outside the 0.6-mm diameter analysis zone.

Solutions prepared for analysis of the H₅ peptide using either TiO₂ or ZrO₂ Glygen NuTips were 66 mg/mL 2,5-DHB in 1% TFA in 80% acetonitrile (wash solution I), 1% TFA in 80% acetonitrile (wash solution II), and 3% NH₄OH (elution solution).⁴

Dried samples of the H_5 peptide with or without protein digest mixture were dissolved in wash solution I. The tips were prerinsed twice with 10 μ L of wash solution I, and then 2 μ L of the H_5 peptide-containing solution was loaded onto the tip and aspirated 50 times. The tips were rinsed with 10 μ L of solution I ten times, followed by 10 μ L of wash solution II ten times. The H_5 peptide was eluted with 2 μ L of 3% NH₄OH (aspirated 6 times) and dried. The dried sample was reconstituted in 1 μ L of water and 1 μ L of acetonitrile and applied to the stainless steel MALDI plate. One μ L of 125 fmol/ μ L of D_5 peptide and 1 μ L of 10 mg/mL 2,5-DHB in 1:1 acetonitrile:1% phosphoric acid were added and allowed to dry.

4.2.6 Instrumentation and Data Analysis

MALDI mass spectra shown here are representative of many similar spectra, as each experiment was repeated three times or more using different modified plates. All mass spectra shown in this chapter were obtained using a MALDI linear ion trap mass spectrometer (Thermo vMALDI LTQ XL), and peptide sequencing was made possible using low energy collision-induced dissociation (CID). Protein Prospector (http://prospector.ucsf.edu) was used to make preliminary assignments to signals in the mass spectra, and assignments were confirmed using CID tandem mass spectrometry. The Protein Prospector website was also used to help confirm assignments of product ions observed in the tandem mass spectra. The thicknesses of polymer films on modified plates were determined using a rotating analyzer spectroscopic ellipsometer (J. A. Woollam, M-44), assuming a film refractive index of 1.5. Reflectance FTIR spectra of

the modified plates were collected using a Nicolet Magna 560 spectrophotometer with a Pike grazing angle (80°) accessory.

4.3 Results and Discussion

4.3.1 Calibration

The synthetic phosphorylated peptides, H₅ and D₅ peptides, are shown in Figure 4.6. Since these peptides are identical with the exception that the D₅ peptide contains a deuterated label, they should desorb and ionize equally in MALDI-MS analysis. Hence, for an equimolar mixture of the H_5 peptide (m/z 1393.6) and the D_5 peptide (m/z 1398.6), we would expect to see approximately equal ion intensities in the MALDI mass spectrum with the isotopic peaks being separated by 5 m/z units. The MALDI-MS linear dynamic range of these phosphorylated peptides was determined to be 8 fmol – 125 fmol. To compensate for any small variations in the sensitivity of MALDI for the two phosphorylated peptides at slightly different concentrations, a calibration curve (Figure 4.7) was prepared and used to calculate the percent recovery of the H₅ peptide using the D₅ peptide as the internal standard. Since the D₅ peptide was the internal standard, the 5point calibration curve was created by analyzing mixtures containing 125 fmol of the D₅ peptide and varying amounts of the H_5 peptide (125, 62, 31, 16, and 8 fmol). The ratio of the peak intensities due to the H_5 and D_5 peptides (I_{H5}/I_{D5}) in the MALDI mass spectra were plotted versus the amount of the H₅ peptide as shown in Figure 4.7 to obtain a highly linear plot that reveals essentially equal sensitivities for the two peptides.

$$H_3C$$
 CH_2
 $LFTGHPEpSLEK$

a) H_5 peptide (m/z 1393.6)

 D_3C
 CD_2
 $LFTGHPEpSLEK$

b) D_5 peptide (m/z 1398.6)

Figure 4.6: Sequence of the labeled synthetic phosphopeptides a) H_5 peptide and b) D_5 peptide with their respective m/z values.

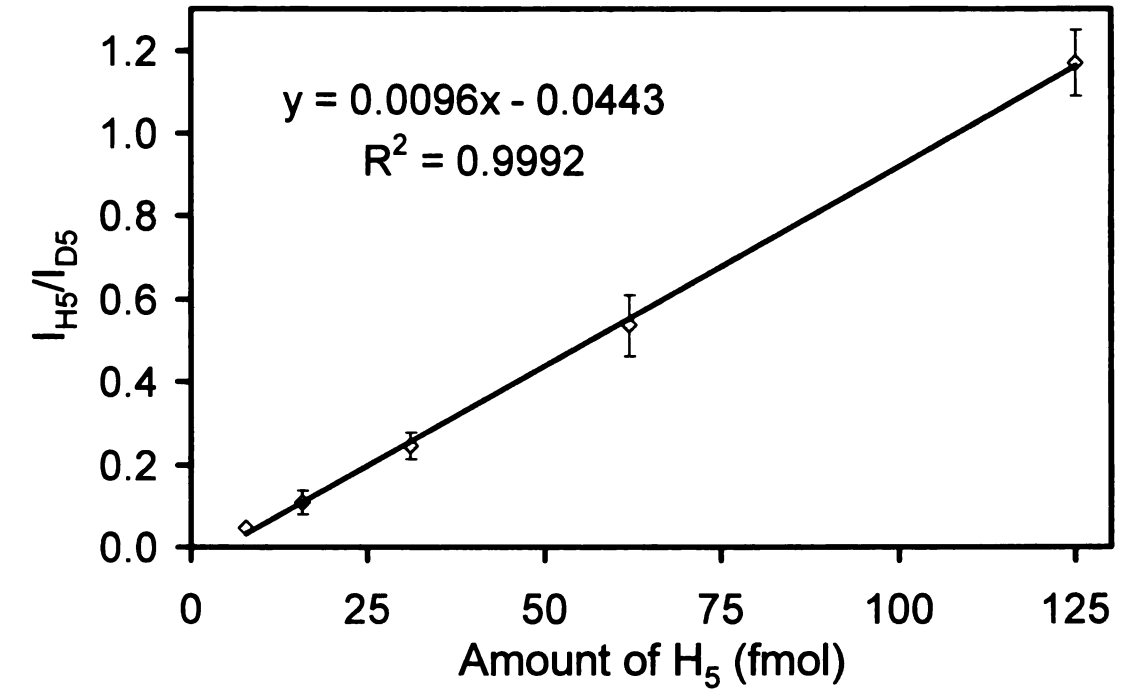


Figure 4.7: Calibration curved prepared by plotting the ratio of the peak intensities due to the H_5 and D_5 peptides (I_{H5}/I_{D5}) in MALDI mass spectra. 125 fmol of the D_5 peptide was present in all samples, and the amount of the H_5 peptide was varied from 8 to 125 fmol.

4.3.2 Recovery of the H₅ Peptide Using Monolayer-modified and Polymer-modified MALDI Plates

Figure 4.8 illustrates the procedure used to examine the efficiency of on-plate enrichment of the H₅ peptide in the absence of the protein digest mixture using MALDI plates modified with Fe(III)-NTA-MUA or Fe(III)-NTA-PHEMA. These plates differ greatly in the ellipsometric thicknesses of the NTA-Fe(III) films, which were ~10 Å, ~30 Å, and ~500 Å for Fe(III)-NTA-MUA, Fe(III)-NTA-PAA, and Fe(III)-NTA-PHEMA, respectively.

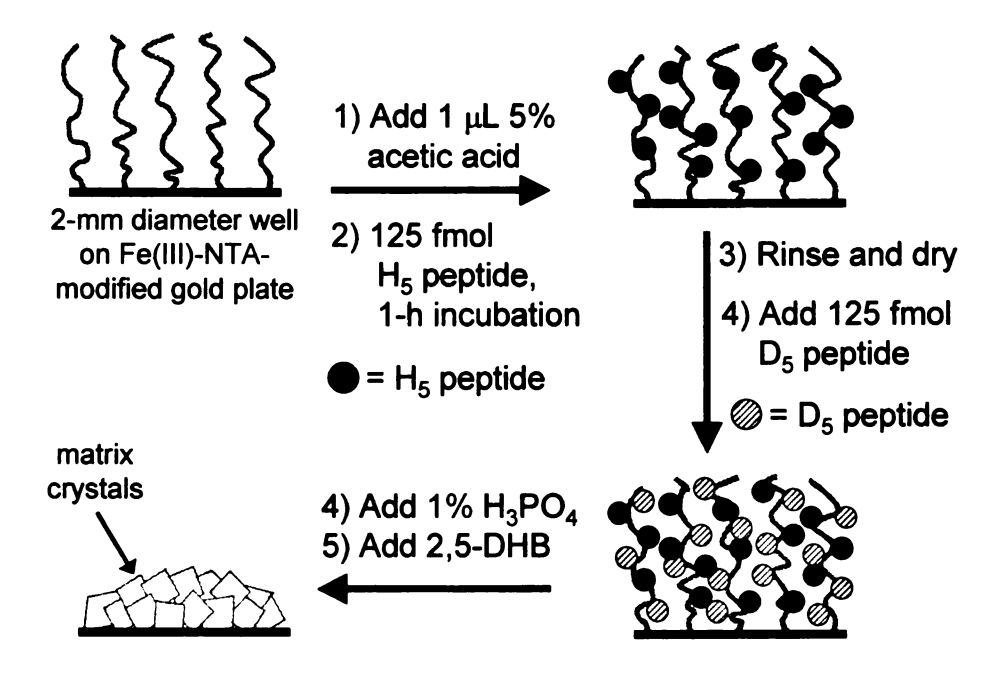


Figure 4.8: Procedure used to recover the H₅ peptide (no digest) using Fe(III)-NTA-MUA-modified or Fe(III)-NTA-PHEMA-modified plates.

First, 5% acetic acid is applied to the 2-mm diameter sample, followed immediately by addition of 125 fmol of the H₅ peptide. The H₅ peptide was incubated with the plate for 1 h, and the plate was thoroughly rinsed with 3:30:67 acetic acid:acetonitrile:water solution to remove any unbound H₅ peptide. Next, 125 fmol of the D₅ peptide, the internal standard, was added followed by the 1% phosphoric acid containing 2,5-DHB. After the

matrix/H₅ peptide/D₅ peptide mixture co-crystallized, this sample was analyzed using MALDI-MS.

When the Fe-(III)-NTA-MUA-modified plate was used to analyze 125 fmol of the H₅ peptide (in the absence of the protein digest mixture) by MALDI-MS, the ratio of the H₅ peptide to the D₅ peptide signal intensities from the mass spectrum and the use of the equation given in the calibration curve (Figure 4.7) gave a recovery of the H₅ peptide of $14 \pm 5\%$ (Figure 4.9a). In contrast, when the same sample was applied to the Fe(III)-NTA-PHEMA-modified plate, the recovery of the H_5 peptide was 72 ± 3%. The mass spectrum of the H₅ peptide recovered using an Fe(III)-NTA-PHEMA-modified plate is shown in Figure 4.9b. The peak at m/z 1393.6 is due to the H₅ peptide recovered using the modified plate and the peak at m/z 1398.6 is due to the D₅ peptide, the internal standard. The other peaks are the isotopic peaks of the two phosphorylated species, which are present due to the natural abundance of other isotopes. These results clearly demonstrate that these thick polymer films are capable of binding more phosphopeptide than a single layer of Fe(III)-NTA. The recovery of 125 fmol of the H₅ peptide in the absence of protein digest was not determined using the Fe(III)-NTA-PAA-modified plates.

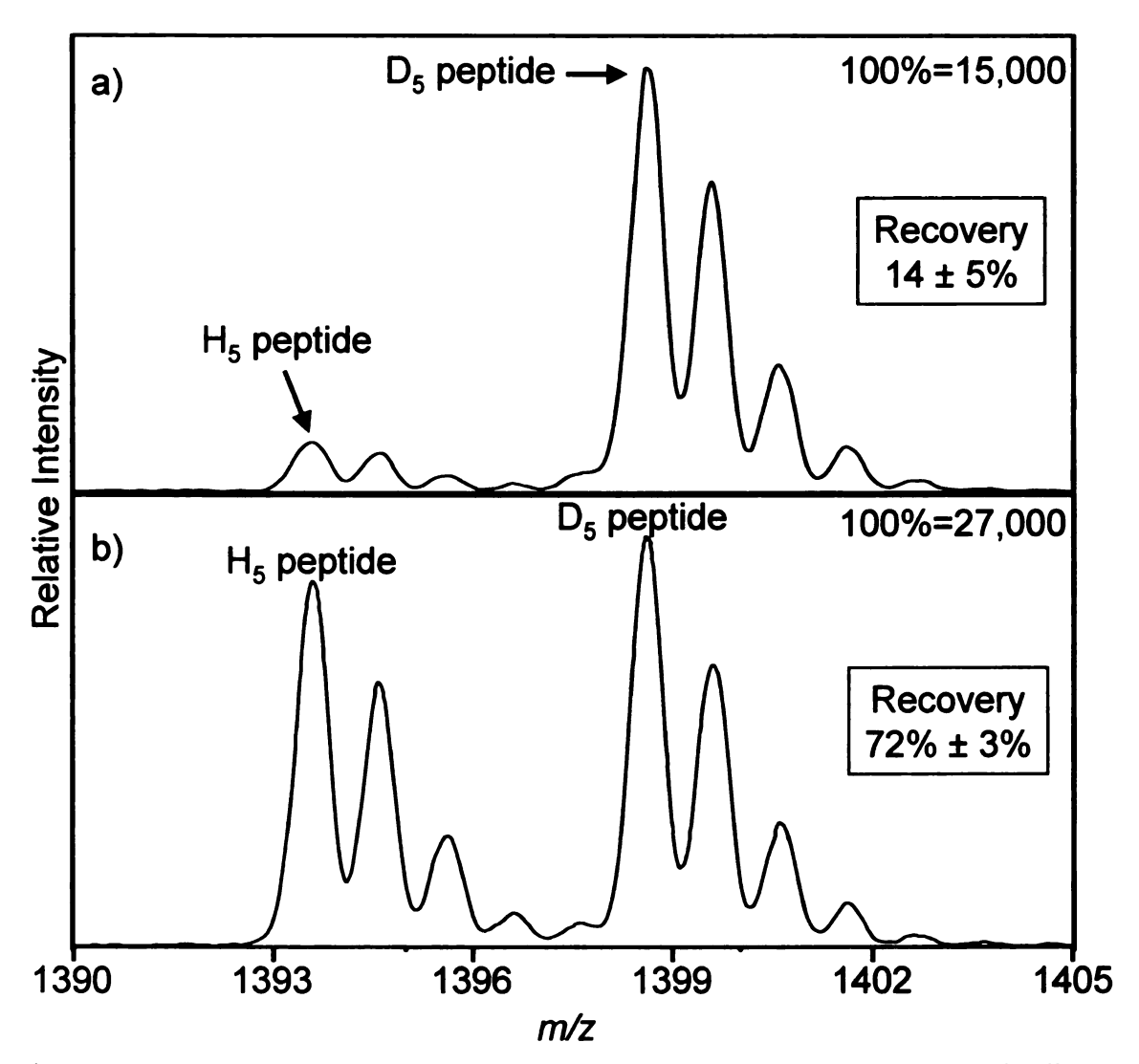


Figure 4.9: MALDI mass spectrum of 125 fmol of the H_5 peptide (no protein digest). The spectra were obtained using a) the Fe(III)-NTA-MUA-modified plate and b) the Fe(III)-NTA-PHEMA-modified plate. After the sample was applied to the plates and rinsed, 125 fmol of the D_5 peptide was added as an internal standard.

We also compared the use of the different Fe(III)-NTA-modified plates in the recovery of 125 fmol of the H₅ peptide from solutions containing a mixture of digested BSA (MW ~66 kDa), phos b (MW ~97 kDa), and esterase (MW ~62 kDa). The protocol for determining the recovery of the H₅ peptide (Figure 4.10) is similar to that used above for examining recoveries from solution of the H₅ peptide without the protein digest mixture. Briefly, the protein digest mixture (370 fmol BSA, 390 fmol esterase, and 240

fmol phos b, 1 pmol total) was first applied to the plate, directly followed by the addition of 125 fmol of the H₅ peptide. Typically, the sample was allowed to incubate for 1 h and then rinsed with acetic acid/acetonitrile solution to remove any nonphosphorylated peptides and digest reagents such as urea and DTT. After the plate was dried completely, 125 fmol of the D₅ peptide was added as the internal standard, followed by addition of a phosphoric acid/2,5-DHB solution release the H₅ peptide and the D₅ peptide from the Fe(III)-NTA complexes. (2,5-DHB also serves as the MALDI matrix.) The samples were then analyzed using MALDI-MS.

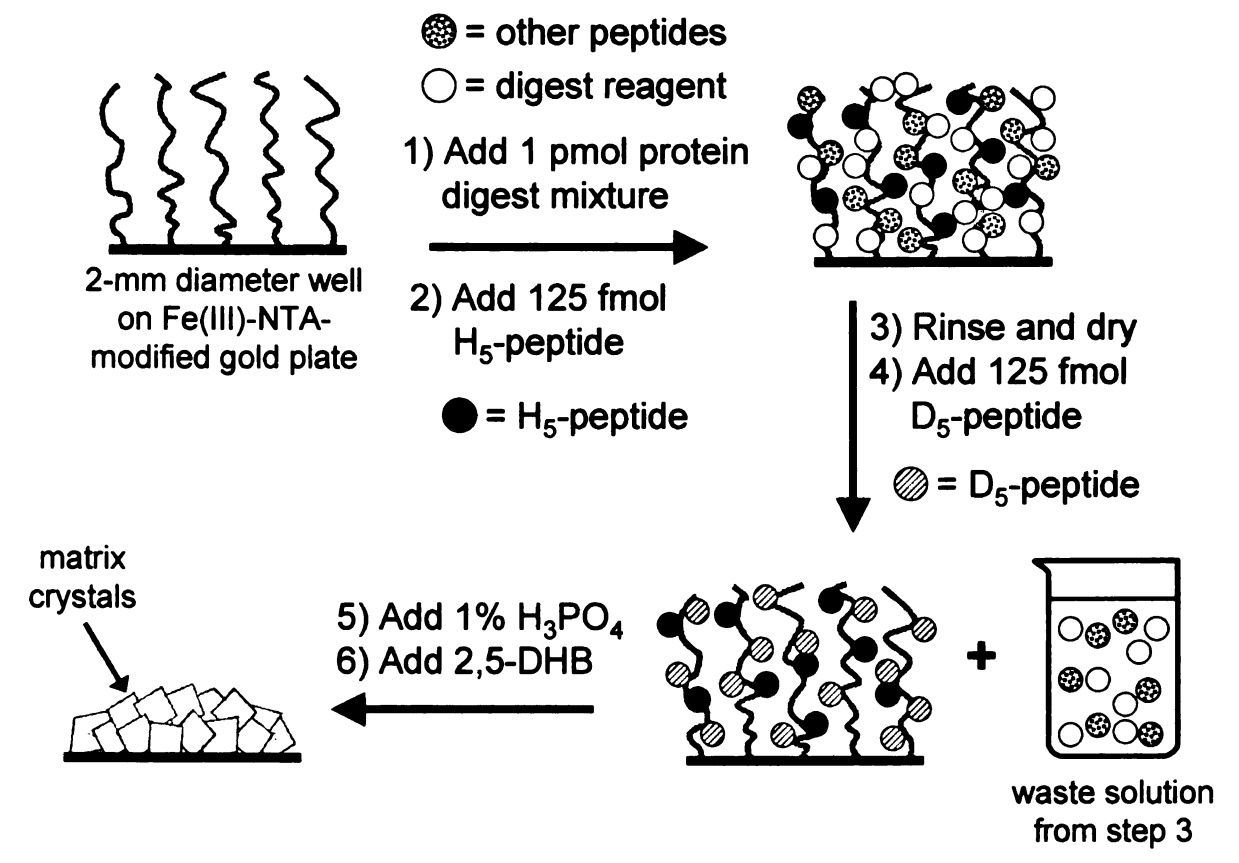


Figure 4.10: Protocol used for determining the recovery of the H₅ peptide from a protein digest mixture using Fe(III)-NTA-MUA-modified, Fe(III)-NTA-PAA-modified, or Fe(III)-PHEMA-modified plates.

The MALDI mass spectra in Figures 4.11, 4.12, and 4.13 show the recovery of the H₅ peptide from the protein digest mixture using Fe(III)-NTA-MUA-modified,

Fe(III)-NTA-PAA-modified, and Fe(III)-NTA-PHEMA-modified plates, respectively. The conventional analysis of 1 pmol of protein digest mixture containing 125 fmol of the H₅ peptide and 125 fmol of the D₅ peptide is also shown in Figures 4.11a, 4.12a, and 4.13a for comparison. In the conventional spectrum, many signals of digested peptides are present, but there were no signals due to the H₅ and the D₅ peptides (see Figure 4.11a). Evidently, ionization of these peptides is suppressed by the excess of digest proteins. The Fe(III)-NTA monolayer-functionalized plate showed minimal signal from digest peptides but was only capable of recovering 9 ± 2% of the H₅ peptide (Figure 4.11). There was a slight improvement when the relatively thin (~30 Å) Fe(III)-NTA-PAA film was utilized, as recovery increased to $23 \pm 12\%$. As shown in the mass spectrum in Figure 4.12a, however, there are a number of peaks (m/z 547, 696, 902, 994, 1439, and 1852) due to peptides from the protein digest mixture. The binding of less nonphosphorylated peptide to the Fe(III)-NTA-MUA-modified plate than to the Fe(III)-NTA-PAA-modified plate most likely occurs because the binding capacity of the monolayer is less than that of the Fe(III)-NTA-PAA film...

As seen in Figure 4.13b, the Fe(III)-NTA-PHEMA film showed a remarkable 73 ± 12% recovery of the H₅ peptide, even in the large excess of digest peptides. In fact, the recovery is the same in the presence and the absence of the protein digest mixture. The mass spectrum of the H₅ peptide-spiked digest obtained using the Fe(III)-NTA-PHEMA film does, however, contain signals due to a number of nonphosphorylated peptides (*m/z* values of 665, 994, 1177, 1249, 1419, 1439, 1532, and 1901). The sequences of these peptides are listed in Table 4.1. Many of the peptides contain histidine residues, which could contribute to their binding to the modified plate

Table 4.1: Positive ions due to nonphosphorylated peptides that were frequently observed when 1 pmol protein digest mixture containing 125 fmol of the H_5 peptide was analyzed using the enrichment methods presented in this chapter. Most of the ions observed are those from BSA and phos b, as determined using using CID MS/MS. The m/z value listed in the table is the theoretical value. The number of histidine (H), glutamic acid (E), and aspartic acid (D) residues for each peptide sequence are also given in the table.

Protein	Peptide Sequence	# H	# D	# E	m/z
BSA	KFWGK	0	0	0	665
	FKDLGEEHFK	1	1	2	1250
	TVMENFVAFVDK	0	1	1	1400
	SLHTLFGDELCK	1	1	1	1420
	RHPEYAVSVLLR	1	0	1	1440
	LKECCDKPLLEK	0	1	2	1533
	NECFLSHKDDSPDLPK	1	3	0	1902
	RHPYFYAPELLYYANK	1	0	1	2045
Phos b	HLHFTLVK	2	0	0	995
	DFYELEPHK	1	1	2	1178
	IHSEILKKTIFK	1	0	1	1457
	ARPEFTLPVHFYGR	1	0	1	1690

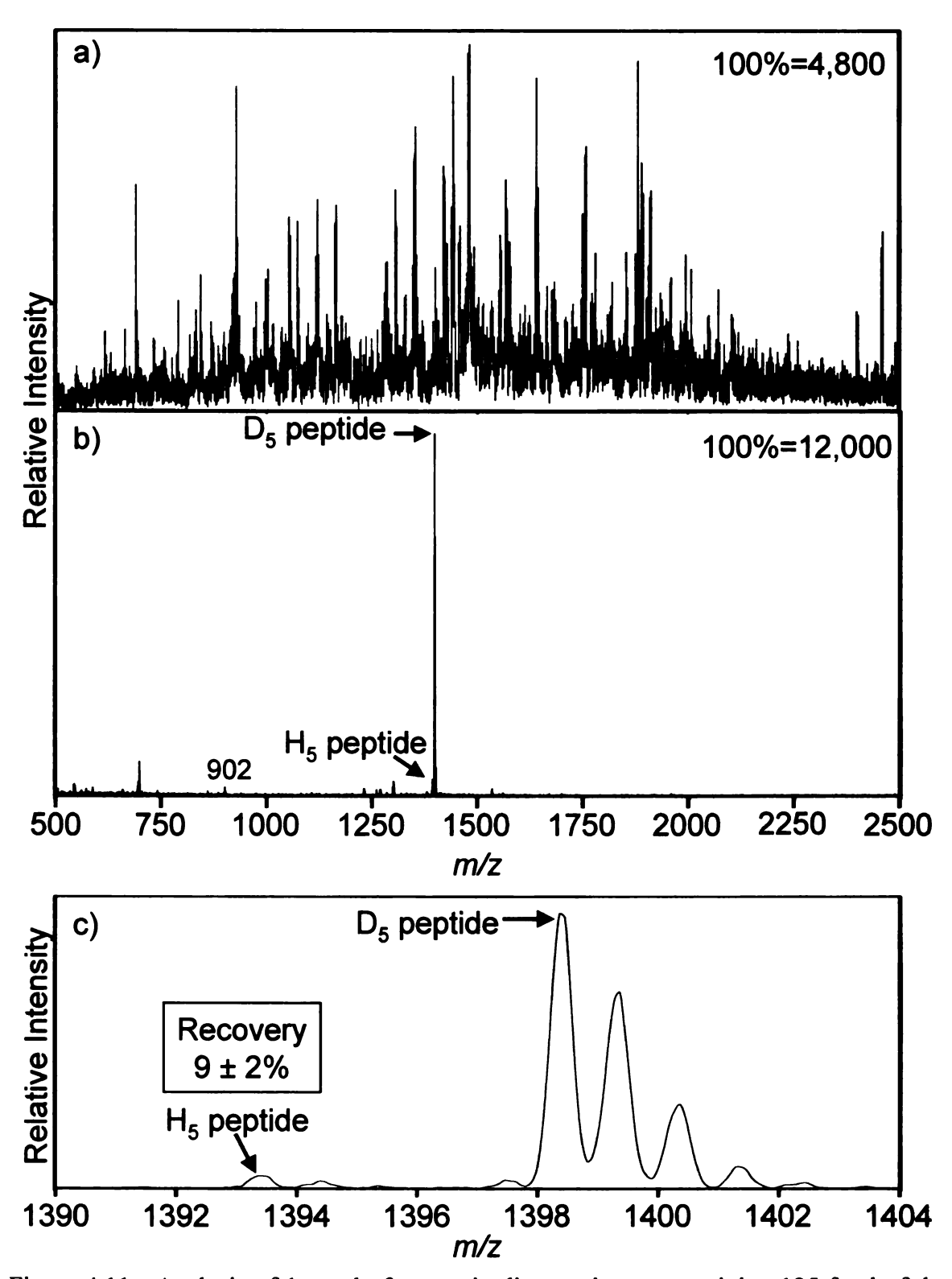


Figure 4.11: Analysis of 1 pmol of a protein digest mixture containing 125 fmol of the H_5 peptide. 125 fmol of the D_5 peptide was added as an internal standard. Spectra were obtained using a) conventional MALDI-MS analysis, and b) and c) a Fe(III)-NTA-MUA-modified plate with incubation and rinsing. Spectrum c) is an expanded portion of spectrum b).

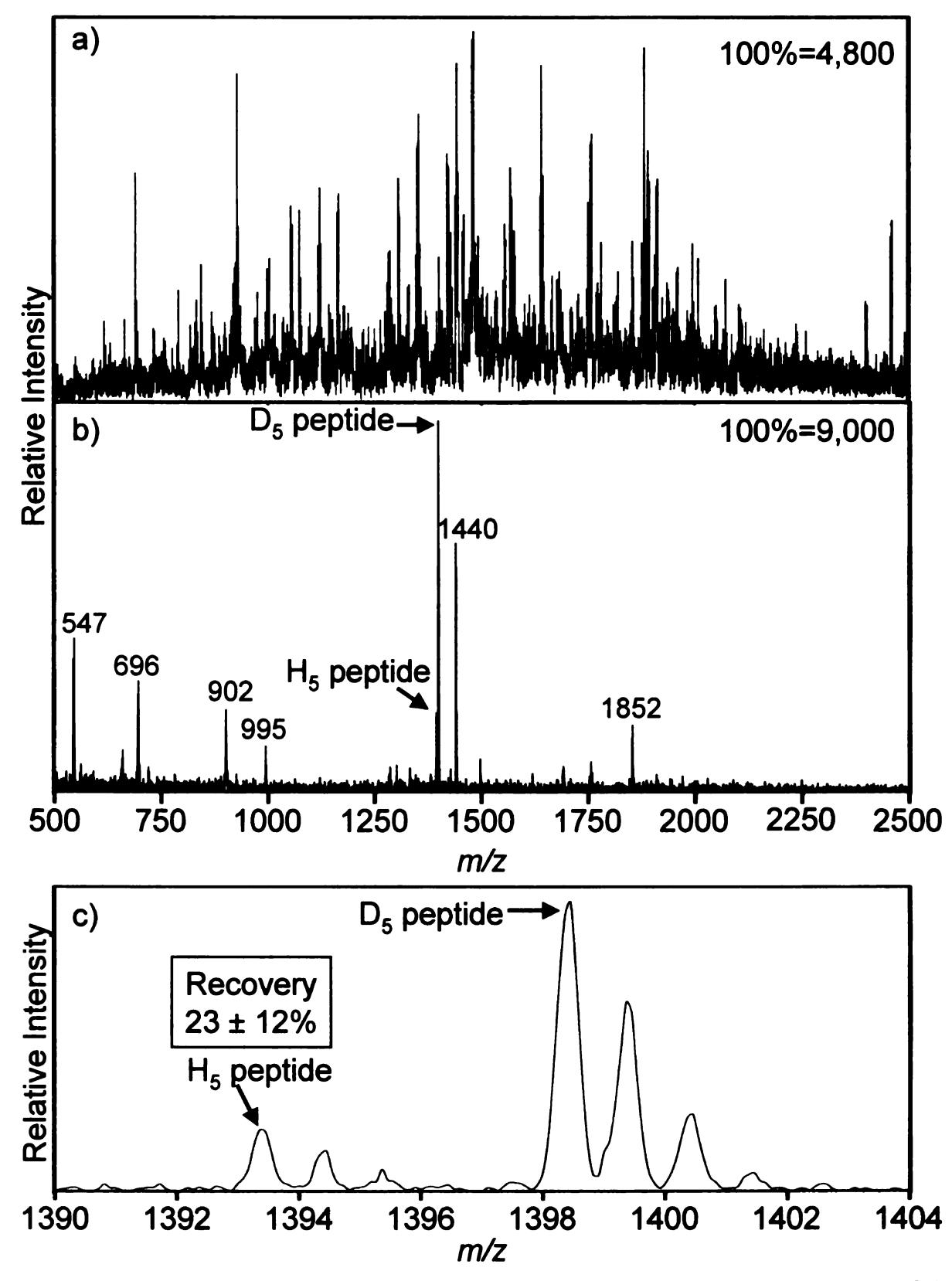


Figure 4.12: Analysis of 1 pmol of a protein digest mixture containing 125 fmol of the H₅ peptide. 125 fmol of the D₅ peptide was added as an internal standard. Spectra were obtained using a) conventional MALDI-MS analysis, and b) and c) a Fe(III)-NTA-PAA-modified plate with incubation and rinsing. Spectrum c) is an expanded portion of spectrum b).

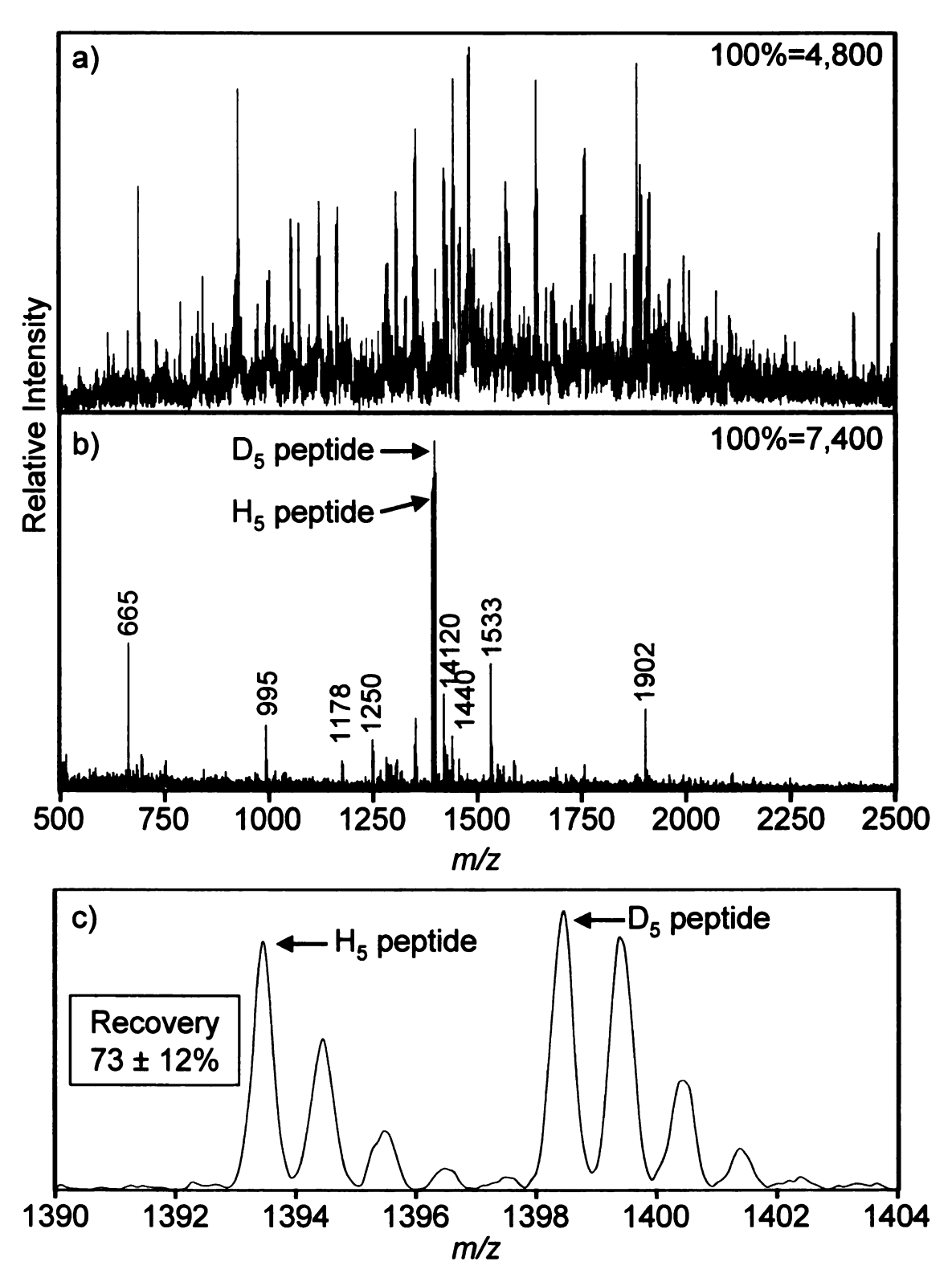


Figure 4.13: Analysis of 1 pmol of a protein digest mixture containing 125 fmol of the H₅ peptide. 125 fmol of the D₅ peptide was added as an internal standard. Spectra were obtained using a) conventional MALDI-MS analysis, and b) and c) a Fe(III)-NTA-PHEMA-modified plate with incubation and rinsing. Spectrum c) is an expanded portion of spectrum b).

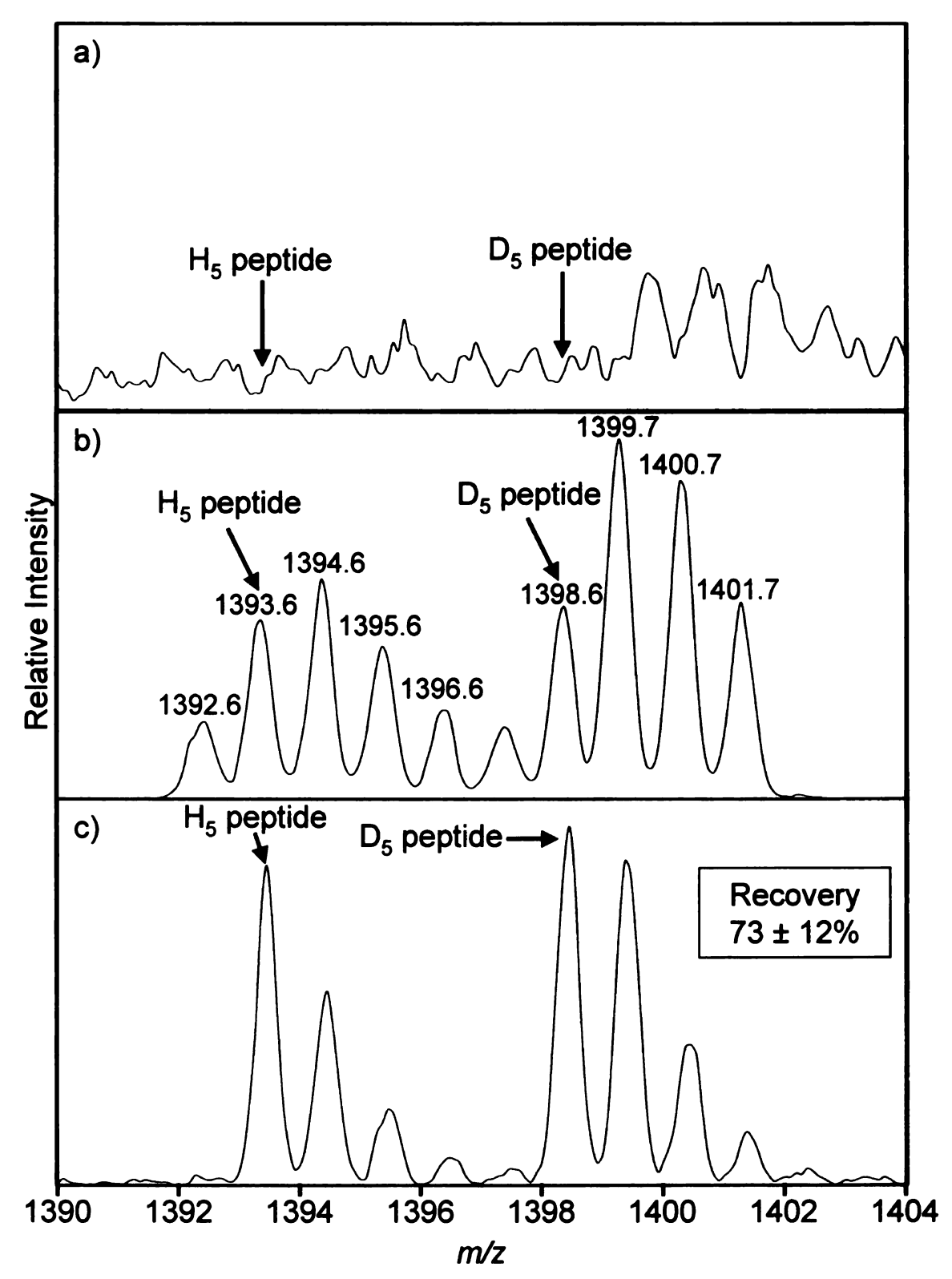


Figure 4.14: Analysis of 1 pmol of protein digest mixture containing 125 fmol of the H_5 peptide and 125 fmol of the D_5 peptide (internal standard) using a) conventional MALDI-MS analysis, b) conventional MALDI-MS analysis with precursor ion isolation with m/z 1396.4 and a m/z window of 10 (no fragmentation), and c) the Fe(III)-NTA-PHEMA-modified plate with incubation and rinsing. In spectrum c), the D_5 peptide was added just prior to addition of matrix.

We considered the possibility that there could be nonphosphorylated peptides from the protein digest mixture with m/z values similar to those of the H_5 and D_5 peptides. Figure 4.14a shows the enlarged region (m/z 1390 – 1404) of the conventional mass spectrum of the 1 pmol protein digest mixture containing 125 fmol of the H₅ and 125 fmol of the D₅ peptides. There appear to be no peaks due to the labeled phosphorylated peptides or any nonphosphorylated peptides. However, when the ions in this region were isolated to increase signal to noise (selected window with m/z 10 centered about 1396.4), the mass spectrum in Figure 4.14b was obtained. This mass spectrum shows that there are peptides that are present at or near m/z 1393.6 and 1398.6 in addition to the isotopes of the D₅ and H₅ peptides. Figure 4.14c shows the enlarged region of the mass spectrum obtained when the H₅ peptide was recovered from the protein digest mixture using the Fe(III)-NTA-PHEMA-modified plate. There is an irregular distribution of the isotopic peaks for the D_5 peptide due to a larger than expected signal at m/z 1399.7. This peak was determined to be due in part to the BSA peptide TVMENFVAFVDE by using CID MS/MS as shown in Figure 4.15. The y_n and b_n -H₂O ions that comprise the MS/MS spectrum are due to the BSA nonphosphorylated peptide. The mass spectrum also shows the product ion due to the loss of phosphoric acid from the isotope of the D₅ peptide that has an m/z value of 1399.

Fortunately, the signal at m/z 1399.7 should not affect our recovery calculations because we are mainly concerned that no nonphosphorylated signals are present at m/z 1393.6 and 1398.6, since only these would skew our results. To insure that our calculated recoveries of the H_5 peptide were accurate, we also calculated percent recovery using MS/MS spectra. A precursor ion was selected at m/z 1396.4 with a

window of m/z 10, which will allow any ions from m/z 1391 to 1401 to be isolated and fragmented using CID. Then the product ions, $[M+H-H_3PO_4]^+$, of the H_5 and D_5 peptides, which are solely representative of the phosphorylated peptides, were used to determine the recovery of the H_5 peptide, and this result was compared with that obtained using the MS data.

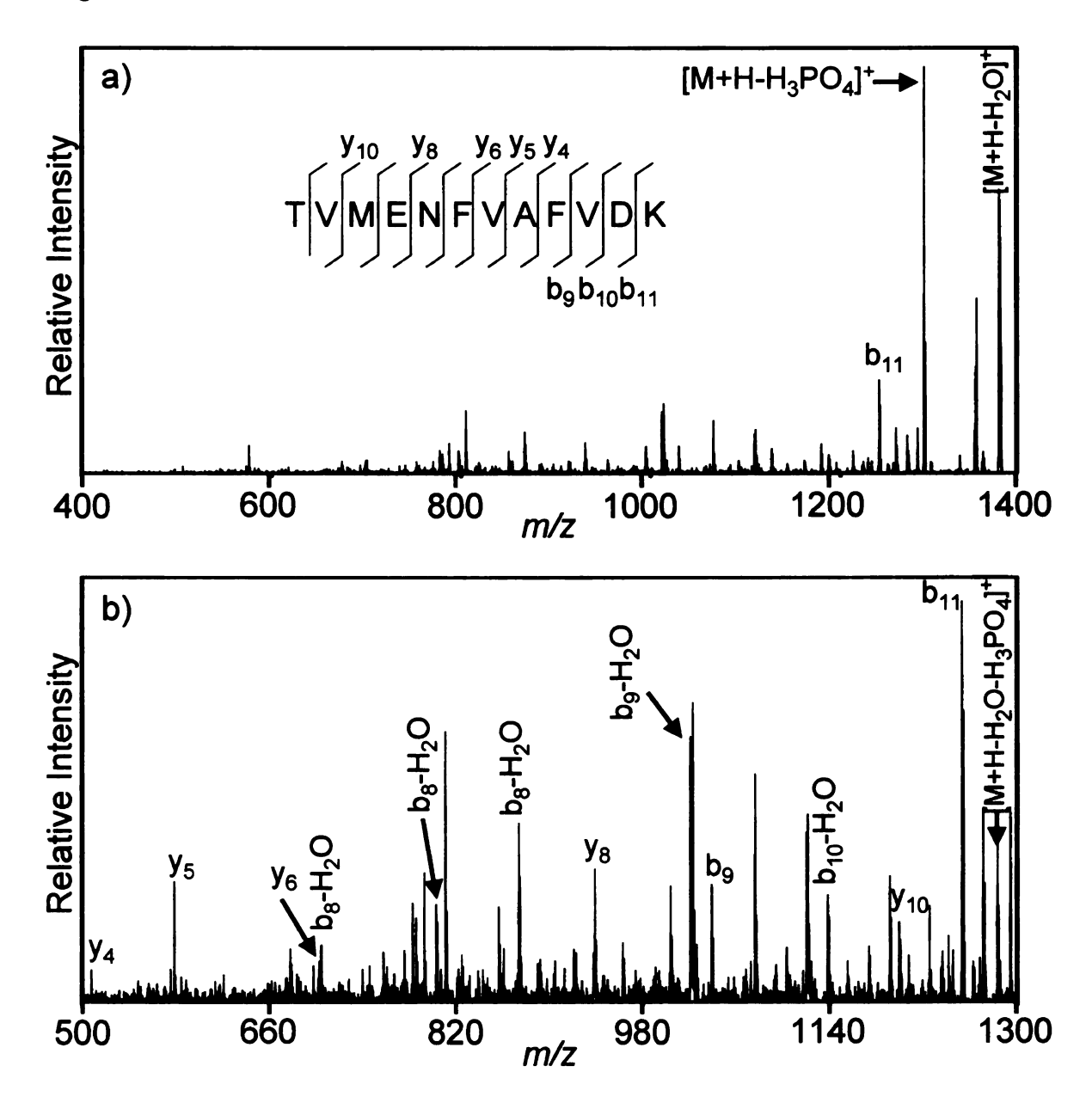


Figure 4.15: CID MS/MS spectrum of m/z 1399.6 observed in the MS spectrum of the peptides recovered from the H₅ peptide/protein digest mixture using an Fe(III)-NTA-PHEMA-modified plate a) m/z region 400 – 1400 and b) enlarged m/z region 500 – 1300. The b and y ions are due to the peptide shown, which originates from BSA.

The loss of H_3PO_4 (-98 Da) from the H_5 and D_5 peptides gives rise to peaks at m/z1295 and 1300, respectively, and these peaks represent the dominant product ions as shown in Figures 4.16 and 4.17. These two peptides are identical in amino acid sequence and will have the same y_n ions, while their b_n and b_n-H₂O ions will differ by 5 Da due to the heavy isotope label that has 5 deuterium atoms incorporated into it. Figure 4.18a shows the CID MS/MS spectrum of the protein digest mixture containing 125 fmol of H₅ and 125 fmol of the D₅ peptides, and Figure 4.18b shows the CID MS/MS spectrum after H₅ peptide is enriched from 1 pmol of the protein digest mixture using the Fe(III)-NTA-PHEMA-modified plate. Using the intensities of the product ion peaks due to the H₅ and D_5 peptides at m/z 1295 and 1300, respectively, the recovery of the H_5 peptide was determined to be $76 \pm 10\%$. An expanded view (m/z 1240 – 1390) of these mass spectra can be seen in Figure 4.19, which shows that the product ion peaks due to nonphosphorylated peptide were absent when the H₅ peptide was recovered using the Fe(III)-NTA-PHEMA-modified gold plate. The recovery of the H₅ peptide from the protein digest mixture was also determined for the same set of samples using the MS data and found to be 67 ± 21 . Since the MS and MS/MS data give similar percent recoveries of the H₅ peptide from the protein digest mixture, from here on, only MS spectra will be shown for the analysis of the H₅ peptide.

For most of the analyses presented here we utilized a 1-h sample incubation period. However, this limits the utility of MALDI-MS as a high throughput technique. The rate of binding of the H₅ peptide to the Fe(III)-NTA complexes in the polymer brushes may be diffusion limited since no stirring or vortex mixing was used after the sample was applied to the Fe(III)-NTA-PHEMA-modified plate (about every 5-10 min

acetic acid was replenished, which could allow some on-plate sample mixing. Additionally, as the sample droplet on the plate evaporates, the solvent molecules allow mixing of the analyte to occur to due to increasing surface tension forces, which can be observed using a stereomicroscope.) However, when 2- μ l of digest mixture containing 125 fmol of the H₅ peptide was applied to the 2-mm diameter well of the polymer-modified plate, it was found that a 10-min incubation time still allowed for an H₅ peptide recovery of 63 \pm 15%, based on MS data, or 78 \pm 15%, based on MS/MS data. Thus, short incubation times should still allow efficient analyses.

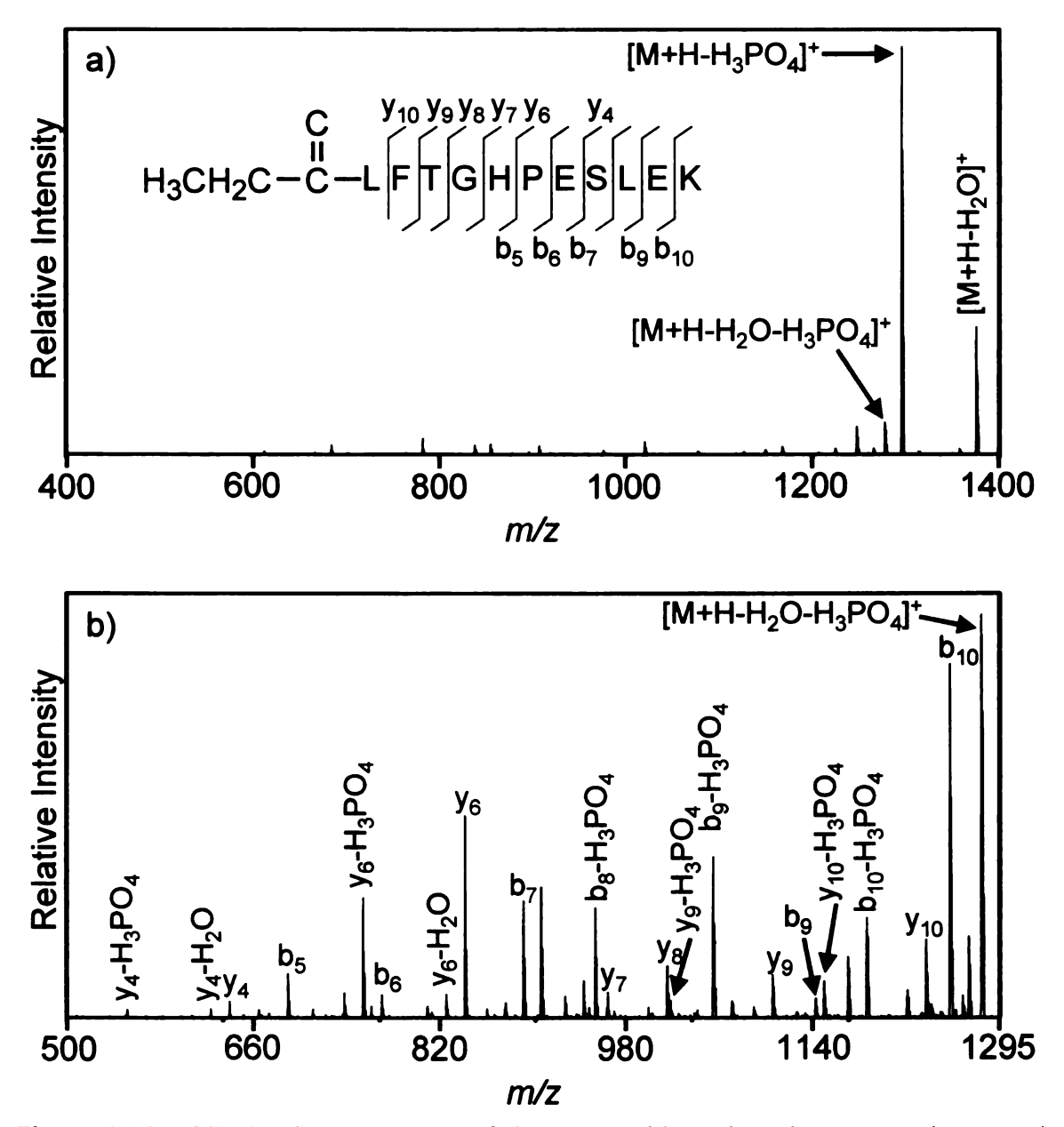


Figure 4.16: CID MS/MS spectrum of the H_5 peptide (selected precursor ion at m/z 1393.6) a) m/z region 400 - 1400 and b) enlarged m/z region 500 - 1295.

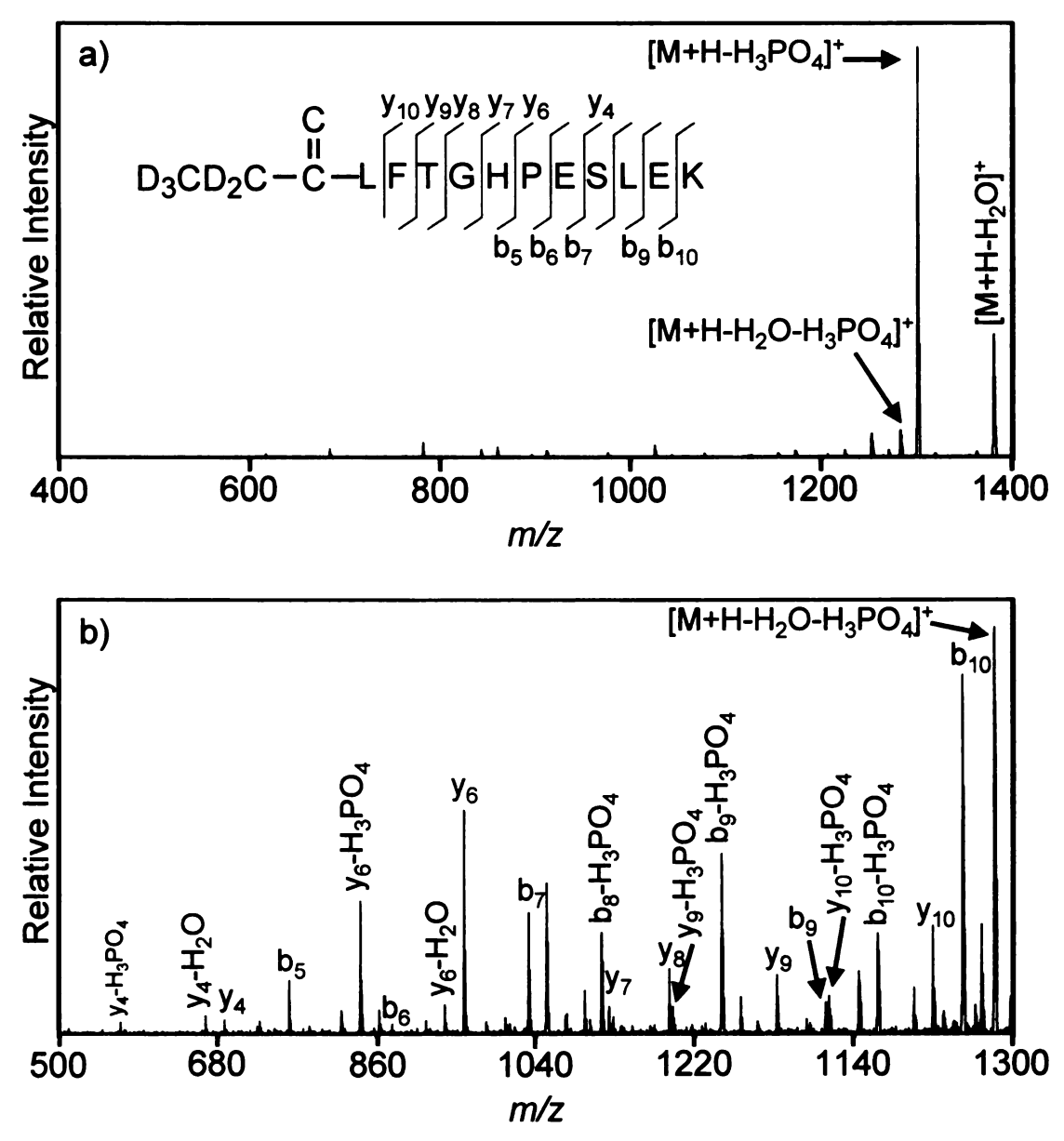


Figure 4.17: CID MS/MS spectrum of the D_5 peptide (selected precursor ion at m/z 1398.6) a) m/z region 400 - 1400 and b) enlarged m/z region 500 - 1295.

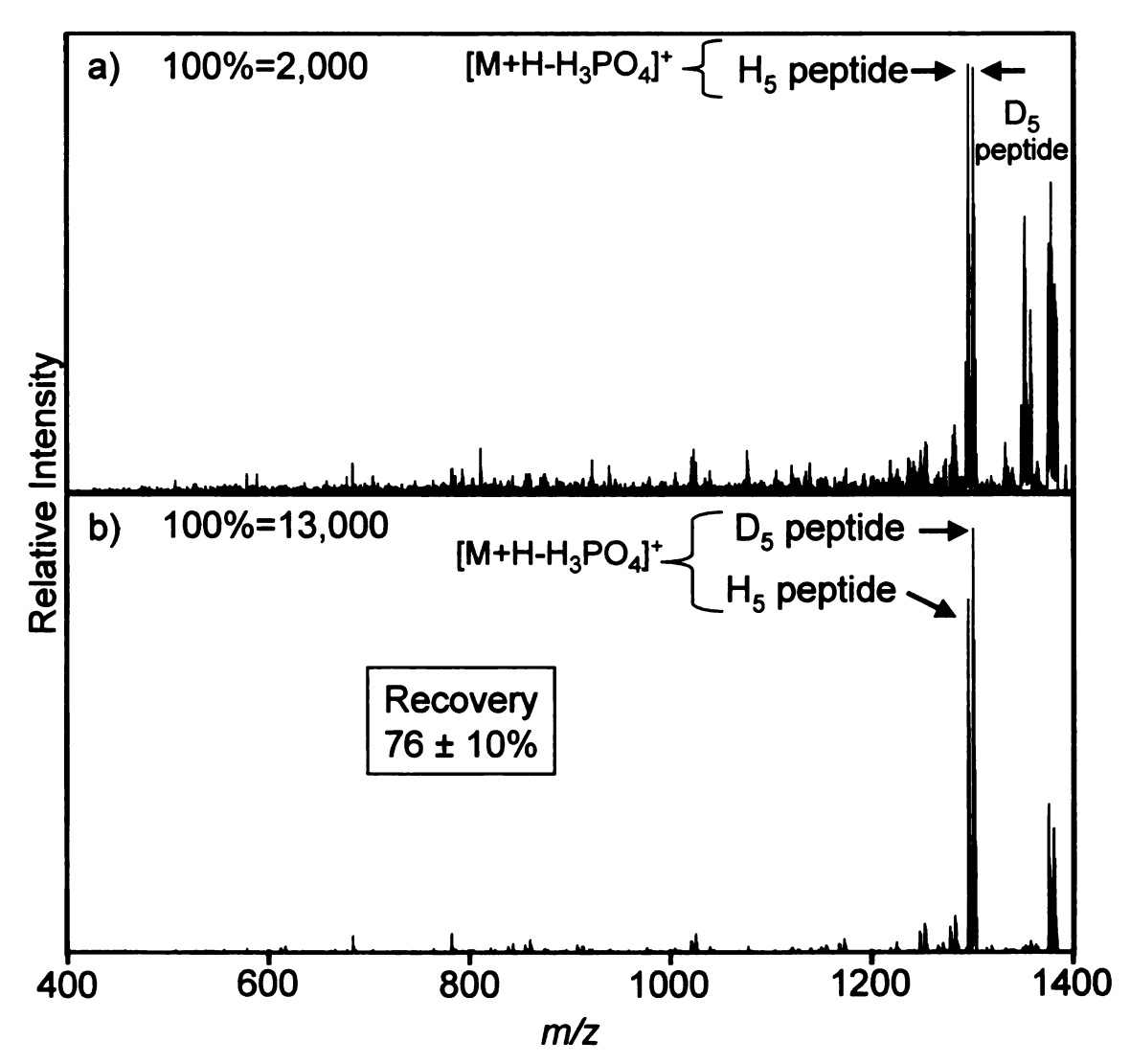


Figure 4.18: CID MS/MS analysis of 1 pmol of a protein digest mixture containing 125 fmol of the H_5 peptide. 125 fmol of the D_5 peptide was added to the digest solution prior to conventional analysis and to the Fe(III)-NTA-PHEMA-modified plate after enrichment. Spectra were obtained using a) conventional MALDI-MS analysis and b) enrichment using a Fe(III)-NTA-PHEMA-modified plate. In both a and b, the precursor ion isolation was m/z 1396.4 with a m/z window of 10.

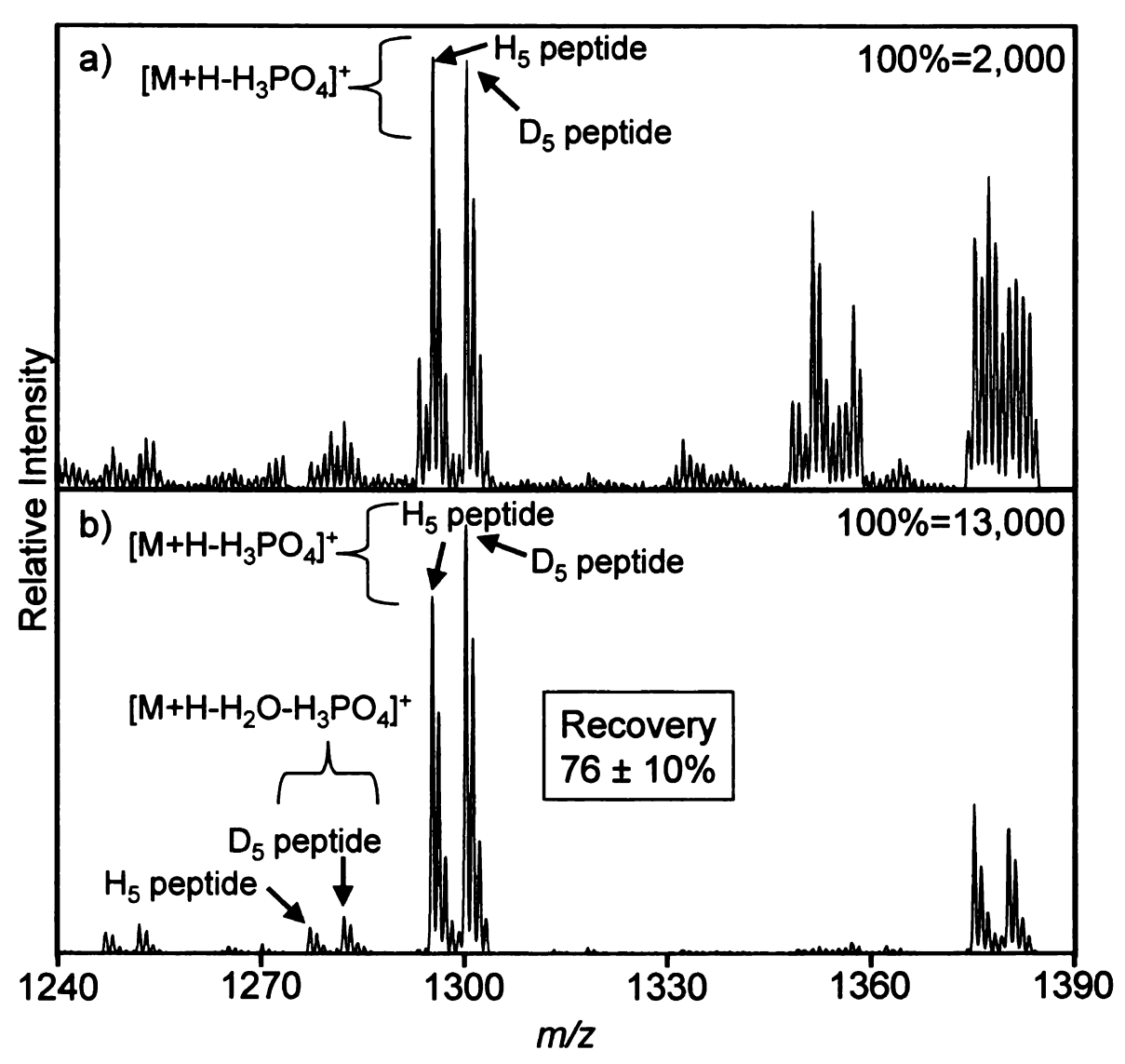


Figure 4.19: Enlarged m/z region 1240 - 1390 of the CID MS/MS analysis of 1 pmol of a protein digest mixture containing 125 fmol of the H₅ peptide. Spectra were obtained using a) conventional MALDI-MS analysis and b) enrichment on a Fe(III)-NTA-PHEMA-modified plate. 125 fmol of the D₅ peptide was added to the digest solution prior to conventional analysis and to the Fe(III)-NTA-PHEMA-modified plate after enrichment. In both a and b, the selected precursor ion had a m/z 1396.4 with a m/z window of 10.

3.3 Recovery of the H₅ Peptide Using Commercial IMAC Materials

As mentioned previously, the commercially available IMAC materials selected for comparison with Fe(III)-NTA-PHEMA films were chosen based on their applicability to low volume samples and low amounts of a particular analyte. Both the Millipore $ZipTip_{MC}$ and Qiagen IMAC chips appear to fit this criterion, while most commercially

available IMAC materials require roughly 50 µL of sample volume. The Qiagen IMAC chips are also attractive because they are manufactured to interface with several different commercial mass spectrometers, including the Thermo vMALDI LTQ XL that we use. Bio-Rad sells affinity chips (these chips were formerly sold by Ciphergen) that utilize IMAC technology, but these are only compatible with a specific Bio-Rad mass spectrometer. We applied the ZipTip_{MC} enrichment and the Qiagen IMAC chip towards the recovery of 125 fmol of the H₅ peptide from the 1 pmol protein digest mixture. Use of the ZipTip_{MC} (selective adsorption on an IMAC resin in a pipette tip followed by elution) resulted in only $12 \pm 2\%$ recovery of the H₅ peptide as demonstrated by the mass spectra in Figure 4.20. Moreover, the mass spectrum in Figure 4.20a shows that some nonphosphorylated peptides (m/z 917, 1260, 1502, and 1749) from the digest mixture were retained on the ZipTip_{MC}. (Using the ZipTip_{MC}, the recovery of the H₅ peptide in the absence of the protein digest mixture was still only $9 \pm 2\%$.) When selective adsorption on the Qiagen IMAC chip was employed, the recovery of the H₅ peptide from a protein digest mixture was $13 \pm 3\%$ (based on MS data) as shown in Figure 4.21. The percent recovery determined from MS/MS data was similar at $16 \pm 3\%$. Even though the percent recoveries of the H₅ peptide obtained using the ZipTip_{MC} and the Qiagen IMAC chip are similar, there are almost no nonphosphorylated peptides recovered from the IMAC chip (Figure 4.21a). Most likely this is due to the lower binding capacity of the Qiagen IMAC chip, which is presumably a monolayer of Fe(III)-NTA complexes. The binding capacity of the ZipTip_{MC} is 400 ng, which corresponds to ~290 pmol of the H₅ peptide. We surmise that the binding capacity of the Qiagen IMAC chip is roughly 5 pmol, assuming that the surface area of the affinity zone is 7 mm², a monolayer of peptide binds to this surface with a density of 1 peptide molecule per 2.5 nm². Even though the Qiagen IMAC chip was estimated to have a binding capacity of 5 pmol, this was not sufficient to recover 125 fmol of the H₅ peptide.

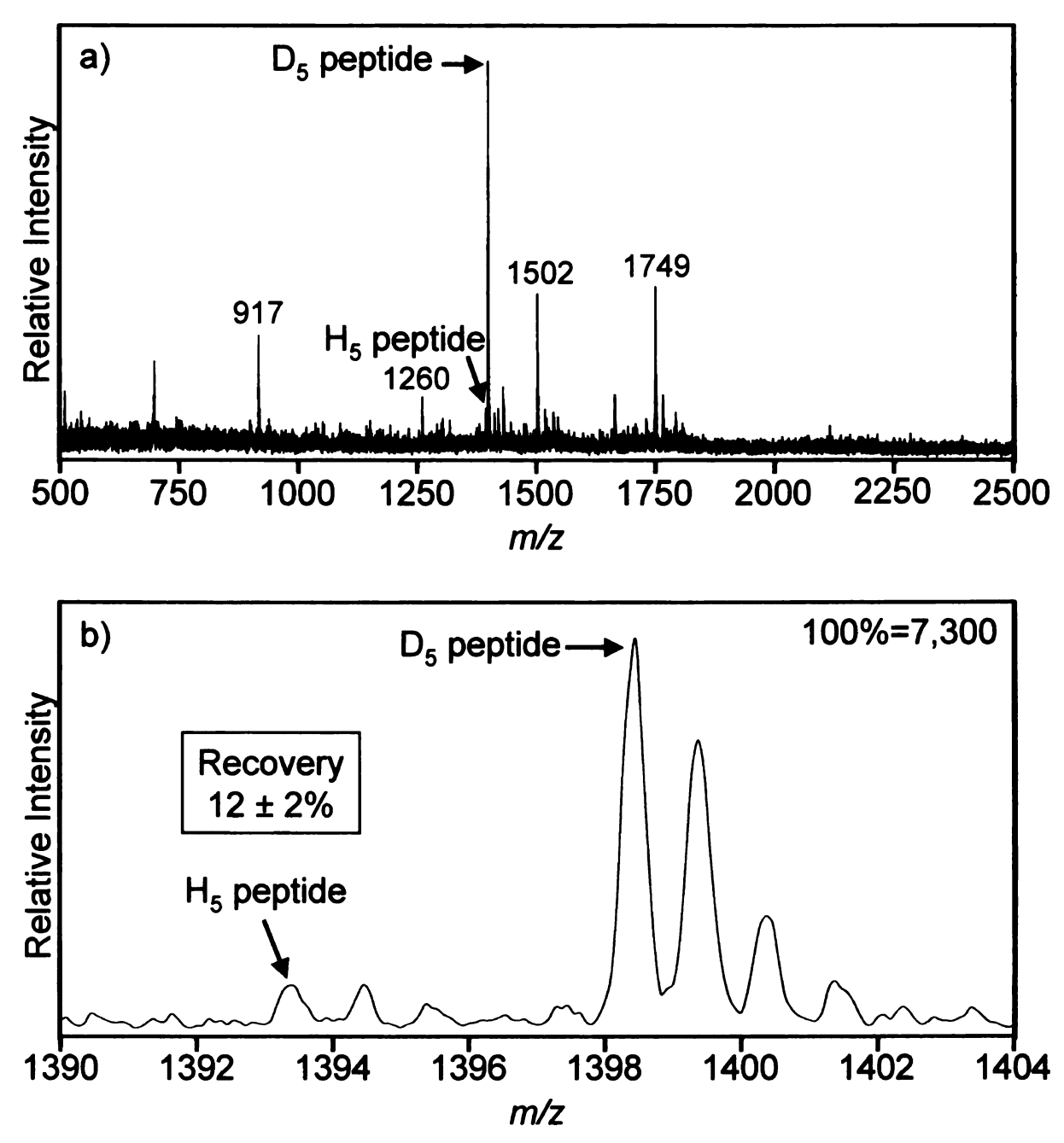


Figure 4.20: Mass spectra of the peptides extracted using a Millipore ZipTip_{MC} and a solution containing a protein digest mixture (1 pmol) and 125 fmol of the H_5 peptide. a) m/z range 500 - 2500 and b) enlarged m/z region 1390 - 1404. The D_5 peptide (125 fmol) was added as an internal standard to the extracted peptides.

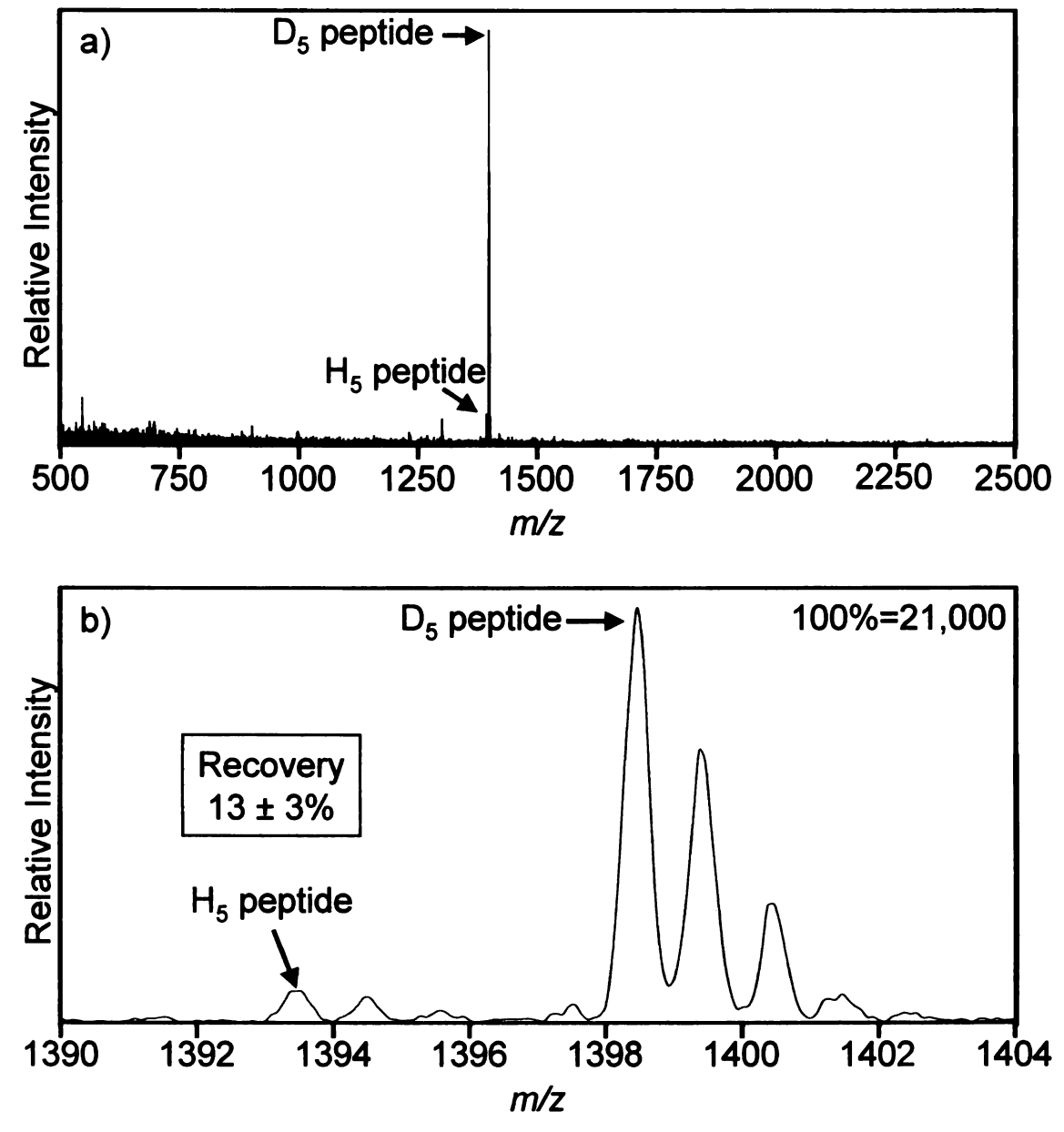


Figure 4.21: Mass spectra of the peptides extracted onto a Qiagen Mass Spec Focus IMAC chip from a solution containing a protein digest mixture (1 pmol) and 125 fmol of the H_5 peptide. a) m/z range 500 - 2500 and b) enlarged m/z region 1390 - 1404. The D_5 peptide was added as an internal standard to the extracted peptides.

4.3.4 Recovery of the H₅ Peptide Using Commercial Metal Oxide Materials

Several recent reports showed highly successful enrichment of phosphopeptides using TiO₂ and ZrO₂ as adsorbents, so we also examined the use of one of these systems for comparison with the Fe(III)-NTA-PHEMA-modified plates. We selected Glygen NuTips because these TiO₂ or ZrO₂-containing pipet tips are capable of analyzing small volumes of solutions containing low amounts of phosphorylated peptides. When a sample of 1 pmol of protein digest mixture containing 125 fmol of the H₅ peptide was treated with the tips using 1% TFA in the rinse solutions and 3% NH₄OH in the elution solution, there was a recovery of $68 \pm 5\%$ and $22 \pm 8\%$ for the TiO₂-containing and ZrO₂containing NuTips, respectively, as shown by the mass spectra in Figures 4.22 and 4.23. (Using the TiO₂ and ZrO₂ NuTips, the recoveries of the H₅ peptide in the absence of the protein digest mixture were $60 \pm 7\%$ and $29 \pm 9\%$, respectively.) When the ZrO₂ NuTip was used there was very little adsorption of nonphosphorylated peptide to the resin as shown in Figure 4.22a. However, one problem we encountered when using the TiO₂ NuTip was that part of the TiO₂ material was eluted from the NuTip when 3% NH₄OH was used as the elution solution, and this eluted resin appeared to interfere with the MS analysis. Peaks presumably due to polymer, which most likely eluted from the tip, gave rise to prominent peaks separated by 338 Da (Figure 4.22). We also examined the use of 0.5% piperidine as an elution solution,⁵ but this caused more titanium dioxide to be leached out of the tips. The presence of the peaks separated by 338 Da made identifying nonphosphorylated peptides from the protein digest mixture more complicated.

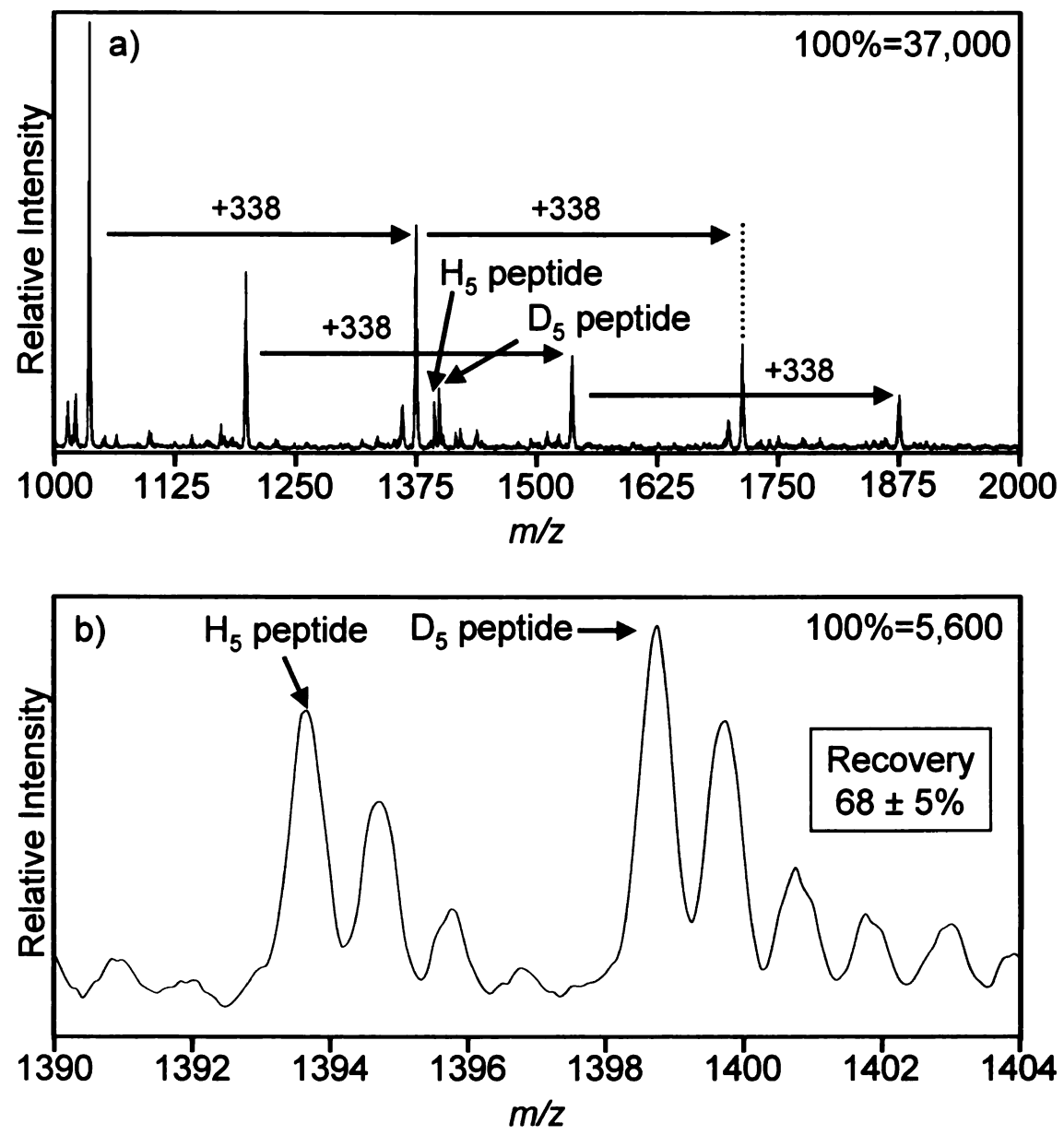


Figure 4.22: Mass spectra of the peptides extracted using a Glygen TiO_2 NuTip and a solution containing a protein digest mixture (1 pmol) and 125 fmol of the H_5 peptide. a) m/z range 1000 - 2000 and b) enlarged m/z region 1390 - 1404. The D_5 peptide (125 fmol) was added as an internal standard to the extracted peptides.

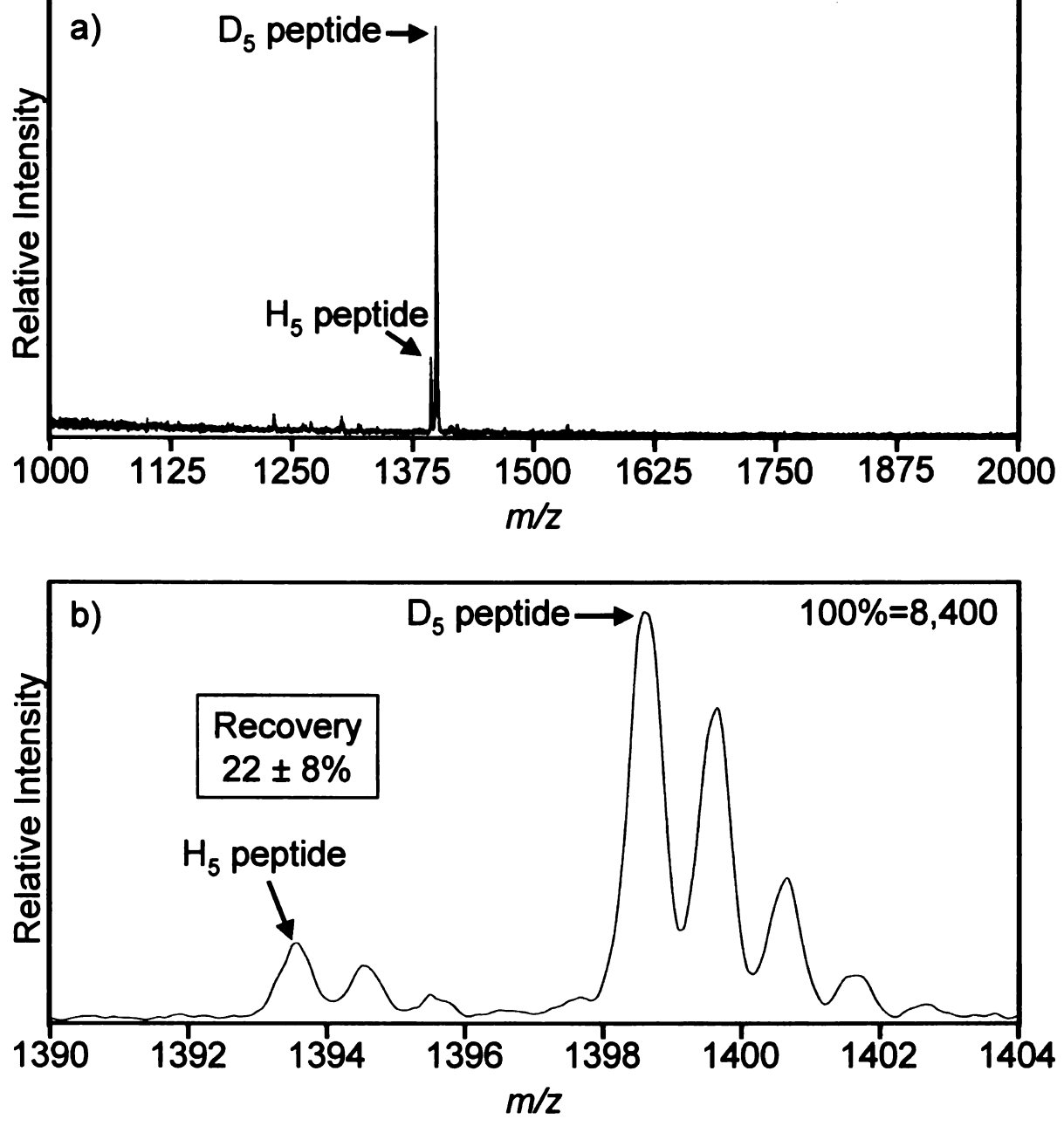


Figure 4.23: Mass spectra of the peptides extracted using a Glygen ZrO_2 NuTip and a solution containing a protein digest mixture (1 pmol) and 125 fmol of the H_5 peptide. a) m/z range 1000 - 2000 and b) enlarged m/z region 1390 - 1404. The D_5 peptide (125 fmol) was added as an internal standard to the extracted peptides.

4.4 Conclusions

This chapter demonstrates that MALDI-MS can be used to quantify the amount of the phosphorylated H₅ peptide that can be recovered from a three-protein digest mixture. We were able to obtain at least 3-fold higher recoveries of the H₅ peptide when using plates modified with relatively thick (500 Å) Fe(III)-NTA-PHEMA films rather than thinner (30 Å) Fe(III)-PAA-NTA films or monolayer films. When comparing our Fe(III)-NTA-PHEMA-modified plate to commercial IMAC and metal oxide materials, we found that the use of Fe(III)-NTA-PHEMA-modified MALDI plates gives several-fold greater recoveries than the use of ZipTip_{MC} pipette tips, ZrO₂ NuTips, and Qiagen MALDI chips. Recovery from TiO₂ NuTips is similar to that obtained with Fe(III)-NTA-PHEMA-modified plates, but we frequently saw interference from TiO₂ resin that had leached out of the tips. Although most of the work on modified plates employed 60-min incubations, 10-min incubations with Fe(III)-NTA-PHEMA-modified plates are sufficient for high recoveries.

4.5 References

- (1) Hillenkamp, F.; Peter-Katalinic, J. MALDI MS: A Practical Guide to Instrumentation, Methods and Applications; Wiley-VCH Verlag GmbH & Co.: KGaA, 2007.
- (2) Belisle, C. M.; Chen, I. Y.; Mirshad, J. K.; Roth, U.; Steinert, K.; John A. Walker, I. American Society for Mass Spectrometry Seattle, WA, May 28-June 1, 2006.
- (3) Garrett, T. J.; Prieto-Conaway, M. C.; Kovtoun, V.; Bui, H.; Izgarian, N.; Stafford, G.; Yost, R. A. *International Journal of Mass Spectrometry* **2007**, *260*, 166-176.
- (4) Simon, E.; Young, M. A.; Andrews, P. C. American Society for Mass Spectrometry Indianapolis, IN, June 3-7, 2007.
- (5) Kweon, H. K.; Hakansson, K. Analytical Chemistry 2006, 78, 1743-1749.

Chapter Five: Conclusions and Future Research

5.1 Conclusions and Future Research

Fe(III)-NTA-PHEMA-modified The of high-capacity plates for use phosphopeptide enrichment and subsequent identification of phosphorylation sites is very promising. These high-capacity plates show at least three-fold greater phosphopeptide recoveries than do MALDI plates derivatized with a monolayer or thin polymer film of Fe(III)-NTA complexes. The binding capacity for the Fe(III)-NTA-PHEMA-modified plate is around 0.6 µg/cm² or roughly 18 pmol of phosphopeptide per 2-mm diameter sample well. Moreover Fe(III)-NTA-PHEMA-modified plates allow as little as 15 fmol of β -case in digest to be detected with a signal to noise ratio of ≥ 6 . However, at this lowfmol level, only the monophosphorylated peptide can be detected, while the recovery of the tetraphosphorylated peptides diminishes when the amount of β-casein digest decreased to below 1 pmol. Additional studies using standard monophosphorylated and tetraphosphorylated β-casein peptides, which are commercially available, should be used to further investigate this phenomenon. Interestingly, at high levels (1 - 7 pmol) of β casein digest, the Fe(III)-NTA-PHEMA-modified plates are able to recovery trace-level impurities (\sim 10% of the β -casein digest) of α -casein phosphopeptides. The α -caseins phosphopeptides are not observed when the Fe(III)-NTA-PAA-modified plates are used to analyze \sim 7 pmol of β -casein digest. This confirms that the high capacity of the PHEMA-modified plates allows a higher percentage of phosphopeptides to be recovered than did use of the Fe(III)-NTA-PAA-modified plates even when the amount of phosphopeptides are present at fmol-levels.

Isotopically labeled peptides are attractive for examining peptide recoveries in onplate purification and MALDI-MS analysis. Such studies show that the Fe(III)-NTAPHEMA-modified MALDI plate is able to recovery over 70% of the H₅ peptide from a
three-protein digest mixture. Commercial IMAC (Millipore ZipTips_{MC} and Qiagen Mass
Spec Focus IMAC chips) and metal oxide materials (Glygen ZrO₂ NuTips) exhibit at
least 3-fold lower phosphopeptide recoveries than the Fe(III)-NTA-PHEMA-modified
plate. In contrast, the recovery of the H₅ peptide (68%) using the commercial Glygen
TiO₂ NuTip was comparable to that the polymer-modified plate. However, mass spectra
of samples enriched by the TiO₂ NuTip show that TiO₂, which had leached out of the tip
during peptide elution with a basic elution solution, significantly interfered in the MS
analysis. Additional purification steps may be required to remove any metal oxide
material from the elution solution when using the TiO₂ microtips for phosphopeptide
analysis by MS.

It appears that histidine-containing nonphosphorylated peptides (from digests of ovalbumin, BSA, and phosphorylase b) were apt to bind to a small degree to our Fe(III)-NTA-PHEMA-modified plates. Thus, the incorporation of a low concentration (< 5 mM) of imidazole into the binding and/or rinsing solution could prove useful for limiting the binding of these peptides to the polymer-modified plates. However, imidazole also has an affinity for Fe(III), and too high of a concentration may prevent the phosphopeptides from binding to Fe(III)-NTA complexes. Other properties of peptides that may affect nonspecific adsorption should also be examined, such as the hydrophobicity and acidity of the peptide.

Potential improvements to the Fe(III)-NTA-PHEMA-modified plates include incorporating smaller sample wells surrounded by a hydrophobic region to help concentrate the sample while isolating the phosphopeptides on the plate. In these experiments, the hydrophobic region allows deposition of a relatively large sample drop that slowly evaporates to the size of the hydrophilic region, thus concentrating the sample. Xu et al. previously demonstrated using patterned surfaces on a MALDI plate for concentration and purification of the analyte, ^{1,2} and applied this technology to the analysis of phosphopeptides. ¹ Additionally, the choice of binding, washing, and matrix solutions used for the polymer-modified plate needs to be optimized in order to maximize the recovery of phosphopeptides and reduce the number of nonphosphorylated peptides that bind to the polymer film. Ndassa et al. showed that using 33:33:33 acetonitrile:methanol:water containing 0.1% acetic allowed the best recovery of phosphorylated peptides (the peptides were methyl esterified) using IMAC.³

It would also be interesting to see if the incorporation of other metals such as Ga(III) or Zr(IV) or other ligands such as IDA or phosphonate into the polymer films could increase the recovery and selectivity of the phosphopeptides. Such affinity systems would include Zr(IV)-NTA, Zr(IV)-phosphonate, and other complexes.

Since commercial TiO₂ microtips had a 68% recovery of phosphopeptide, then perhaps incorporating TiO₂ nanoparticles in polymer films on MALDI plates, could be useful for on-plate enrichment. In this case, TiO₂ would not interfere with the MS analysis since no off-plate elution using a strong base is necessary.

Most importantly, the modified MALDI plates need to be utilized to identify and quantify phosphorylation in important biological samples such as the cancer signaling

pathway of p53, the tumor suppressor protein. p53 is a transcription factor that regulates cellular activity in response to stress such as genetic damage within the cell.⁴ As a cancer prevention mechanism, activated p53 due to DNA damage will halt the growth of the cell and initiate repair.⁴ However, if the cellular damage is too severe, then p53 will stimulate cell apoptosis.⁴ Phosphorylation is one of the posttranslational modifications (others include acetylation, glycosylation, ribosylation, and sumoylation) that activates p53.⁴ Anti-cancer therapy has been targeted towards p53 and kinase activity.⁵ Understanding phosphorylation events of p53 will lead to new drug treatments for cancer.

In summary, optimized phosphopeptide enrichment procedures with high-capacity polymer-modified MALDI plates show great promise for helping to elucidate regulatory mechanisms in important areas such as better understanding cancer.

5.2 References

- (1) Xu, Y. D.; Bruening, M. L.; Watson, J. T. Analytical Chemistry 2004, 76, 3106-3111.
- (2) Xu, Y. D.; Watson, J. T.; Bruening, M. L. Analytical Chemistry 2003, 75, 185-190.
- (3) Ndassa, Y. M.; Orsi, C.; Marto, J. A.; Chen, S.; Ross, M. M. *Journal of Proteome Research* **2006**, *5*, 2789-2799.
- (4) Weinberg, R. A. *The Biology of Cancer*; Garland Science: New York, **2007**.
- (5) Stoklosa, T.; Golab, J. Acta Biochimica Polonica 2005, 52, 321-328.

